PERSPECTIVE RESERVOIR FACIES WITHIN THE BEEKMANTOWN GROUP OF EASTERN NEW YORK STATE

FINAL REPORT

NYSERDA AGREEMENT NUMBER: 4525

DECEMBER, 2005

Submitted by:

Donald Clark
CUNY Graduate Center
365 Fifth Ave., New York, New York 10016
email: CDN194@AOL.COM

Submitted to:

Dr. John Martin, NYSERDA Project Manager
New York State Energy Research and Development Authority
17 Columbia Circle, Albany, New York 12203-6399

Notice

This report was prepared by Donald Clark in the course of performing work contracted for and sponsored by the New York State Energy Research and Development Authority and the Northeastern Science Foundation (Hereafter the "Sponsors"). The opinions expressed in this report do not necessarily reflect those of the Sponsors or the State of New York, and reference to any specific product, service process, or method does not constitute an implied or expressed recommendation or endorsement of it. Further, the Sponsors and the State of new York make no warranties or representations, expressed or implied, as to the fitness for particular purpose or merchantability of any product, apparatus, or service, or the usefulness, completeness, or accuracy of any processes, methods or other information contained, described, disclosed, or referred to in this report. The Sponsors, the State of New York and the contractor make no representation that the use of any product, apparatus, process, method or other information will not infringe privately owned rights and will assume no liability for any loss, injury or damage resulting from, or occurring in connection with the use of information contained, described, disclosed, or referred to in this report.

ABSTRACT

PERSPECTIVE RESERVOIR FACIES WITHIN THE BEEKMANTOWN GROUP OF EASTERN NEW YORK STATE

Fracture information was collected from a series of cores taken from the shallow-water Beekmantown Group (Sauk Sequence) carbonates from both the Mohawk River and Champlain Valleys. Fracture information of interest included type of fracture, fracture spacing and the spatial relationship that the fractures have with the normal faults that bisect both valleys.

The majority of the fractures found were extension (mode I) fractures. This is consistent with the tectonic forces that affected the area during the Taconic orogeny. During this time, upwarping due to the cratonward migration of a peripheral bulge resulted in extension in the upper portion of the lithosphere. A more substantial cause of extension in the upper lithosphere was the bending of the plate as it entered the subduction zone beneath the Taconic allochthon. Cores that did not intersect fault zones contained mostly extension fractures whereas cores that were very close to, or intersected fault zones, contained both extension and shear fractures, in near equal numbers. Both extension and shear fractures increased in number as the cores approached fault zones. As a result, the average fracture spacing between the extension fractures was found to decrease as the fault zones were approached.

The spatial relationship between fractures and faults in individual cores was determined using chi-square goodness of fit testing. The regional spatial relationship between fractures and faults was determined graphically, by plotting the average number of fractures that occurred in equal length intervals along selected cores against the distance between the core locations and the closest surface exposures of adjacent faults. In both cases, there is a direct relationship between the occurrence of fractures and faults.

It was determined that the fractures found within the Beekmantown Group carbonates are clustered in a series of fracture swarms, or process zones. The fracture swarms preceded faulting by preparing the rock for eventual fault slip. Fracture swarms that did not experience faulting are also found within these rocks. Despite the fact that these fracture swarms did not experience faulting, they still identify areas of stress build up and were produced by the tectonic forces that produced the faulting.

Fractures act as conduits for meteoric water, hydrothermal fluids, natural gas and oil. During the Post Sauk period of subaerial exposure, meteoric water flowed through the Beekmantown Group formations forming karst features by dissolving both carbonate rocks and evaporite deposits. The highest porosity will be found in the rocks within and surrounding the fracture swarms and in the rock that is just beneath the unconformity surface. This is due to the fact that these rock surfaces were the first surfaces that the meteoric water was in contact with, when the meteoric water was in a state of undersaturation. The increased matrix porosity and enlarged preexisting fractures greatly increased the quality of the reservoir rock.

Key Words: Taconic Orogeny, Beekmantown Group, fractures, reservoir, karst

ACKNOWLEDGMENTS

I would like to thank Richard Nyahay and the geology staff at the New York State Museum for allowing me access to the core samples; John Martin and the New York State Energy Research Development Authority (NYSERDA) for funding; the Northeast Science Foundation for allowing me to use their laboratory and to Prof. Gerald M. Friedman and Mrs. Friedman for the tremendous amount of support and encouragement that they have given me during the course of this project.

TABLE OF CONTENTS

SUMMARY....1
PREVEOUS STUDIES....2
GEOLOGIC SETTING....9
LITHOLOGY....12
PROCEDURES....14
Identification of Fracture Types....14
Fracture Distribution Patterns....16
Fracture Spacing....17
Regional Fracture Patterns....18
RESULTS....19
Core 74-NY-11....19
Core 75-NY-2....37
Core 75-NY-14....49
Core 74-NY-10....62
Core 74-NY-6....73
Core 74-NY-7....90
Core 74-NY-13....101
Core 74-NY-9....111
Imperial Paper Co. core....118
Comstock core....132
Beekmantown core....139
Localized Changes in Fracture Density....153
Regional Changes in Fracture Density....160
Differences between Shear and Extension Fracture Distribution Patterns....164
Fracture Spacing Comparisons between Surface Fractures and Subsurface Fractures....166
DISCUSSION....170
Fracture controls....170
Fracture and Fault Development within Eastern New York State....178
Strike Slip Analog....181
Porosity and Permeability within Fracture Zones....183
Error Analysis....200
Fault process zone – Fracture Intensification Domain comparison....204
CONCLUSION....208
REFERENCES....210

TABLES

Table — Page

1. Core 74-NY-11. Chi-square goodness of fit results for the distribution of all the fractures on this core 23
2. Core 74-NY-11. Chi-square goodness of fit results for the distribution of fractures with common dip angles 27
3. Core 74-NY-11. Chi-square goodness of fit results for the distribution of fractures with 60° and 90° dip angles 30
4. Core 74-NY-11. The average fracture spacing for the 90° dipping fractures 32
5. Core 75-NY-2. Chi-square goodness of fit results for the distribution of all the fractures on this core 40
6. Core 75-NY-2. The average fracture spacing for the 90° dipping fractures 45
7. Core 75-NY-14. Chi-square goodness of fit results for the distribution of all the fractures on this core 53
8. Core 75-NY-14. Chi-square goodness of fit results for the distribution of fractures with common dip angles 55
9. Core 75-NY-14. Chi-square goodness of fit results for the distribution of all the shear fractures on the core 57
10. Core 75-NY-14. The average fracture spacing for the 90° dipping fractures 59
11. Core 74-NY-10. Chi-square goodness of fit results for the distribution of all the fractures on this core 64
12. Core 74-NY-10. Chi-square goodness of fit results for the distribution of fractures with common dip angles 67
13. Core 74-NY-10. The average fracture spacing for the 90° dipping fractures 70
14. Core 74-NY-6. Chi-square goodness of fit results for the distribution of all the fractures on this core 76
15. Core 74-NY-6. Chi-square goodness of fit results for the distribution of fractures with 90° and 60° dip angles 79
16. Core 74-NY-6. The average fracture spacing for the 90° dipping fractures 80
17. Core 74-NY-7. The average fracture spacing for the 90° dipping fractures 98
18. Core 74-NY-13. Chi-square goodness of fit results for the distribution of all the fractures on this core 104
19. Core 74-NY-13. Chi-square goodness of fit results for the distribution of fractures with 60° and 75° dip angles 107
20. Core 74-NY-13. The average fracture spacing for the 90° dipping fractures 108

21. Core 74-NY-9. Chi-square goodness of fit results for the distribution of all the fractures on this core.....113
22. Core 74-NY-9. Chi-square goodness of fit results for the distribution of fractures with 90° and 60° dip angles.....116
23. Core 74-NY-9. The average fracture spacing for the 90° dipping fractures.....119
24. Imperial Paper Company Core. Chi-square goodness of fit results for the distribution of all the fractures on this core.....125
25. Imperial Paper Company Core. Chi-square goodness of fit results for the distribution of fractures with 90° and 60° dip angles.....127
26. Imperial Paper Company Core. The average fracture spacing for the 90° dipping fractures.....129
27. Comstock Core. The average fracture spacing for the 90° dipping fractures.....136
28. Beekmantown Core. Chi-square goodness of fit results for the distribution of all the fractures on this core.....142
29. Beekmantown Core. Chi-square goodness of fit results for the distribution of fractures with common dip angles.....147
30. A comparison between the widths of the fracture zones in footwall blocks and hanging wall blocks.....157
31. A comparison between the widths of three fault process zones.....159
32. A comparison between the fracture types from cores that intersected fault zones versus cores that were taken greater distances from fault zones.....165
33. Surface fracture measurements from outcrops in the Mohawk River Valley.....168
34. The depth where the greatest number of extension fractures, per interval of core, was found.....176
35. Core 74-NY-10. Fracture porosity for the vertical extension fractures.....189
36. Core 74-NY-10. The extension fracture and matrix porosity volumes.....192
37. Core 74-NY-11. Fracture porosity for the vertical extension fractures.....194
38. Core 74-NY-11. The extension fracture and matrix porosity volumes.....197

FIGURES

Figure Page

1. The locations of the north-northeast striking normal faults that bisect the Mohawk River Valley....4
2. A generalized map of the carbonate shelf, foredeep and overthrust sheets that occupied the area that is now eastern New York State....5
3. A diagrammatic representation of the behavior of the lithosphere at a subduction zone....7
4. Extension fractures interpreted to be neotectonic joints in Devonian strata south of Syracuse, New York....8
5. The regional stratigraphy of the Sauk Sequence from the central Mohawk Valley to the southern Champlain Valley, New York State....10
6. The core locations in the Mohawk Valley, New York....15
7. The locations of cores 74-NY-9, 74-NY-10 and 74-NY-11....20
8. Core 74-NY-11. The total number of fractures per 12-meter interval of core....21
9. Carbonate rubble from core 74-NY-11....22
10. Core 74-NY-11. The number of 30°, 40°, 60° and 90° dipping fractures per 12-meter interval of core....25
11. Core 74-NY-11. The number of 65°, 70°, 75° and 80° dipping fractures per 12-meter interval of core....26
12. Core 74-NY-11. The increase in the combined number of 60° and 90° dipping fractures with depth....29
13. Core 74-NY-11. The change in the average fracture spacing with depth....33
14. Core 74-NY-11. The change in the average fracture spacing with depth....34
15. The geometric relationship between the core, the fault and the breccia zone surrounding the fault....36
16. The location of core 75-NY-2....38
17. Core 75-NY-2. The total number of fractures per 12-meter interval of core....39
18. Core 75-NY-2. The number of 90° dipping fractures per 12-meter interval of core....42
19. Core 75-NY-2. The number of 50°, 60°, 70°, and 75° dipping fractures per 12-meter interval of core....43
20. Core 75-NY-2. The change in the average fracture spacing for each interval, 90° dipping fractures....46

21. Core 75-NY-2. The change in the average fracture spacing for the 90° dipping fractures 47
22. The polynomial curve modeling the rate of change in the average fracture spacing for cores 74-NY-11 and 75-NY-2 48
23. The location of core 75-NY-14 50
24. Core 75-NY-14. The total number of fractures per 12-meter interval 52
25. Core 75-NY-14. The number of 45°, 55°, 60° and 90° dipping fractures per 12-meter interval of core 54
26. Core 75-NY-14. The number of shear fractures and the number of extension fractures per 12-meter interval 56
27. Core 75-NY-14. The change in the average fracture spacing for each interval for the extension fractures 60
28. Core 75-NY-14. The change in the average fracture spacing for the extension fractures with depth 61
29. The polynomial curves modeling the rate of change of the average fracture spacing for cores 74-NY-11, 75-NY-2 and 75-NY-14 63
30. Core 74-NY-10. The total number of fractures per 12-meter interval 65
31. Core 74-NY-10. The number of 70°, 75° and 90° dipping fractures per 24-meter interval of core 68
32. Core 74-NY-10. The change in average fracture spacing for each interval, with depth, for the extension fractures 71
33. Core 74-NY-10. The change in the average fracture spacing, with depth, for the extension fractures 72
34. The location of core 74-NY-6. 74
35. Core 74-NY-6. The total number of fractures per 12-meter interval of core 75
36. Core 74-NY-6. The number of 60°, 70° and 90° dipping fractures per 12-meter interval 78
37. Core 74-NY-6. The change in average fracture spacing for each interval, with depth, for the extension fractures 81
38. Core 74-NY-6. The change in average fracture spacing, with depth, for the extension fractures 83
39. Core 74-NY-6. The change in average fracture spacing, with depth, for the extension fractures 84
40. The changes in fracture frequency values along a line perpendicular to a fault in the Pretoria series quartzite, South Africa 85
41. The joint frequency associated with a fault that passed through sandstone in the Invincible colliery, New South Wales, Australia 86

42. Fracture frequency wave....88
43. The fracture frequency waves along three horizontal profiles....89
44. The fracture spacing curves for core 74-NY-10 and core 74-NY-6....91
45. The location of core 74-NY-7....92
46. Core 74-NY-7. The total number of fractures per 12-meter interval of core....94
47. Core 74-NY-7. Vuggy porosity....95
48. Core 74-NY-7. The number of 45°, 60°, 70° and 90° dipping fractures per 12-meter interval of core....96
49. Core 74-NY-7. The change in average fracture spacing for each interval, with depth, for the extension fractures....99
50. Core 74-NY-7. The change in average fracture spacing, with depth, for the extension fractures....100
51. The location of core 74-NY-13....102
52. Core 74-NY-13. The total number of fractures per 24-meter interval....103
53. Core 74-NY-13. The number of 60°, 75° and 90° dipping fractures per 12-meter interval of core....105
54. Core 74-NY-13. The change in average fracture spacing for each interval, with depth, for the extension fractures....109
55. Core 74-NY-13. The change in average fracture spacing, with depth, for the extension fractures....110
56. Core 74-NY-9. The total number of fractures per 12-meter interval of core....112
57. Core 74-NY-9. The number of 60° and 90° dipping fractures per 12-meter interval of core....115
58. Core 74-NY-9. The number of 60° and 90° dipping fractures per 36-meter interval of core....117
59. Core 74-NY-9. The change in average fracture spacing for each interval, with depth, for the extension fractures....120
60. Core 74-NY-9. The change in average fracture spacing with depth for the extension fractures....121
61. The location of the Imperial Paper Co. core....122
62. Imperial Paper Co. Core. The total number of fractures per 12-meter interval of core....124
63. Imperial Paper Company Core. The number of 90° and 60° dipping fractures per 12-meter interval of core....126
64. Imperial Paper Company Core. The change in average fracture spacing for each interval....130

65. Imperial Paper Company Core. The change in average fracture spacing with depth....131
66. The location where the DOT Comstock core was taken....133
67. Comstock Core. The total number of fractures per 12-meter interval of core....134
68. Comstock Core. The change in average fracture spacing for each interval....137
69. Comstock Core. The change in average fracture spacing with depth....138
70. The location of the Beekmantown core....140
71. Beekmantown core. The total number of fractures, per 12-meter interval of core....141
72. The Beekmantown core. The number of 90°, 70°-75°, 55°-60°, 45° and 30°-35° dipping fractures, per 12-meter interval of core....144
73. The Beekmantown Core. Two parallel 75° dipping fractures orientated approximately 90° from a vertical fracture....145
74. The Beekmantown Core. A small, 35° dipping reverse fault at a depth of 45 meters....146
75. Dissolution enlarged fractures at the Beekmantown core location....149
76. A type I fracture pattern....150
77. A type II fracture pattern....151
78. A diagrammatic representation of the fracture gradient zones that parallel the plane of the fault....154
79. The geometric relationship between the core interval length and the fracture gradient zones....155
80. The decrease in the average number of extension fractures per 12 meter interval of core....161
81. The increase in the fracture spacing between the extension fractures with increasing distance from the nearest fault....163
82. Map of the study area showing the locations of the outcrops where fractures measurements were taken....167
83. Beekmantown core. An extension fracture passing through a parasequence boundary....172
84. Beekmantown core. A comparison between the change in the number of fractures (per 24 meter interval) with depth....173
85. Vertical fracture set found in association with a normal fault in chalk in the Beer Sheva Syncline, Israel....177
86. The first stage of fracture development....179
87. The second stage of fracture development....180

88. The third stage of fracture development.....182
89. Diagrammatic representation of joint and fault development within the Sella Group dolomites of Northern Italy.....184
90. The principal stress axes corresponding to (A) normal faults and (B) strike slip faults.....185
91. Paleohighs from the Bakersville natural gas field.....187
92. Core 74-NY-10. The change in fracture porosity and fracture spacing with depth.....190
93. Core 74-NY-11. The change in fracture porosity and fracture spacing with depth.....195
94. Core 74-NY-9. A stylolite at a depth of 311 meters.....198
95. North-northwest striking Fracture Intensification Domain on the south western shore of Seneca Lake, New York.....205

SUMMARY

A subsurface study within the Mohawk River and Champlain Valleys was conducted using fracture distribution and fracture spacing patterns that were found in core samples. A subsurface study was performed since surface exposures within the study area are at a minimum due to soil cover. Using data collected from the subsurface is also beneficial since surface exposures are often in a state of fracture saturation from a variety sources, such as unloading. Therefore, a subsurface study will minimize problems associated with overprinting by a regional joint system when attempting to link the origin of the fractures with orogenic events.

The purpose of this study was to obtain a better understanding of the type, origin and development of the fractures within the subsurface Beekmantown Group carbonates of eastern and east central New York State. This knowledge was then used to integrate fracture development within the Beekmantown carbonates with the development of the normal fault system that formed in eastern New York State during the Taconic Orogeny.

Fractures and faults act as conduits for meteoric water flow. Secondary porosity, due to the dissolution of bedrock by meteoric water flow, has long been known to enhance the quality of reservoirs that lacks substantial primary porosity, or adds to the value of a reservoir by adding to the already existing primary porosity found within the rock. Fractures also add to the porosity of the rock and, in some cases, accounts for a significant amount of the porosity within the rock. For these reasons, it is expected that the highest porosity will be found near and within the fracture swarms that are found in association with faults.

Fractures and fault networks also act as conduits for the flow of natural gas. The permeability created by the fault and fracture networks allows for the migration and concentration of substantial amounts of natural gas into the porous reservoir. Just as important, the permeability allows for the economical extraction of the natural gas.

A clear understanding of the origin and development of fractures is vital, so that the areas most likely to have the most productive reservoirs can be identified.

PREVIOUS STUDIES

Geraghty and Isachsen (1981) reported their findings from a two-year surface study of the McGregor-Saratoga-Ballston Lake Fault system in eastern New York State. This particular fault system trends north to north-north-east from Altamont, N.Y to Glens Falls, N.Y. The steeply dipping fault is 85 km long and is part of a series of similar high angle faults that extend northward into Canada. The eastern block is the downthrown block. The study divided the fault system into 25 sections. Surface fractures along these sections were studied to try to gain evidence as to the relative movement of the fault. Most fractures were steeply dipping. Only 39, of 920 measured fractures, had dips less than 45°. From the sections where surface fractures could be measured, the strike of the fractures along the fault zone showed good correlation to the strike of the fault along 14 sections and no clear correlation along only 2 sections. It was noted in the report that although there are regional fractures within the study area, no attempt was made to separate them from the fault induced fracturing. The authors of the study suggested that such a study would be useful in eliminating background noise. It was also noted that no slickensided fractures were found.

Geraghty and Isachsen (1981) also reported on the fault movement history of the fault system. They indicated that the earliest movement was during the Late Proterozoic, when block faulting affected the area. Periods of extension may have occurred during the Early Ordovician, Late Medial Ordovician and after the Taconic, Acadian and Alleghany orogenies. Reactivation of the faults may also have occurred during the Triassic and Jurassic, when rifting occurred in eastern North America during the breakup of Pangea. They also felt that the most recent fault movement was during the Neogene and is related to the uplifting of the Adirondack dome. Where it could be measured in surface exposure, the width of the fault zone was reported to be 10 meters or less. As part of this study, a 175 meter deep core was examined that was drilled southwest of Saratoga Springs, N. Y. This core was taken 0.7 km from the trace of the Saratoga fault. The core did not penetrate the fault and only a single localized fracture zone 0.5 meters thick was intersected. This subsurface data supports the surface data, which indicated that the width of the fracture zone surrounding the fault is very narrow.

Bradley and Kidd (1991) investigated the cause of the faulting in the Mohawk River and Champlain Valleys of New York State (Figure 1). The study area of Bradley and Kidd (1991) and the study area of this report overlap. The predominant strike of these faults is north to north-northeast and parallel to the Taconic orogenic front. The majority of these faults dip east, toward the orogenic front, with dip angles that average approximately 60° (Figure 2). Westward dipping faults are found in the Mohawk River Valley, but are much less numerous and have smaller displacements than their eastward dipping counterparts. The major faults are spaced about 10 to 20 km apart. The Champlain Valley has fewer westward dipping faults than the Mohawk River Valley. The displacement of the faults increases to the east, as the Taconic orogenic front is approached.

Major faults, between 100 and 200 km from the leading edge of the thrust sheets, have vertical displacements of up to a few tens of meters. Major faults, less than 100 km from the leading edge of the thrust sheets, have vertical displacements that increase to 100 to 400 meters. Beneath the thrust sheets, the Taconic Allochthon, the vertical displacement of the major faults increases even more due to loading. An example of this increased vertical displacement is seen in the log of the Finnegan boring in southern Washington Co., N.Y., which is just east of the leading edge of the thrust sheets (Guo, Sanders and Friedman, 1990). The bottom of the Taconic Allochthon was encountered at a depth of 842 meters (2764 ft.). It is not known whether this amount of vertical displacement is due to displacement along one or several faults, but it does indicate that the total vertical displacement due to faulting increases abruptly beneath the thrust sheets. The combination of having a majority of the faults dip to the east and an increase in fault displacement to the east is in direct response to loading by the thrust sheets.

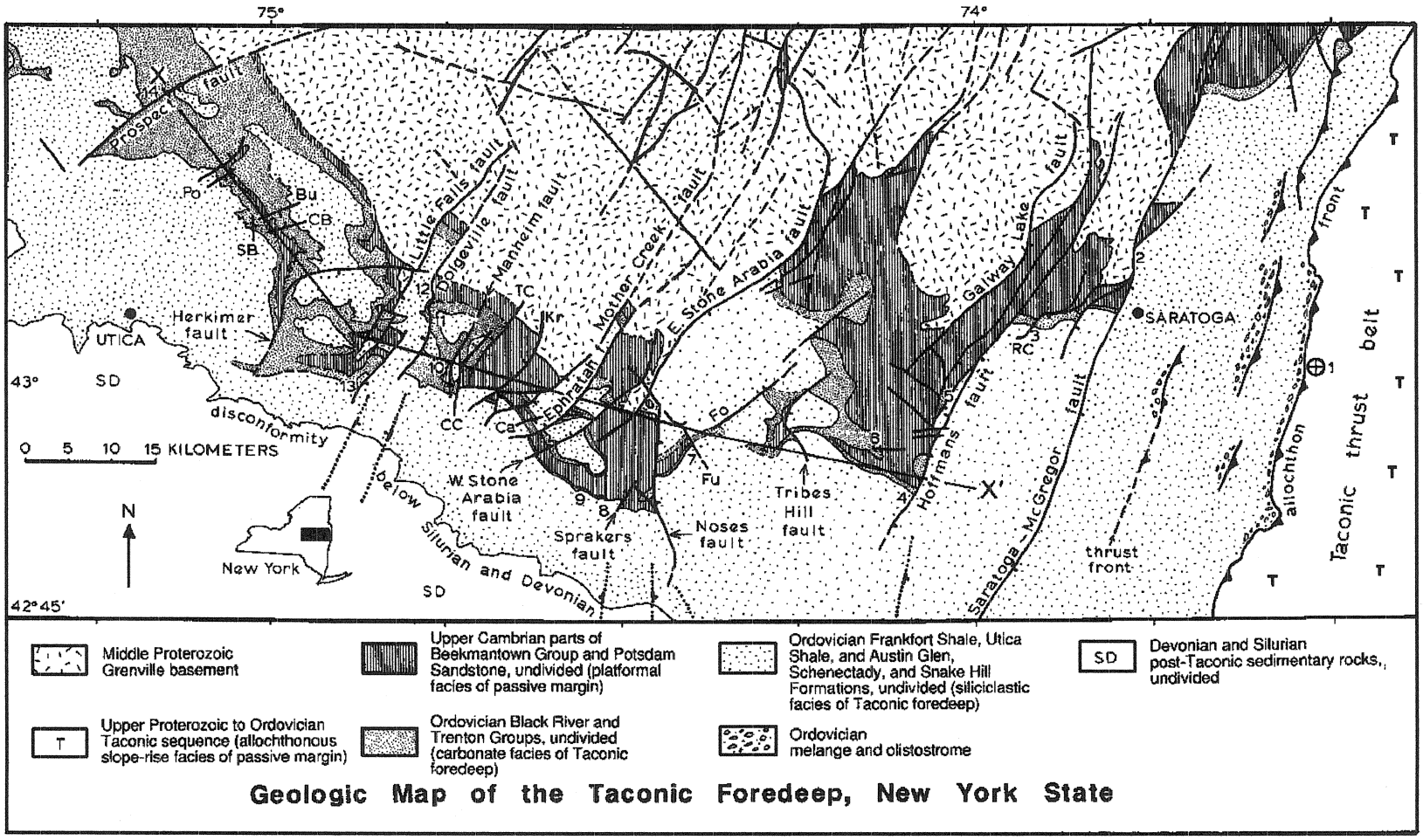

Figure 1. The locations of the north-northeast striking normal faults (black lines) that bisect the Mohawk River Valley.

Source. Bradley and Kidd, 1991.

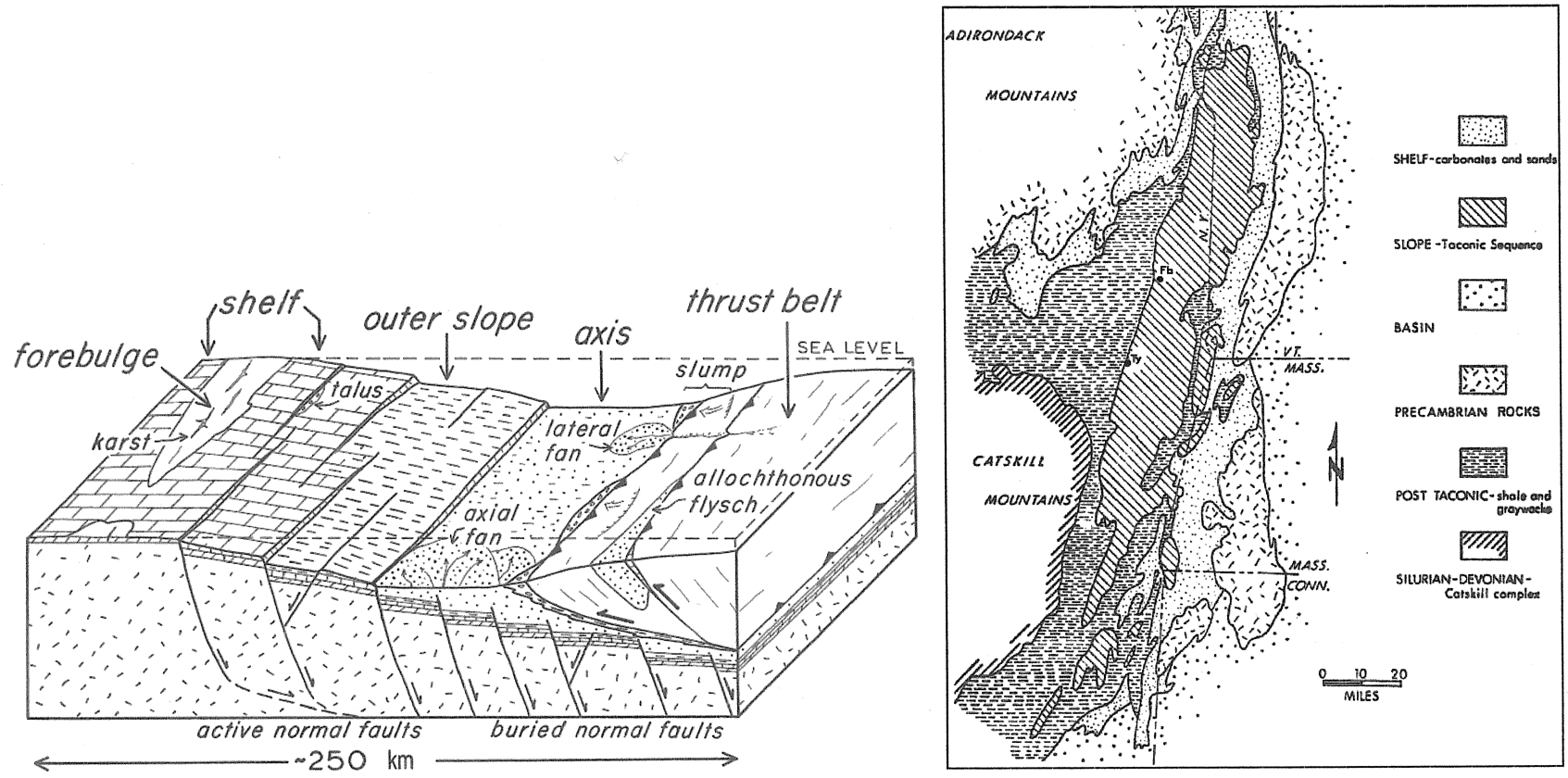

Figure 2. A generalized map of the carbonate shelf, foredeep and overthrust belts that occupied the area that is now eastern New York State during the Taconic Orogeny (A) and the area as it appears today (B). The Taconic Allochthon (Sequence) is made up of the Taconic thrust sheets.

Source. Bradley and Kidd, 1991 (A) and Keith and Friedman (1977) (B).

Bradley and Kidd (1991) indicated that the majority of the faulting within this area occurred during the Taconic Orogeny, under conditions that have been described as flexural extension. At the subduction zone, the continental plate was forced to bend as it dipped beneath the overriding Taconic Allochthon, resulting in extension in the outer crust and compression in the lower crust (Figure 3). The bending of the lithosphere beyond its elastic limit (on the convex side of the bend) is credited as the mechanism by which the normal faults formed. This resulted in a systematic series of gently rotated normal fault blocks that die out at a depth of about 17.5 km. Therefore, the depth separating brittle from ductile behavior has been estimated to be at a depth of between 15 and 20 km. Although Bradley and Kidd (1991) addressed the development of the normal faults that bisect the study area, the paper did not attempt address the development of fractures.

Hancock and Engelder (1989) documented the presence of neotectonic joints south of Syracuse, New York (Figure 4). This region is just south and to the west of the study area of this report. These joints were found in Devonian rocks that are part of the Appalachian Plateau. Neotectonic joints are the most recent joint systems to form in an area that has been subjected to uplift and erosion. Neotectonic joints form within the upper 0.5 km of the crust where the minimum effective stress (σ_3') is tensile. Uplift and the removal of overburden are the mechanisms that produce the tensile stress, which produce the joints. Since they are the most recently formed joints, they form approximately parallel to the current maximum horizontal stress direction (N 75° E to N 90° E). Neotectonic joints usually form as parallel to subparallel vertical sets (+/- 10° about the mean strike orientation) and are interpreted to be extension fractures perpendicular to the minimum effective stress direction. Joint spacing tends to be wider in massive rocks than in thinly bedded rocks and is usually evenly spaced. Less commonly there are steeply dipping conjugate striking joints parallel to the strike of the vertical joints. The dihedral angle separating the conjugate joints averages between 10° and 45°. Joints with a dihedral angle in this range are considered to be transitional between extension and shear fractures and are classified as hybrid- shear or hybrid extension fractures.

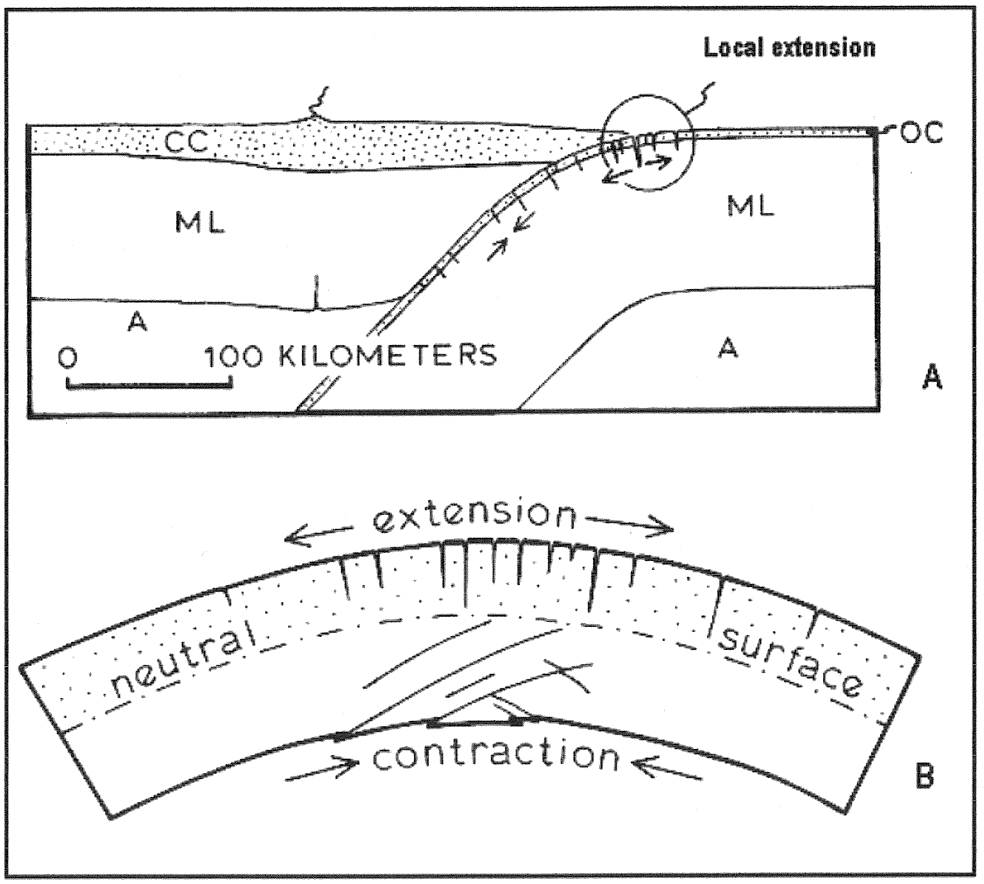

Figure 3. A diagrammatic representation of the behavior of the lithosphere at a subduction zone. CC is the continental crust; OC is the ocean crust; ML is the mantle layer and A is the asthenosphere. (A) The greatest amount of extensional stress occurs where bending is the greatest. (B) The zones of extension and contraction are separated by a neutral surface.

Source. Bradley and Kidd, 1991.

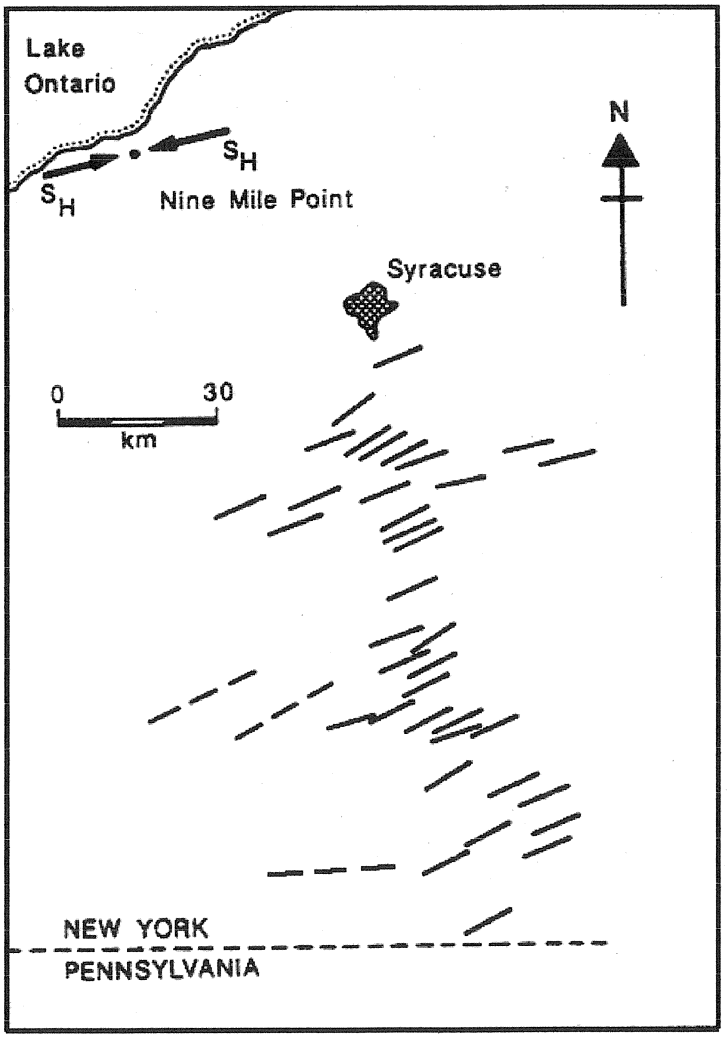

Figure 4. Extension fractures interpreted to be neotectonic joints in Devonian strata south of Syracuse, New York. The strike of the joints is subparallel to the present orientation of the maximum principal stress direction.

Source. Hancock and Engelder (1989).

GEOLOGIC SETTING

The sediments that became the carbonate rocks of the Beekmantown Group (Sauk Sequence) were deposited on the bottom of the continental shelf of the Iapetus Ocean during the Late Cambrian and Early Ordovician (Dolfi and Friedman, 1983; Bradley and Kidd, 1991; Dykstra and Longman, 1995; Condie, 1997; Phillips and Friedman 2001). The Iapetus Ocean formed as rifting separated Laurentia from Baltica during the breakup of the Proterozoic Supercontinent, Rodinia, between 750 and 600 Ma. This rifting produced normal faults in the Precambrian crust in some areas and resulted in the widening of the Iapetus Sea. The base unit of the Sauk sequence is the Cambrian Potsdam sandstone, which was deposited on eroded Precambrian metamorphics and on top of the fault blocks. Dykstra and Longman (1995) report that thickness variations in the Potsdam are seen in seismic lines in the Quebec lowlands. This indicates that some normal faults may have been active when the Potsdam sandstone was deposited. The sands were produced by the erosion of the Laurentian highlands, to the north. As the transgressing sea moved inland, a series of carbonate formations were deposited on the Potsdam sandstone. These formations include the Little Falls and Tribes Hill formations in the Mohawk Valley, the Galway, Hoyt and Gailor in the Saratoga Springs area and the Theresa (Galway) and the Cutting, Spellman, Fort Cassin and Providence Island formations in the Champlain Valley (Figure 5).

The proximity of the Laurentian continental shelf to the paleoequator during the Early Ordovician, approximately 20° south latitude, combined with the shallow water marine environment, was responsible for the formation of extensive amounts of carbonate sediments (Rubin and Friedman, 1977; Conway and Friedman, 1984; Friedman, 1994; Friedman, Kolkas and Ching, 1999; Kolkas and Friedman 1999).

Periods of emergence in this hot, arid climate favored the development of sabkhas (Friedman, 1980; Friedman and Sanders, 1967). The combined conditions of a hot, arid climate, extremely shallow water and intermittent exposure created excessive evaporation. High evaporation rates in turn produced evaporite minerals and hypersaline brines, which were largely responsible for the production of dolostone, both at the surface and in the subsurface in this area.

After deposition and dolomitization, vast areas of the continental shelf became subaerially exposed during the initial stages of the Taconic Orogeny as a peripheral bulge progressively moved inland, in advance of one, or several island arcs (Dykstra and Longman, 1995; Jacobi, 1981; Bradley and Kidd, 1991; Knight, James and Lane, 1991; Dix, Robinson and McGregor, 1998). The passage of the peripheral bulge resulted in uplift as high as 100 meters, or more, above sea level. This resulted in erosion and the formation of a karst topography and possible reactivation of some of the Precambrian normal faults. This unconformity, known as the Knox unconformity in the Appalachians and the St.

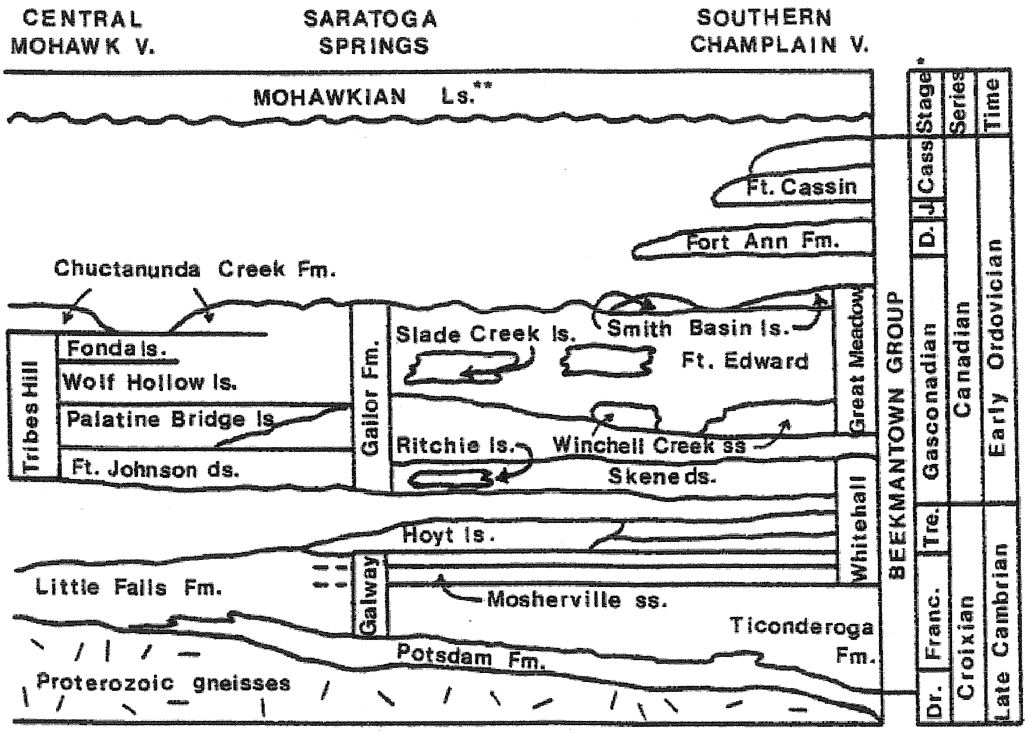

Figure 5. The regional stratigraphy of the Sauk Sequence from the central Mohawk River Valley to the Southern Champlain Valley, New York State. The Mohawkian limestones are part of the Tippecanoe Sequence.

Source. Zagorski, 1981.

George unconformity in Newfoundland, records the change from a passive to a convergent plate boundary. The time that this unconformity lasted is estimated to be in the range of 1 to 3 million years. As the unconformity surface submerged into the foredeep basin, which formed as a result of downward loading from the approaching island arc, the shallow water Black River limestone and overlying deeper water Trenton limestone formations were deposited.

The Taconic orogeny, of the mid to late Ordovician, was the end result of the collision of an island arc, which had formed in the Iapetus Ocean, with Laurentia (Dykstra and Longman, 1995; Bradley and Kidd, 1991; Knight, James and Lane, 1991; Dix, Robinson and McGregor, 1998). The Taconic orogeny pushed a series of thrust sheets, of mostly deeper water deposits, onto the carbonate shelf (Figure 2). These thrust sheets are preserved as the Taconic Allochthon. The roughly north-south trending normal faults that are found throughout the Mohawk and Champlain Valleys were formed during this time under conditions of flexural extension caused by crustal bending of the subducting plate (Bradley and Kidd, 1991). A restricted basin formed between the thrust front and the shoreline. This was the depositional environment of the organic rich Utica shale. Above the Utica shale are the turbidite greywackes and shales of the Schenectady Formation and the Frankfort Shale, which were deposited as submarine fan deposits. Covering all of these formations is the Queenston clastic wedge, which formed from the erosional remnants of the Taconic Mountains.

Northeastern North America was subjected to the tectonic forces of the Acadian Orogeny during the Devonian period and the Alleghany Orogeny during the Mississippian, Pennsylvanian and Permian Periods. The final major tectonic event to affect the area was the breakup of Pangea during the Mesozoic. The break up of Pangea started during the Triassic period, which resulted in tensional rifting and block faulting in northeastern North America.

LITHOLOGY

The lithology of the Sauk Sequence carbonates is predominantly dolostone, with both limestone and sandstone interbedded within the various dolostone formations (Figure 5). Zenger (1981) subdivided the Little Falls into four subdivisions, A, B, C and D near the type locality town of Little Falls, New York. The lowest unit, unit A is approximately 30 meters thick. This unit has a one meter thick basal layer of coarse sandstone and pebble conglomerate. The remainder of the unit is a low quartz, medium to coarse crystalline dolostone. Laminae and interclasts are common. The next layer, unit B, is a quartzose dolostone approximately 60 meters thick. Unit B is composed primarily of fine to medium crystalline dolostone with interbedded sandstone. Vuggy intervals are very prominent in this layer. Algal stromatolites are distributed throughout this unit. Unit C is approximately 12 to 18 meters thick and is made up of medium to coarse crystalline, low quartz to quartzose dolostone. Vuggy intervals are very prominent in this unit as well. Unit D is approximately 10 meters thick. This unit is made up of very fine to fine crystalline, low quartz dolostone. Edgewise breccia is present near the contact with the overlying Tribes Hill formation.

The Tribes Hill Formation overlies the Little Falls Formation (Phillips and Friedman, 2001). The lowest member, the Fort Johnson member, is the facies equivalent of the Gailor Formation to the east. It is a dolomitic limestone to calcitic dolostone and feldspathic dolostone. The Palatine Bridge member is a thinly bedded quartzite limestone with interbedded shales. The Wolf Hollow member is a massive, dolomitic limestone and mottled dolostone. The Fonda member is a fossiliferous, coarse limestone with flat pebble conglomerates, dolostones, oolitic and skeletal grainstones and packstones.

Mazzullo, et al. (1978) reported that the Galway Formation is 47.6 meters thick in the Saratoga Springs area. This formation is made up of a cherty, nonfossiliferous, medium to thick bedded, medium to coarsely crystalline, sandy dolostone. The sand content decreases toward the top of the formation. Vugs, commonly filled with sparry cement, are abundant near the top of the unit. The one meter thick Mosherville sandstone occurs 5.5 meters from the top of the Galway. The Potsdam Sandstone lies beneath the Galway in this area.

The Hoyt Formation is approximately 12 meters thick and overlies the Galway Formation in the Saratoga Springs area (Mazzullo et al., 1978; Phillips and Friedman, 2001). It is composed of fine to coarse textured limestone. Columnar and domal stromatolites are common in this unit.

The Gailor Formation is approximately 70 meters thick in the Saratoga Springs – Schenectady area (Conway and Friedman, 1984; Mazzullo et al., 1978; Phillips and Friedman, 2001). It is generally a thick to medium bedded, fine to medium bedded, somewhat cherty dolostone. There are two limestone

members within this unit, the Ritchie Member and the Slade Creek Member. Local dissolution collapse structures can be found in the upper part of the Gailor. Conway and Friedman (1984) have indicated that there is a great deal of variability within the Gailor Formation. This indicates there were fairly rapid changes in depositional environments in this area. An example of this variability is the prominence of the Hoyt, Ritchie and Slade Creek limestones in the area studied by Mazzullo, et al. (1978), but not in the area studied by Conway and Friedman (1984). The two areas are separated by a difference of about 20 miles.

The similar lithology of the bedrock from which the cores were taken eliminated the possibility that lithology was a factor controlling the fracture pattern within the bedrock.

PROCEDURES

Cores from Montgomery, Fulton, Herkimer, Schoharie, Saratoga, Clinton, Essex, Jefferson, Warren and Washington Counties, were examined to determine fracture type and fracture spacing (Figure 6). Most of these cores are housed in the New York State Museum's core repository. Two cores were drilled specifically for this study. One was from an abandoned rock quarry in the town of Willsboro, New York. The other was from the town of Beekmantown, New York.

Fractures of a size visible to the naked eye were used for this study. Fracture type, length, dip angle, aperture size and location along each core was recorded. Fracture distribution patterns and fracture spacing patterns were also determined. The details for each of these methods are outlined below.

IDENTIFICATION OF FRACTURE TYPES

Both shear and extension fractures are typically found with faults, so it was expected that both would be found on the cores (Nelson, 2001; Nelson, 2004; Stearns and Friedman, 1972). Shear fractures, by definition, have a sense of movement parallel to the fracture plane and are typically identified by an offset in bedding, slickensides or gouge. It is important to note that shear fractures may not show visible offset. This is especially true for shear fractures that are found associated with folding. Extension fractures are defined by a sense of movement perpendicular to and away from the fracture plane and are typically identified by plumose marking or a lack of offset on either side of the fracture plane. Plumose patterns mark the propagation of the fracture front. It should be noted that any movement parallel to the fracture plane can obliterate the plumose patterns, as can mineral growth or weathering.

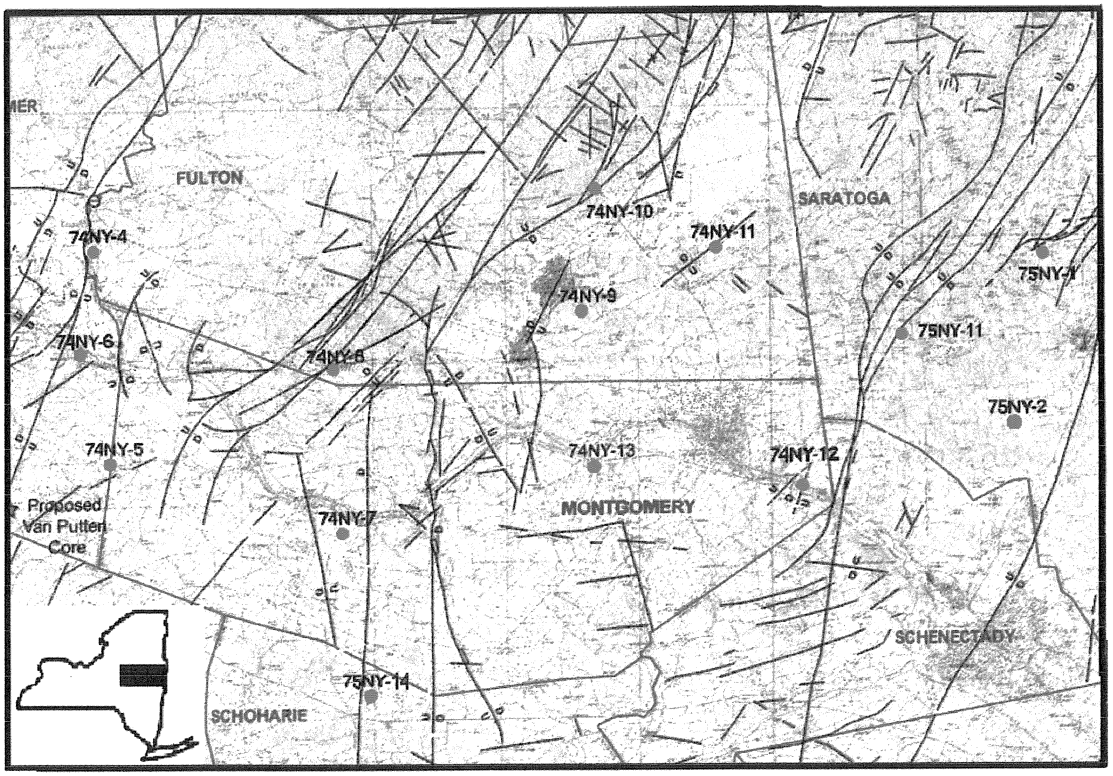

Figure 6. The core locations in the Mohawk River Valley, New York. The cores are identified by numerical codes (74-NY-9, 74-NY-10 and 74-NY-11) and red circles. The black lines are the north-northeast striking faults, U and D indicates upthrown or downthrown blocks, respectively. The blue lines are the county borders.

Source. New York State Museum.

If surface markings, such as plumose patterns or striations, were absent or if there was no measurable offset on either side of the fault plane, the geometric relationship between the fractures was used to make the final determination as to the types of fractures present (shear or extension fracture). Shear fractures usually form conjugate pairs at acute angles to the greatest principal stress axis and parallel to the intermediate stress axis (Price, 1966). Extension fractures bisect the conjugate angle between the shear fracture planes and are parallel to the greatest and intermediate principal stress axes and perpendicular to the least principal stress axis.

Core alignment was used to estimate the orientation of the fractures relative to each other and, along with the dip of the fractures, to group the fractures into sets.

FRACTURE DISTRIBUTION PATTERNS

The numbers of shear and extension fractures, per 12 meter interval of core, were plotted against depth to determine if there were any fracture distribution patterns. Once plotted, chi-square goodness of fit testing was used to determine if the distribution of fractures was dependent or independent of position along the length of the core. Of particular interest, were the fracture distribution patterns in the bedrock surrounding faults. For all the cores, the null hypothesis was: there is no relationship between the positions of the fractures along the length of the core with respect to an adjacent fault. In other words, there should ideally be an equal number of fractures in each of the intervals, if the fractures developed independently from the faults. If the distribution of fractures deviated significantly from the null hypothesis, it indicated that there was a statistically significant fracture gradient along the core, using the chosen core interval length. A statistically significant fracture gradient indicates that there was a stress gradient within the bedrock that was directly related to the faults.

The initial interval length used was 12 meters. If the distribution of fractures using this interval length was not found to be significantly different than the null hypothesis, the interval length was increased by 12 meter increments until it was. Unless otherwise stated, all analyses were done using core interval lengths that had statistically significant distributions of fractures.

FRACTURE SPACING

Fracture spacing was determined using the average fracture spacing method developed by Narr (1996). This method treats the core as a three dimensional sample of the bedrock from which it was taken and measures both fracture spacing and fracture porosity. It requires that fractures occur in arrays of parallel fractures that form sets, are perpendicular to bedding and are long relative to the core diameter. Each set must be evaluated separately. This method was ideally suited for the extension fractures found in the study cores, since they fit these requirements. This technique could not be used for the shear fractures, mainly due to the fact that the cores were not orientated at the time of drilling. Without an orientated core, it was impossible to determine which of the conjugate fracture sets the shear fractures should be placed.

Despite the fact that the cores were not orientated at the time of drilling, the strike of the fractures should be parallel to the strike of the faults, since the fractures associated with faults are the result of the same stress field that caused the faulting (Stearns and Friedman, 1972; Nelson, 2001). This will result in fracture strikes that parallel the fault strikes. This has already been shown to be true in the study area. Geraghty and Isachsen (1981) reported that the strike of the fractures adjacent to the McGregor-Saratoga-Ballston fault system had a good correspondence with the strike of the fault trend in 14 out of 16 segments of the fault that were studied. Narr (1996) also indicated that fracture development is in a state of saturation at the surface and fewer fracture sets are typically found with depth. These facts indicate that there is a very high degree of certainty that the strikes of the subsurface fractures are parallel to the strikes of the faults.

Narr (1996) indicated that longer cores provide a better estimation of the average fracture spacing than shorter cores. This presented a potential problem for the use of this method for this study. There was a dramatic increase in the number of fractures found along the cores that approached faults. If excessively long intervals of core were used, the actual changes in fracture spacing as the faults were approached would not be recorded correctly. If too short an interval of core was used, the calculated fracture spacing value may not be accurate. The results of the chi-square goodness of fit testing, outlined above, was used to determine the appropriate core interval length to be used for average fracture spacing calculations. Specifically, core interval lengths that just deviated from the null hypothesis were used as a compromise between an interval length that was long enough, so that the fracture distribution was statistically significant, but short enough that the changes in average fracture spacing could be plotted.

Changes in average fracture spacing with depth were plotted using a polynomial curve. This polynomial curve was then extrapolated to depths that were past the ends of the core. This allowed for the estimation of the fracture spacing where no core was available for testing. Subsurface fracture spacing values, calculated from core samples, will be compared to surface fracture spacing values in order to clarify the source of the subsurface fractures.

REGIONAL FRACTURE PATTERNS

For those cores that showed no fracture gradient, the average number of fractures, per 12 meter interval of core, was plotted against the distance to the nearest fault affecting the area where the core was taken. This was done to determine if there is a regional spatial relationship between the number of fractures that can be found in the bedrock and the distance that the bedrock is located from the faults.

RESULTS

CORE 74-NY-11

CORE LOCATION

Core 74-NY-11 is 120 meters long (129 to 249 meters) and was taken adjacent to the surface exposure of a northwestward dipping normal fault that is part of the graben that holds the Sacandaga Lake to the northeast (Figure 7). The top of the core was taken from the Little Falls Formation. The contact with the Galway Formation is at a depth of approximately 200 meters. There is a thin layer, approximately 10 meters thick, of Potsdam sandstone at the base of the core. The contact with the Precambrian is at a depth of 248 meters.

FRACTURE PATTERN: TOTAL NUMBER OF FRACTURES

Initially, there was a fairly consistent number of fractures in each of the intervals down to a depth of 202 meters, where there was a dramatic increase in the number of fractures (Figure 8). From a depth of 214 to 239 meters, the core was all rubble, so it could not accurately be examined for fractures (Figure 9). In addition to the 26 fractures in the 12-meter interval of core from 202 to 214 meters, there were also three sections of core, each approximately 60 cm long, that were rubble. For an interval length of 12 meters, chi-square testing indicated that the distribution pattern for the total number of fractures was significantly different than if there were an equal number of fractures in each of the intervals (Figure 8 and Table 1).

INTERPRETATION

This core penetrated the hanging wall and the fault zone of the normal fault that is adjacent to the area where the core was drilled. This determination was based on the fact that there was a statistically significant increase in the number of fractures with depth and a rubble zone from 214 to 239 meters. The actual fault plane passed through the rubble zone. This interpretation is reinforced by the fact that the normal fault dips in the direction of the core (Figure 7).

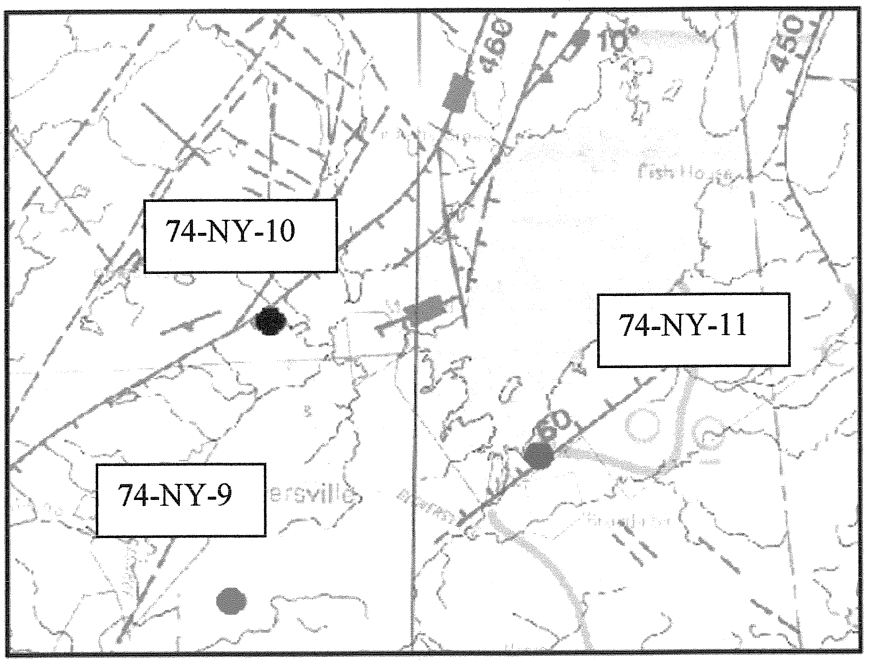

Figure 7. The locations of cores 74-NY-9, 74-NY-10 and 74-NY-11. The Sacandaga Lake is in the center of the map. The circles are the CORE locations. The solid lines are normal faults, hachure marks are on the relatively downthrown side of the faults. Rectangular bar over fault indicates a near vertical normal fault. Fault lines are dashed where inferred. Numbers indicate minimum estimated displacement, in meters. Map width approximately 23 km.

Modified from Isachsen and McKendree, 1977

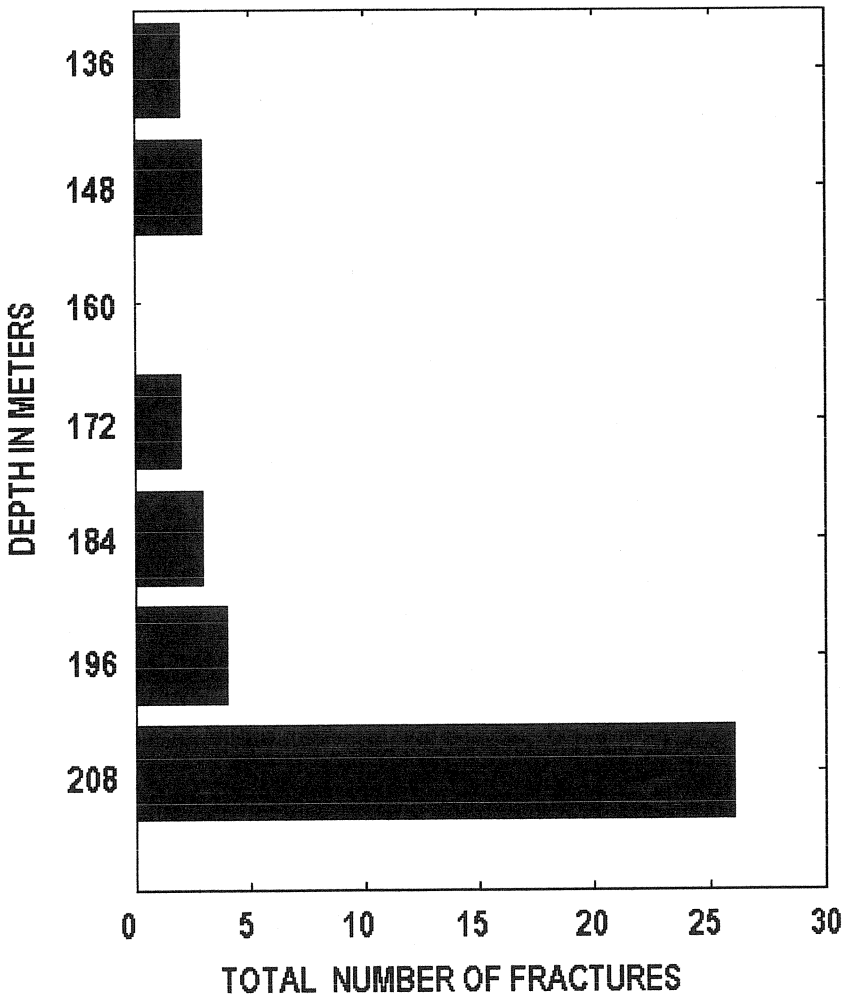

Figure 8. Core 74-NY-11. The total number of fractures per 12-meter interval of core (7 total). Total core length, 120 meters (129 to 249 meters below the surface). From 214 to 239 meters, the core was all rubble and is not represented here.

Figure 9. Carbonate rubble from core sample 74-NY-11. Depth interval 231 to 234 meters (757 to 767 feet). Despite the severe degree of deformation, some shear fractures can be seen in the core. These fractures intersect the core at an acute angle to the vertical axis of the core.

Table 1. Core 74-NY-11. Chi-square goodness of fit results for the distribution of all the fractures on this core (95 % confidence interval). Interval length - 12 meters.

Number of intervals	Number of fractures	Expected number of fractures per interval	Chi-square Computed	Chi-square Table
7	39	5.571	88.622	12.592

Table values from Davis (1986).

FRACTURE PATTERN: INDIVIDUAL FRACTURE SETS

There was considerable variation in the dip angles of the fractures found on this core (Figures 10 and 11). Fractures, with dip angles of 30°, 40°, 60° and 90° were all found along the length of the core. The 30° dipping fractures were clustered near the top of the core. The 40° dipping fractures were located near the middle of the core and toward the section of core that contained the rubble. Both the 60° and 90° dipping fractures increased in number with depth. Below a depth of 160 meters, the majority of the 60° dipping fractures were clustered in a narrow band at a depth of 208 meters. The 90° dipping fractures, on the other hand, steadily increased in number with depth below 160 meters.

Fractures with dip angles of 65°, 70°, 75° and 80° were found in the highly fractured interval before the rubble zone, between depths of 202 and 214 meters (Figure 11). These dip angles were unique to this last interval. This interval also had three 60 cm long sections of core that were rubble and, out of the intervals, clearly had the highest number of fractures.

No plumose markings or striations were observed on any of the fracture faces. Most of the fractures showed little to no offset.

For an interval length of 12 meters, chi-square testing indicated that the distribution of the 60° and 90° dipping fractures was significantly different than if there were an equal number of fractures in each of the intervals (Table 2). The distribution of the 30° dipping fractures was also significantly different than if there were an equal number of fractures in each of the intervals, whereas the distribution of the 40° dipping fractures was not. The distribution of the 65°, 70°, 75° and 80° dipping fractures was significantly different than if there were an equal number of fractures in each of the intervals (Table 2).

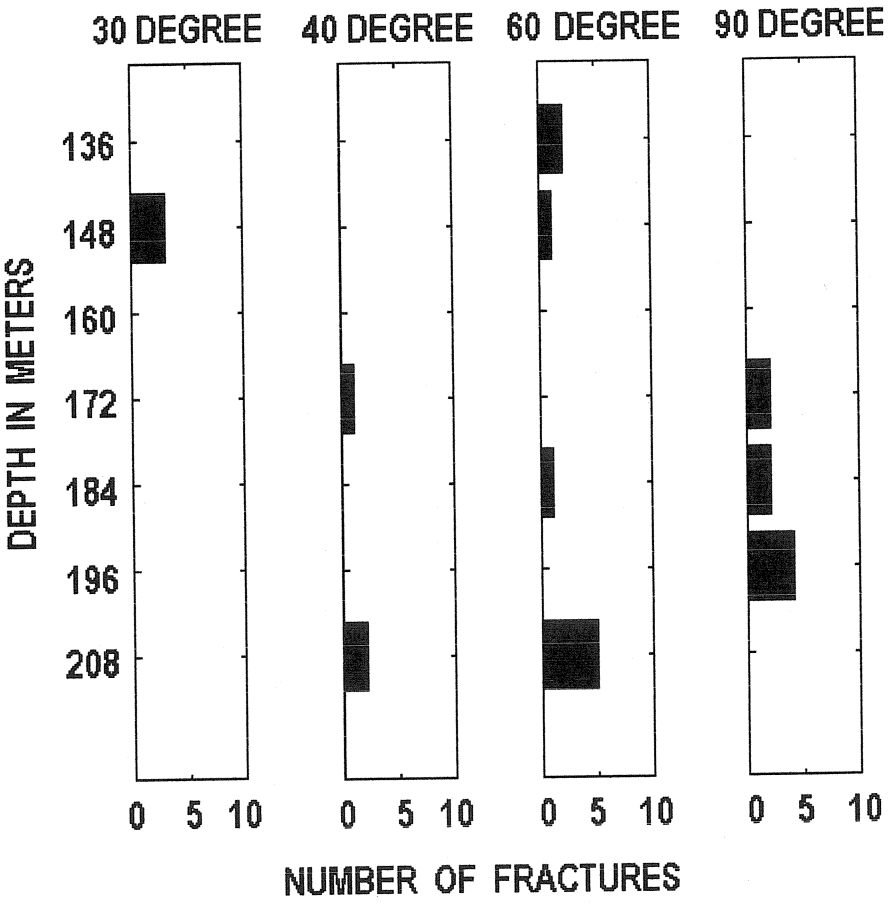

Figure 10. Core 74-NY-11. The number of 30° dipping fractures, 40° dipping fractures, 60° dipping fractures and 90° dipping fractures per 12-meter interval of core (7 total). From 214 to 239 meters, the core was all rubble and is not represented here.

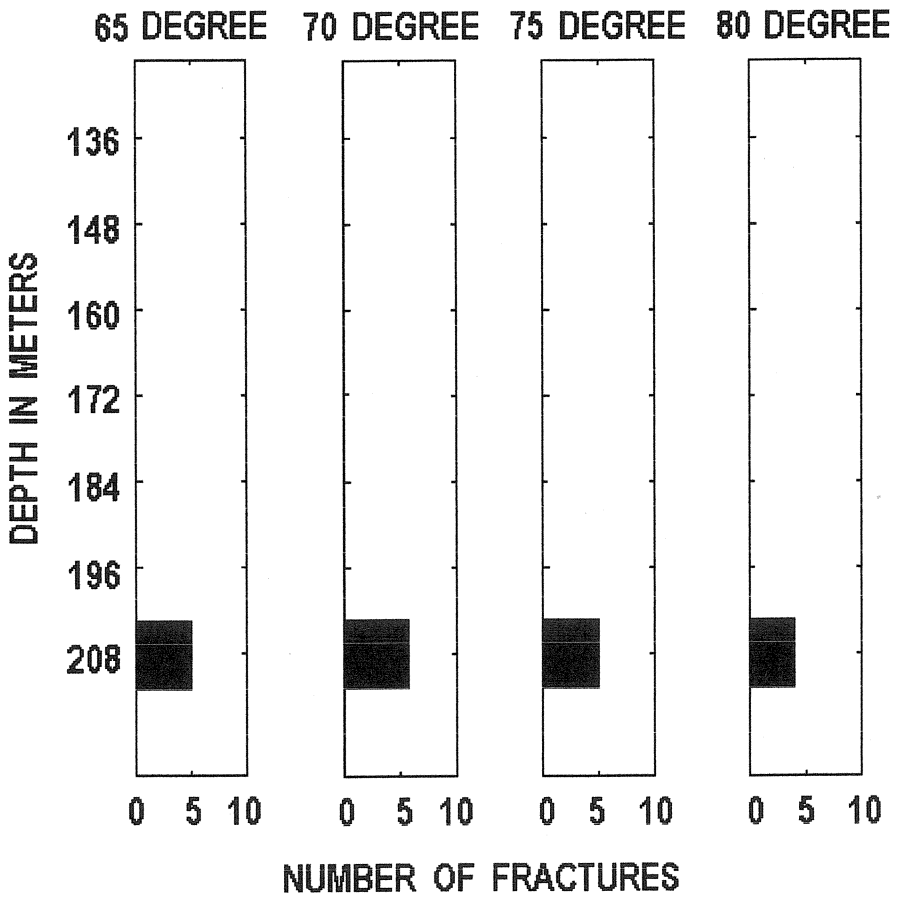

Figure 11. Core 74-NY-11. The number of 65° dipping fractures, 70° dipping fractures, 75° dipping fractures and 80° dipping fractures per 12-meter interval of core (7 total). From 214 to 239 meters, the core was all rubble and is not represented here.

Table 2. Core 74-NY-11. Chi-square goodness of fit results for the distribution of fractures with common dip angles (95 % confidence interval). Interval length - 12 meters.

Dip angle	Number of intervals	Number of fractures	Expected number of fractures per interval	Chi-square Computed	Chi-square Table
30°	7	3	0.43	15.921	12.592
40°	7	3	0.43	7.690	12.592
60°	7	9	1.29	15.108	12.592
90°	7	8	1.14	12.998	12.592
65°	7	5	0.71	30.181	12.592
70°	7	6	0.86	35.881	12.592
75°	7	5	0.71	30.181	12.592
80°	7	4	0.57	24.060	12.592

Table values from Davis (1986).

INTERPRETATION

Based on the geometric relationship between the fractures, it was determined that the 90° dipping fractures are extension, or mode I fractures. Extension fractures typically form under conditions of low confining stress and indicate that the mode of deformation was brittle behavior (Dennis, 1972, Price, 1966 and Nelson, 2001). The 60° dipping fractures are shear fractures.

The stress field that produces normal faulting is one where the major principal stress axis is vertical and the minor and intermediate principal stresses axes are horizontal (Price, 1966). The angle of shearing as a result of this stress field is determined by $\theta = 45° - \varphi/2$, where θ is the angle between the shear plane and the vertical major principal stress axis and φ is the angle of internal friction. Price (1966) chose a reasonable value of 30° for φ, which gives a value of 30° for θ. This is equal to a 60° dip angle. Price (1966) supported the theoretical with data from the field that showed a high percentage of normal faults with dips in the range of 60° to 65°.

Steeper and shallower normal faults do occur though. The acute angle between the conjugate shear planes is often bisected by a vertical extension fracture. The classification of the 60° dipping fractures found on the core as shear fractures and the classification of the 90° dipping fractures as extension fractures is consistent with the stress field that produces normal faults.

If the 60° and 90° dipping fractures are viewed as the most probable to have formed as a result of the stress field that had caused the normal faulting, then they should be examined together. When both fracture sets are combined, there is a dramatic increase in the number of fractures with depth, as the fault rubble zone is approached (Figure 12). The distribution of the combined number of fractures along the length of the core was significantly different than if there were an equal number of fractures in each of the intervals when the interval length was 24 meters (Table 3). The statistically significant increase in the combined number of 60° and 90° dipping fractures with depth is further evidence that these fractures were produced by the same stress field that caused the faulting and that this core was taken from the hanging wall block.

The interval just above the rubble zone (202-214 meters) had a high number of fractures, all dipping at a variety of angles. This section of core also had several sections, each approximately 60 cm long, that were rubble. The bedrock at this depth is very close to the fault plane and the damage zone surrounding the fault. The damage zone surrounding the fault plane is a very complex zone of changing stress and strain states (Nelson, 2001). This would explain the unique fracture sets found in this last section of core.

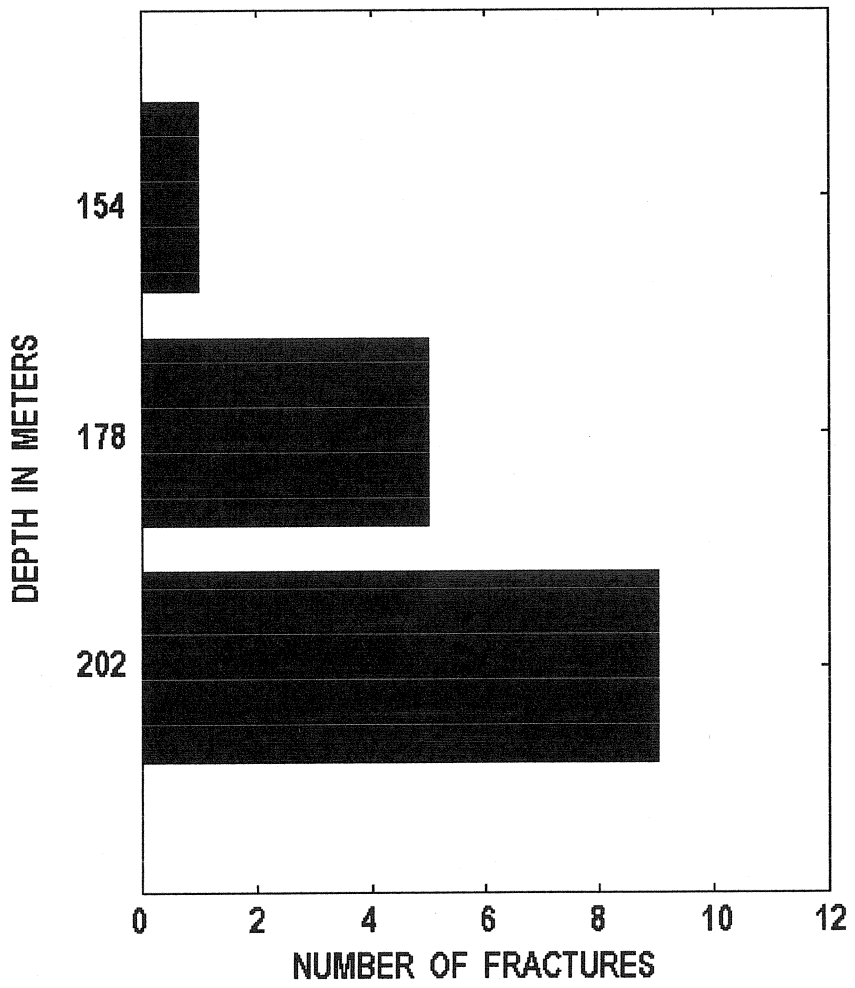

Figure 12. Core 74-NY-11. The increase in the combined number of 60° and 90° dipping fractures with depth. Core interval length - 24 meters.

Table 3. Core 74-NY-11. Chi-square goodness of fit results for the distribution of fractures with 60° and 90° dip angles (95 % confidence interval). Interval length - 24 meters.

Number of intervals	Number of fractures	Expected number of fractures per interval	Chi-square Computed	Chi-square Table
3	13	4.333	6.400	5.991

Table values from Davis (1986).

The fractures with 30° and 40° dip angles are not related to the stress field that produced the normal fault. Their angle is more suggestive of having been formed by a compressive stress field, when the major principal stress axis was horizontal (Price, 1966 and Nelson, 2001). The source of these fractures is certainly from one of the past compressive orogenic events that this area experienced.

AVERAGE FRACTURE SPACING FOR THE EXTENSION FRACTURES, 12-METER INTERVALS

The average fracture spacing was calculated for the 90° dipping fractures after Narr (1996). For each interval below 160 meters, there is a clear decrease in the average fracture spacing with depth, as the rubble zone is approached (Table 4 and Figure 13).

A sixth order polynomial was used to model the rate of change in average fracture spacing value from one interval to the next (Figure 14). A sixth order polynomial was used, since lower order polynomial lines descended below the 0-meter fracture spacing intercept, an impossible condition. The polynomial curve was extrapolated to a hypothetical location for the fault, at a depth of 220 meters, to model the rate of change in fracture spacing closer to the fault. This depth was chosen for the location of the fault since it is near the center of the rubble zone. It should be stressed though, that the fault could have passed anywhere through the rubble zone. A value of 0.001 meter was used for the average fracture spacing minimum, which ideally, should be located at the fault plane.

The polynomial was also extrapolated to shallower depths, where the average fracture spacing increased to approximately 5 meters at a depth of about 160 meters (Figure 14). This is a very good indication that the curve modeled the fracture behavior of the rock quite well, since there were no 90° fractures found on the core above this elevation. Overall, the change in fracture spacing, with distance from the fault, is non-linear.

Table 4. Core 74-NY-11. The average fractures spacing for the 90° dipping fractures. Interval length - 12 meters.

Method	Interval depth (m)	Average fracture spacing (m)
Narr (1996)	130-142	∞ (1)
	142-154	∞
	154-166	∞
	166-178	2.67
	178-190	1.26
	190-202	0.42
	202-214	∞

(1) values of infinity are due to absence of fractures

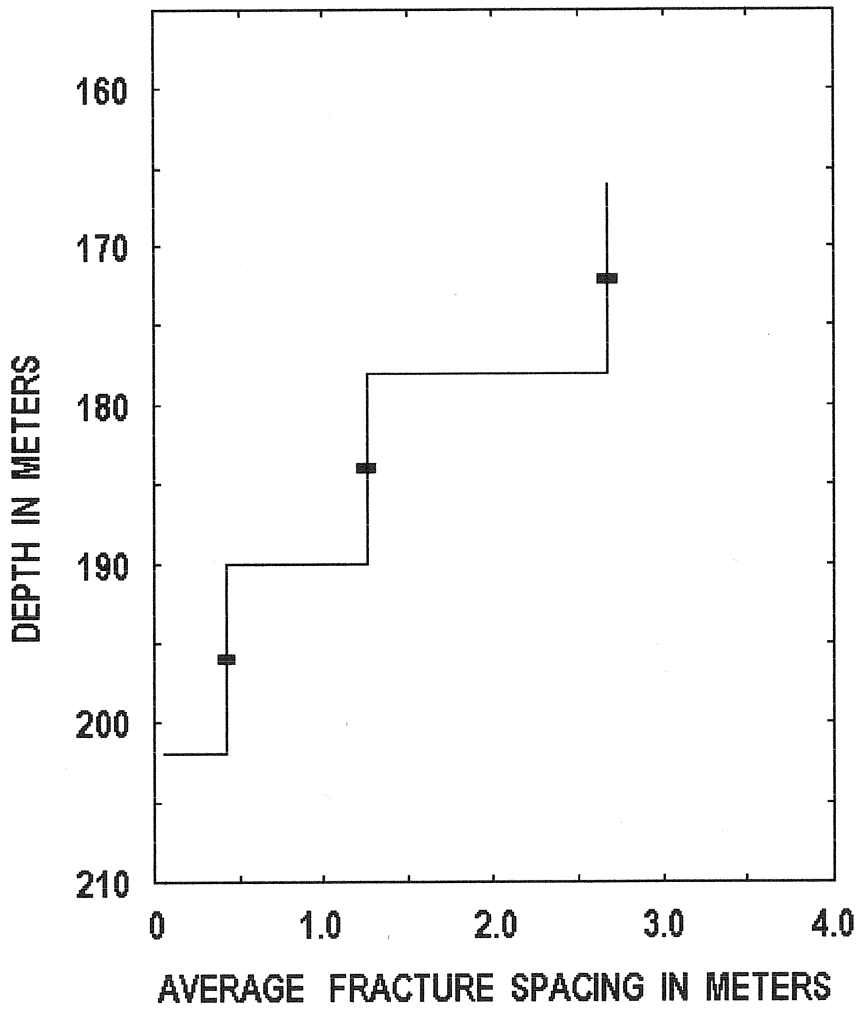

Figure 13. Core 74-NY-11. The change in average fracture spacing with depth (after Narr, 1996). The stair step size is the length of the interval, 12 meters. The bars are the centers of the intervals. Interval length - 12 meters.

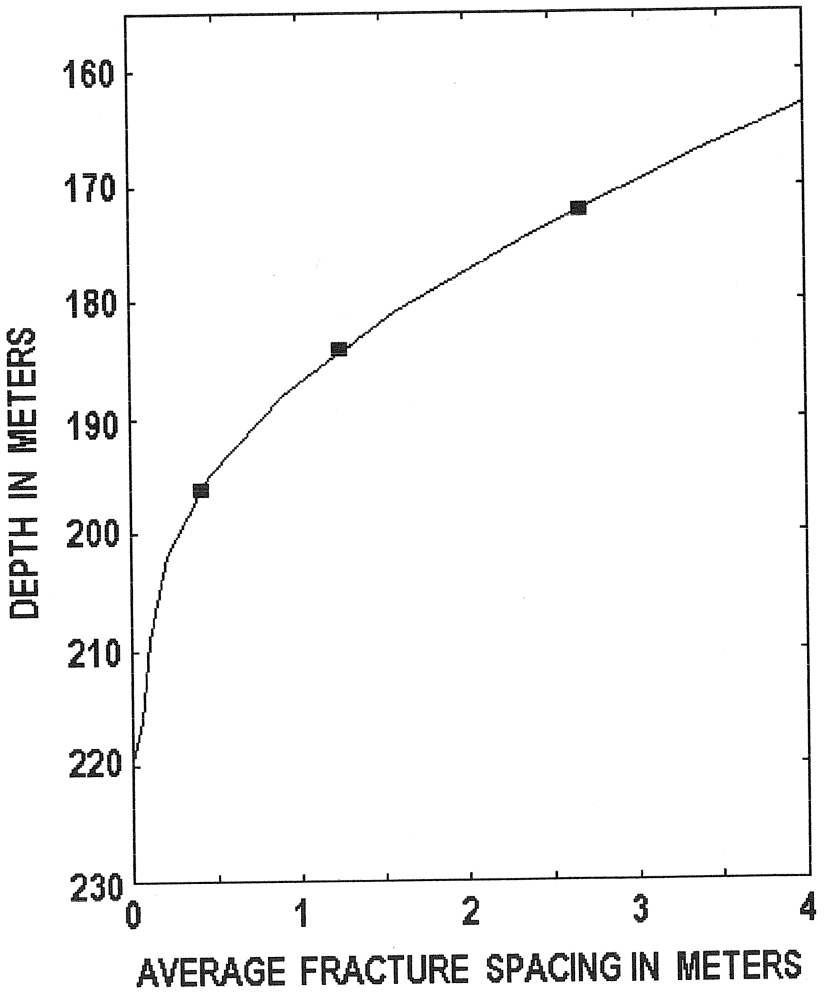

Figure 14. Core 74-NY-11. The change in the average fracture spacing with depth (after Narr, 1996). The line is a sixth order polynomial regression line linking the centers of the intervals (bars) to the approximate location of the fault plane, at a depth of 220 meters. The fracture spacing is estimated to be 0.001 meter at the fault plane.

Interval length - 12 meters.

INTERPRETATION

The pattern of decreasing fracture spacing with depth for the extension fractures (90° dipping) is consistent with the above interpretation that the core was taken from the hanging wall block of the fault that is adjacent to where the core was drilled. The centimeter to millimeter scale fracture spacing within the bedrock between 214 and 239 meters severely weakened the bedrock and allowed the fault plane to pass through it. Nelson (2004) refers to this zone of fractured rock as a process zone. By definition, a process zone is an orientated volume of fractured rock that prepares the rock for eventual offset (faulting).

WIDTH OF THE FAULT RUBBLE ZONE PARALLEL TO THE EARTH'S SURFACE

The fact that this core completely recovered the fault rubble zone was important, since this allowed for the calculation of the total width of the rubble zone, both normal to the fault plane and parallel to the Earth's surface. This was done using Pythagorean's theorem (Figure 15). Using the twenty five meter length of core that passed through the fault rubble as the hypotenuse of a right triangle and an estimated fault dip of 60° gives a breccia zone 12.5 meters wide, normal to the plane of the fault and 10.8 meters wide parallel to the surface of the Earth.

Interpretation

Geraghty and Isachsen (1981) reported that the fault zones around the McGregor-Saratoga-Ballston Lake fault system were generally less than 10 meter wide in surface exposure (parallel to the Earth's surface). This particular fault system has an estimated displacement of 85 meters at Saratoga Springs, which is 32 km east of the location where core 74-NY-11 was taken. If all the faults that bisect the Mohawk River Valley were the result of the same tectonic events, then there is a very good chance that there will be similarities in fault geometry. The similarity between the width of the breccia zones surrounding the McGregor-Saratoga-Ballston Lake fault system, generally less than 10 meters, and the fault penetrated by core 74-NY-11, approximately 10.8 meters, seems to support this theory.

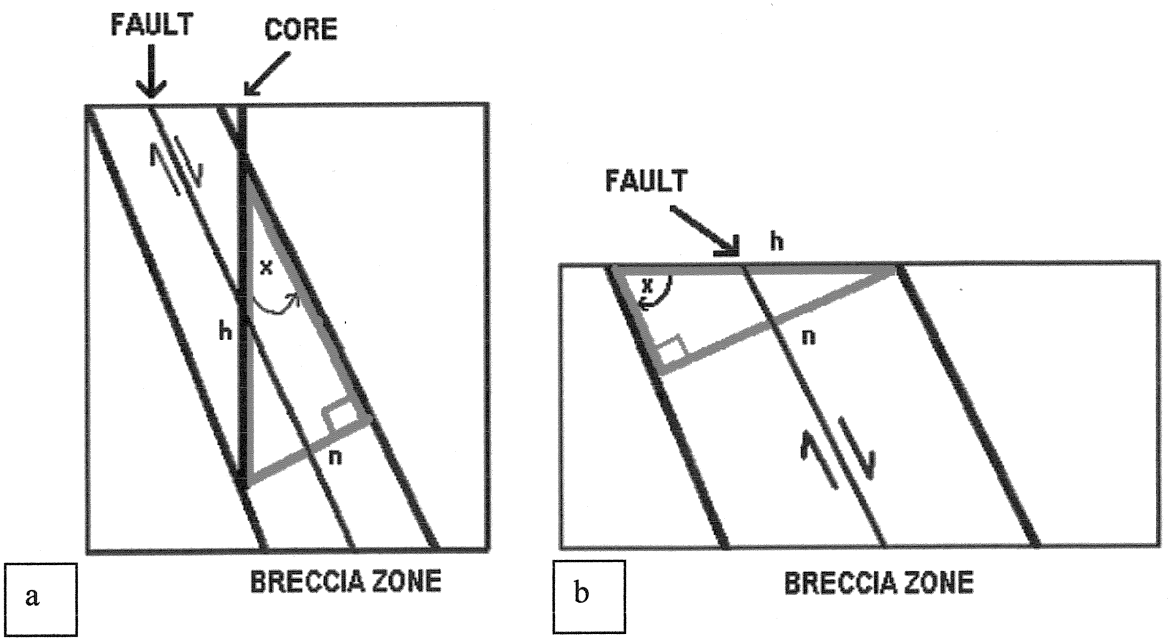

sin x = n/h

where **x** is equal to 90° – dip angle

n is normal to the fault plane

h is the hypotenuse

sin x = n/h

where **x** is equal to the dip angle

n is normal to the fault plane

h is parallel to Earth's surface

Figure 15. The geometric relationship between the core, the fault and the breccia zone surrounding the fault. (a) The width of the breccia zone normal to the fault plane and (b) the width of the breccia zone parallel to the Earth's surface.

CORE 75-NY-2

CORE LOCATION

Core 75-NY-2 is 202 meters long and was taken from a depth of 306 to 508 meters. Of all the cores studied, core 75-NY-2 was taken the furthest distance from the nearest faults (Figure 16) (Isachsen and McKendree, 1977). It is located approximately 12 km east of the Hoffman's faults to the west and approximately 4 km from the Saratoga-McGregor fault to the east. The Hoffman's fault to the west has an estimated minimum displacement of approximately 430 meters. The Saratoga-McGregor fault to the east has an estimated minimum displacement of approximately 440 meters (Geraghty and Isachsen, 1981).

From the top of the core, to a depth of 324 meters, the core passed through the Canajoharie Shale. Rickard (1973) has indicted that just beneath the Canajoharie Shale in this area there is a thin veneer (10 – 20 meters) of Trenton Group limestones. This places the contact of the Trenton and the underlying Gailor formation at a depth of approximately 340 meters. The Hoyt limestone lies between the Gailor and the underlying Galway formation, which begins at a depth of approximately 440 meters.

FRACTURE PATTERN: TOTAL NUMBER OF FRACTURES

All of the fractures found in this core are clustered near the bottom of the core, in the Galway formation (Figure 17). For an interval length of 12 meters, chi-square testing indicated that the distribution pattern for the total number of fractures was significantly different than if there were an equal number of fractures in each of the intervals (Table 5).

INTERPRETATION

The most obvious reason for the lack of fracturing in this core is the fact that it was taken from a part of the study area that was located the furthest distance from the surface exposures of the nearest faults. As a result, this core showed the least amount of fracturing out of all the cores studied and showed no evidence of having interested a fault. It could certainly be argued that both the limestone units at the top of the core were not fractured because limestones are less brittle than dolostone (Nelson, 2001). The relatively minor amounts of limestone within the Gailor should not have prevented fracturing within this unit, so fracturing was probably controlled by distance to the nearest fault and not by lithology.

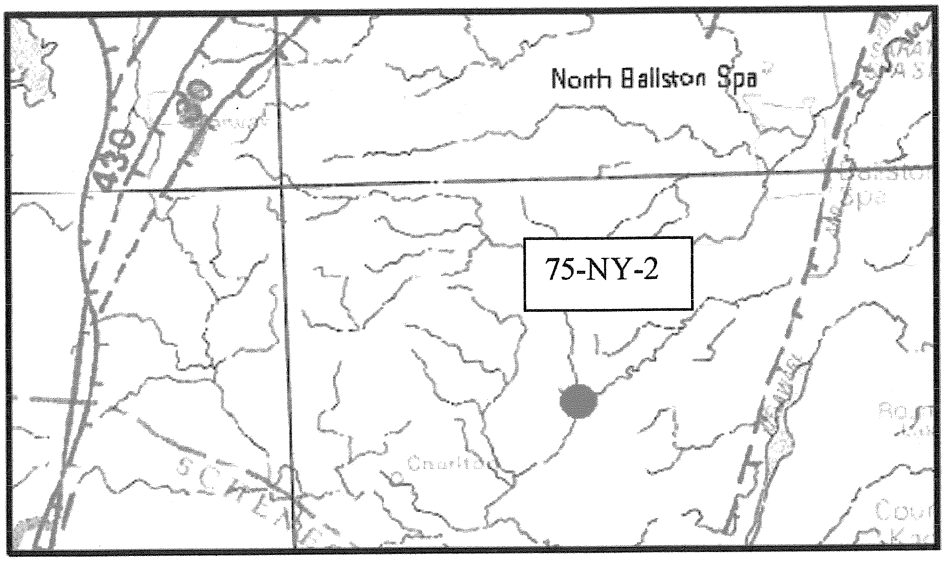

Figure 16. The location of core 75-NY-2. The circle is the core location. The solid lines are normal faults, the hachure marks are on the relatively downthrown side of the faults. The Saratoga-McGregor fault is the fault to the east, the Hoffman's faults are the faults to the west. Fault lines are dashed where inferred. Numbers indicate minimum estimated displacement, in meters. Map width approximately 23 km.

Modified from Isachsen and McKendree, 1977.

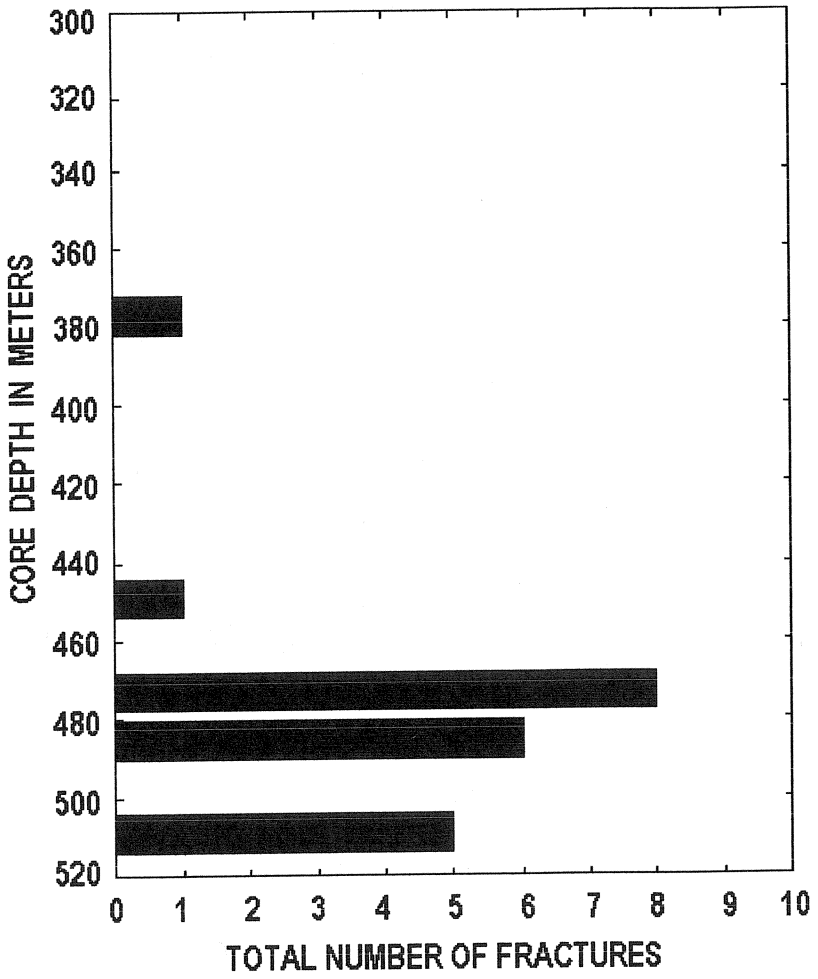

Figure 17. Core 75-NY-2. The total number of fractures per 12-meter interval of core (16 total). The total core length is 202 meters (306 to 508 meters below the surface).

Table 5. Core 75-NY-2. Chi-square goodness of fit results for the distribution of all fractures on this core (95 % confidence interval). Interval length - 12 meters.

Number of intervals	Number of fractures	Expected number of fractures per interval	Chi-square Computed	Chi-square Table
16	21	1.3	760.42	24.996

Table values from Davis (1986).

FRACTURE PATTERN: INDIVIDUAL FRACTURE SETS

There was considerable variation in the dips of the fractures on this core. The fractures had 90°, 75°, 70°, 60° and 50° dips. These five sets of fractures were all found clustered at a depth of approximately 480 meters (Figures 18 and 19). The 90° dipping fractures are the dominant set, both in terms of numbers of fractures and the number of intervals that contained the fractures.

INTERPRETATION

The way the different fracture sets were clustered at the same depth indicates that the stress concentration which caused the fracturing originated near that depth and is not related to the faults seen in surface view.

The 90° dipping fractures are extension fractures. Extension fractures typically form under conditions of low confining stress and indicate that the mode of deformation was brittle behavior (Dennis, 1972, Price, 1966 and Nelson, 2001). The 50° and 60° dipping fractures are shear fractures. These fractures are thought to be conjugate to each other, but since the core was not orientated at the time of drilling there is no way to determine if this is true. These angles are consistent with the expected angle of shearing for normal faulting (Price, 1966).

The 70° and 75° dipping fractures are interpreted as hybrid extension fractures, since the dihedral angle separating the conjugate planes is less than 45° (Hancock et al., 1984). Hybrid extension fractures form conjugate sets with the acute angle separating the fracture planes bisected by the maximum principal stress. The angle between hybrid extension fractures and true tensile cracks (parallel to the maximum and intermediate stress axes) decreases with decreasing confining pressure, which would indicate a shallow depth of burial at the time of deformation (Hancock and Engelder, 1989). Dennis (1972) referred to fractures of this type as oblique extension fractures and considered them to be the result of extension across the fracture surface under a tensile normal stress component. The majority of the displacement in this case is extensional, with only a negligible shear component. These fractures may become faults with continuing deformation. As with the extension fractures, the strike of the hybrid extension fractures is parallel to the strike of the fault that the fractures are associated with.

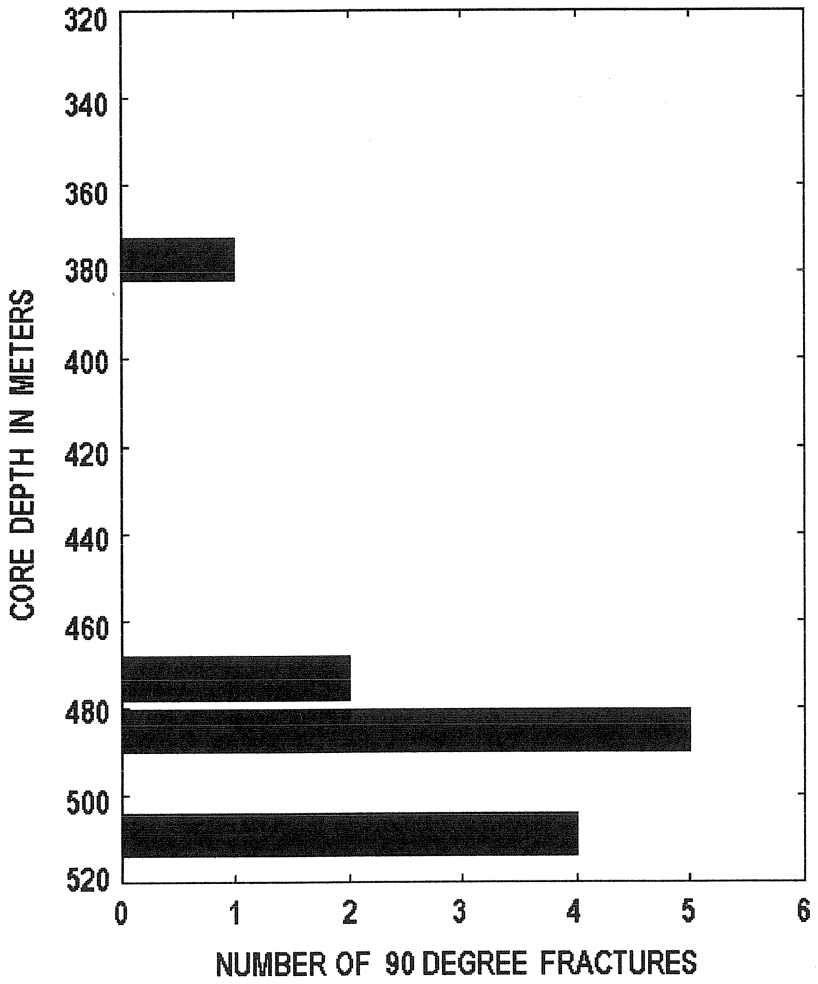

Figure 18. Core 75-NY-2. The number of 90° dipping fractures per 12-meter interval of core (16 total). The total core length is 202 meters (306 to 508 meters below the surface).

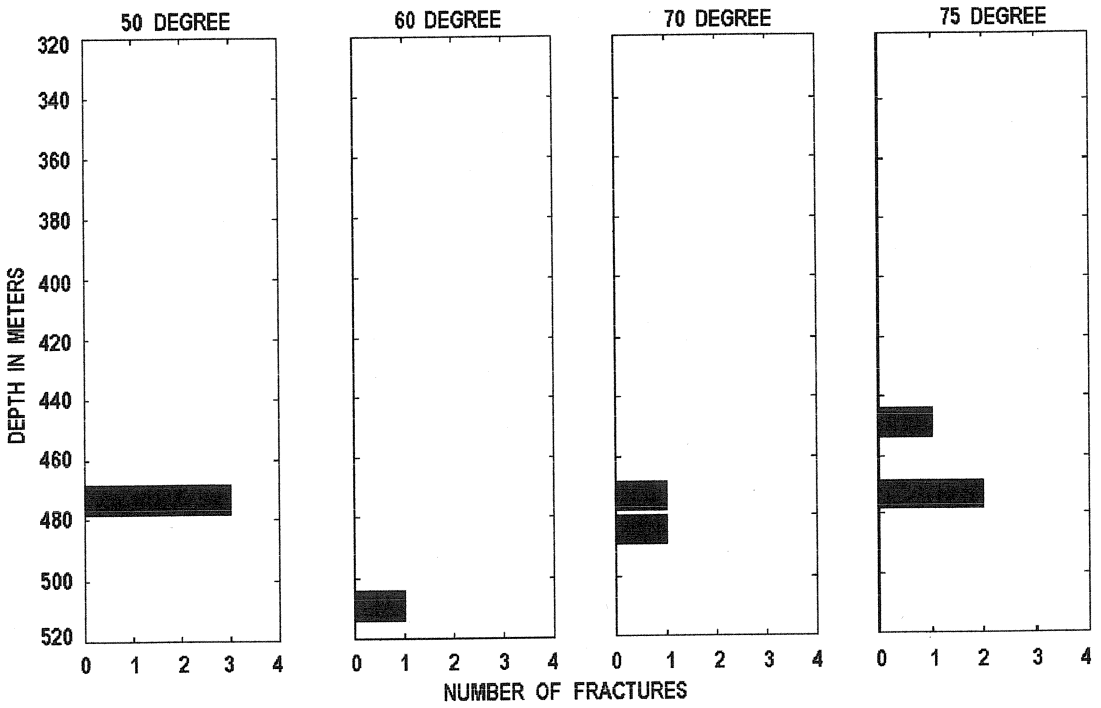

Figure 19. Core 75-NY-2. The number of 50°, 60°, 70°, and 75° dipping fractures per 12-meter interval of core (16 total). The total core length is 202 meters (306 to 508 meters below the surface).

AVERAGE FRACTURE SPACING FOR THE EXTENSION FRACTURES, 12-METER INTERVALS

The average fracture spacing that was calculated for the extension fractures decreased from a high of 10.66 meters at an interval depth of 371 to 383 meters to a minimum of 0.5 meters at a depth interval of 479 to 491 meters (Table 6 and Figure 20).

A third order polynomial was used to model the change in the average fracture spacing between the widely spaced data points and to extrapolate the fracture spacing at a shallower depth (Figure 21). The polynomial curve indicates that the average fracture spacing minimum, estimated to be 0.3 meters, is at a depth of approximately 495 meters.

Although the polynomial was calculated using only a few data points, it is very similar in shape to the curve drawn through the interval centers for core 74-NY-11, which is known to have been taken from a hanging wall block and underlying fault zone (Figure 22). Several important observations can be made from comparing the two curves, and the two cores. First, the fracture spacing curve for core 75-NY-2 lies within the fracture spacing curve for core 74-NY-11. Second, there was no fault rubble found in core 75-NY-2. Third, the average fracture spacing minimum for core 75-NY-2, estimated to be 0.3 meters, is much wider than the 0.001 meters fracture spacing that was estimated to be near the fault plane intersected by cores 74-NY-11.

INTERPRETATION

The fact that the fracture spacing curve for core 75-NY-2 fits inside the fracture spacing curve for core 74-NY-11 indicates that the fracturing within the bedrock penetrated by core 75-NY-2 isn't as extensive as the fracturing in the bedrock penetrated by core 74-NY-11. The lack of fault rubble in core 75-NY-2 is a strong indication that faulting did not occur in the bedrock penetrated by core 75-NY-2. If this is the case, then the difference between the average fracture spacing minimums, 0.001 meters and 0.3 meters for cores 74-NY-11 and 75-NY-2, respectively, starts to better define the minimum fracture spacing threshold that needs to be reached before faulting can occur. This means that the fracture spacing needs to be closer than 0.3 meters before fault movement can occur.

Table 6. Core 75-NY-2. The average fracture spacing for the 90° dipping fractures (after Narr, 1996). Values of infinity are calculated for intervals that did not have any fractures. Interval length - 12 meters.

Method	Interval depth (m)	Average fracture spacing (m)
Narr, 1996	371 – 383	10.660
	383 – 395	∞[1]
	395 – 407	∞
	407 – 419	∞
	419 – 431	∞
	431 – 443	∞
	443 – 455	∞
	455 – 467	∞
	467 – 479	2.133
	479 – 491	0.519
	491 – 503	∞
	503 – 515	1.557

(1) values of infinity are due to absence of fractures

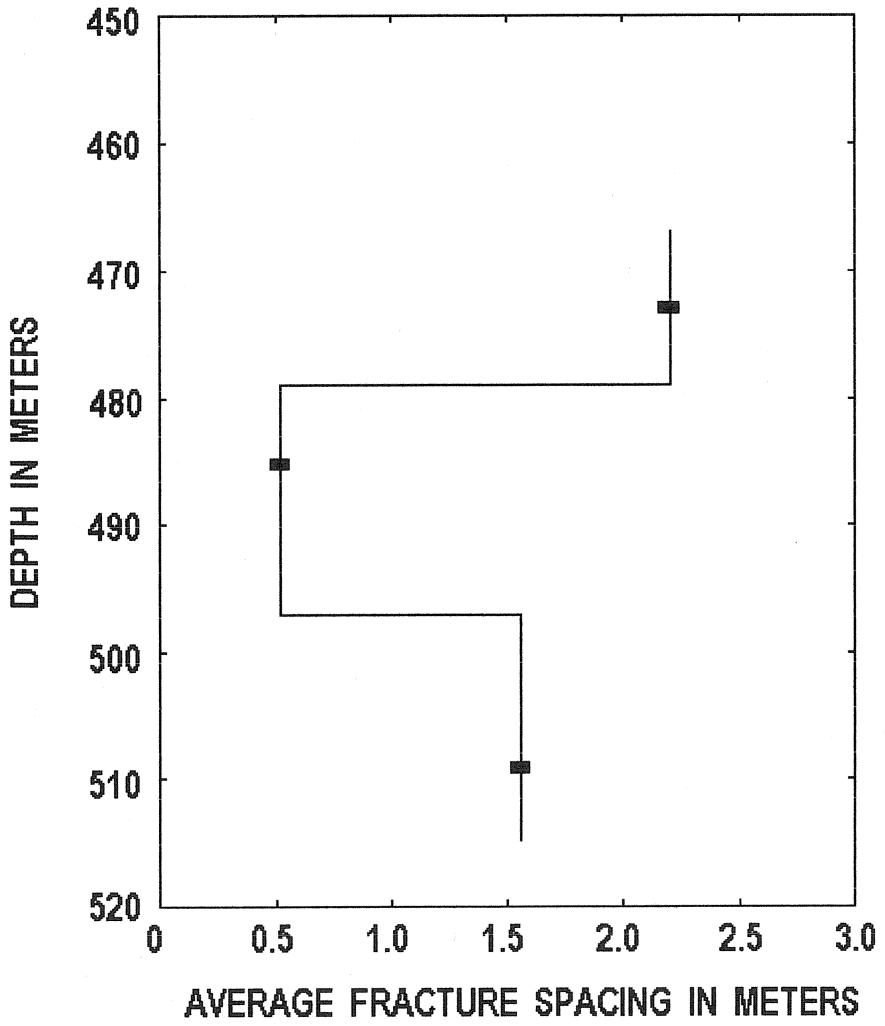

Figure 20. Core 75-NY-2. The change in the average fracture spacing for each interval, 90° dipping fractures (after Narr, 1996). The bars are the centers of the 12-meter intervals listed in table 6. There was no data for the 12-meter interval centered at 497 meters, as a result, the intervals adjacent to the interval centered at 497 meters were extended 6 meters each to fill in the "gap" in the data.

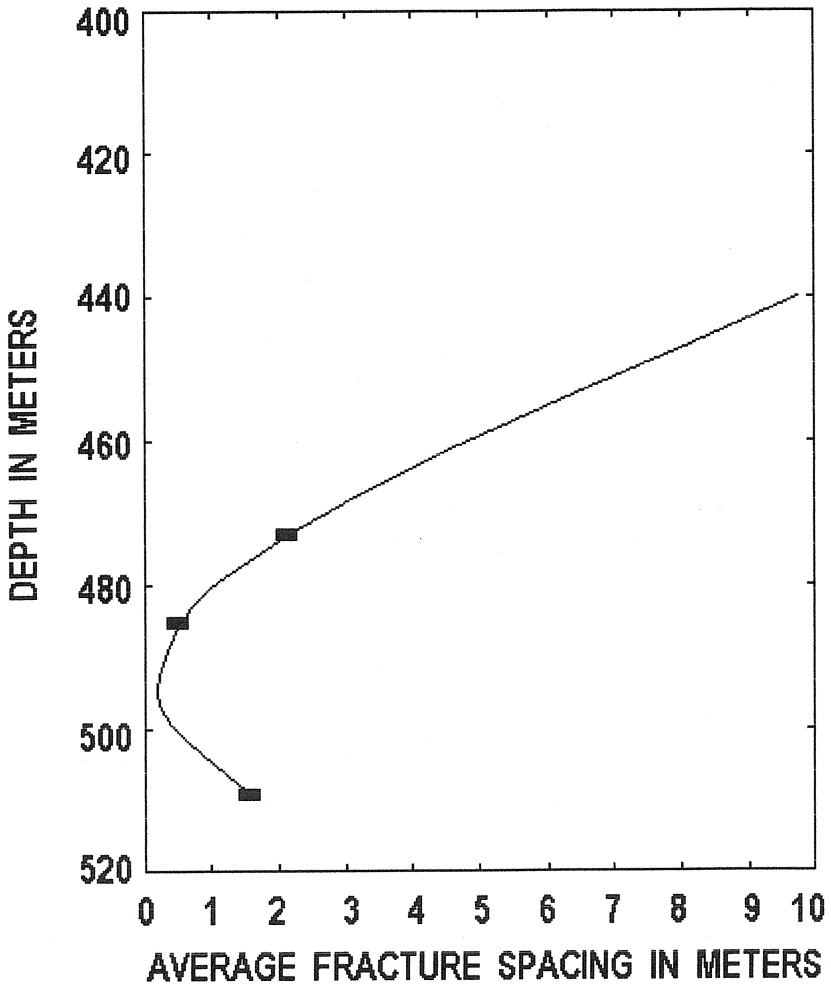

Figure 21. Core 75-NY-2. The change in the average fracture spacing for the 90° dipping fractures between 440 and 520 meters (after Narr, 1996). The line is a third order polynomial. The bars are the centers of each of the 12-meter intervals listed in table 6.

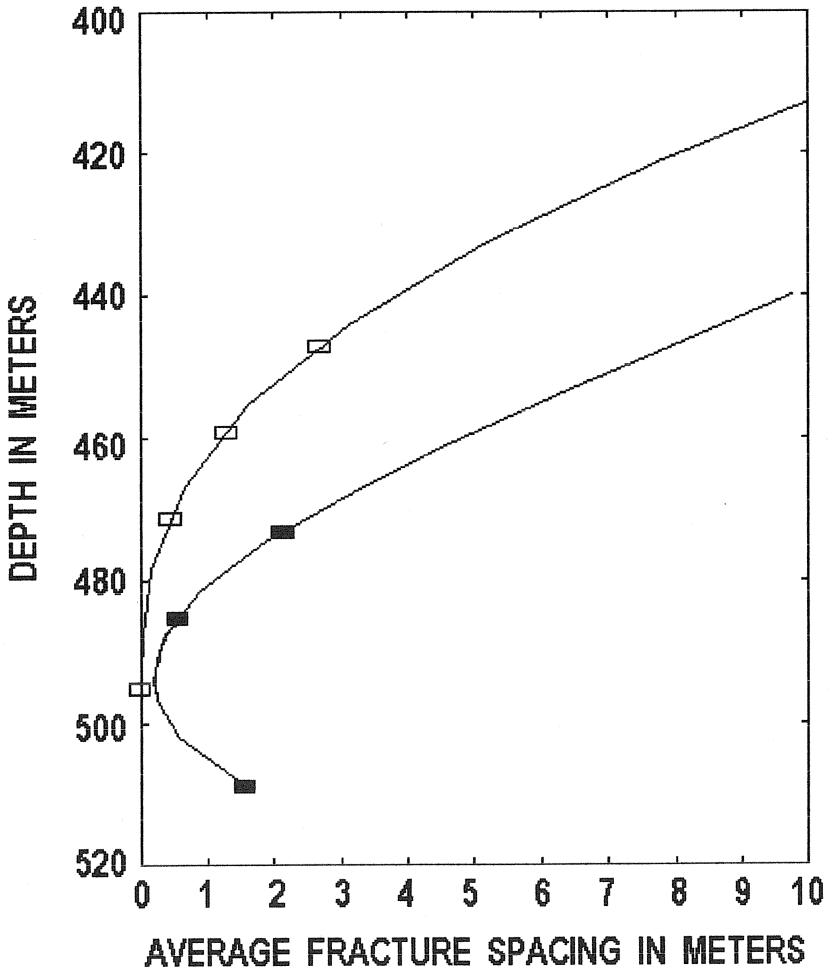

Figure 22. The polynomial curve modeling the rate of change in the average fracture spacing for core 74-NY-11 (-□-) superimposed on the polynomial curve modeling the rate of change in the average fracture spacing for core 75-NY-2 (-■-). On this graph, the fault location for core 74-NY-11 was aligned with the average fracture spacing minimum for core 75-NY-2, estimated to be 0.30 meters at a depth of 495 meters.

Taking all of this into consideration, it appears that the bedrock recovered by core 75-NY-2 is a fault process zone at this stage and that no fault movement has taken place. A process zone is an orientated volume of fractured rock that the fault plane passes through (Nelson, 2004). The fracture intensity within the process zone is much higher than in the surrounding bedrock. The increase in fracture spacing below a depth of 495 meters indicates that the core had passed all the way through the process zone and was moving away from it. Given the fact that this section of core is close to the Precambrian contact may indicate that there is a preexisting fault in the Precambrian metamorphic rocks in this area, which did not fully reactivate during the Taconic orogeny.

CORE 75-NY-14

CORE LOCATION

Core 75-NY-14 is 104 meters long and was taken from a horst structure which was formed by the Sprakers fault to the west and Noses fault to the east (Figure 23) (Isachsen and McKendree, 1977). The Sprakers fault has a minimum estimated displacement of 60 meters and the Noses fault has a minimum estimated displacement of 200 meters. The core was taken from the Little Falls formation, just beneath the contact with the overlying Tribes Hill formation (Curl, 1983).

FRACTURE PATTERN: TOTAL NUMBER OF FRACTURES

Although there were some missing sections of core between the depths of 724 and 736 meters (9 out of 12 meters was missing, the 3 meter section that was not missing had no fractures in it), this core still provides valuable fracture information. When the total number of fractures per 12-meter interval of core was plotted against depth, there was a peak in the number of fractures at a depth of 718 meters (Figure 24). In addition to the 21 fractures that were found in this interval, some rubble was found at a depth of 715 meters. The number of fractures per interval rapidly decreased both above and below this depth. This fracture distribution was significantly different than if there were an equal number of fractures in each of the intervals (Table 7).

The peak number of fractures, 21, per 12-meter interval in this core was slightly less than the peak number of fractures, 26, per 12-meter interval in core 74-NY-11. This interval, for core 74-NY-11, was just above the fault zone.

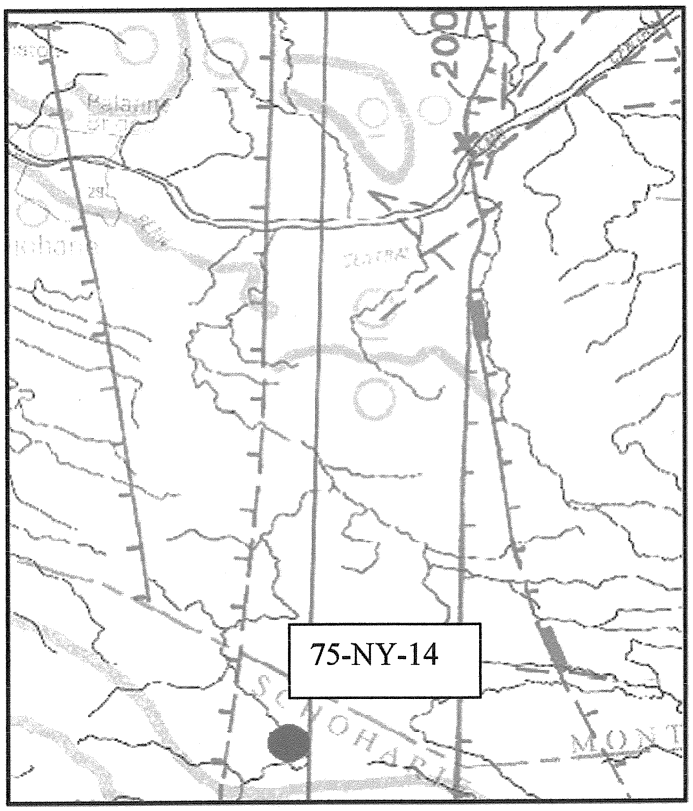

Figure 23. The location of core 75-NY-14. The circle is the core location. The solid lines are normal faults. Hachure marks are on the relatively downthrown side of the faults. Rectangular bar next to fault indicates a high angle normal fault. Fault lines are dashed where inferred. Numbers next to faults indicate minimum estimated displacement, in meters. Map width approximately 17 km.

Modified from Isachsen and McKendree, 1977.

INTERPRETATION

This core passed completely through a process zone and either an incipient fault or a low displacement fault plane at an approximate depth of 718 to 730 meters. The fact that the number of fractures, per 12-meter interval of core, decreases above and below this depth range, indicates that this depth is the most probable location of the fault plane. The similarities in the high number of fractures, per 12-meter interval of core, between this core and core 74-NY-11 and the presence of rubble in both cores indicates that some movement probably had occurred along the fault plane intersected by this core.

What is particular interesting about this core intersecting a fault plane is the location of the core, which was on a horst structure (Figure 23). Since the faults to either side of the core dip in opposite directions, a fault at a depth of 718 to 730 meters was not expected. This indicates that there is a subsurface fault within the horst. This subsurface fault is probably parallel or subparallel to the Sprakers fault to the west, since this core is closer to that fault. It is not known if the dip of the fault is parallel to or conjugate to the Sprakers fault.

FRACTURE PATTERN: INDIVIDUAL FRACTURE SETS

The fractures on this core had 90°, 60°, 55° and 45° dips. The 90° dipping fractures are the dominant fracture set, both in terms of number of fractures and the number of 12-meter intervals that contain fractures (Figure 25). All of these fractures peaked at the same depth, 718 meters. Chi-square testing indicated that the distributions of the 90° and 45° dipping fractures was significantly different than if there were an equal number of fractures in each of the intervals using a 12-meter interval length whereas the distributions of the other fracture sets were not (Table 8).

INTERPRETATION

Based on the geometric relationship between the fractures, the 90° dipping fractures are interpreted as extension, or mode I fractures, and the 45°, 55° and 60° dipping fractures are interpreted as shear fractures. Since the 45°, 55° and 60° dipping fractures were all classified as shear fractures, it is appropriate to group them together and compare them to the extension fractures. The combined shear fracture distribution pattern is the same as the extension fracture distribution pattern, but there were fewer shear fracture (Figure 26). The distribution pattern for the total number of shear fractures was significantly different than if there were an equal number of fractures in each of the 12-meter intervals (Table 9). Both the extension and the shear fractures peaked at the same depth, 718 meters. This

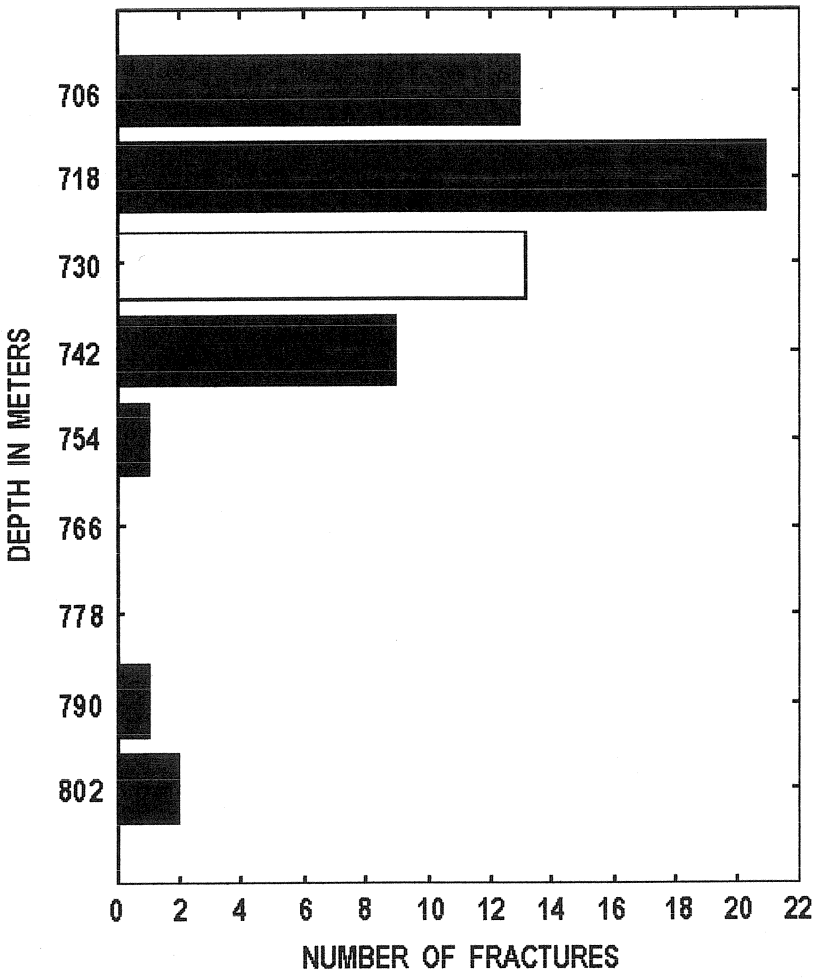

Figure 24. Core 75-NY-14. The total number of fractures per 12-meter interval (9 total). Total core length 104 meters (700 to 804 meters). Note: there was missing data for the 12-meter interval at 730 meters, which is represented by the blank bar.

Table 7. Core 75-NY-14. Chi-square goodness of fit results for the distribution of all the fractures on this core (95 % confidence interval). Interval length - 12 meters.

Number of intervals	Number of fractures	Expected number of fractures per interval	Chi-square computed	Chi-square table
8 (1)	47	5.875	71.638	14.067

(1) Excluding the interval that had missing data.

Table values from Davis (1986).

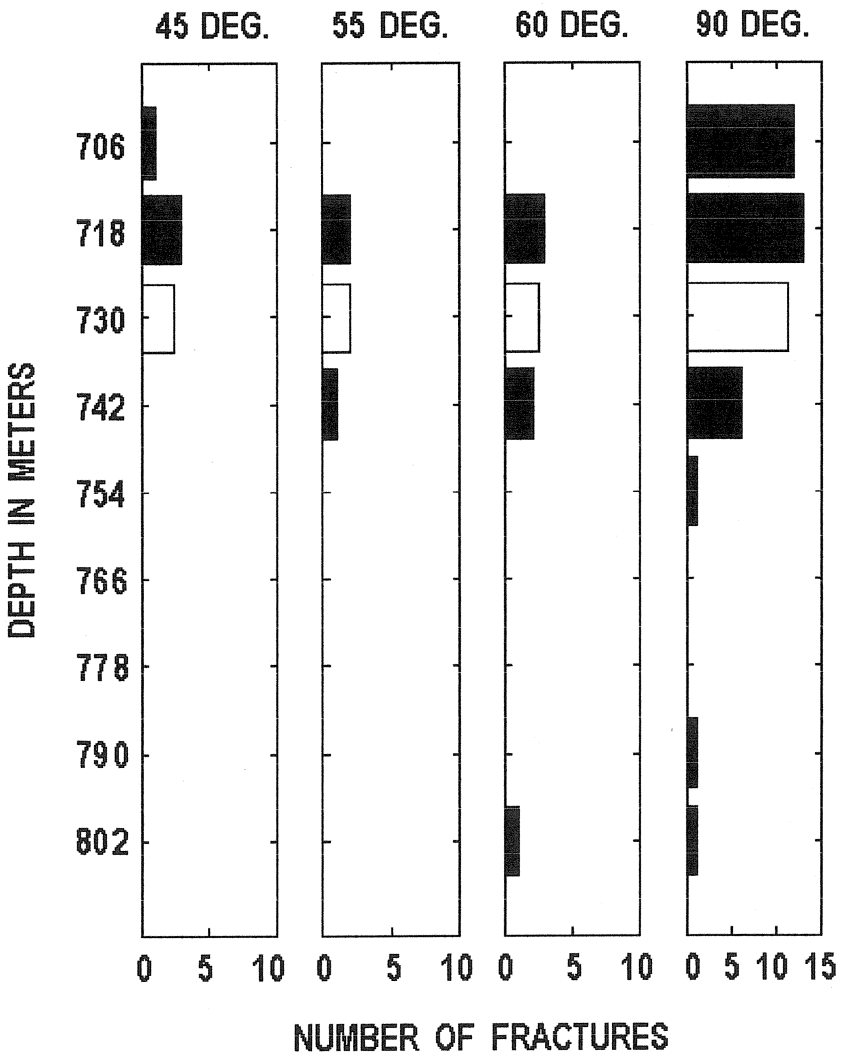

Figure 25. Core 75-NY-14. The number of 45°, 55°, 60° and 90° dipping fractures per 12-meter interval of core (9 total). Total core length 104 meters, 700 to 804 meters. Note: there was missing data for the 12-meter interval at 730 meters, which is represented by the blank bars.

Table 8. Core 75-NY-14. Chi-square goodness of fit results for the distribution of fractures with common dip angles (95 % confidence interval). Interval length - 12 meters.

Dip angle	Number of intervals	Number of fractures	Expected number of fractures per interval	Chi-square computed	Chi-square table
45°	8 (1)	4	0.500	16.000	14.067
55°	8 (1)	3	0.375	10.333	14.067
60°	8 (1)	6	0.750	12.667	14.067
90°	8 (1)	34	4.250	53.412	14.067

(1) Excluding the interval that was missing.

Table values from Davis (1986).

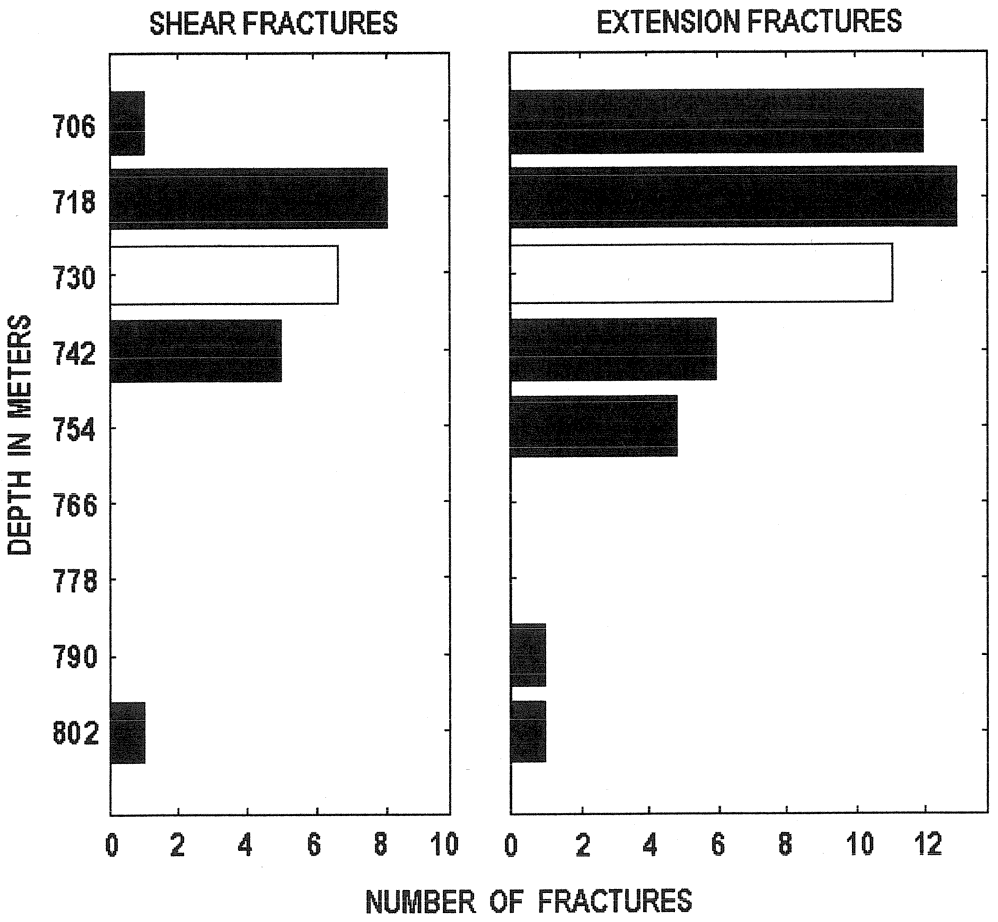

Figure 26. Core 75-NY-14. The number of shear fractures and the number of extension fractures per 12-meter interval (9 total). Total core length 104 meters, 700 to 804 meters. Note: there was missing data for the 12-meter interval at 730 meters, which is represented by the blank bars.

Table 9. Core 75-NY-14. Chi-square goodness of fit results for the distribution of all the shear fractures on the core (95 % confidence interval). Interval length - 12 meters.

Number of intervals	Number of fractures	Expected number of fractures per interval	Chi-square computed	Chi-square table
8 (1)	13	1.625	33.154	14.067

(1) Excluding the interval that had data missing.

Table values from Davis (1986).

supports the above interpretation that the core passed completely through a process zone and a fault plane, at an approximate depth of 718 to 730 meters. The fact that the shear fractures are confined to a tighter zone around the fault plane than the extension fractures may indicate that their development is more closely associated with the formation of the fault plane than the extension fractures.

AVERAGE FRACTURE SPACING FOR THE EXTENSION FRACTURES, 12-METER INTERVALS

The average fracture spacing for the extension fractures is at a minimum value, 0.205 meters, at a depth of 718 meters (Table 10 and Figure 27). Fracture spacing increases both above and below this depth.

A second order polynomial was used to model the change in the average fracture spacing with depth and to extrapolate the fracture spacing at a shallower depth, where there was no data collected (Figure 28). The polynomial curve approaches the "0-meter" fracture spacing intercept at a depth of approximately 710 to 718 meters. It should be remembered that there was missing data for the interval that was centered at 730 meters. Had there been data for this interval, the shape of the polynomial curve may have been different.

INTERPRETATION

Despite missing several meters of core, the fracture spacing curve indicated that the average fracture spacing minimum was in the centimeter to millimeter range at the same depth where the rubble in the core was found, 715 meters. This is a very strong indication that the fault plane is located at, or very close to this depth. The presence of rubble and fracture spacing in the centimeter to millimeter range indicates that some minor offset along the fault plane may have occurred. Since there is only a minor amount of rubble at this depth, any offset is along the fault plane is thought to be minor. This interpretation is based on the fact that there was 29 meters of rubble found in the vertical section of core 74-NY-11 that passed through the fault plane. The offset along the fault intersected by core 74-NY-11 is estimated to be 60 meters.

Table 10. Core 75-NY-14. The average fracture spacing for the 90° dipping fractures (after Narr, 1996). Values of infinity are calculated for intervals that did not have any fractures. Interval length - 12 meters.

Method	Interval depth (m)	Average fracture spacing (m)
Narr, 1996	700 – 712	0.400
	712 – 724	0.205
	724 – 736	N/A
	736 – 748	0.383
	748 – 760	4.800
	760 – 772	∞
	772 – 784	∞

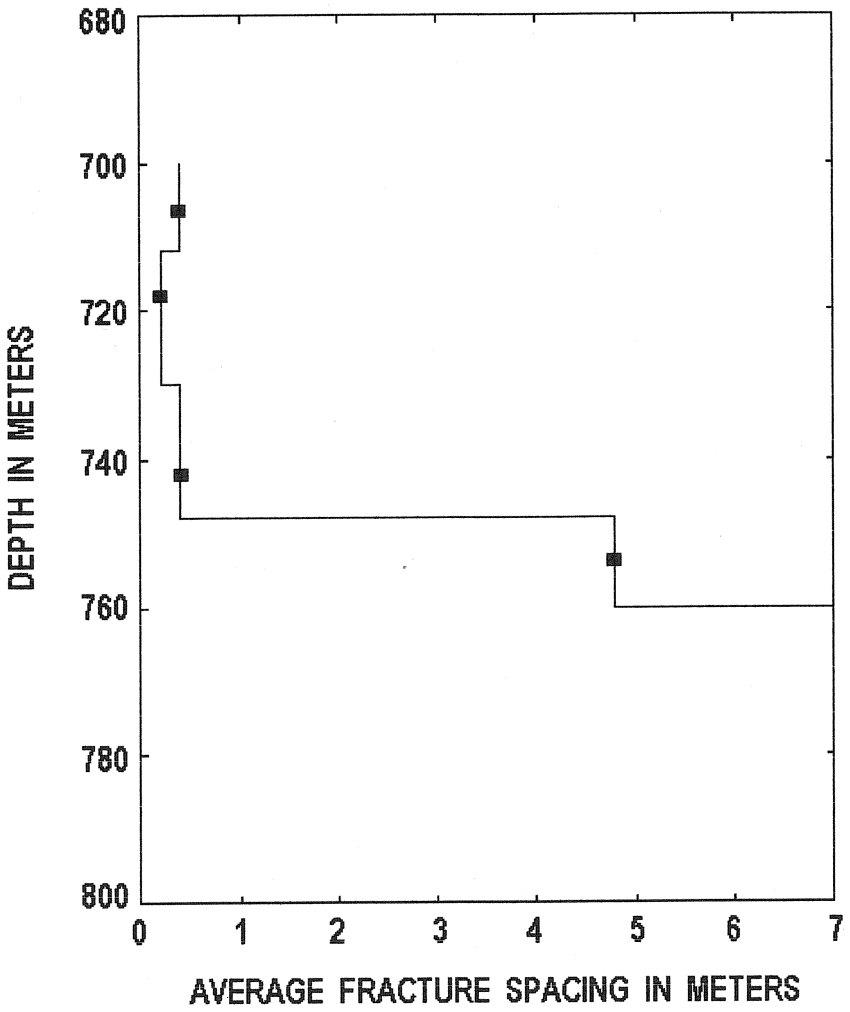

Figure 27. Core 75-NY-14. The change in the average fracture spacing for each interval for the extension fractures (after Narr, 1996). The bars are the centers of the 12-meter intervals listed in table 10. There was missing data for the 12-meter interval centered at 730 meters, as a result, the two intervals adjacent to this interval were extended 6 meters each to fill in the data "gap".

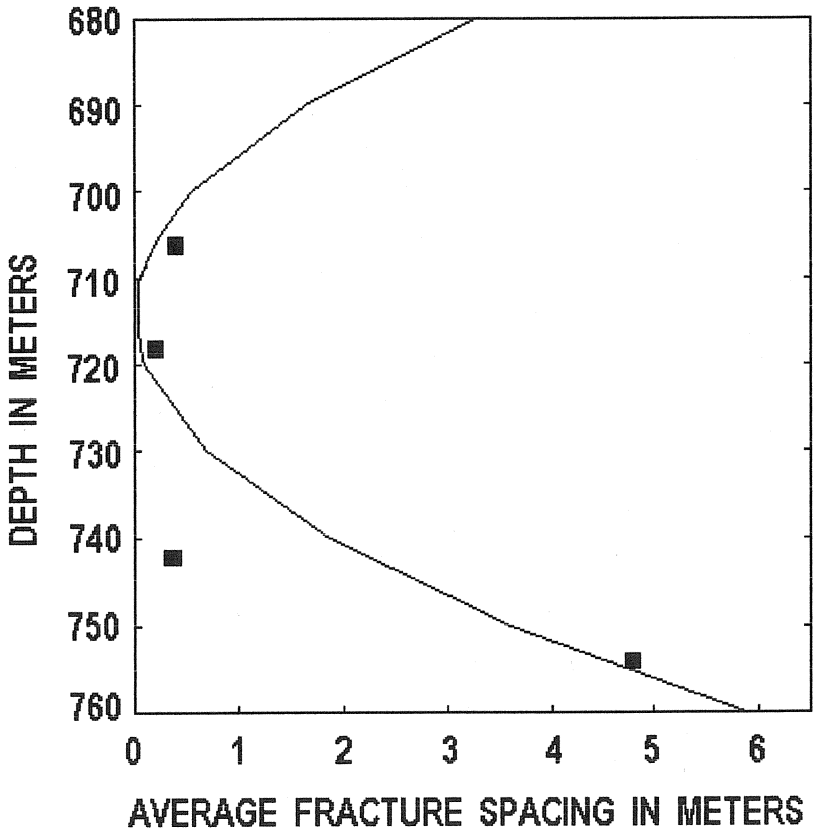

Figure 28. Core 75-NY-14. The change in the average fracture spacing for the extension fractures with depth. The line is a second order polynomial. The bars are the centers of each of the 12-meter intervals listed in table 10.

It was determined that core 75-NY-2 passed through a process zone and that core 74-NY-11 passed through a fault plane that had an estimated displacement of approximately 60 meters. Accordingly, the fracture spacing curve for core 75-NY-2 fit inside the fracture spacing curve for core 74-NY-11, which indicated that the fracturing within the bedrock penetrated by core 75-NY-2 isn't as extensive as the fracturing in the bedrock penetrated by core 74-NY-11 (Figure 22).

When the fracture spacing curves for cores 74-NY-11 and 75-NY-2 were superimposed on the fracture spacing curve for core 75-NY-14, the fracture spacing curve for core 75-NY-14 fell between the fracture spacing curves for cores 74-NY-11 and 75-NY-2 (Figure 29). This indicates that the fracture spacing in the bedrock penetrated by this core is intermediate between the bedrock penetrated by cores 74-NY-11 and 75-NY-2. It had been determined above, that core 75-NY-14 penetrated an incipient fault zone. Clearly, as a fault process zone (core 75-NY-2) develops into an incipient fault (core 75-NY-14) and finally into a fault with tens of meters of offset (core 74-NY-11) the spacing between the fractures will get closer as the rock weakens and finally experiences offset. The comparison between these three fracture spacing curves is in agreement with and clearly shows this development.

CORE 74-NY-10

CORE LOCATION

Core 74-NY-10 measures 76 meters in length and was taken from a depth of 241 to 317 meters. The site where the core was taken is very close to the surface exposure of the East Stone Arabia fault, just to the west of the Sacandaga Lake (Figure 7) (Bradley and Kidd, 1991; Isachsen and McKendree, 1977). The minimum displacement of this fault is estimated to be 350 to 400 meters and the dip of this fault is near vertical. This core was taken from the Little Falls Formation.

FRACTURE PATTERN: TOTAL NUMBER OF FRACTURES

The distribution of the total number of fractures was significantly different than if there were an equal number of fractures in each of the intervals when using an interval length of 12 meters (Table 11 and Figure 30). The total number of fractures decreases with depth from a high of 11 fractures to a low of 0 fractures over a distance of approximately 60 meters. The final interval had no fractures in it at all. No plumose markings or striations were observed on any of the fracture faces.

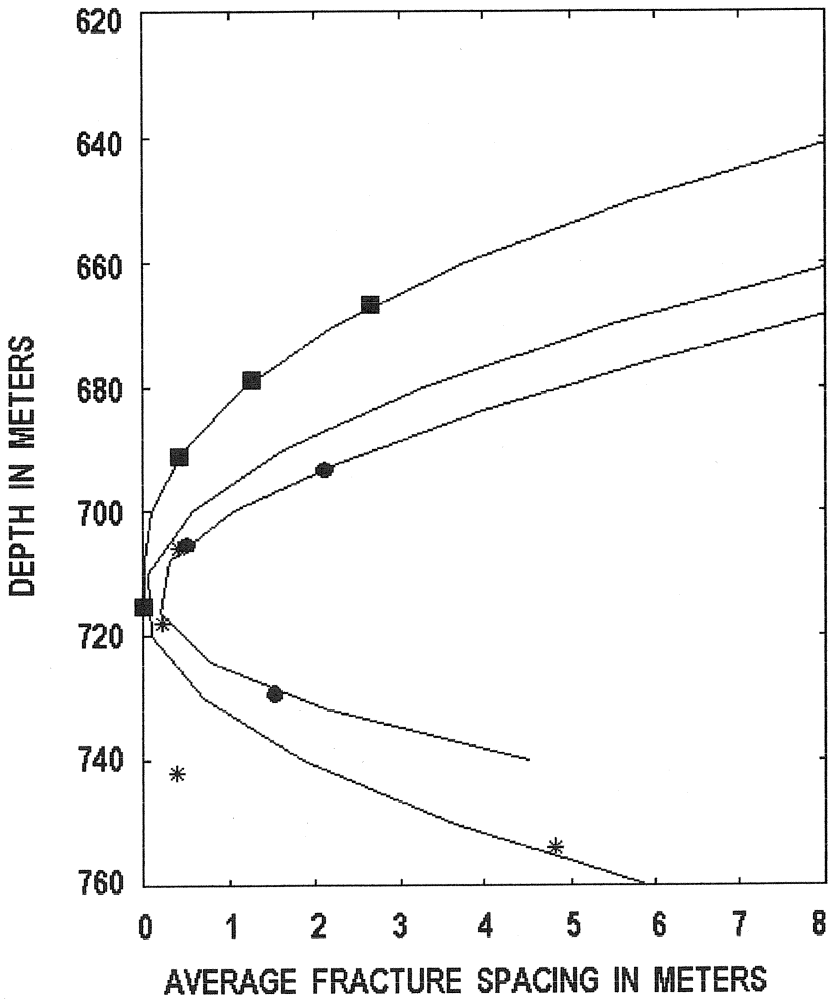

Figure 29. The polynomial curves modeling the rate of change of the average fracture spacing for cores 74-NY-11 (-■-) and 75-NY-2 (-●-) superimposed on the polynomial curve modeling the rate of average fracture spacing change in core 75-NY-14 (--*--). On this graph, the fracture spacing minimums for cores 74-NY-11 and 75-NY-2 were aligned with the fracture spacing minimum for core 75-NY-14. Core 75-NY-2 passed through a process zone, core 75-NY-14 passed through a process zone and an incipient fault and core 74-NY-11 passed through a fault that had an estimated displacement of 60 meter.

Table 11. Core 74-NY-10. Chi-square goodness of fit results for the distribution of all the fractures on this core (95 % confidence interval). Interval length - 12 meters.

Number of intervals	Number of fractures	Expected number of fractures per interval	Chi-square Computed	Chi-square Table
6	27	4.500	15.444	11.070

Table values from Davis (1986).

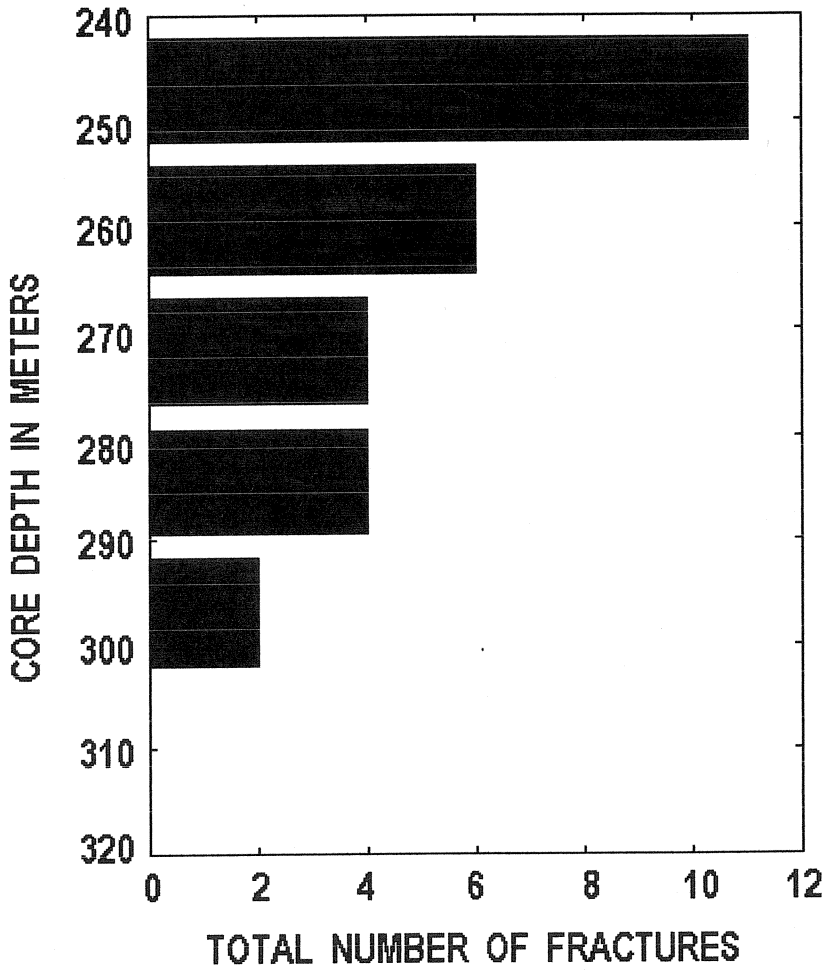

Figure 30. Core 74-NY-10. The total number of fractures per 12-meter interval of core (6 total). Total core length, 76 meters (241 to 317 meters below the surface).

INTERPRETATION

The fracture distribution pattern was due to the fact that the core had been taken from the footwall block, below the fault zone, of the steeply dipping normal fault (East Stone Arabia Fault) that is adjacent to the area where the core was taken. The diminishing number of fractures with depth indicates that the fault is not truly vertical, but does dip to the west at a very steep angle. If the fault was vertical, there would be a relatively consistent number of fractures, with depth, along a vertical core.

FRACTURE PATTERN: INDIVIDUAL FRACTURE SETS

All of the fractures on this core had a 90° dip, a 75° dip or a 70° dip. The 90° dipping fractures were the dominant set, both in terms of number and the number of intervals that contained the fractures. The distribution of each set of fractures was significantly different than if there were an equal number of fractures in each of the intervals when the interval length was 24 meters (Table 12, Figure 31). There was a consistent decrease in the number of 90° dipping fractures with depth. The 75° dipping fractures were found in a cluster at a depth of 254 meters whereas the 70° dipping fractures were found in a cluster at a depth of 278 meters.

INTERPRETATION

Based on the geometric relationship between the fractures, it was determined that the 90° dipping fractures are extension, or mode I fractures. Extension fractures typically form under low confining stress conditions (Dennis, 1972, Price, 1966 and Nelson, 2001). Extension fractures form parallel to the maximum and intermediate principal stresses and perpendicular to the minimum principal stress. The geometric relationship between the fractures was also used to identify the 70° and 75° dipping fractures as hybrid extension fractures. Hybrid extension fractures are characterized by a dihedral angle, separating the two conjugate fracture planes, less than 45° (Hancock et al., 1984). As with conjugate shear fractures, the angle between conjugate hybrid extension fractures is bisected by the maximum principal stress. The angle between hybrid extension fractures and true tensile, or extension fractures decreases with decreasing confining pressure (Hancock and Engelder, 1989). This would indicate a shallow depth of burial at the time of deformation. Dennis (1972) referred to fractures of this type as oblique extension fractures and considered them to be the result of extension across the fracture surface under a tensile normal stress component. The majority of the displacement in this case is extensional, with only a negligible shear component. These fractures may become faults with

Table 12. Core 74-NY-10. Chi-square goodness of fit results for the distribution of fractures with common dip angles (95 % confidence interval). Interval length - 24 meters.

Dip	Number of intervals	Number of fractures	Expected number of fractures per interval	Chi-square computed	Chi-square table
90°	3	19	6.333	6.456	5.991
75°	3	5	1.667	9.998	5.991
70°	3	3	1.000	6.000	5.991

Table values from Davis (1986).

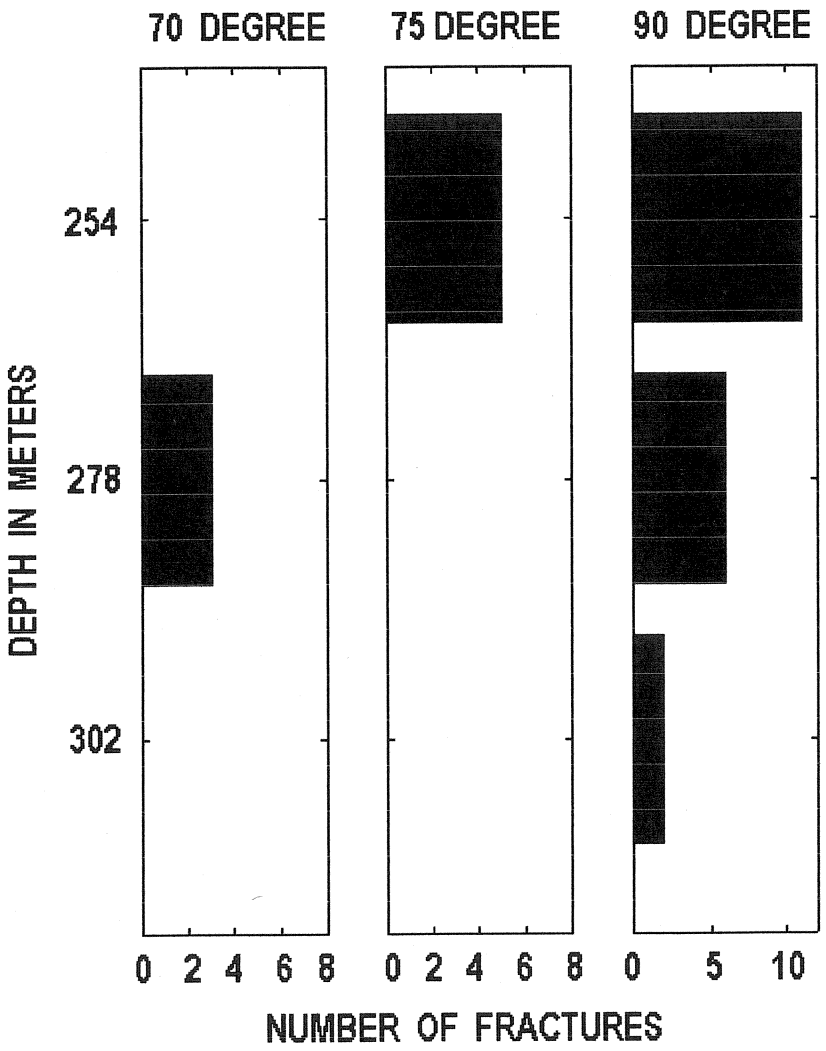

Figure 31. Core 74-NY-10. The number of 70°, 75° and 90° dipping fractures per 24-meter interval of core (3 total).

continuing deformation. As with the strike of the extension fractures, the strike of the hybrid extension fractures is parallel to the strike of the fault that the fractures are associated with. The 75° and 70° dipping fractures are thought to be conjugate to each other, but since the core was not orientated at the time of drilling there is no way to determine if this is true.

AVERAGE FRACTURE SPACING FOR THE EXTENSION FRACTURES, 24-METER INTERVALS

The average fracture spacing was calculated after Narr (1996) using an interval length of 24 meters, since these fractures did not have a statistically significant distribution using a 12-meter interval (Table 13 and Figure 32).

A ninth order polynomial was used to model the rate of change in the average fracture spacing value from one interval to the next (Figure 33). This polynomial curve passed through the centers of each of the 24-meter intervals. Lower order polynomials were not used since they formed parabolas, which did not accurately model the change in the average fracture spacing from one interval to the next. When extrapolated to a shallower depth, the polynomial curve did not intercept the 0-meter fracture spacing intercept, but approached a minimum value at a depth of approximately 220 meters.

INTERPRETATION

The pattern of increasing fracture spacing with depth for the extension fractures is consistent with the above interpretation that the core was taken from the foot wall block of the East Stone Arabia Fault. The extrapolation of the polynomial to a shallower depth indicates that there is a least centimeter scale (or smaller) fracture spacing at a depth of 220 meters. It is very probable that the fault plane is located very close to this depth.

Table 13. Core 74-NY-10. The average fracture spacing for the 90° dipping fractures. Interval length - 24 meters.

Method	Interval depth (m)	Average fracture spacing (m)
Narr, 1996	241 – 265	0.34
	265 – 289	1.13
	289 – 313	3.68

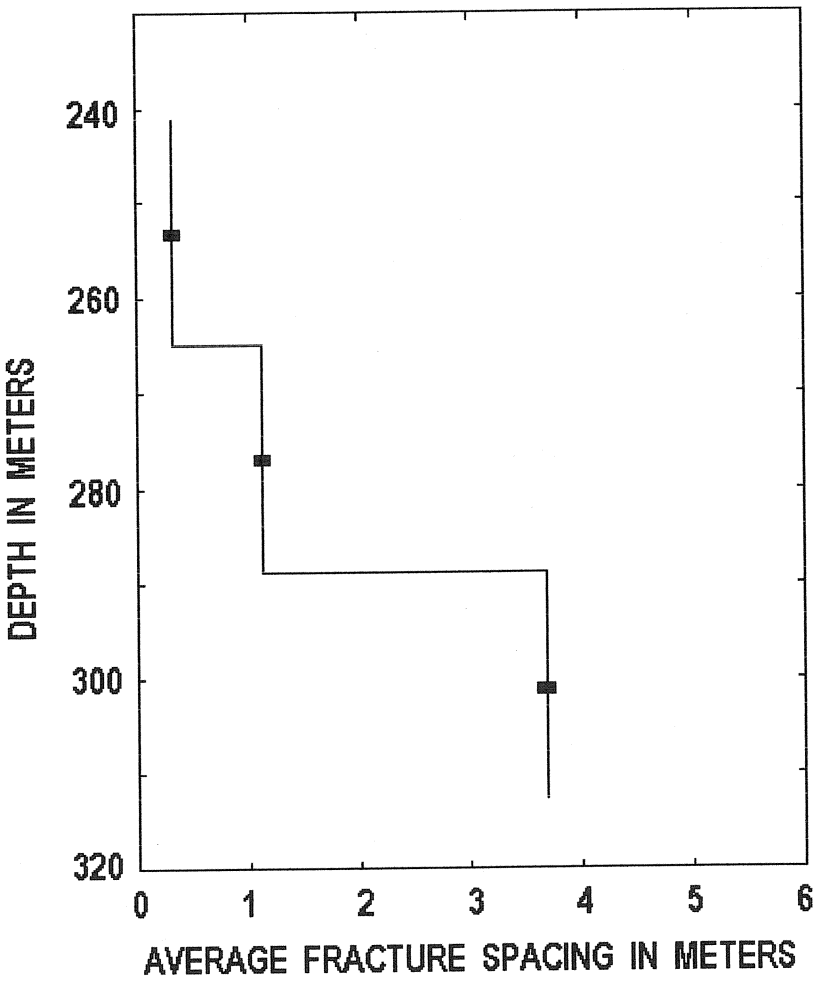

Figure 32. Core 74-NY-10. The change in average fracture spacing for each interval, with depth, for the extension fractures (after Narr, 1996). The stair step size is the length of the interval, 12 meters. The bars are the centers of the intervals. Interval length - 24 meters.

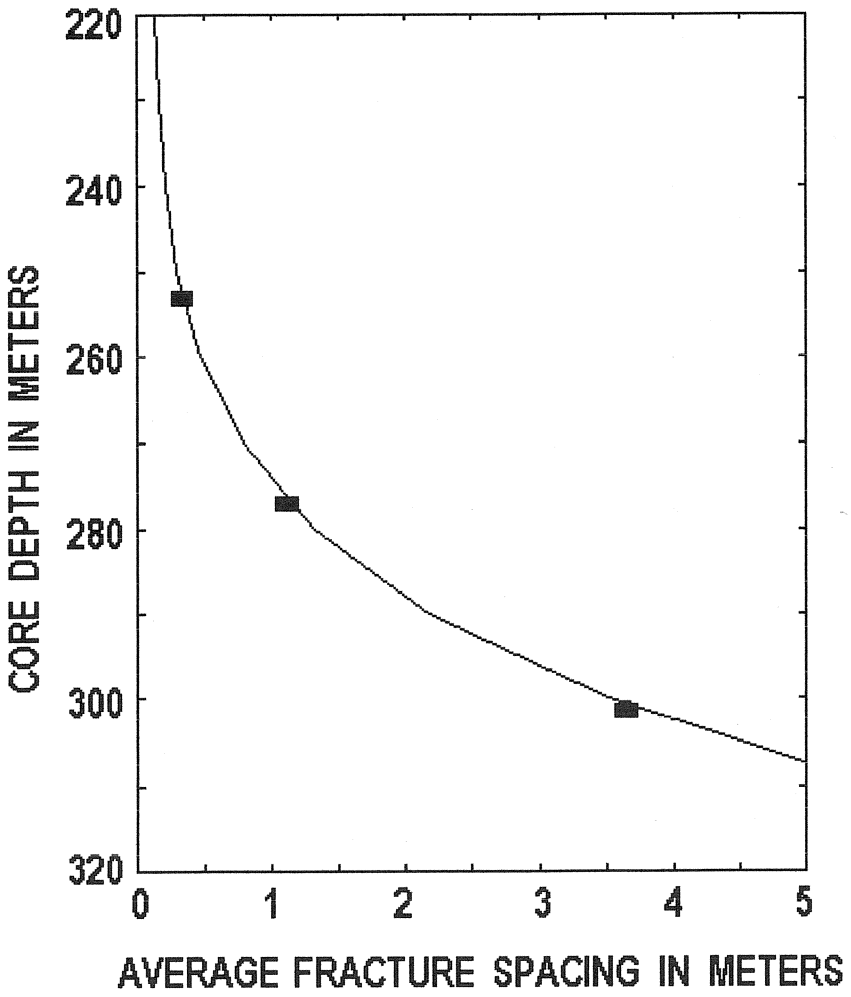

Figure 33. Core 74-NY-10. The change in the average fracture spacing with depth (after Narr, 1996). The line is a ninth order polynomial regression line linking the centers of the intervals (bars). The centimeter scale fracture spacing at 220 meters indicates that the fault is near this location. Interval length - 24 meters.

CORE 74-NY-6

CORE LOCATION

Core 74-NY-6 was taken just to the east of the near vertical Dolgeville fault (Figure 34) (Bradley and Kidd, 1991; Isachsen and McKendree, 1977). This fault is part of a north-northeast striking graben that is approximately 70 km long. The 76 meter long core was taken from a depth of 80 to 156 meters, where it intersected the Precambrian metamorphics.

The core was taken from the lower two units of the Little Falls Formation. The contact between the two layers on this core is estimated to be at a depth of 125 to 135 meters.

FRACTURE PATTERN: TOTAL NUMBER OF FRACTURES

When the total number of fractures, per 12 meter interval, was plotted against depth, the overall trend indicated that there was a decreasing number of fractures with depth (Figure 35). The trend was not a smooth one, due to a spike in the number of fractures as a depth of 122 meters. Chi-square testing indicated that the distribution of fractures was significantly different than if there were an equal number in each of the intervals (Table 14).

INTERPRETATION

The fracture pattern, along with the core location, would indicate that the core was taken from the footwall block of the Dolgeville fault, seen in map view, or a fault that formed parallel to the Dolgeville fault (Figure 34). This particular fracture pattern is similar to the fracture pattern seen in core 74-NY-10, since there is an overall decrease in the number of fractures with depth for both cores (Figure 30). The major difference between the two cores is core 74-NY-10 had a relatively smooth decrease in the number of fractures with depth whereas core 74-NY-6 did not. It was determined that core 74-NY-10 was taken from a footwall block.

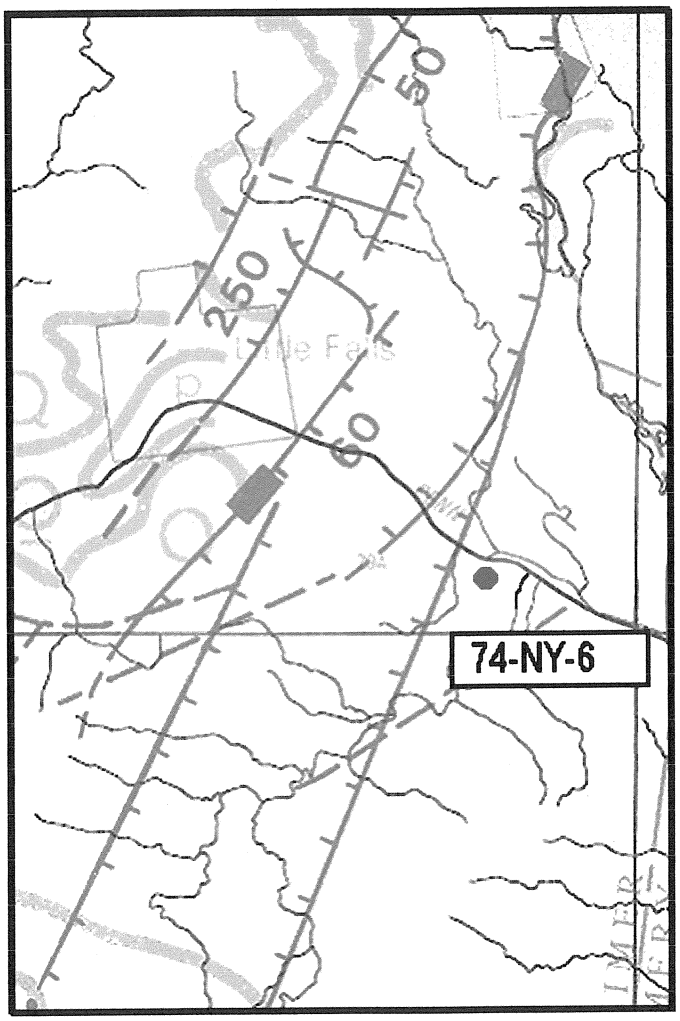

Figure. 34. The location of core 74-NY-6. The circle is the core location. The solid lines are normal faults, the hachure marks are on the relatively downthrown side of the faults. The rectangular bars over the faults indicate near vertical faults. The numbers indicate the estimated minimum fault displacement. Faults are dashed where inferred. Map width approximately 13 km.

Modified from Isachsen and McKendree, 1977.

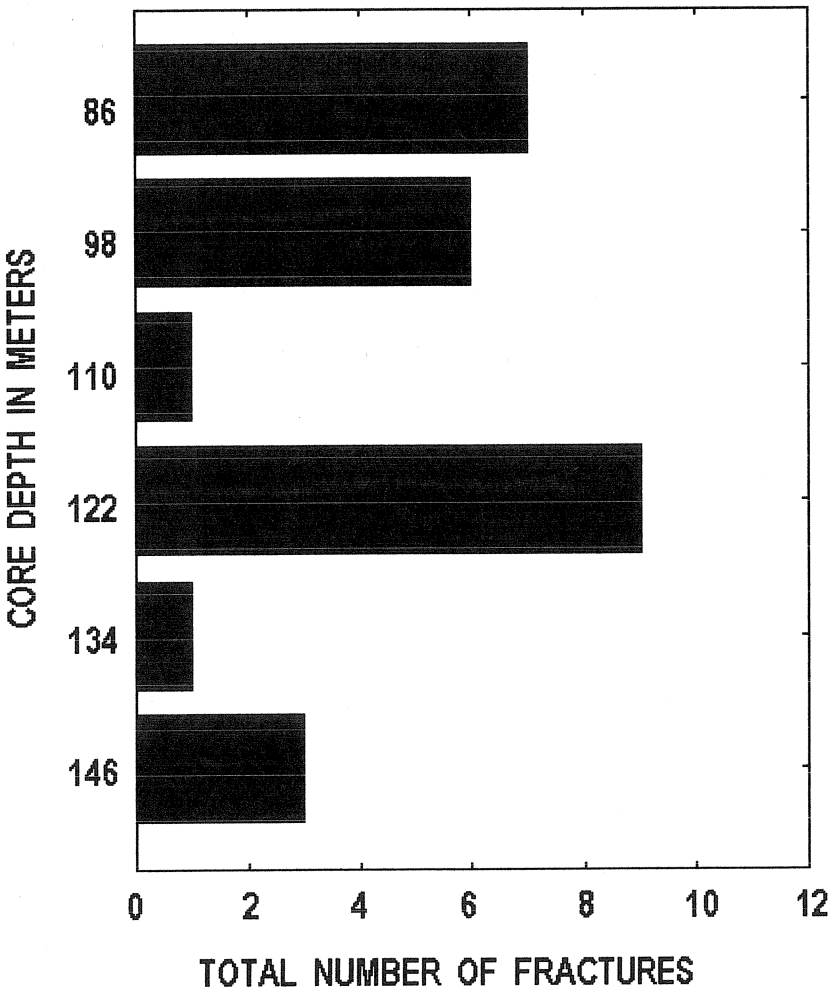

Figure 35. Core 74-NY-6. The total number of fractures per 12-meter interval of core (6 total). Total core length, 76 meters (80 to 156 meters).

Table 14. Core 74-NY-6. Chi-square goodness of fit results for the distribution of all the fractures on this core (95 % confidence interval). Interval length - 12 meters.

Number of intervals	Number of fractures	Expected number of fractures per interval	Chi-square Computed	Chi-square Table
6	27	4.5	12.333	11.070

Table values from Davis (1986).

FRACTURE PATTERN: INDIVIDUAL FRACTURE SETS

The fractures on this core had 90°, 60° and 70° dips (Figure 36). The 90° dipping fractures are the dominant fracture set. This was true both in terms of numbers of fractures and the number of intervals that contained the fractures. Despite the two intervals at depths of 110 and 134 meters, the 90° dipping fractures decreased steadily with depth. This is very similar to the fracture pattern for the 90° dipping fractures that was observed in core 74-NY-10, using a 24-meter core interval (Figure 31). The 60° dipping fractures were clustered at a depth of 122 meters and the single 70° dipping fracture was a depth of 146 meters.

INTERPRETATION

Based on the geometric relationship between the fractures, it was determined that the 90° dipping fractures are extension, or mode I fractures. Extension fractures typically form under low confining stress conditions and indicate that the rock behaved as a brittle material when subjected to stress (Dennis, 1972, Price, 1966 and Nelson, 2001). The geometric relationship between the fractures was also used to identify the 60° dipping fractures as shear fractures and the single 70° dipping fracture as a hybrid extension fracture. Chi-square testing indicated that the distribution of these fractures was significantly different than if there were an equal number in each of the intervals (Table 15).

The presence of the both the shear and the extension fractures is consistent with the stresses that would have produced normal faulting. In this case, the maximum principal stress axis would have been vertical and the minimum and intermediate principal stress axes would have been horizontal.

The cluster of shear fractures at a depth of 122 meters is an indication of a stress build up at that depth, which may have eventually lead to the formation of another fault in this area.

AVERAGE FRACTURE SPACING FOR THE EXTENSION FRACTURES, 12-METER INTERVALS

The average fracture spacing for each of the intervals was calculated after Narr (1996) using an interval length of 12 meters (Table 16 and Figure 37). The high fracture spacing values, at 110 and 134 meters, coincide with the intervals that had one and no fractures in them, respectively. Narr's (1996) method calculates a fracture spacing value of infinity for intervals that contain no fractures.

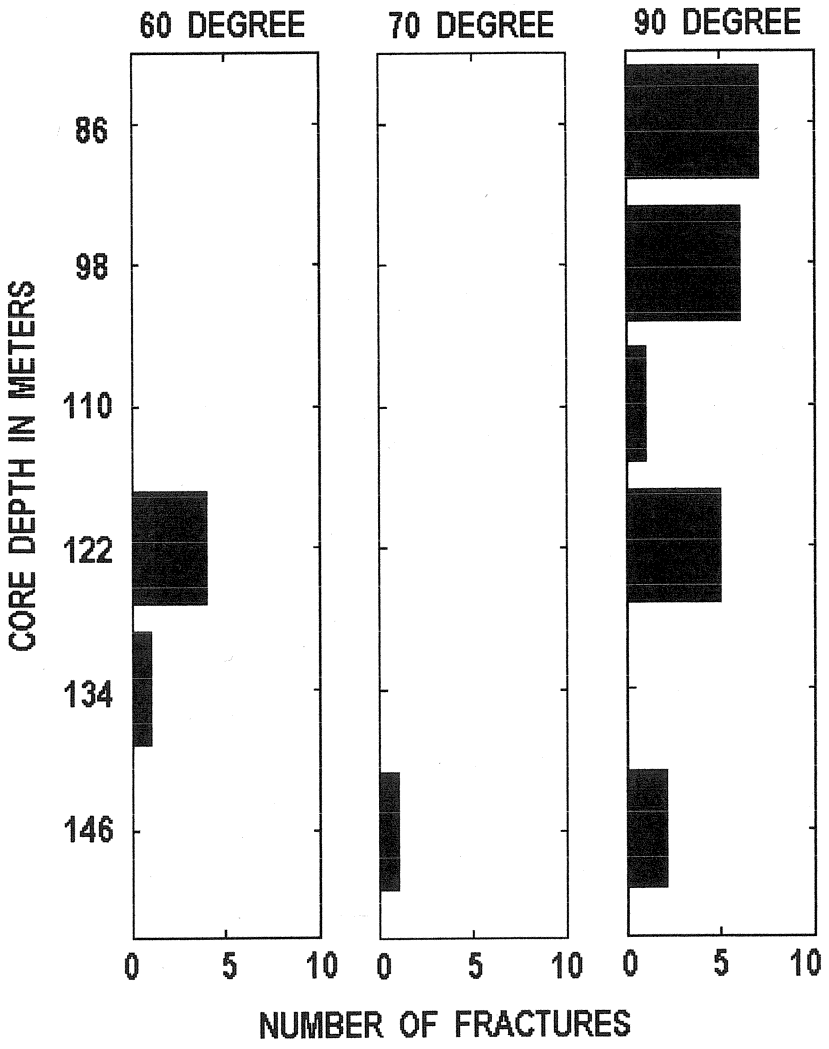

Figure 36. Core 74-NY-6. The number of 60°, 70° and 90° dipping fractures per 12-meter interval (6 total).

Table 15. Core 74-NY-6. Chi-square goodness of fit results for the distribution of fractures with 90° and 60° dip angles (95 % confidence interval). Interval length - 12 meters.

Dip	Number of intervals	Number of fractures	Expected number of fractures per interval	Chi-square computed	Chi-square table
90°	6	21	3.5	11.857	11.070
60°	6	5	0.833	15.462	11.070

Table values from Davis (1986).

Table 16. Core 74-NY-6. The average fracture spacing for the 90° dipping fractures (after Narr, 1996). Interval length - 12 meters.

Method	Interval depth (m)	Average fracture spacing (m)
Narr, 1996	80 – 92	0.36
	92 – 104	0.69
	104 – 116	6.00
	116 – 128	1.61
	128 – 140	∞ (1)
	140 – 152	2.18

(1) Values of infinity are calculated if there are no fractures in the interval.

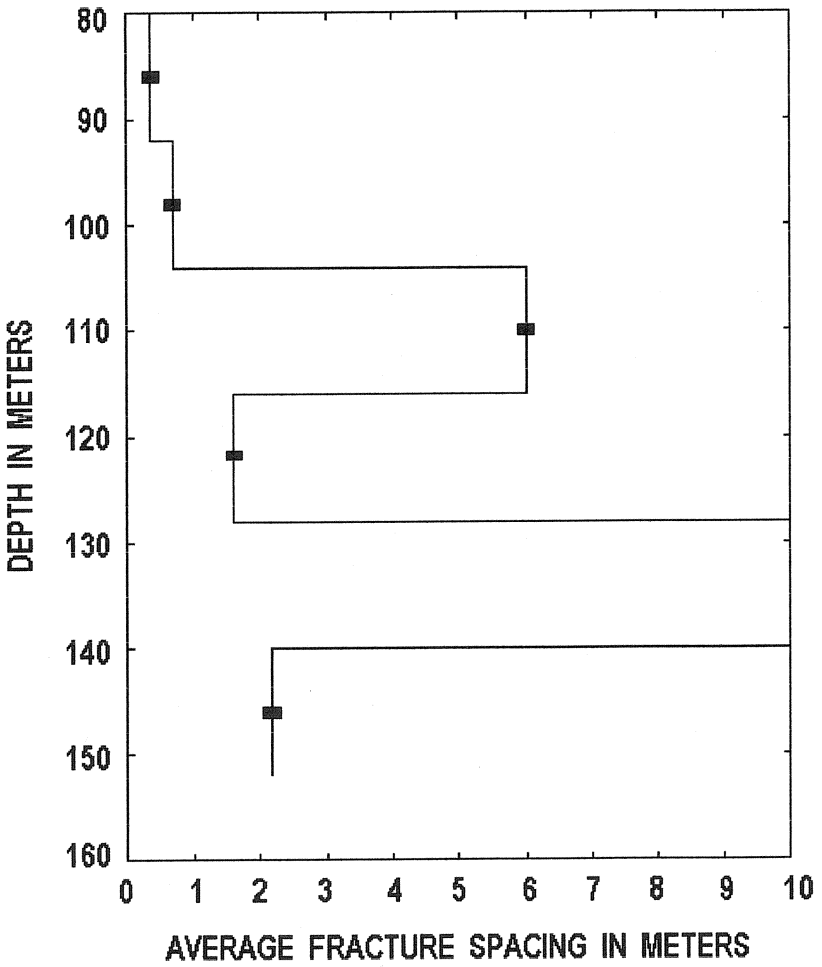

Figure 37. Core 74-NY-6. The change in average fracture spacing for each interval, with depth, for the extension fractures. The bars are the centers of each of the 12-meter intervals.

The rate of fracture spacing change with depth can be examined two different ways. The first way to examine the change in fracture spacing with depth is to drawn a curve through all the data points (Figure 38). A third order polynomial was used for this. This curve is sigmoidal in shape and the overall fracture spacing trend indicated that there was an increase in fracture spacing with depth.

The second way to examine the change in fracture spacing with depth is to model the rate of change by smoothing the curve to eliminate the high fracture spacing values at 110 and 134 meters (Figure 39). When this was done, the rate of increase in fracture spacing with depth was both smooth and slightly non-linear using a third order polynomial. When the polynomial was extrapolated to a shallower elevation, it approaches a minimum fracture spacing value at a depth of approximately 50 – 60 meters.

INTERPRETATION

The high fracture spacing values at 110 and 134 meters is consistent with the few fractures and no fractures, respectively, that were found in these intervals. Narr's (1996) method calculates an average fracture spacing value of infinity for intervals of core that don't contain any fractures.

The sigmoidal shaped curve may be recording multiple layers of a horizontal pattern of alternating high and low fracture frequency values (inverse of fracture spacing) that diminishes in intensity with increasing distance from a fault. This horizontal pattern has been documented by several workers (Shepherd, et al., 1981; Thamm 1939).

Thamm (1939) mapped fracture frequencies along several horizontal lines perpendicular to faults in the Pretoria series (quartzite) and Dolomite series of the West Witwatersrand area of South Africa (Figure 40). This mapping revealed a fairly symmetrical pattern on both sides of the fault line with the highest fracture frequency values adjacent to the fault; there was a distinct pattern of alternating high and low fracture frequency values that diminished in intensity with distance from the fault. This pattern was observed in both the quartzite and the dolomite.

Shepherd, et al. (1981) mapped fracture frequencies in sandstone in underground coal mines in Australia and found distinct and mappable increases in fracture frequency as faults were approached (Figure 41). As with Thamm's (1939) earlier work, Shepard et al. (1981) found a pattern of alternating high and low joint frequencies that diminished in intensity with distance from the faults along horizontal lines that were perpendicular to faults. The work of Shepherd, et al. (1981) indicated that the surface patterns of Thamm (1939) are also present in the subsurface.

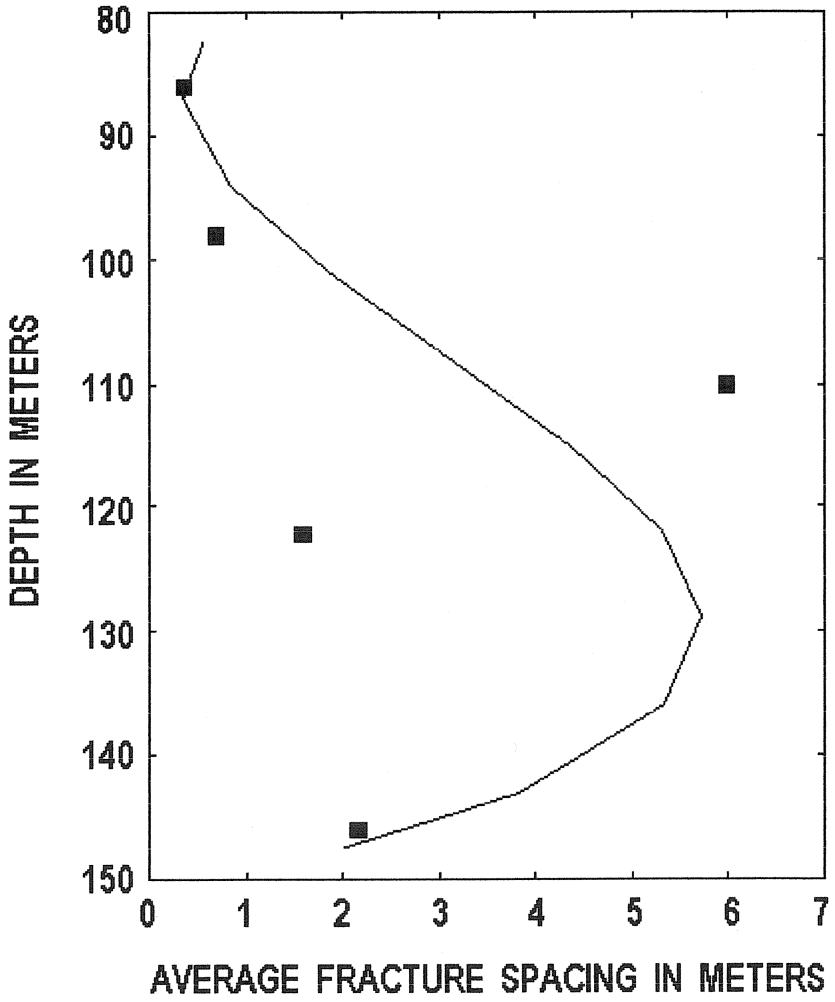

Figure 38. Core 74-NY-6. The change in average fracture spacing, with depth, for the extension fractures. The line is a third order polynomial. The bars are the centers of each of the 12-meter intervals. The fracture spacing value at a depth of 134 meters is infinity and is not on the graph.

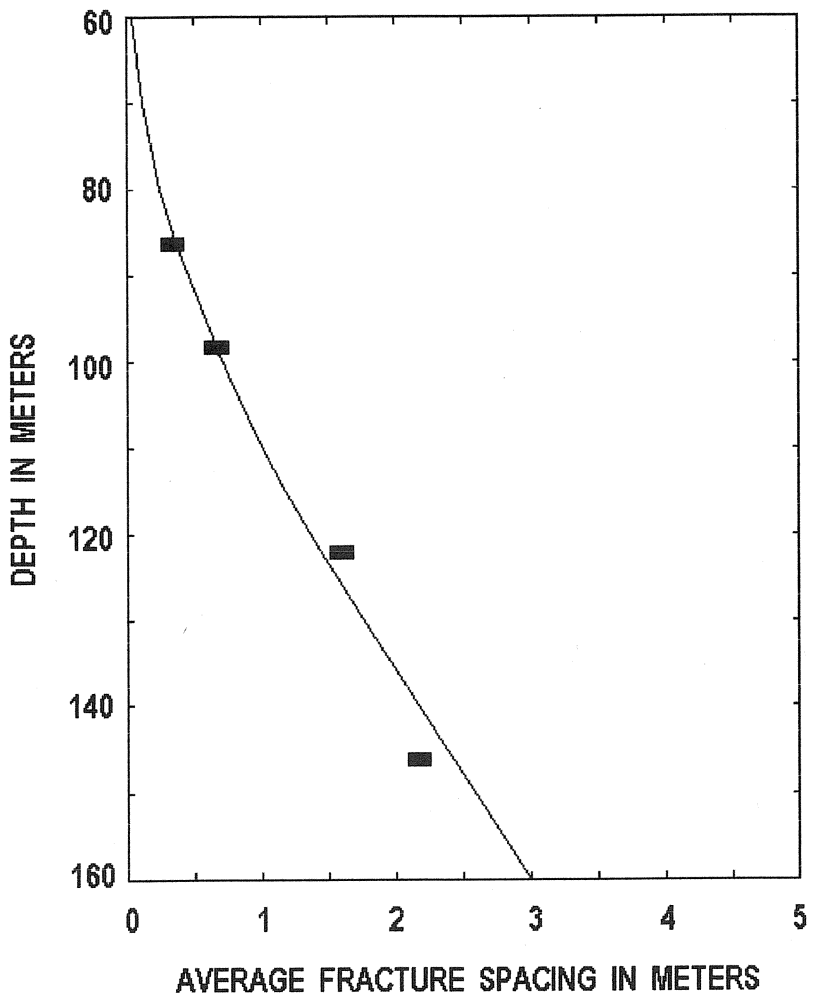

Figure 39. Core 74-NY-6. The change in average fracture spacing, with depth, for the extension fractures. The high average fracture spacing values, at depths of 110 and 134 meters, were not included so that the sigmoidal curve in Figure 38 could be smoothed. The bars are the centers of each of the 12-meter intervals. The line is a third order polynomial that was extrapolated to a depth of 60 meters.

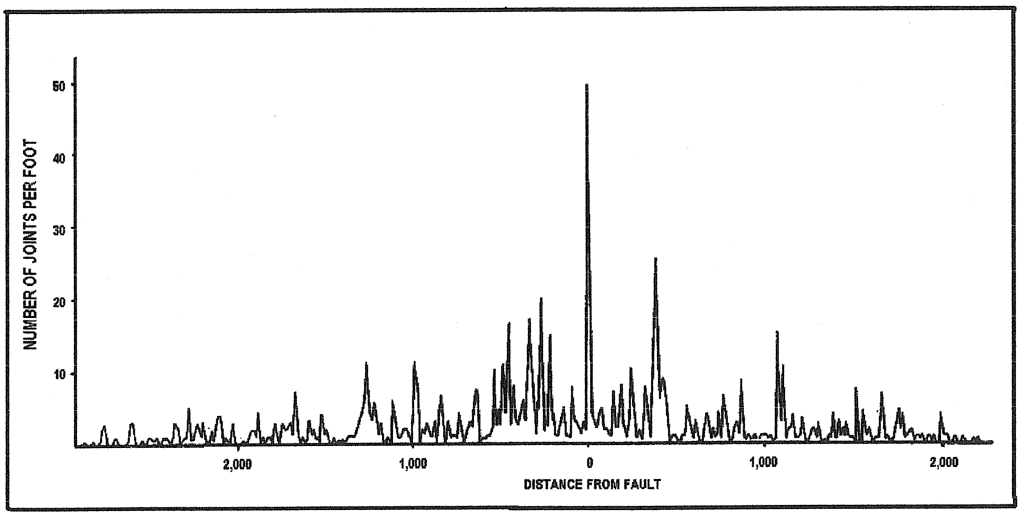

Figure 40. The changes in fracture frequency values along a line perpendicular to a fault in the Pretoria series quartzite, South Africa. Fracture frequency, in this case, records the number of fractures per foot. There is a pattern of alternating high and low fracture frequency values that decreases in value with distance from the fault. The overall trend is a decrease in fracture frequency with distance from the fault.

Source. Thamm, 1939.

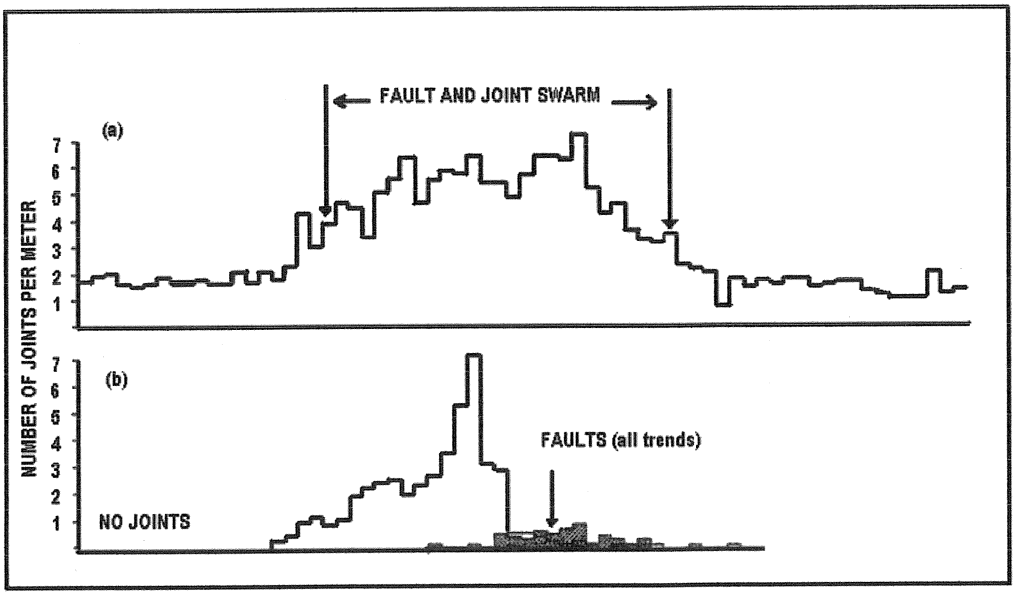

Figure 41. The joint frequency (number of joints per meter) associated with a fault that passed through sandstone in the Invincible colliery, New South Wales, Australia. The joint frequency values were measured along a line perpendicular to the fault.
Figure a - Northeast-southwest trending joints. The total width of the fault and joint swarm is 300 meters.
Figure b - North-south trending joints.

Modified from Shepherd, et al. (1981)

A pattern of alternating high and low fracture frequencies, or fracture spacing values that diminishes in intensity with distance from a fault is easy to recognize along a horizontal line. Graphically, this pattern can be represented by a fracture frequency, or fracture spacing wave (Figure 42). Due to the dip of the fault, the start of the wave along any horizontal plane is offset in the dip direction with depth (Figure 43). The amount of offset can be determined using Pythagorean's theorem, $\tan A = x / y$, where A is the angle between the fault plane and the vertical plane and x is the horizontal offset due to the change in depth, y. If the dip angle of the fault is 60°, the angle between the fault plane and the vertical plane is 30° and the horizontal offset of the wave, at a depth of 50 meters, is 28.8 meters. Thamm (1939) measured the alternating high and low fracture frequency pattern for over 600 meters, normal to the fault (Figure 40). This indicates that this pattern should be detected vertically for over 1,000 meters.

Depending on the wavelength of the fracture frequency wave, there is a very good chance that the fracture frequency waves of several horizontal profiles will not be in phase (Figure 43). As a result, a vertically drilled core may alternately intersect horizons of high and low fracture frequencies with depth. This will be recorded as a pattern of vertically alternating high and low fracture frequency values, or fracture spacing values, along the length of the core. This may be the cause of the sigmoidal fracture spacing pattern seen in cores 74-NY-6 (Figure 38).

Smoothing the sigmoidal curve allowed for additional interpretations that, while different, do not contradict, or diminish the interpretations made from the sigmoidal curve. The increase in fracture spacing with depth for the smoothed curve indicates that the Dolgeville fault is not truly vertical. If it were, there would have been a relatively constant number of fractures along the vertically drilled core.

If the section of curve, that was extrapolated to a shallower depth, accurately models the change in fracture spacing, it would indicate that there is either a fault present at a depth close to 60 meters, or a highly fractured fault process zone that did not achieve faulting. The lack of shear fractures toward the top of the core suggests that faulting did not occur, since cores 74-NY-10 and 74-NY-11 had an increase in both the number of extension and shear fractures as the cores approached faults.

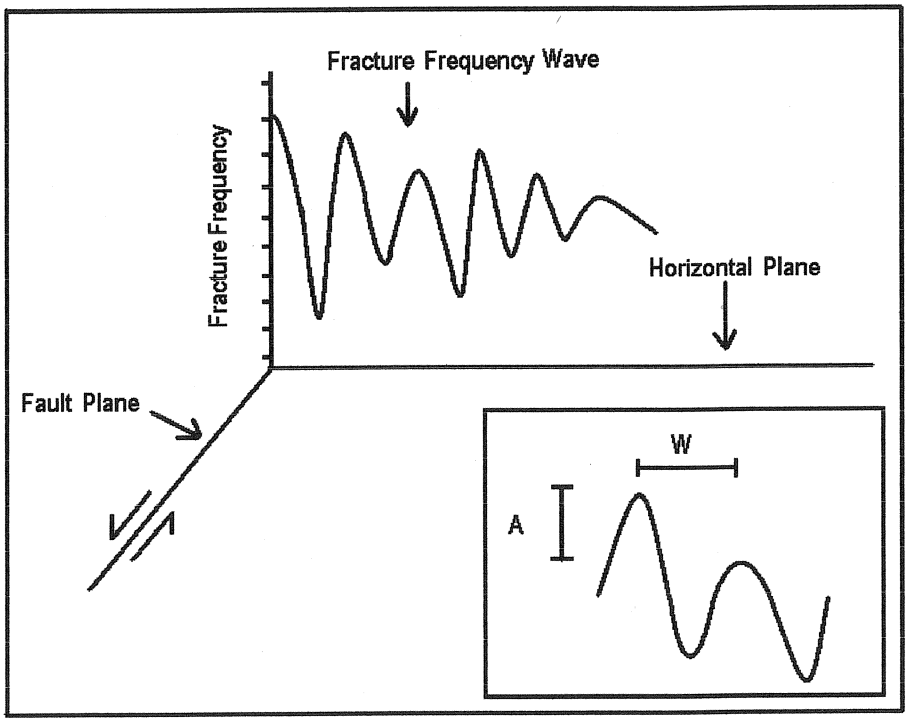

Figure 42. Fracture frequency wave. The pattern of alternating high and low fracture frequency values that diminishes in intensity with distance from a fault along a horizontal plane can be modeled by a wave. The wavelength and amplitude of this wave may vary considerably (W and A, respectively, in the insert).

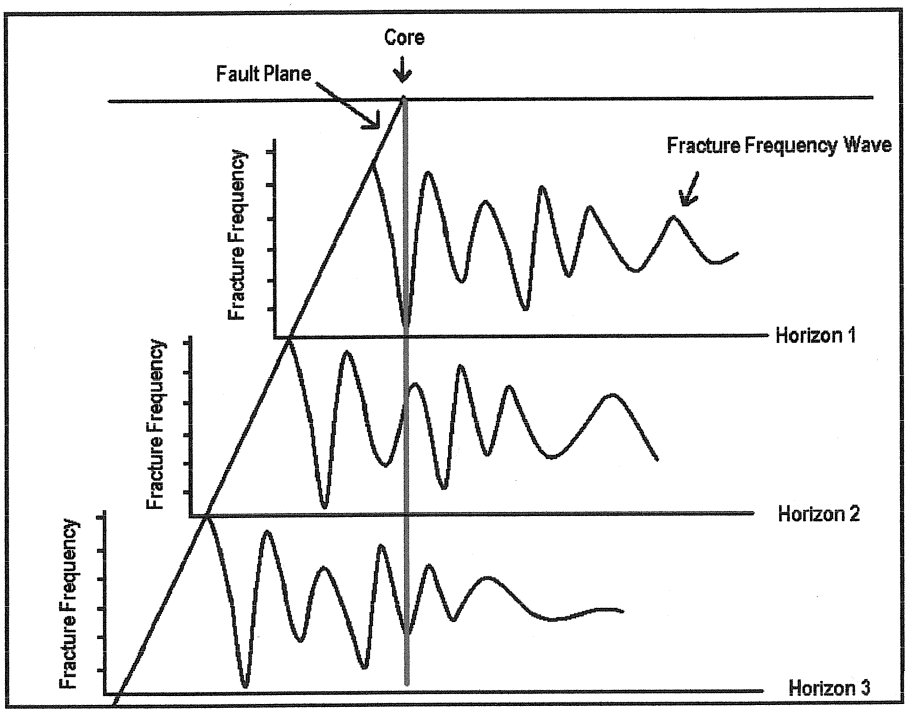

Figure 43. The fracture frequency waves along three horizontal profiles. Each wave is at s different depth below the surface. Each wave has a pattern of diminishing high and low values as the distance from the fault plane increases. The intersection of a vertical core with the fracture frequency wave at each horizon is out of phase with the fracture frequency wave of the overlying horizon as the core gets deeper. This results in an increasing and decreasing number of fractures along the length of a vertical core. This wave can also be used to record fracture spacing, which is the inverse of fracture frequency.

It is appropriate to make a comparison between the rate of increase in fracture spacing for cores 74-NY-6 and 74-NY-10, since they both came from the footwall blocks of near vertical faults. In order to make a more legitimate comparison, the rate of increase in fracture spacing for core 74-NY-10 was recalculated using 12 meter intervals, since the fracture spacing for this core was originally calculated using 24 meter intervals. When the fracture spacing curve, using 12-meter intervals was superimposed over the fracture spacing curve for core 74-NY-6, the curves were virtually identical (Figure 44). The identical shape of these curves is consistent with the fact that both cores passed through the same lithologies, the Little Falls formation, and both areas share the same stress history. Their identical shape also indicates that the width of the fracture zones within these two footwall blocks is the same.

CORE 74-NY-7

CORE LOCATION

Core 74-NY-7 is 84 meters long and was taken from a depth of 130 to 214 meters between two parallel, westward dipping normal faults (Figure 45) (Isachsen and McKendree, 1977). The core location is approximately 2 km from each fault. The fault to the east, the Sprakers fault, has a minimum estimated displacement of 40 meters, the displacement of the fault to the west is unknown.

The core was taken from the Little Falls Formation, just below the contact with the overlying Fort Johnson member of the Tribes Hill Formation (Curl, 1983). The top of the core was taken from unit D of the Little Falls Formation. Below unit D, unit C extends downward to a depth of approximately 150 meters. Unit B extends downward to a depth of approximately 200 meters. Below 200 meters, the dolomitic portion of unit A extends downward to a depth of 218 meters where it comes into contact with the basal sandstone and conglomerate layer. The Precambrian contact is at a depth of 219 meters.

FRACTURE PATTERN: TOTAL NUMBER OF FRACTURES

When analyzing this particular core, chi-square testing was performed using interval lengths of 12, 24 and 36 meters. In each case, chi-square testing indicted that the distribution of fractures was not significantly different than if there were an equal number of fractures in each of the intervals. An interval length of 12 meters was used for the fracture analyses so that this core could be better compared to the others, which were mostly analyzed using 12-meter core intervals.

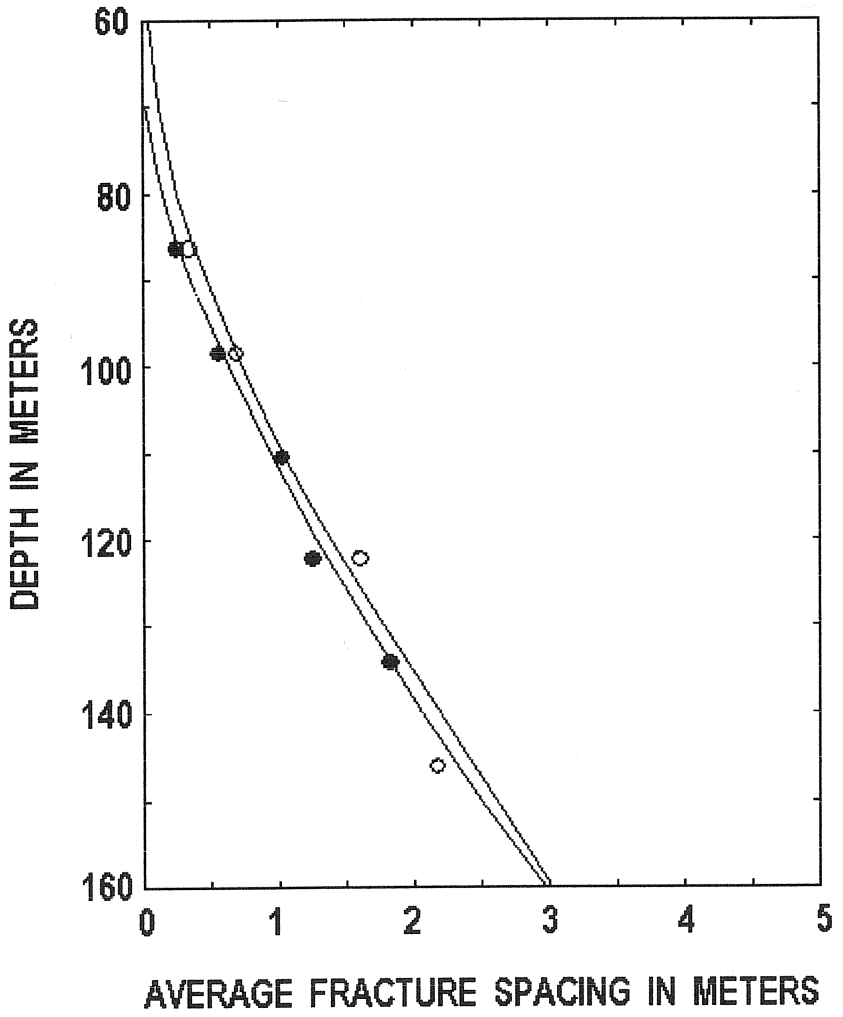

Figure 44. The fracture spacing curve for core 74-NY-10 (-●-) superimposed over the fracture spacing curve for core 74-NY-6 (-○-). The fracture spacing curves for both cores were calculated using 12-meter intervals, so that a direct comparison between the two could be made.

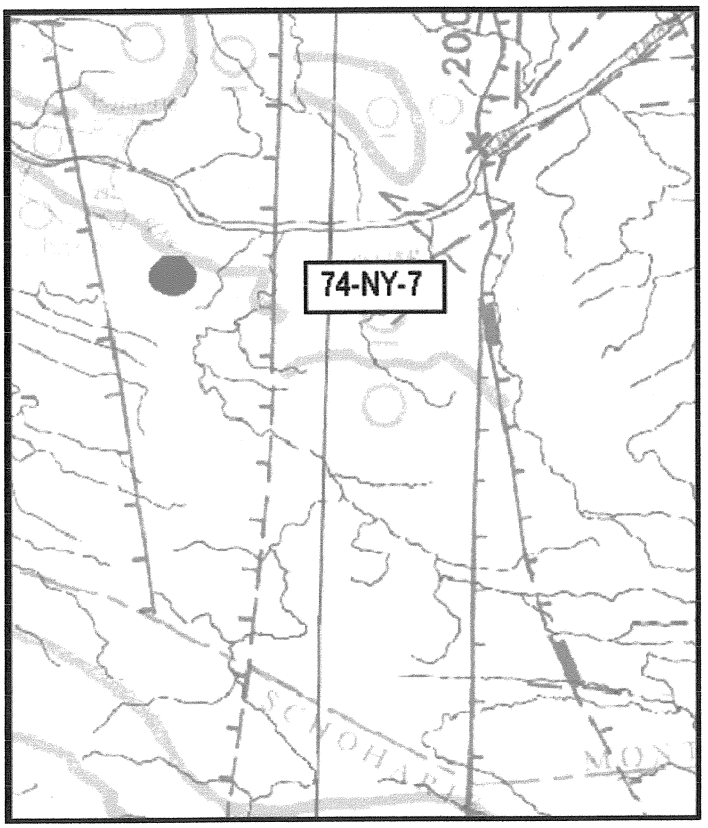

Figure 45. The location of core 74-NY-7. The circle is the core location. The solid lines are normal faults, dashed where inferred. Hachure marks are on the relatively downthrown side of the faults. The rectangular bars next to the fault indicate a high angle normal faults. Fault lines are dashed where inferred. Numbers indicate minimum estimated displacement, in meters.

Modified from Isachsen and McKendree, 1977. Map width approximately 17 km.

When the total number of fractures per 12-meter interval of core was plotted against depth, the number of fractures was found to be both fairly high and consistent with depth (Figure 46).

This core had the largest number of vugs of all the core samples examined for this study (Figure 47). This core also had the most fractures out of any of the cores that were examined for this study.

INTERPRETATION

It was determined that the high number of fractures was due to its position between two closely spaced faults. This is consistent with the findings of Nelson (2004), who has indicated that the area between two closely spaced faults is an area of intense fracturing due to the propagation of two different faults. In this case, there is a process zone for each one of the faults. The process zones overlap each other, since they are so close together. This increases the amount of fractures that are found within the bedrock between the two faults. Slip-related fractures from each of the faults may be an additional source of fractures within this bedrock.

Concerning the large amount of vugs that were found in this core, it is very possible that the high number of fractures found within the core aided the flow of the diagenetic fluid that produced the vugs.

FRACTURE PATTERN: INDIVIDUAL FRACTURE SETS

All but three of the fractures on this core had a 90° dip (Figure 48). These three fractures had dips of 70°, 60° and 45°. Quite clearly, the 90° dipping fractures were the dominant set, both in terms of number of fractures and the number of intervals that contained the fractures. There were also noticeably fewer shear fractures in this core, when compared to the other cores which were examined.

As with the distribution of the total number of fractures, the distributions of the individual sets of fractures were not significantly different than if there were an equal number of fractures in each of the intervals using interval lengths of 12, 24 and 36 meters. An interval length of 12 meters was used for the analyses, so that the results could be compared to the other cores, which mostly had statistically significant distributions using 12-meter intervals.

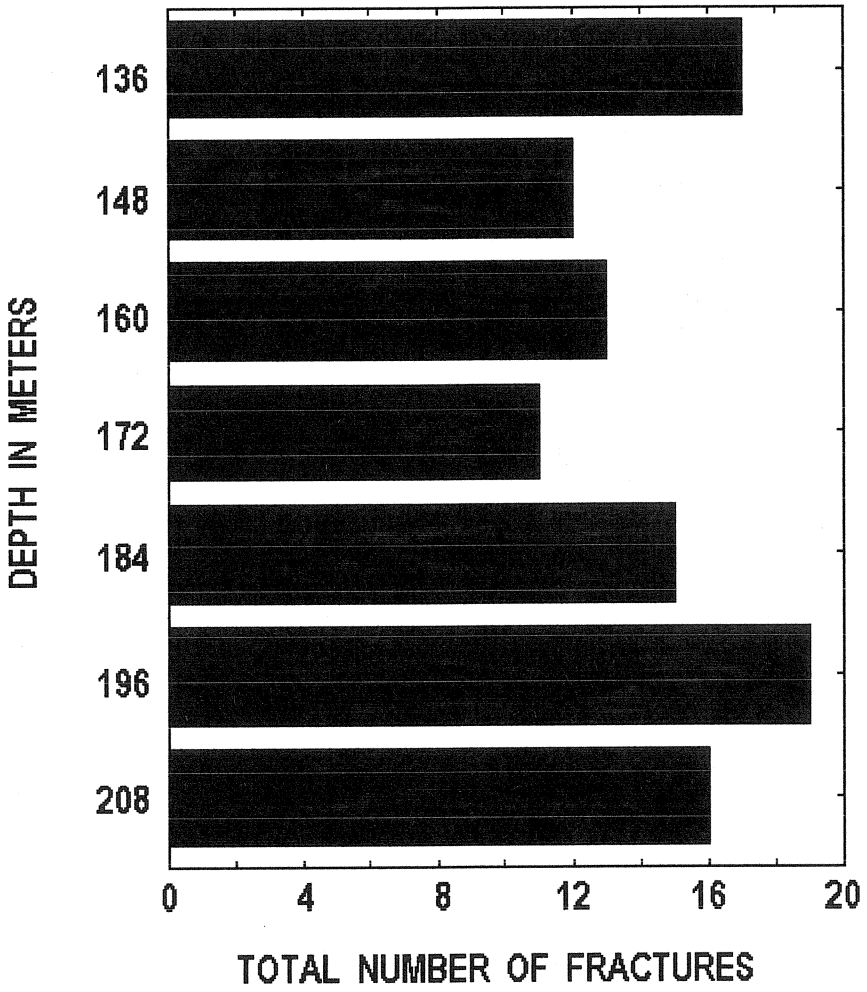

Figure 46. Core 74-NY-7. The total number of fractures per 12-meter interval of core (7 total). Total core length, 85 meters (130 – 215 meters below the surface).

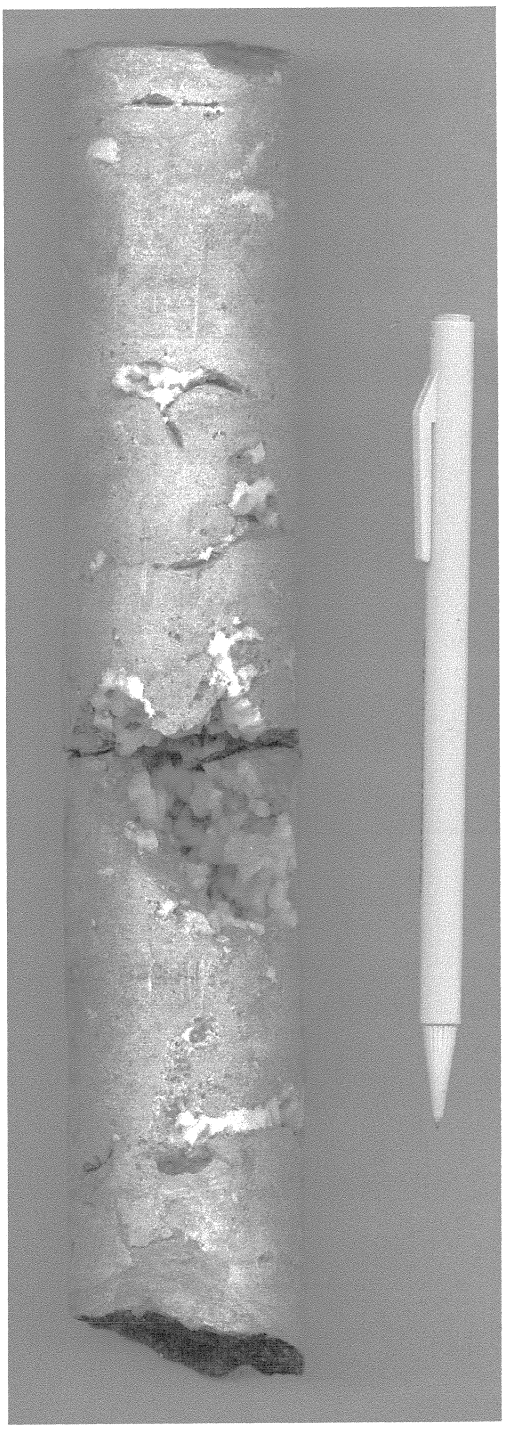

Figure 47. Core 74-NY-7. Vuggy porosity. The large vug is approximately 4 cm across. The crystals within the vug are dolomite. Core diameter 5.08 cm, core depth 190 meters.

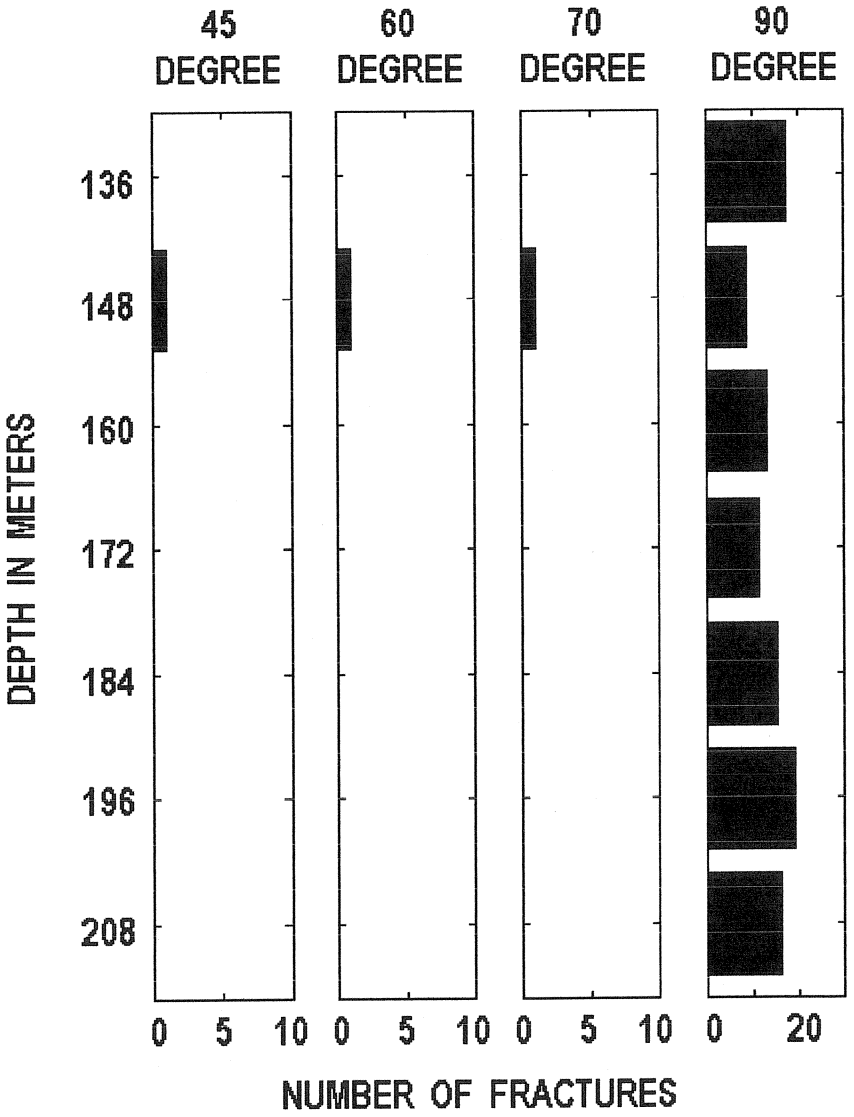

Figure 48. Core 74-NY-7. The number of 45°, 60°, 70° and 90° dipping fractures per 12-meter interval of core (7 total).

INTERPRETATION

Based on the geometric relationship between the fractures, it was determined that the 90° dipping fractures are extension, or mode I fractures. Extension fractures typically form under low confining stress conditions and indicate that the rock behaved as a brittle material when subjected to stress (Dennis, 1972, Price, 1966 and Nelson, 2001). The geometric relationship between the fractures was also used to identify the 60° and 45° dipping fractures as shear fractures and the 70° dipping fracture as a hybrid extension fracture. Considering the fact that this core was taken several kilometers from the closest fault, the few number of shear fractures found along this core may indicate that shear fractures are more prevalent near faults.

AVERAGE FRACTURE SPACING FOR THE EXTENSION FRACTURES, 12-METER INTERVALS

The average fracture spacing was calculated for the extension fractures using an interval length of 12 meters (Table 17 and Figure 49). There is no clear indication if there is a pattern of increasing or decreasing fracture spacing with depth.

When a third order polynomial was drawn through the centers of the 12-meter intervals, a very distinct sigmoidal pattern of increasing and decreasing average fracture spacing values with depth became apparent (Figure 50).

INTERPRETATION

The sigmoidal pattern, of increasing and decreasing average fracture spacing values with depth, that was seen in this core is very similar to the sigmoidal pattern observed in core 74-NY-6. As detailed above, this sigmoidal shaped curve may be recording multiple layers of a horizontal pattern of alternating high and low fracture frequency values (inverse of fracture spacing) that diminishes in intensity with increasing distance from a fault. Refer to the analysis of core 74-NY-6 for a detailed explanation.

Table 17. Core 74-NY-7. The average fracture spacing for the 90° dipping fractures. Interval length - 12 meters.

Method	Interval depth (m)	Average fracture spacing (m)
Narr, 1996	130 – 142	0.19
	142 – 154	0.60
	154 – 166	0.50
	166 – 178	0.44
	178 – 190	0.13
	190 – 202	0.16
	202 – 214	0.36
	130 – 214(1)	0.25

(1) Values if the entire length of the core was used as a single interval.

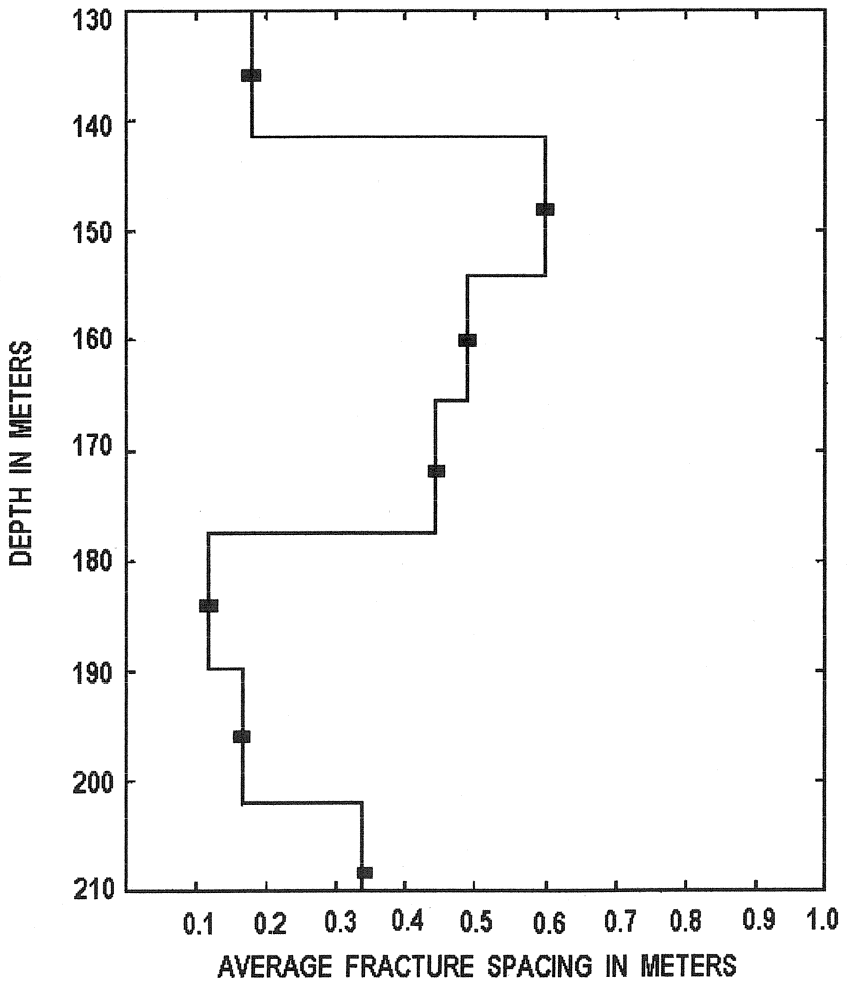

Figure 49. Core 74-NY-7. The change in average fracture spacing for each interval, with depth, for the extension fractures. The size of the stair step is the size of the interval. The bars are the centers of the 12-meter intervals.

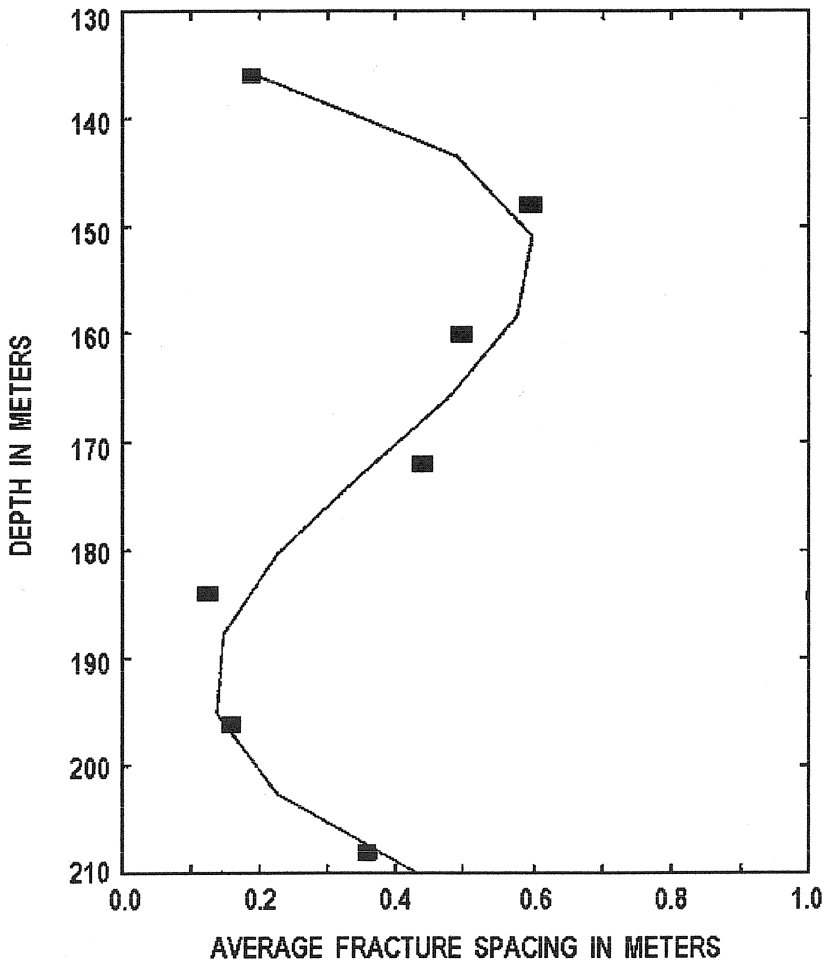

Figure 50. Core 74-NY-7. The change in average fracture spacing, with depth, for the extension fractures. The line is a third order polynomial, the bars are the centers of the 12-meter intervals.

CORE 74-NY-13

CORE LOCATION

Core 74-NY-13 was taken from a location that was approximately 5 to 6 km from both the Fultonville and Tribes Hill faults (Figure 51) (Bradley and Kidd, 1991; Isachsen and McKendree, 1977). Both faults dip to the east. Core 74-NY-13 is 104 meters long and was taken from a depth of 181 to 285 meters (596 – 935 feet). The top of the core was taken from the Little Falls formation, the bottom was taken from the Galway formation (Phillips and Friedman, 2001; Rickard, 1973; Zagorski, 1981). The contact with the underlying Galway formation was placed at a depth of approximately 230 to 260 meters.

FRACTURE PATTERN: TOTAL NUMBER OF FRACTURES

When the total number of fractures per 24-meter interval of core was plotted against depth, there was a spike in the number of fractures at a depth of 251 meters (Figure 52). No rubble was found at this depth, or anywhere else in the core. Chi-square testing indicted that this fracture distribution was significantly different than having an equal number of fractures in each of the intervals using an interval length of 24 meters, but not at 12 meters (Table 18).

INTERPRETATION

The peak in the number of fractures at a depth of 251 meters indicates that there was a stress build up at that depth. The fact that the peak, at 251 meters, has a lower number of fractures both above and below it indicates that this core did not approach a fault zone. The lack of rubble within the core also indicates that the core did not pass through a fault zone. The peak in the number of fractures suggests that a process zone was starting to develop at this depth.

FRACTURE PATTERN: INDIVIDUAL FRACTURE SETS

All the fractures on this core had either a 90°, 75°, or a 60° dip (Figure 53). The 90° dipping fractures were the dominant set, both in terms of number and the number of intervals that contained the fractures. The number of 90° dipping fractures was low and relatively constant with depth, except for a spike in number at a depth of 245 meters. Despite this spike in fracture number, the distribution of the 90° dipping fractures was not significantly different than if there were an equal number of fractures in each of the intervals, using interval lengths of 12, 24 or 36 meters.

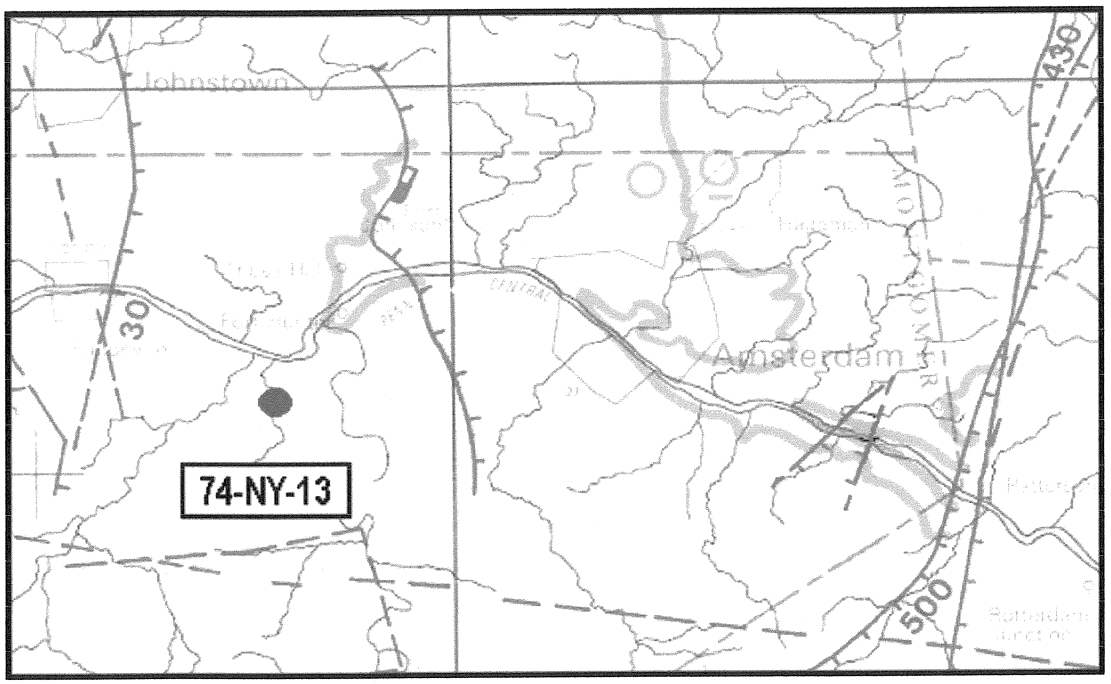

Figure 51. The location of core 74-NY-13. The circle is the location of the core. The solid lines are normal faults, dashed where inferred. Hachure marks are on the relatively downthrown side of the faults. The rectangular bar (half solid - half open) next to fault line indicates a low angle normal fault. The numbers next to the fault lines indicate the estimated minimum displacement, in meters.
Map width approximately 30 km

Modified from Isachsen and McKendree, 1977.

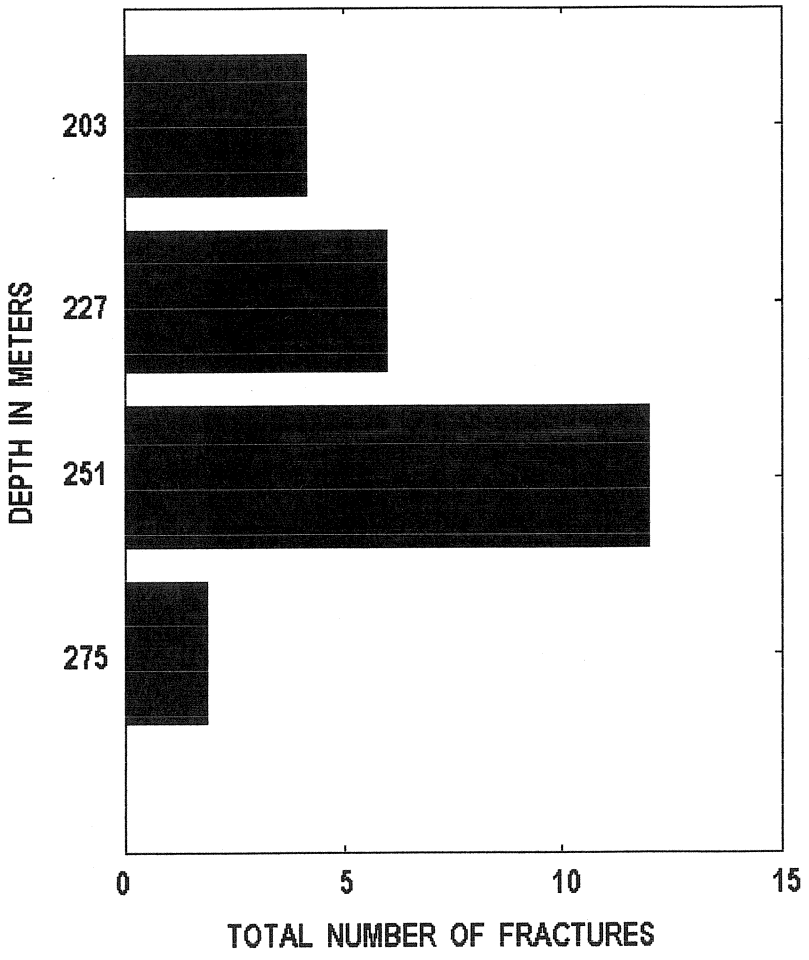

Figure 52. Core 74-NY-13. The total number of fractures per 24-meter interval of core (9 total).

Table 18. Core 74-NY-13. Chi-square goodness of fit results for the distribution of all the fractures on this core (95 % confidence interval). Interval length - 24 meters.

Number of intervals	Number of fractures	Expected number of fractures per interval	Chi-square computed	Chi-square table
4	24	6.0	9.33	7.815

Table values from Davis (1986).

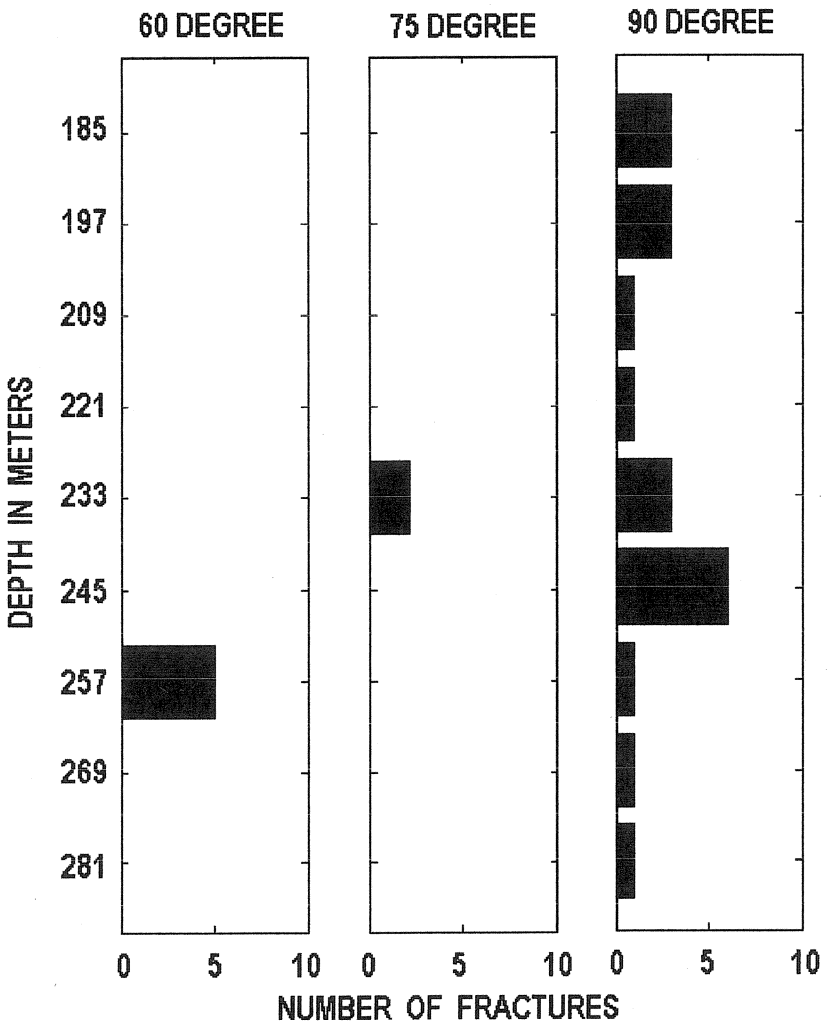

Figure 53. Core 74-NY-13. The number of 60°, 75° and 90° dipping fractures per 12-meter interval of core (6 total).

There are much fewer 90° dipping fractures on this core, than on core 74-NY-7 (Figures. 48 and 53). Despite the differences in the number of 90° dipping fractures between these two cores, the distributions are similar. These differences are noted, since both cores were taken between parallel to subparallel normal faults and did not intersect a fault zone.

The 75° and 60° dipping fractures were clustered at depths of 233 and 257 meters, respectively (Figure 53). These depths are very close to the depth where the spike in the number of 90° dipping fractures was found. The distributions of the 75° and 60° dipping fractures were significantly different than if there were an equal number of fractures in each of the intervals, using an interval length of 12 meters (Table 19).

INTERPRETATION

Based on the geometric relationship between the fractures, it was determined that the 90° dipping fractures are extension, or mode I fractures. The geometric relationship between the fractures was also used to identify the 60° dipping fractures as shear fractures and the 75° dipping fractures as hybrid extension fractures.

The fact that all three types of fractures peaked at roughly the same depth strengthens the initial interpretation that a process zone was in the initial stages of formation at a depth of approximately 230 to 260 meters.

The low number of fractures on this core, as opposed to core 74-NY-7, is due to the fact that this core was taken between two widely spaced faults of low displacement. The core's position between the two faults was at the outside edges of the area affected by the process zones of either fault. As a result, this core did not have nearly the number of fractures as core 74-NY-7. The comparison between cores 74-NY-7 and 74-NY-13 indicates that the amount of fracturing within the bedrock is directly proportional to the distance that the bedrock is from a fault.

AVERAGE FRACTURE SPACING FOR THE EXTENSION FRACTURES, 12-METER INTERVALS

The average fracture spacing was calculated for the extension fractures using an interval length of 12 meters (Table 20 and Figure 54). There was no clear indication of a pattern of either increasing or decreasing fracture spacing with depth, although a slight increase in spacing with depth may be present.

Table 19. Core 74-NY-13. Chi-square goodness of fit results for the distribution of fractures with 60° and 75° dip angles (95 % confidence interval). Interval length - 12 meters.

Dip	Number of intervals	Number of fractures	Expected number of fractures per interval	Chi-square computed	Chi-square table
60°	9	5	0.555	40.040	15.507
75°	9	2	0.222	16.016	15.507

Table values from Davis (1986).

Table 20. Core 74-NY-13. The average fracture spacing for the 90° dipping fractures. Interval length - 12 meters.

Method	Interval depth (m)	Average fracture spacing (m)
Narr, 1996	179 – 191	0.88
	191 – 203	1.57
	203 – 215	2.91
	215 – 227	6.00
	227 – 239	2.04
	239 – 251	0.76
	251 – 263	13.70
	263 – 275	4.80
	275 – 287	2.30

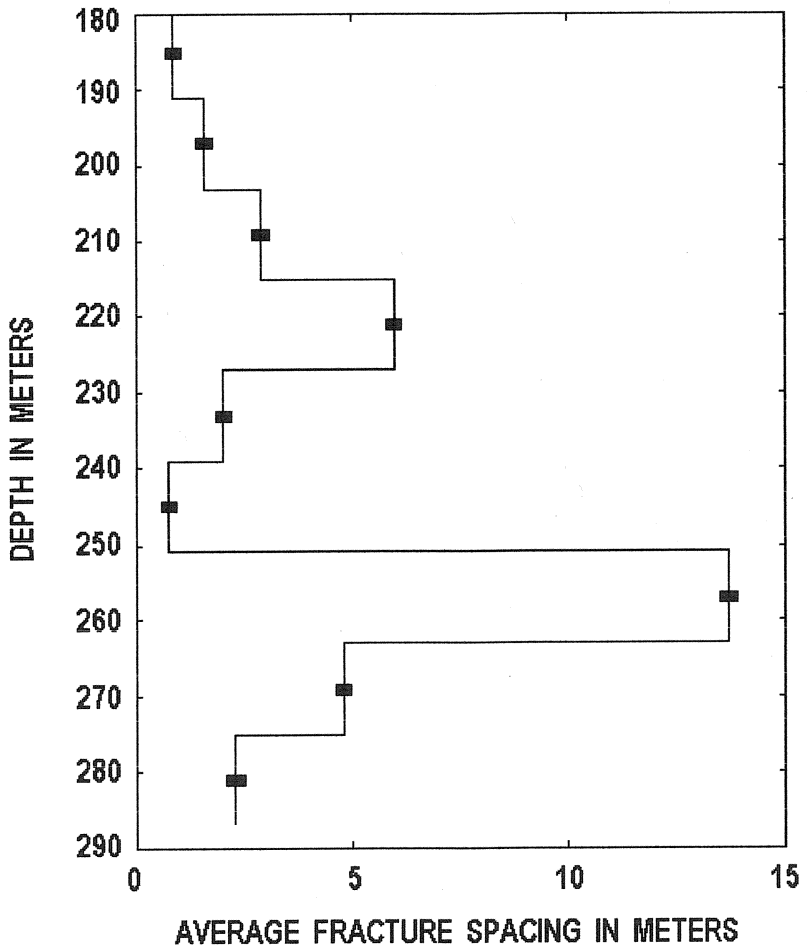

Figure 54. Core 74-NY-13. The change in average fracture spacing for each interval, with depth, for the extension fractures. The stair step size is the size of the interval, 12-meters. The bars are the centers of the 12-meter intervals.

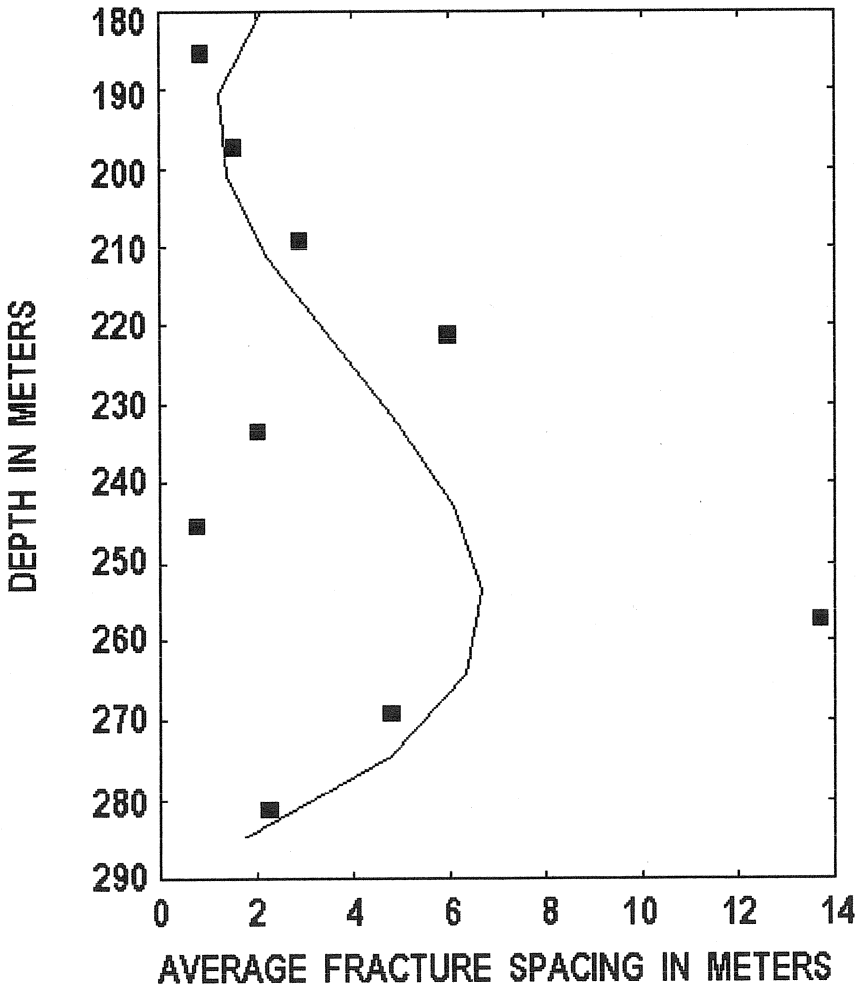

Figure 55. Core 74-NY-13. The change in average fracture spacing, with depth, for the extension fractures. The bars are the centers of the 12-meter intervals. The line is a third order polynomial.

CORE 74-NY-9

CORE LOCATION

Core 74-NY-9 is 106 meters long and was taken from within the graben that holds the Sacandaga Lake (Figure 7). The core was taken from a depth of 257 to 363 meters. The upper 76 meters of core was taken from the Little Falls Formation whereas the final 30 meters was taken from the Galway Formation (Zagorski, 1981). The contact between the two formations is at a depth of approximately 333 meters.

This particular core was taken just northwest of the strike line of the northwestward dipping normal fault that was intersected by core 74-NY-11 (Figure 7). It is not known if this fault continues to the south in the subsurface.

FRACTURE PATTERN: TOTAL NUMBER OF FRACTURES

Initially, when the total number of the fractures per 12-meter interval of core was plotted against depth, two distinct peaks, and an overall decrease in the number of fractures per interval were observed with depth (Figure 56). This fracture distribution was significantly different than if there were an equal number of fractures in each of the intervals (Table 21). There was no rubble within the two intervals where the peak numbers of fractures were found.

INTERPRETATION

The diminishing number of fractures with depth suggests that the core had been taken from a footwall block, below a normal fault. It is very probable that the fracture peaks seen at these two depths is a result of the same stresses that produced the normal fault that was intersected by core 74-NY-11 (Figure 7). The fact that this fault dips toward the area where core 74-NY-9 was taken, strengths this interpretation. The lack of fault rubble within the intervals that had high number of fractures indicates that the core did not pass through a fault zone, but may have passed through a process zone what was in the early stages of development.

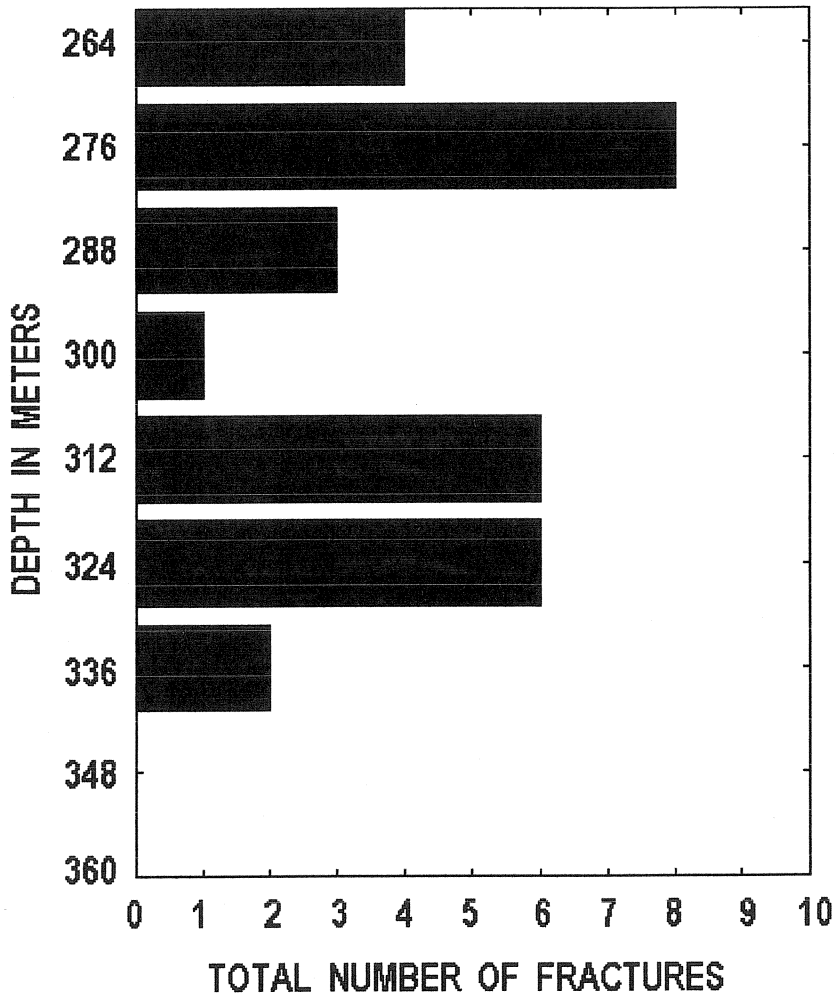

Figure 56. Core 74-NY-9. The total number of fractures per 12-meter interval of core (9 total). The last two intervals contained no fractures. Total core length, 106 meters (257 to 363 meters below the surface).

Table 21. Core 74-NY-9. Chi-square goodness of fit results for the distribution of all the fractures on this core (95 % confidence interval). Interval length - 12 meters.

Number of intervals	Number of fractures	Expected number of fractures per interval	Chi-square computed	Chi-square table
9	30	3.333	19.820	15.507

Table values from Davis (1986).

FRACTURE PATTERN: INDIVIDUAL FRACTURE SETS

All of the fractures on this core had either a 90°, or a 60° dip. The 90° dipping fractures are the dominant fracture set, both in terms of number of fractures and the number of 12-meter intervals that contain fractures (Figure 57). Both the 60° and 90° dipping fractures peaked at the same depths, 276 and 312-324 meters. Chi-square testing indicated that the distribution of these fractures was not significantly different than if there were an equal number of fractures in each of the intervals using 12-meter interval lengths. Separating these fractures into individual sets changed the statistically significant distribution of the total number of fractures into statistically non-significant distributions.

The distribution of the 90° dipping fractures was significantly different than if there were an equal number of fractures in each of the intervals when the interval length was increased to 36 meters (Table 22 and Figure 58). The distribution of the 60° dipping fractures never achieved statistical significance.

Using a 36 meter interval length, the number of extension fractures decreased with depth, but the number of shear fractures showed no trend of either increasing or decreasing with depth (Table 22 and Figure 58).

INTERPRETATION

Based on the geometric relationship between the fractures, the 90° dipping fractures are interpreted as extension, or mode I fractures, and the 60° dipping fractures are interpreted as shear fractures. Interpretations can be made from the individual fracture sets using both 12-meter and 36-meter intervals. Initially, chi-square testing indicated that the peaks in the numbers of fractures, at 276 and 317 to 324 meters, are not statistically significant for the individual fracture sets using 12-meter intervals, but it should be remembered that when the two sets were combined these peaks were significant. The fact that both sets of fractures peaked at the same depths indicates a common source of fracture producing stresses at these respective depths.

Increasing the interval length to 36 meters resulted in a fracture distribution (90° dipping fractures) that was significantly different than if there were an equal number of fractures in each of the intervals. Statistically, this helps to identify the area where there are an increased number of fractures, between 260 and 330 meters.

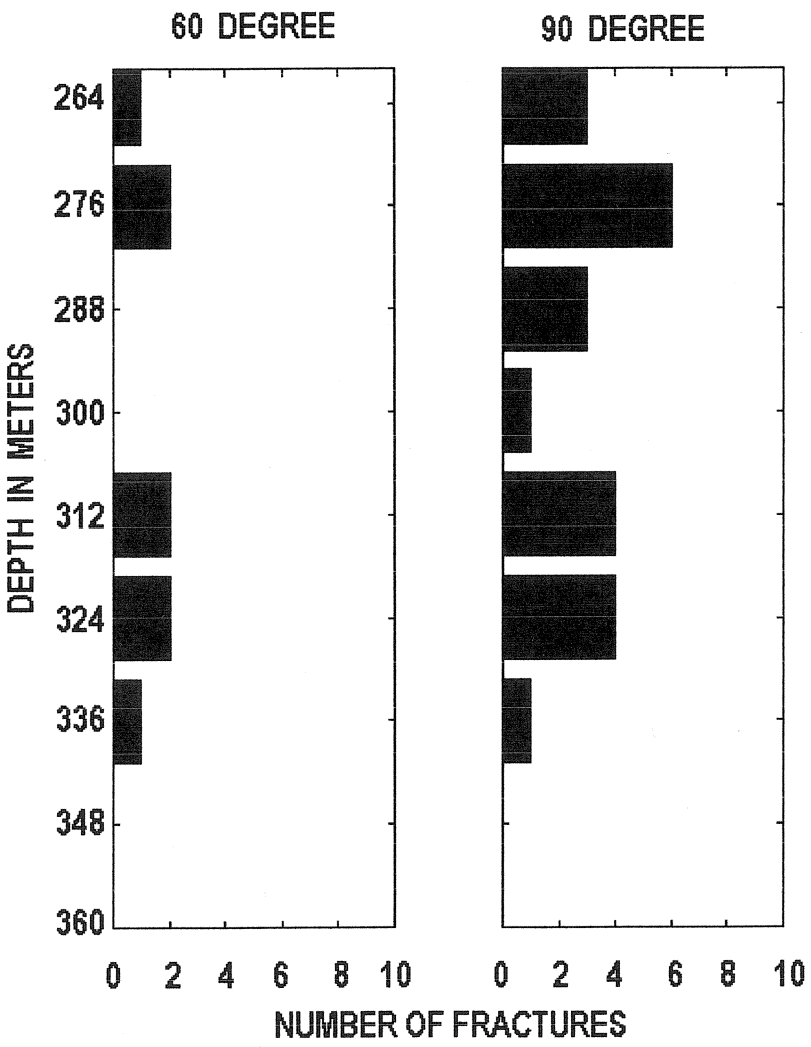

Figure 57. Core 74-NY-9. The number of 60° and 90° dipping fractures per 12-meter interval of core (9 total). The last two intervals contained no fractures. Total core length, 106 meters (257 to 363 meters below the surface).

Table 22. Core 74-NY-9. Chi-square goodness of fit results for the distribution of fractures with 90° and 60° dip angles (95 % confidence interval). Interval length - 36 meters.

Dip	Number of intervals	Number of fractures	Expected number of fractures per interval	Chi-square computed	Chi-square table
90°	9	22	7.333	8.819	5.991
60°	9	8	2.667	1.750	5.991

Table values from Davis (1986).

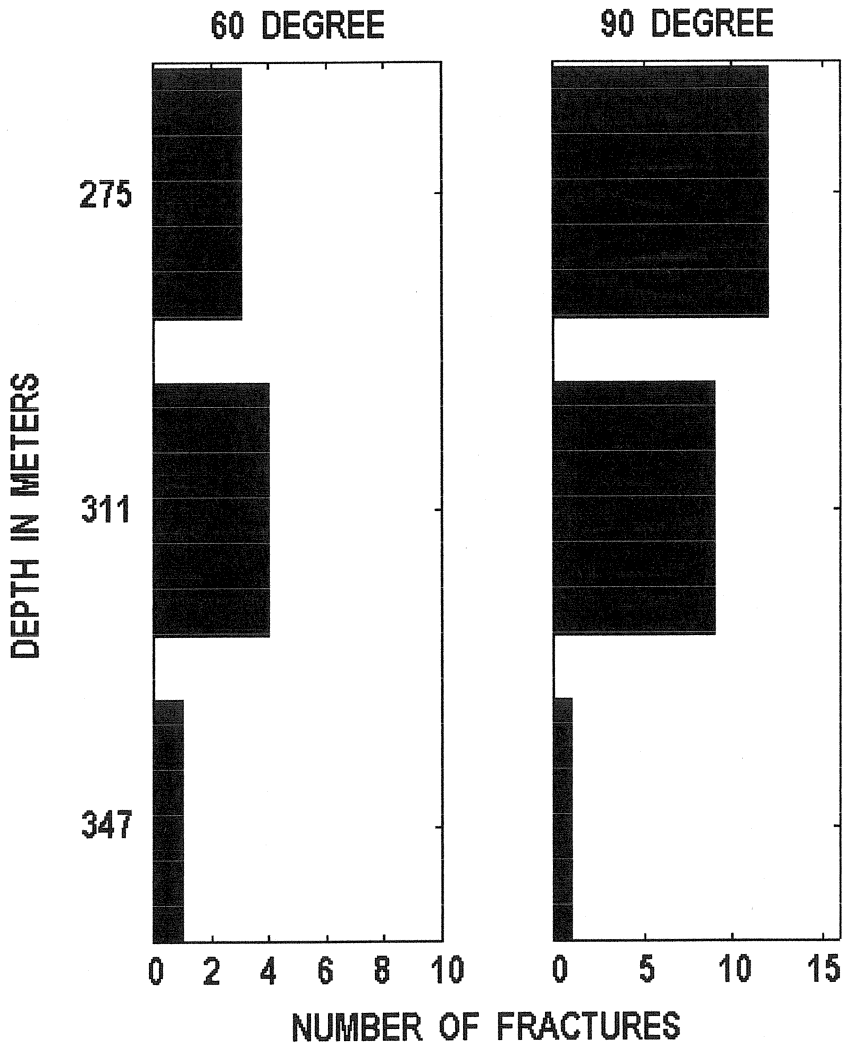

Figure 58. Core 74-NY-9. The number of 60° and 90° dipping fractures per 36-meter interval of core (9 total). Total core length, 106 meters (257 to 363 meters below the surface).

These fracture distribution patterns indicate that the area, between 260 and 330 meters, is a process zone for the fault that passes by core 74-NY-11 (Figure 4). As mentioned above, the fact that this fault dips toward the area where core 74-NY-9 was taken, strengths this interpretation. The lack of any fault rubble between 260 and 330 meters is further evidence that this area has not experienced any fault movement and is only a process zone at this time.

AVERAGE FRACTURE SPACING FOR THE EXTENSION FRACTURES, 36-METER INTERVALS

The average fracture spacing was calculated for the extension fractures using an interval length of 36 meters (Table 23, Figure 59). Using this interval length, the average fracture spacing minimum extends from a depth of 260 to a depth of 320 meters. Below 325 meters there was a very abrupt increase in fracture spacing with depth. The minimum fracture spacing values, 0.65 and 0.58 meters, are close to, but above the minimum average fracture spacing value, 0.52, that was calculated for core 75-NY-2 (Table 6). A curve was "hand-fitted" to the data points in order to try and determine the change in fracture spacing with depth (Figure 60). Unfortunately, the data points were too widely spaced to realistically model the rate of fracture spacing change with depth using polynomials.

INTERPRETATION

When analyzing core 75-NY-2, it was determined that fracture spacing under 0.3 meters was required before fault movement could occur. The minimum fracture spacing in the bedrock penetrated by this core, 0.58 meters, supports the above interpretation that this core passed through a fault process zone and that no faulting has occurred. The abrupt increase in fracture spacing below a depth of 320 meters indicates that the width of the process zone is very narrow.

IMPERIAL PAPER CO. CORE

CORE LOCATION

The Imperial Paper Co. core was taken from Glens Falls, Warren County, New York (Figure 61). The core was taken from a depth of 221 to 305 meters. The core passed through the Ticonderoga formation, which is composed of quartzose dolostones, and the underlying Potsdam Sandstone (Rickard, 1973). The Ticonderoga formation is the stratigraphic equivalent of the Galway formation to the west. The contact between the two formations is at a depth of approximately 265 meters. The core was taken from within the series of grabens that holds Lake George and is located approximately 5 km from the normal fault to the east and approximately 10 km from the fault to the west.

Table 23. Core 74-NY-9. The average fracture spacing for the 90° dipping fractures. Interval length - 36 meters.

Interval depth (m)	Average fracture spacing (m)
257 – 293	0.65
293 – 329	0.58
329 – 365	12.00

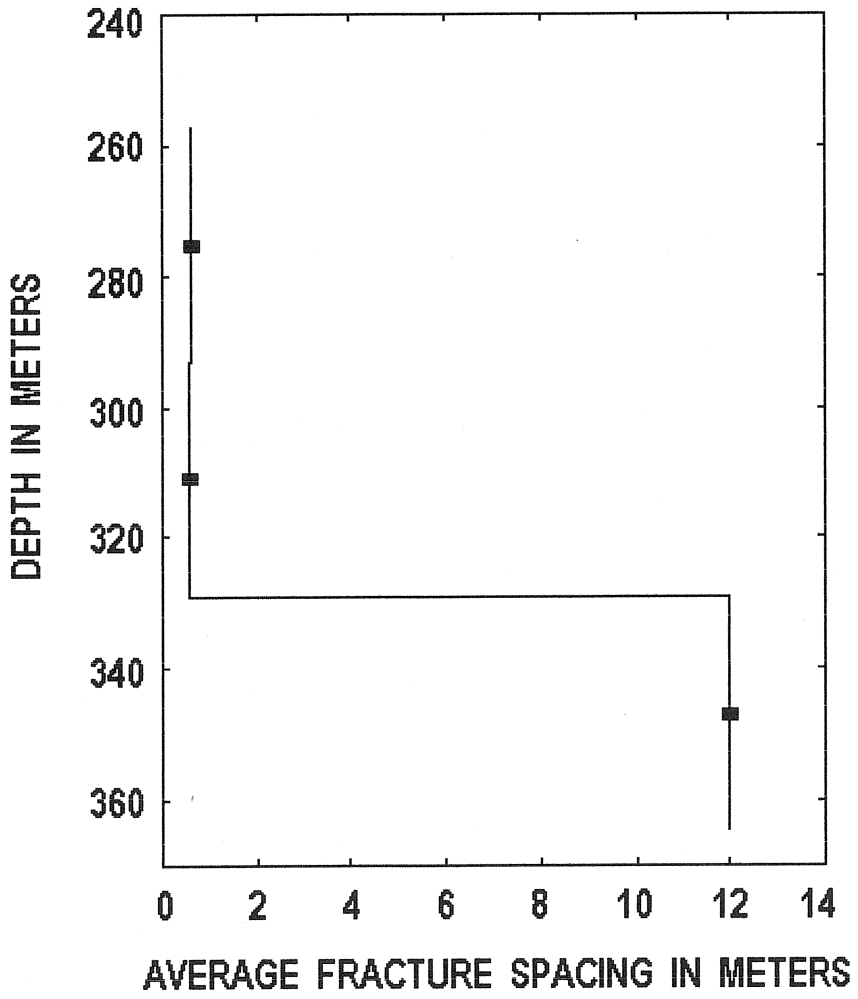

Figure 59. Core 74-NY-9. The change in average fracture spacing for each interval, with depth, for the extension fractures. The stair step size is the size of the interval, 36-meters. The bars are the centers of the 36-meter intervals.

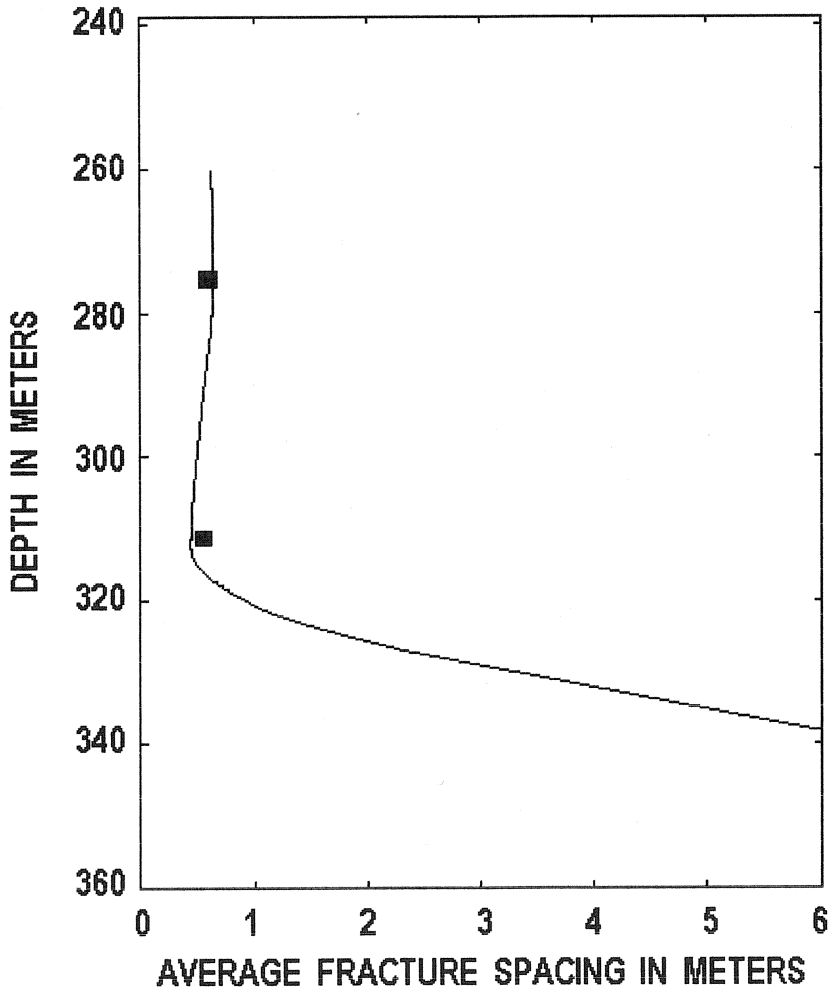

Figure 60. Core 74-NY-9. The change in average fracture spacing with depth for the extension fractures. The bars are the centers of the 36-meter intervals.

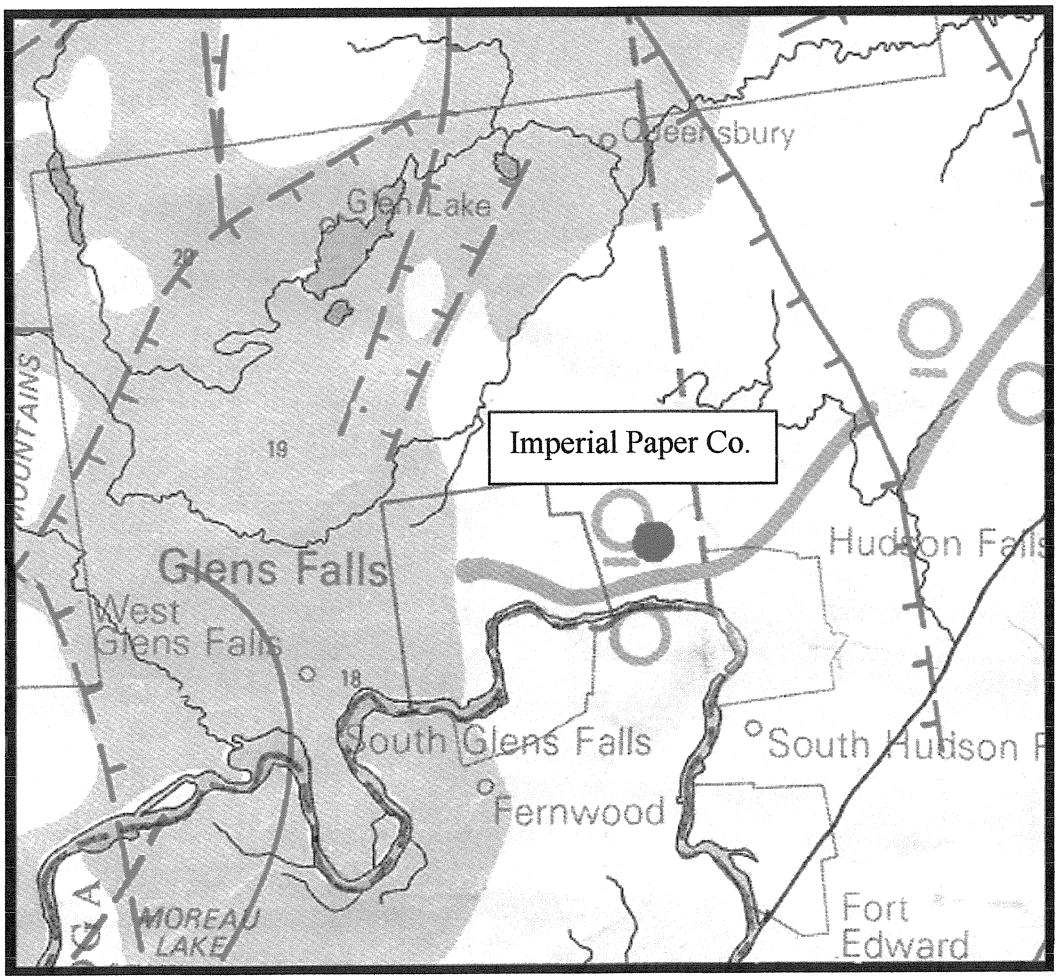

Figure 61. The location of the Imperial Paper Co. core. The circle is the location of the core. The solid lines are normal faults, dashed where inferred. Hachure marks are on the relatively downthrown side of the faults.

Map width approximately 20 km

Modified from Isachsen and McKendree, 1977.

FRACTURE PATTERN: TOTAL NUMBER OF FRACTURES

Initially, when the total number of the fractures per 12-meter interval of core was plotted against depth, there was a fairly consistent number of fractures until the final interval where there was a dramatic increase in the number of fractures (Figure 62). The fracture pattern was very similar to the one seen in core 75-NY-11 (Figure 8). Unlike core 74-NY-11, there was no rubble within the section of core that was examined. The fracture distribution was significantly different than if there were an equal number of fractures in each of the 12-meter intervals (Table 24).

INTERPRETATION

The fracture pattern and the similarity between this core and core 74-NY-11 indicate that this core was taken from the hanging wall block of a fault. Given the fact that the core was taken from the center of a large graben structure strongly suggests that this fault is a normal fault. This fault is a subsurface fault and not the fault that is 5 km to the east (Figure 61). This interpretation was made using Pythagorean's theorem, since the dip of the fault located 5 km to the east would need to be approximately 4° if the core was to intersect it at a depth of 300 meters.

FRACTURE PATTERN: INDIVIDUAL FRACTURE SETS

All of the fractures on this core had either 90°, or 60° dips. The 90° dipping fractures are the dominant fracture set, both in terms of number of fractures and the number of 12-meter intervals that contain fractures (Figure 63). Both the 60° and 90° dipping fractures increased in number with depth. Chi-square testing indicated that only the distribution of the 90° dipping fractures was significantly different than if there were an equal number of fractures in each of the 12-meter intervals (Table 25). Increasing the interval length to 24 and then to 36 meters did not result in a fracture distribution that was significantly different than if there were an equal number of fractures in each of the intervals for the 60° dipping fractures.

INTERPRETATION

Based on the geometric relationship between the fractures, it was determined that the 90° dipping fractures are extension, or mode I fractures. Extension fractures typically form under low confining stress conditions (Dennis, 1972, Price, 1966 and Nelson, 2001). Extension fractures form parallel to the maximum and intermediate principal stress axes and perpendicular to the minimum principal stress axis. The 60° dipping fractures are shear fractures. Shear fractures with 60° dips are

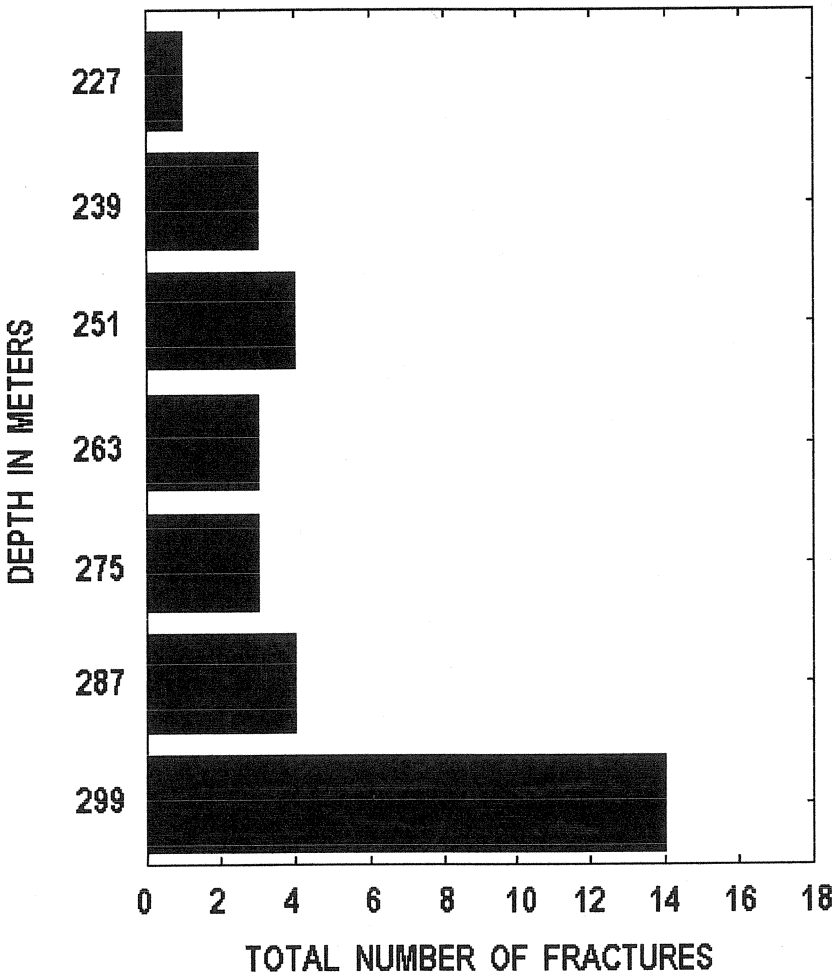

Figure 62. Imperial Paper Co. Core. The total number of fractures per 12-meter interval of core (7 total). Total core length, 84 meters (221 to 305 meters below the surface).

Table 24. Imperial Paper Company Core. Chi-square goodness of fit results for the distribution of all the fractures on this core (95 % confidence interval). Interval length – 12 meters.

Number of intervals	Number of fractures	Expected number of fractures per interval	Chi-square computed	Chi-square table
7	31	4.42	25.727	12.592

Table values from Davis (1986).

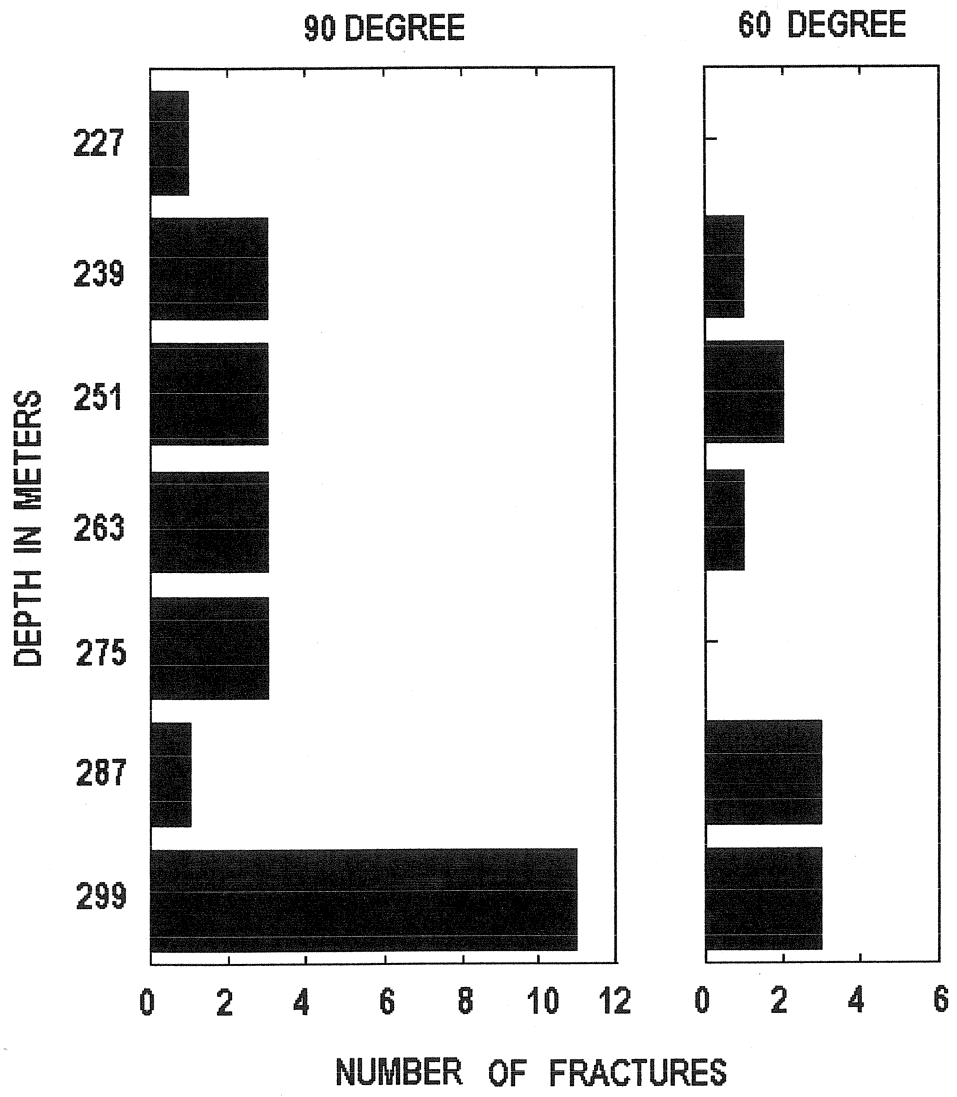

Figure 63. Imperial Paper Company Core. The number of 90° and 60° dipping fractures per 12-meter interval of core (7 total). Total core length, 84 meters (221 to 305 meters below the surface).

Table 25. Imperial Paper Company Core. Chi-square goodness of fit results for the distribution of fractures with 90° and 60° dip angles (95 % confidence interval). Interval length – 12 meters.

Dip	Number of intervals	Number of fractures	Expected number of fractures per interval	Chi-square computed	Chi-square table
90°	7	21	3.00	25.333	12.592
60°	7	10	1.43	6.793	12.592

Table values from Davis (1986).

consistent with the stress field that would have caused normal faulting to take place (Price, 1966). This and the fact that both the 60° and the 90° dipping fractures increased in number with depth, strengthens the interpretation that this core passed through the hanging wall block of a normal fault.

AVERAGE FRACTURE SPACING FOR THE EXTENSION FRACTURES, 12-METER INTERVALS

The average fracture spacing was calculated for the extension fractures using an interval length of 12 meters (Table 26, Figure 64). There is a pattern of alternating high and low fracture spacing values that diminishes in value with depth. The minimum fracture spacing value, 0.12 meters, is below the 0.3 meter fracture spacing threshold that had been determined to be required to allow faulting to occur using cores 74-NY-11, 75-NY-2 and 75-NY-14.

A third order polynomial was used to model the change in fracture spacing with depth (Figure 65). This curve is sigmoidal in shape and is very similar to the patterns seen in cores 74-NY-6, 74-NY-7 and 74-NY-13 (Figures. 38, 50 and 55, respectively). The polynomial intercepts the 0-meter fracture spacing intercept at a depth of approximately 300 meters.

INTERPRETATION

As detailed above, the sigmoidal shaped curve may be recording multiple layers of a horizontal pattern of alternating high and low fracture frequency values (inverse of fracture spacing) that diminishes in intensity with increasing distance from the fault plane. Refer to the analysis of core 74-NY-6 for a detailed explanation.

The average fracture spacing minimum, 0.12 meters, and the shape of the polynomial curve plotting the change in fracture spacing with depth, indicates that a fault may be located at a depth of 300 to 310 meters. This interpretation is consistent with the interpretations made above, that this core was taken from the hanging wall block of a normal fault.

Table 26. Imperial Paper Company Core. The average fracture spacing for the 90° dipping fractures. Interval length - 12 meters.

Interval depth (m)	Average fracture spacing (m)
221 – 233	3.00
233 – 245	0.86
245 – 257	1.50
257 – 269	0.64
269 – 281	0.92
281 – 293	2.40
293 – 305	0.12

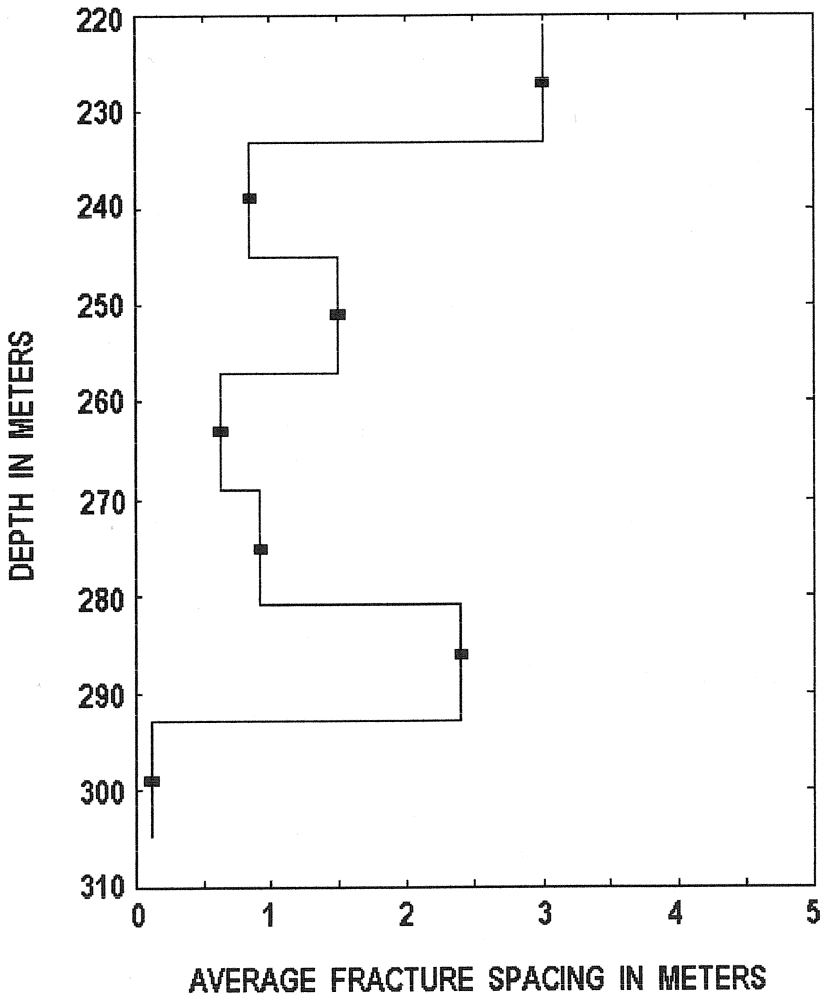

Figure 64. Imperial Paper Company Core. The change in average fracture spacing for each interval. The stair step size is the size of the interval, 12-meters. The bars are the centers of the 12-meter intervals. The overall trend is a decrease in fracture spacing with depth.

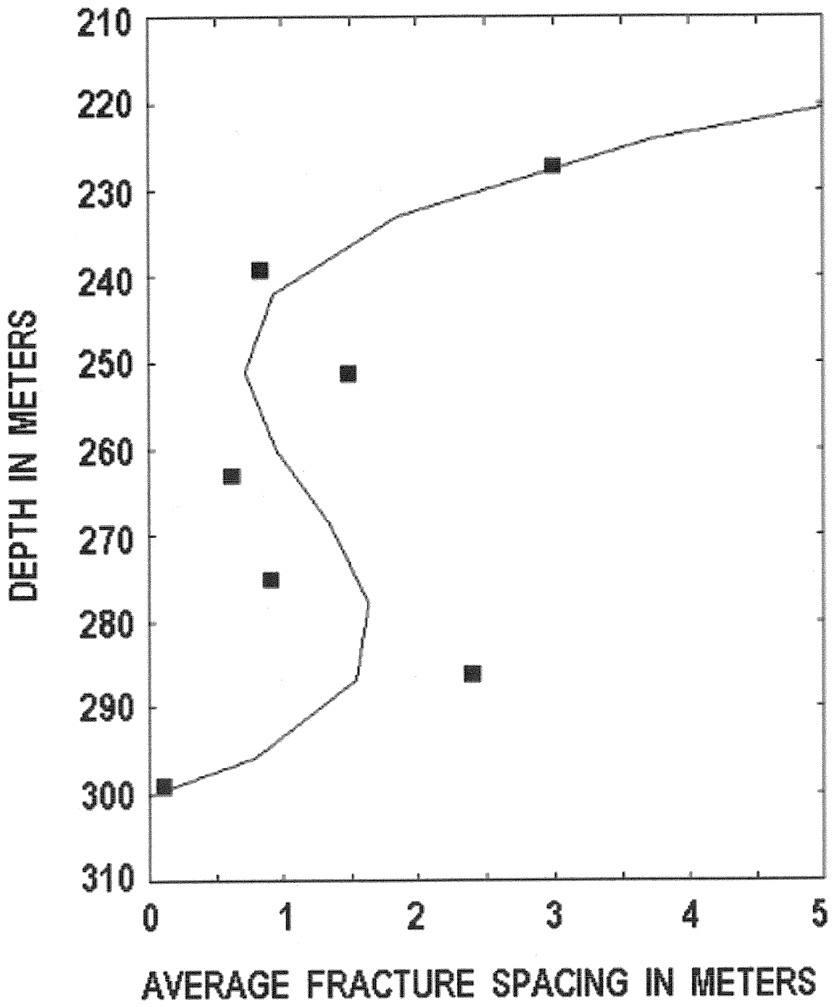

Figure 65. Imperial Paper Company Core. The change in average fracture spacing with depth. The curve is a third order polynomial, the bars are the centers of the 12-meter intervals.

COMSTOCK CORE

CORE LOCATION

The Comstock core was taken near the town of Comstock, New York (Figure 66). This core was taken approximately 2 km east of a normal fault and was taken from the eastern edge of the study area. The core is 60 meters long, was taken from a depth of 4 to 64 meters and penetrated the Galway and Potsdam Formations. Due to the interfingering of the dolostone and sandstone, the exact contact depth between the Galway and Potsdam Formations was not determined. The contact with the Precambrian was at a depth of 61 meters.

FRACTURE PATTERN: TOTAL NUMBER OF FRACTURES

The number of fractures found along the length of this core was relatively constant with depth (Figure 67). All of the fractures had 90° dips. Chi-square testing was performed using interval lengths of 12, 24 and 36 meters. Each test indicted that the distribution of fractures was not significantly different than if there were an equal number of fractures in each of the intervals. As a result, an interval length of 12 meters was used for the analyses so that this core could be better compared to the others, which in most cases used core intervals of 12 meters.

INTERPRETATION

All of the fractures on this core are interpreted to be extension fractures. This makes this core very similar to cores 74-NY-7 and 74-NY-13, since each of these cores was dominated by extension fractures.

The constant number of extension fractures with depth was attributed to the fact that the core was taken approximately 2 km away from the nearest fault. This also makes this core similar to cores 74-NY-7 and 74-NY-13, since they too were drilled several kilometers from the surface exposure of the nearest fault.

The average number of extension fractures per 12-meter interval, 7.4, was half the average number per 12-meter interval for core 74-NY-7, 14.3. The most obvious reason for this is the fact that the Comstock core was drilled 2 km from a single fault as opposed to 2 km from two separate faults, as core 74-NY-7 had. The higher number of fractures in core 74-NY-7 was attributed to the fact that the core was taken from an area that was affected by the process zones from two separate and subparallel

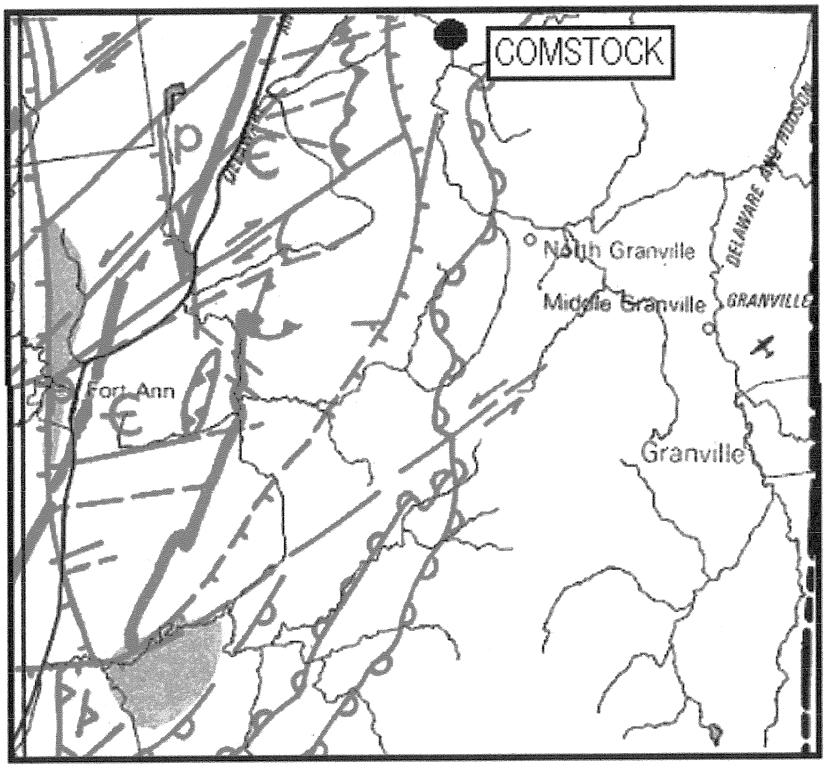

Figure 66. The location where the DOT Comstock core was taken. Solid lines indicate faults. Hachure marks are on the relatively downthrown side of normal faults. Fault lines are dashed where inferred. Half circles are on gravity slides. Map width approximately 20 km.

Source: Isachsen and McKendree, 1977.

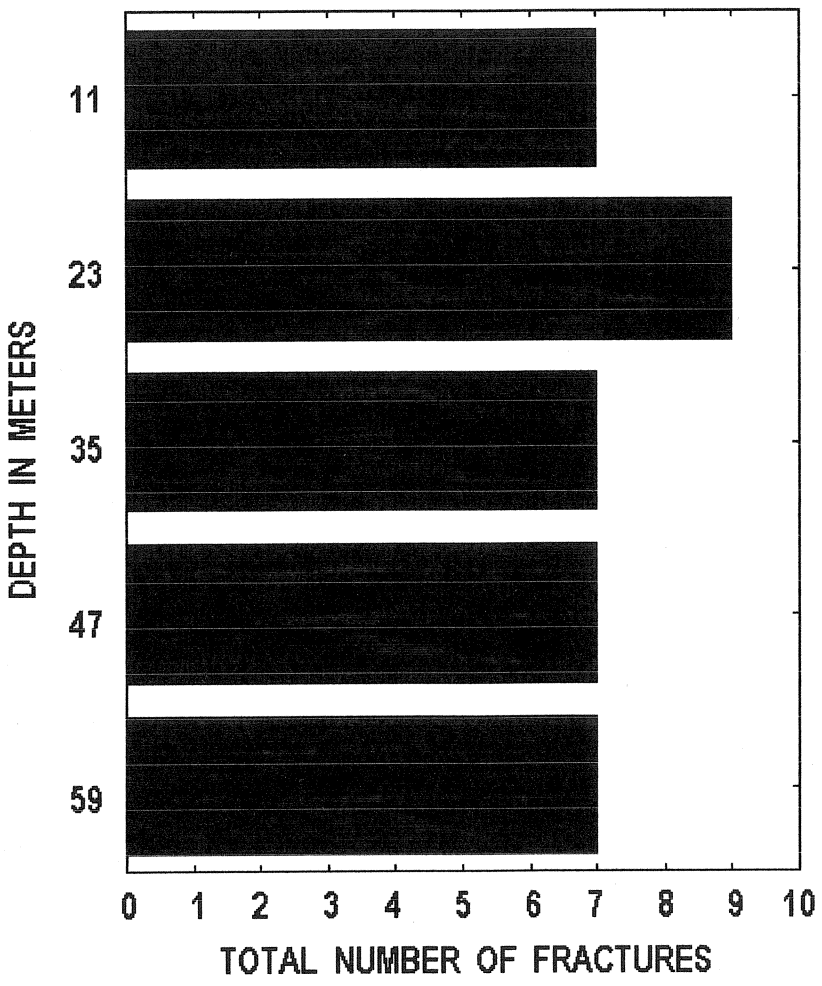

Figure 67. Comstock Core. The total number of fractures per 12- meter interval of core (5 total). All of these fractures have a 90° dip. Total core length, 60 meters (4 to 64 meters below the surface.

faults. The Comstock core, on the other hand, only penetrated one process zone, which resulted in half the average number of fractures per 12-meter interval.

The average number of extension fractures per 12-meter interval, 7.4, was much greater than the 2.2 extension fractures per 12-meter interval for core 74-NY-13. The most obvious reason for this is the fact that the Comstock core was drilled 2 km from a single fault as opposed to 5-6 km from two separate faults, as core 74-NY-13 had. In this case, the further distance that core 74-NY-13 was from the nearest adjacent faults resulted in fewer fractures per 12-meter interval of core.

AVERAGE FRACTURE SPACING FOR THE EXTENSION FRACTURES, 12-METER INTERVALS

The average fracture spacing was calculated for the extension fractures using an interval length of 12 meters (Table 27 and Figure 68). The change in average fracture spacing with depth was fairly consistent and gave no clear indication if there was a pattern of increasing or decreasing fracture spacing with depth.

When a third order polynomial was drawn through the centers of the 12-meter intervals, a sigmoidal fracture spacing curve was revealed (Figure 69). This fracture spacing curve is very similar to the pattern observed in cores 74-NY-6, 74-NY-7, 74-NY-13 and the Imperial Paper Company core (Figures. 38, 50, 55 and 65, respectively).

INTERPRETATION

As detailed above, the sigmoidal shaped curve may be recording multiple layers of a horizontal pattern of alternating high and low fracture frequency values (inverse of fracture spacing) that diminishes in intensity with increasing distance from a fault. Refer to the analysis of core 74-NY-6 for a detailed explanation.

Table 27. Comstock Core. The average fracture spacing for the 90° dipping fractures. Interval length - 12 meters.

Interval depth (m)	Average fracture spacing (m)
4 – 16	0.533
16 – 28	0.414
28 – 40	0.381
40 – 52	0.857
52 – 64	0.511

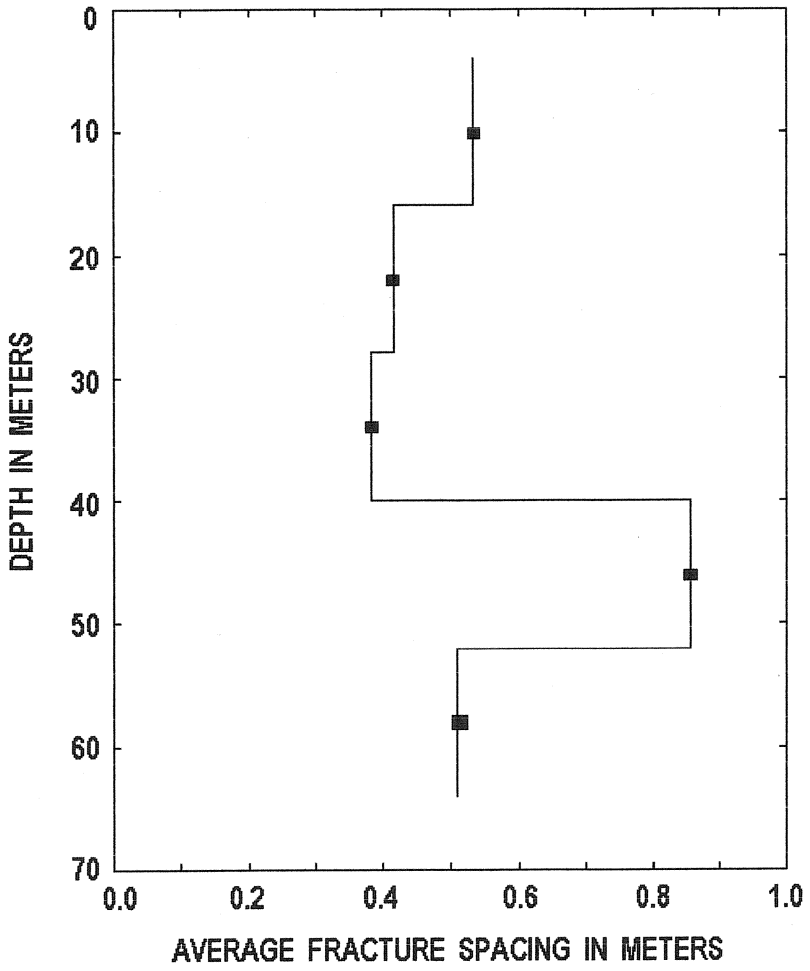

Figure 68. Comstock Core. The change in average fracture spacing for each interval. The stair step size is the size of the interval, 12-meters. The bars are the centers of the 12-meter intervals.

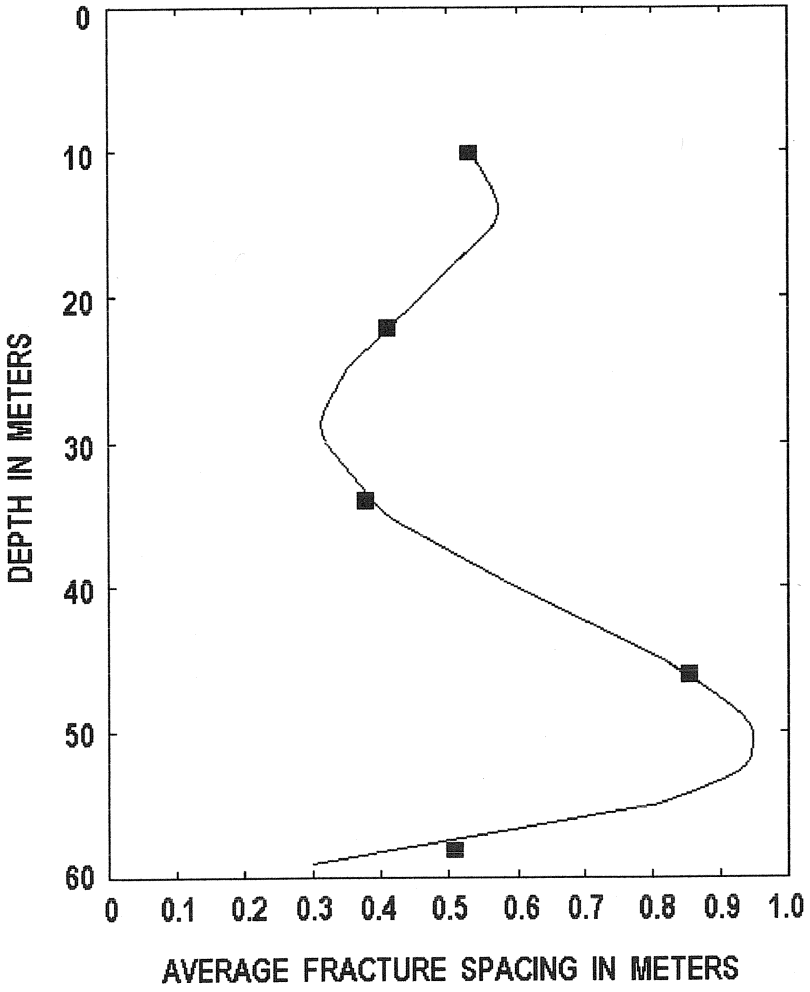

Figure 69. Comstock Core. The change in average fracture spacing with depth. The curve is a third order polynomial; the bars are the centers of the 12-meter intervals.

BEEKMANTOWN CORE

CORE LOCATION

The Beekmantown core was taken from the footwall block of a small fault, right at the edge of the fault scarp, in the town of Beekmantown, New York (Figure 70). This fault appears to be a small and very localized feature and is not nearly as long as the faults that bisect the Mohawk River Valley (Figure 1). The site where the core was taken had been completely covered by the Isle La Motte thrust sheet, as evidenced by the klippe, just to the west of the site (Fisher, 1968). The core is 47 meters long and was taken from the Providence Island formation. The Providence Island formation is medium to thickly bedded and has been pervasively dolomitized.

FRACTURE PATTERN: TOTAL NUMBER OF FRACTURES

The number of fractures found along the length of this core decreased abruptly with depth (Figure 71). Chi-square testing indicated that this fracture distribution was significantly different than if there were an equal number of fractures in each of the intervals (Table 28). Out of all the cores examined, the first 12-meter interval of this core contained more fractures than any other 12-meter interval. Cores 74-NY-11 and 75-NY-14 also had high numbers of fractures in a single 12-meter interval. Core 74-NY-11 had 26 fractures and core 75-NY-14 had 21 fractures. It should be noted that core 75-NY-14 was only 3.8 cm in diameter and not 5.08 cm as the other two were. Had it been thicker it may have contained even more fractures. Core 74-NY-11 was taken immediately above a fault zone whereas core 75-NY-14 passed completely through an incipient fault.

The fracture distribution pattern along this core is similar to the fracture distribution patterns found along cores 74-NY-10 and 74-NY-6 (Figures. 30 and 35 respectively). Despite the large difference in the number of fractures in the first interval for all three cores, the numbers of fractures in the second intervals were very similar. Both core 74-NY-10 and core 74-NY-6 had 6 fractures in the second interval whereas the Beekmantown core had 5.

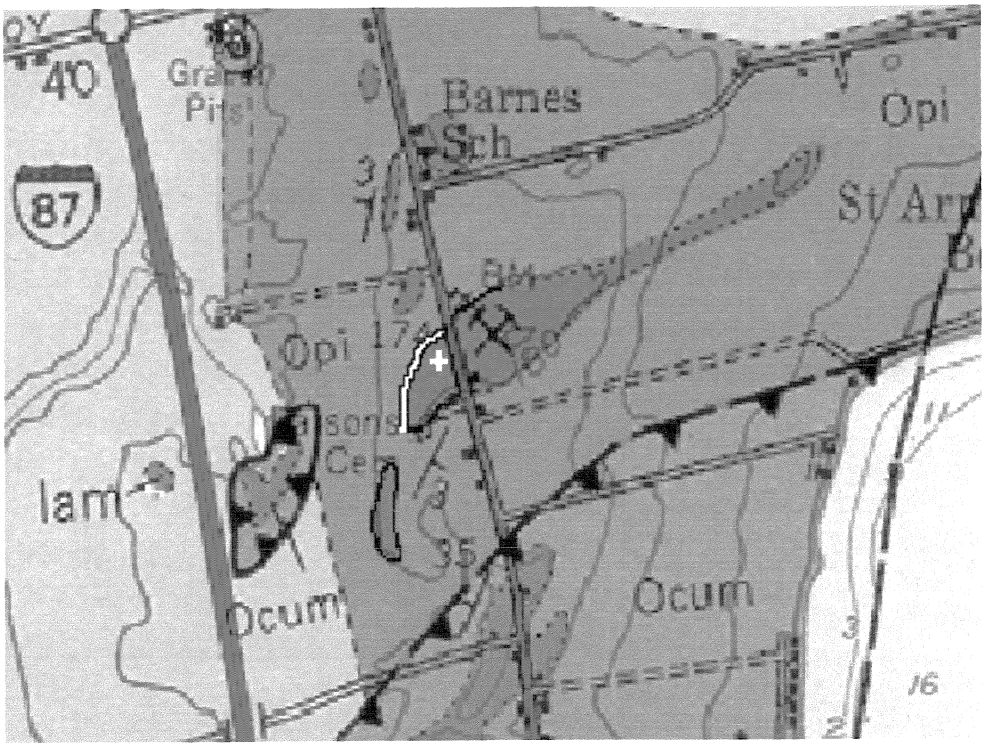

Figure 70. The location of the Beekmantown core in Beekmantown, N.Y. The white cross, just west of route 9, marks core location. The white line north and west of the core location is a normal fault, which dips to the north and west. This fault extends east of route 9. Opi is the Ordovician Providence Island formation of the Beekmantown Group, pink areas are covered with Pleistocene overburden and Iam is the Lacolle Mélange. The saw-tooth line is the leading edge of the Isle La Motte thrust sheet, the saw-teeth on the overriding block, which is composed of the Ordovician Cumberland Head Argillite, Ocum. Darker colors on the map represent outcropped rock.

Map width approximately 3 km.

Modified from Fisher, 1968.

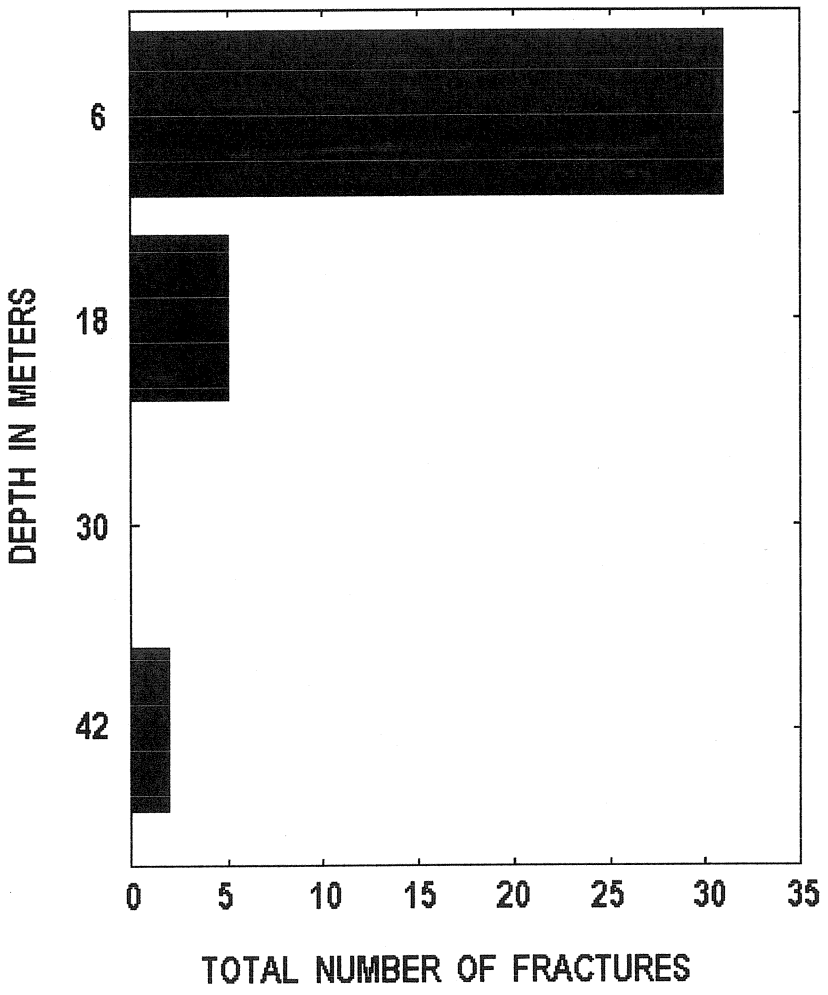

Figure 71. Beekmantown core. The total number of fractures, per 12-meter interval of core (4 total). Total core length, 47 meters (0 to 47 meters).

Table 28. Beekmantown Core. Beekmantown Core. Chi-square goodness of fit results for the distribution of all the fractures on this core (95 % confidence interval). Interval length – 12 meters.

Number of intervals	Number of fractures	Expected number of fractures per interval	Chi-square computed	Chi-square table
4	38	9.5	66.211	7.815

Table values from Davis (1986).

INTERPRETATION

The similarities in the high numbers of fractures in this core and cores 74-NY-11 and 75-NY-14 is consistent with the fact that all three cores were taken immediately adjacent to or passed directly through a fault zone. The higher number of fractures in the first interval of the Beekmantown core may be due to the fact that the Beekmantown core was taken from the surface whereas cores 74-NY-11 and 75-NY-14 were taken from depths of 130 to 214 meters and 700 to 804 meters, respectively. Narr (1996) indicated that the surface is generally in a state of saturation with respect to fracture development. This may be the reason that the highest number of fractures found in a 12-meter interval of core was from this core.

The decrease in the number of fractures with depth is consistent with the fact that the core was taken from the footwall block of a normal fault. The similarities with the fracture pattern observed in this core and the fracture patterns observed in cores 74-NY-10 and 74-NY-6 reinforce the interpretation that those cores were taken from footwall blocks as well.

FRACTURE PATTERN: INDIVIDUAL FRACTURE SETS

The fractures on this core had 90°, 70°-75°, 55°-60°, 45° and 30°-35° dips (Figure 72). The 90° and 70°-75° dipping fractures are the dominant fractures and are confined, with the exception of one 70° fracture, to the top interval. These fractures had multiple orientations. They intersected each other at 50°, 70° and 90° angles and were also found to be parallel to each other (Figure 73).

The 55°-60° dipping fractures were found in equal numbers in the top two 12-meter intervals (Figure 72). The two 45° and the 30°-35° dipping fractures were also confined to the top interval. The reverse fault with centimeter scale offset at a depth of 45 meters has a 35° dip (Figure 74).

Chi-square testing indicated that the distributions of the 90°, 70°-75°, 55°-60° and 30°-35° dipping fractures were significantly different than if there were an equal number of fractures in each of the intervals (Table 29). Increasing the interval length to 24 meters did not result in a fracture distribution that was significantly different than if there were an equal number of fractures in each of the intervals for the 45° dipping fractures.

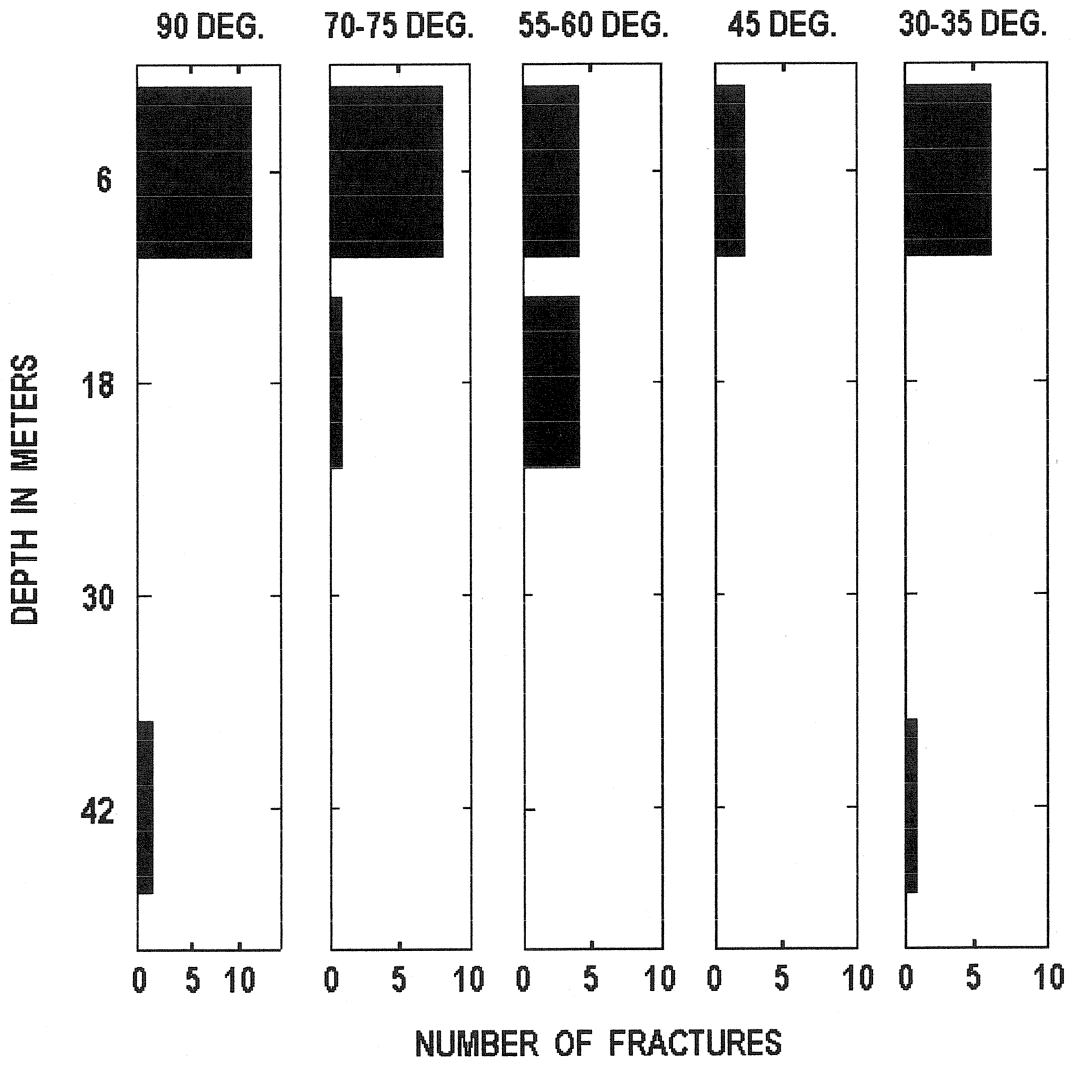

Figure 72. The Beekmantown core. The number of 90°, 70°-75°, 55°-60°, 45° and 30°-35° dipping fractures, per 12-meter interval of core (4 total). Total core length, 47 meters (0 to 47 meters).

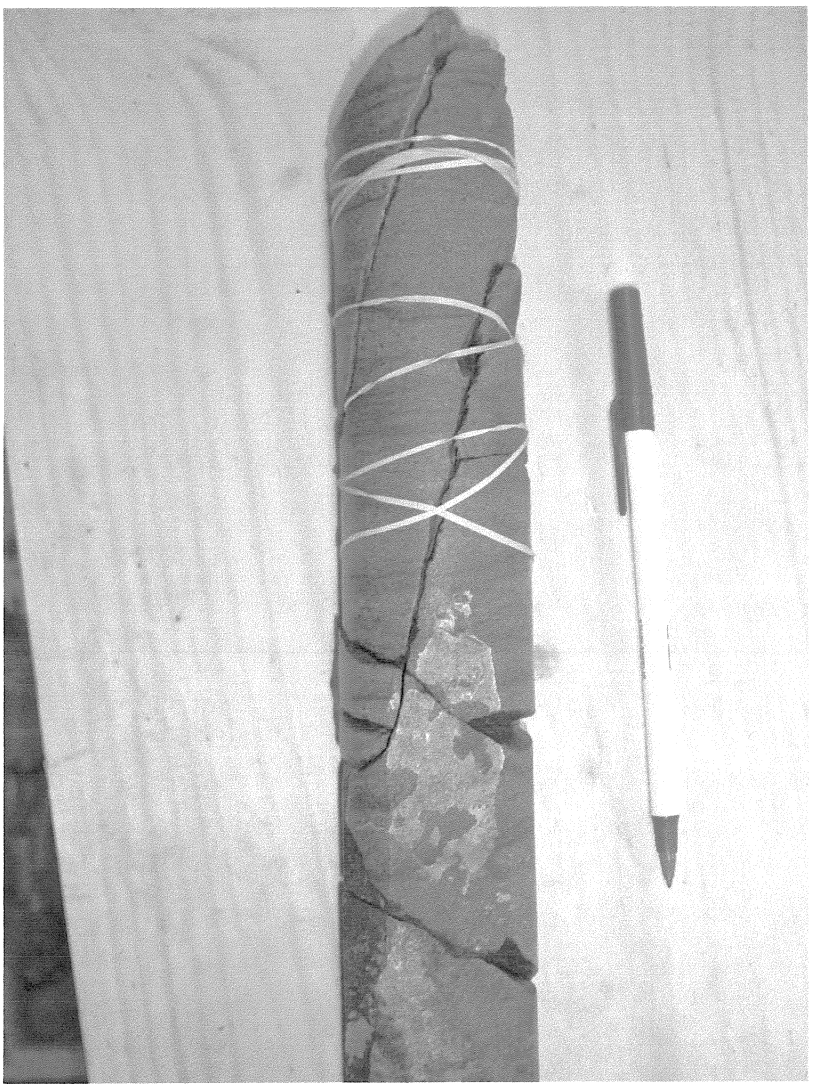

Figure 73. The Beekmantown Core. Two parallel 75° dipping fractures orientated approximately 90° from a vertical fracture. There is no displacement along either of the 75° dipping fractures. Note the presence of carbonate cement on the vertical fracture surface. The top of the core is at the top of the picture.

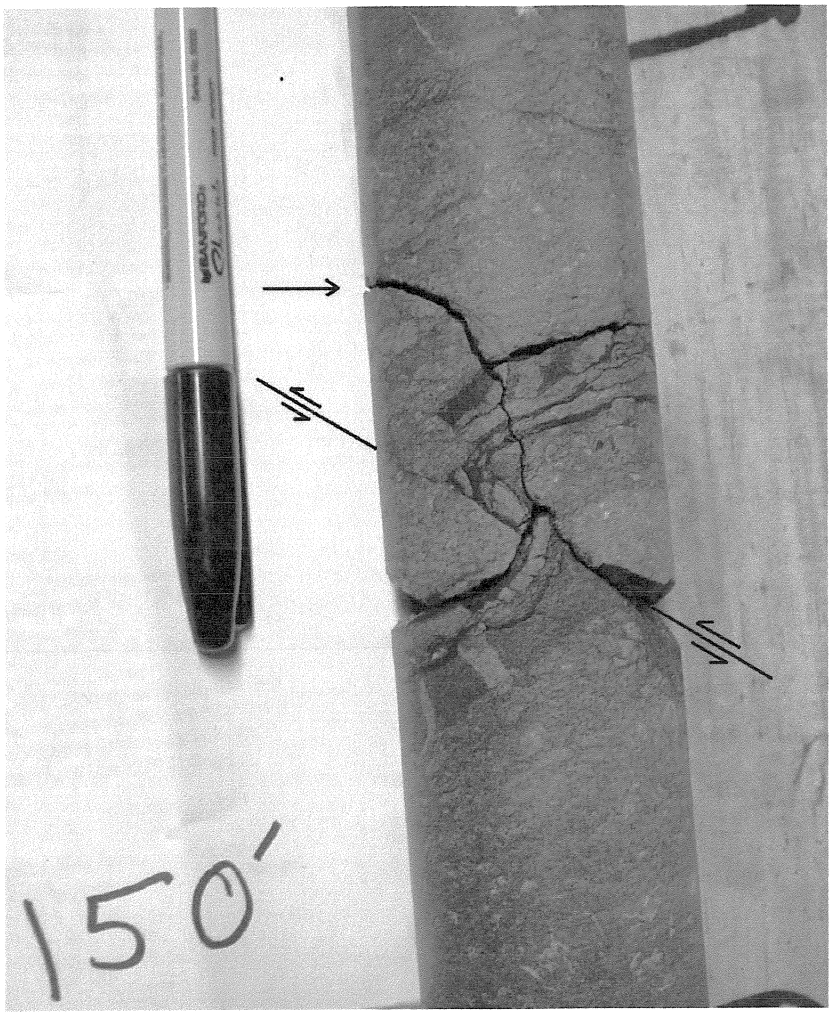

Figure 74. The Beekmantown Core. A small, 35° dipping reverse fault at a depth of 45 meters. The fracture pointed out by the arrow was drilling induced.

Table 29. Beekmantown Core. Chi-square goodness of fit results for the distribution of fractures with common dip angles (95 % confidence interval). Interval length – 12 meters.

Dip angle	Number of intervals	Number of fractures	Expected number of fractures per interval	Chi-square computed	Chi-square table
90°	4	12	3.00	28.667	7.815
70°-75°	4	9	2.25	27.000	7.815
55°-60°	4	8	2.00	8.000	7.815
45°	4	2	0.50	6.000	7.815
30°-35°	4	7	1.75	14.143	7.815

Table values from Davis (1986).

Fractures with strikes of N60°E, N90°E N100°E, N15°E, N-S and N15°W were measured in surface exposure (Figure 75). These fractures formed conjugate sets that had north-south and east-west orientations. Several of the conjugate sets of fractures were bisected by a third fracture set. Many of the fractures have been greatly enlarged due to karst dissolution. Karst dissolution was present along the entire length of the core.

INTERPRETATION

The area where this core was taken was subjected to a very complex deformational history. Much of this deformational history was recorded by fracture patterns, both in core and at the surface. The compressional forces of the Taconic Orogeny produced gently dipping anticlines and synclines in the area (Fisher, 1968). Strike and dip symbols on the geologic map of the area indicate that the location where the core was taken is a small, gently dipping anticline (Figure 70). The beds, just south of the core location, strike N 28° E and dip 3° to the east-southeast. The beds just north of the core location strike N 10° E and dip 3° to the west. The strike of the anticline is approximately N 10 ° E to N 20 ° E.

Several conjugate sets of shear fractures are observed in surface exposure where the core was drilled (Figure 75). Extension fractures bisect both conjugate sets of shear fractures. The conjugate sets of shear fractures that have an overall east-west orientation form a type I fracture pattern (Figures 75 and 76) (Stearns and Friedman, 1972). This pattern indicates a shortening in the dip direction and elongation in the strike direction. Horizontal compressive stresses from the east would have set up a stress field that would have produced these fractures.

The conjugate set of shear fractures that have an overall north-south orientation form a type II fracture pattern (Figure 77) (Stearns and Friedman, 1972). The strike of the extension fractures is parallel to the strike of the anticline. This fracture pattern indicates a shortening parallel to the strike direction and elongation parallel to the dip direction. Downward stresses, to the east of this location, would have set up a stress field that would have produced these fractures.

The extension fractures and the shear fractures for both the type I and type II fracture patterns are perpendicular to the bedding surface. The bedding was horizontal at the core site, as a result, all of the fractures associated with the type I and type II fracture patterns have 90° dips.

Stearns and Friedman (1972) indicated that type I and type II fracture patterns are commonly found together and that the type I fracture pattern is probably the first to have formed. This relationship has tentatively been identified here, since many type II fractures terminate at type I fractures.

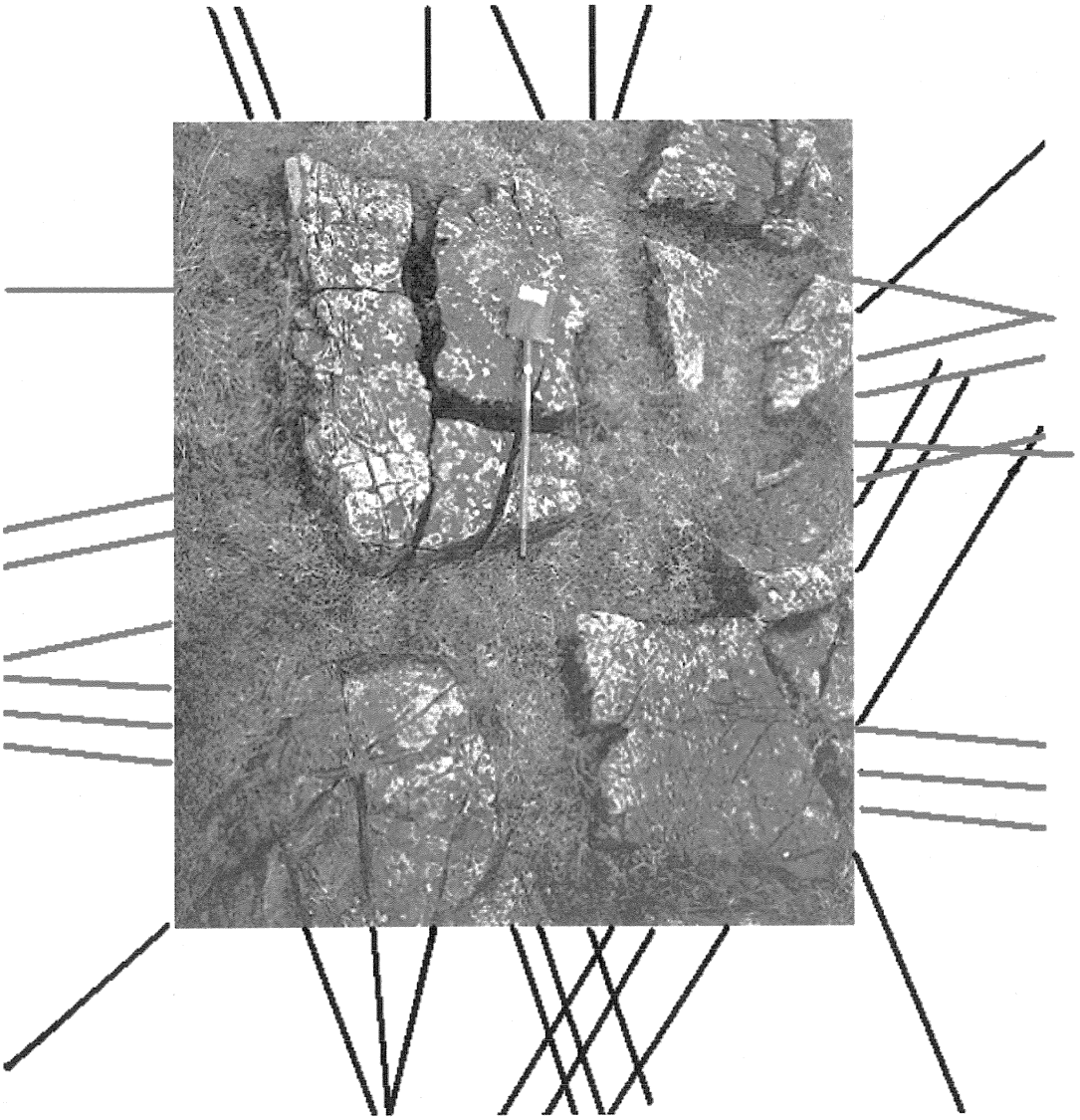

Figure 75. Dissolution enlarged fractures at the Beekmantown core location. The blade of the shovel is pointing north. The fault scarp is directly to the north and has a strike of approximately N-60°-E to N-70°-E. The black lines trace a type II fold related fracture pattern. The red lines trace a type I fold related fracture pattern. Both sets are made up of conjugate sets of shear fractures that are bisected by extension fractures. The Type I fracture set appears to have formed first.

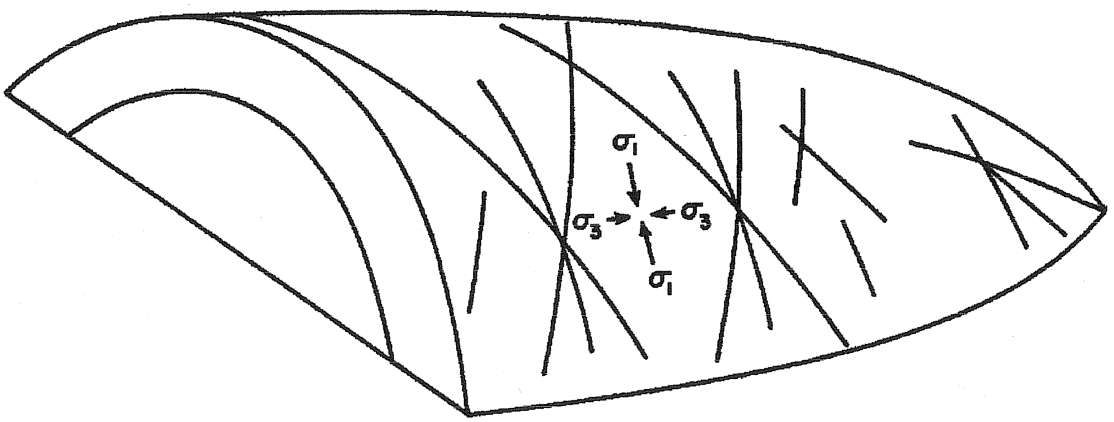

Figure 76. A type I fracture pattern. σ_1 is the greatest principal stress and σ_3 is the least principal stress. The conjugate fractures are shear fractures which are bisected by extension fractures. Both types of fractures have vertical dips. This pattern indicates a shortening in the dip direction and elongation in the strike direction.

Source: Stearns and Friedman, 1972.

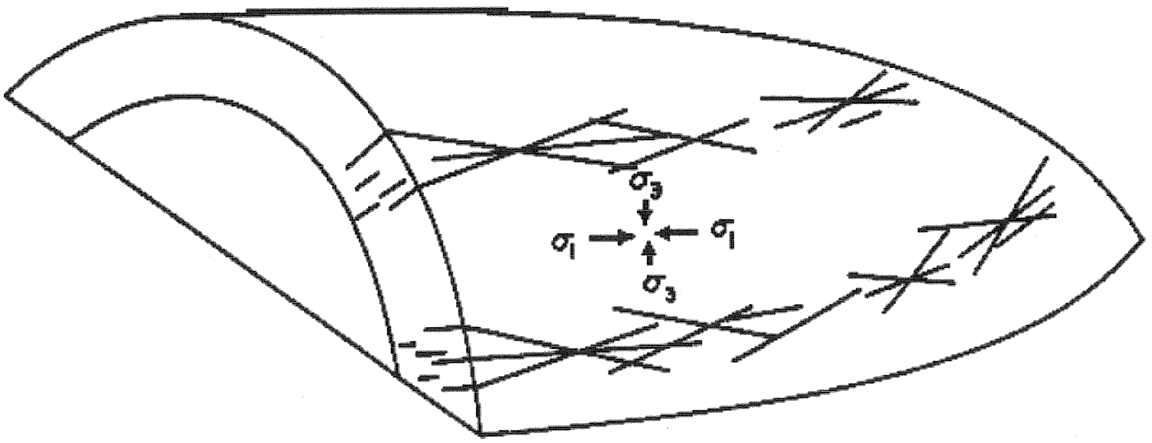

Figure 77. A type II fracture pattern. σ_1 is the greatest principal stress and σ_3 is the least principal stress. The conjugate fractures are shear fractures which are bisected by extension fractures. Both types of fractures are perpendicular to the bedding, so their dips will vary depending upon the dip of the limb of the anticline that they are found on. This pattern indicates a shortening in the strike direction and an elongation in the dip direction.

Source: Stearns and Friedman, 1972.

The 70°-75° dipping fractures are hybrid extension fractures. Dennis (1972) indicated that the hybrid extension fractures (oblique extension fractures) may become faults with continuing deformation. These fractures strike parallel or subparallel to the strike of the fault that they are associated with and were produced by the same tensional forces that caused normal faulting to occur.

The 45° and the 55°-60° dipping fractures are shear fractures. Shear fractures with dips of between 45° and 60° are formed by the same tensional forces and stress field as normal faults (Price, 1966). This indicates that these fractures were formed during the same time as the normal fault.

The 30°-35° dipping fractures are shear fractures. Shear fractures with this dip angle are produced by horizontal compressional forces (Price, 1966). The small, 35° dipping reverse fault at a depth of 45 meters was produced by horizontal compressive forces (Figure 74).

A northeast striking graben, 3.5 kilometers south of the core location, cut through the Isle La Motte thrust sheet (Cumberland Head argillite) and the underlying Beekmantown carbonates (the graben now holds Woodruff pond). This indicates that there were some tensional forces in the area, either post or late Taconic. The small normal fault where the core was drilled is most likely formed during this tensional period and may be linked to the graben to the south.

A core drilled through this bedrock would undoubtedly have intersected fractures that formed both during folding and faulting. Intersecting both fault and fold generated fractures may be the reason that the first 12-meter interval of this core had the highest number of fractures, per 12-meter interval, out of all the cores that were examined for this study.

Many of the fractures associated with the type I pattern have a strike that is subparallel to the strike of the fault and the fractures that are associated with the fault. In core, type I fractures and fault generated fractures would be virtually indistinguishable. Many of the fractures that are part of the type II fracture pattern have a strike that is roughly perpendicular to the strike of the fault generated fractures. This relationship was clearly seen in the core (Figure 73).

LOCALIZED CHANGES IN FRACTURE DENSITY

FRACTURES SURROUNDING FAULTS

The fracture patterns along cores 74-NY-10, 74-NY-6, 74-NY-11, the Imperial Paper Co. core and the Beekmantown core were attributed to the fact that these cores intersected fault zones. Cores 74-NY-10, 74-NY-6 and the Beekmantown core were taken from footwall blocks (Figures. 30, 35 and 71 respectively). Core 74-NY-11 and the Imperial Paper Co. core were taken from hanging wall blocks (Figures. 8 and 62, respectively).

It is clear from the fracture patterns on these cores that there is a distinct fracture gradient surrounding these faults that is roughly perpendicular to the fault plane (Figure 78). Obviously the greatest amount of fracturing occurs adjacent to the fault. Fracturing then diminishes in intensity with distance from the fault. It is fairly straightforward to determine the width of the fracture gradient zone normal to the plane of the fault using Pythagorean's theorem, if the core is used as the hypotenuse of the right triangle (Figure 79). This can be done for individual gradient zones, as pictured in Figure 78, or for the entire width of the fracture zone.

It is important to calculate the width of the fracture zone in the footwall block separately from the width of the fracture zone in the hanging wall block, since the hanging wall block is often more highly fractured than the footwall block (Nelson, 2004). This is due to the fact that the hanging wall block slides over the irregular fault surface, which produces an increased amount of fracturing in that block.

The widths of the fracture zones within the hanging wall and footwall blocks intersected by cores 74-NY-10, 74-NY-6, 74-NY-11 and the Imperial Paper Co. core were calculated and compared. The calculated width was the distance it took for fracture spacing to increase from 0.001 meters to 3 meter. A value of 0.001 meters was used to represent the fracture spacing at the fault plane. The location of the fault plane was estimated from the polynomial extrapolations on the graphs plotting fracture spacing against depth. The calculations were made using 85° fault dips for the faults intersected by cores 74-NY-10 and 74-NY-6 and 60° fault dips for the faults intersected by core 74-NY-11 and the Imperial Paper Co. core (Isachsen and McKendree, 1977 and Bradley and Kidd, 1991).

The displacement of the fault adjacent to core 74-NY-6 (Dolgeville fault) is approximately 37 meters (Bradley and Kidd, 1991). The displacement of the fault adjacent to core 74-NY-10 (East Stone Arabia fault) is approximately 350 – 400 meters (Isachsen and McKendree, 1977). The displacement of the fault intersected by core 74-NY-11 is estimated to be 60 meters (Isachsen and McKendree, 1977). The displacement of the fault intersected by the Imperial Paper Co. core is not

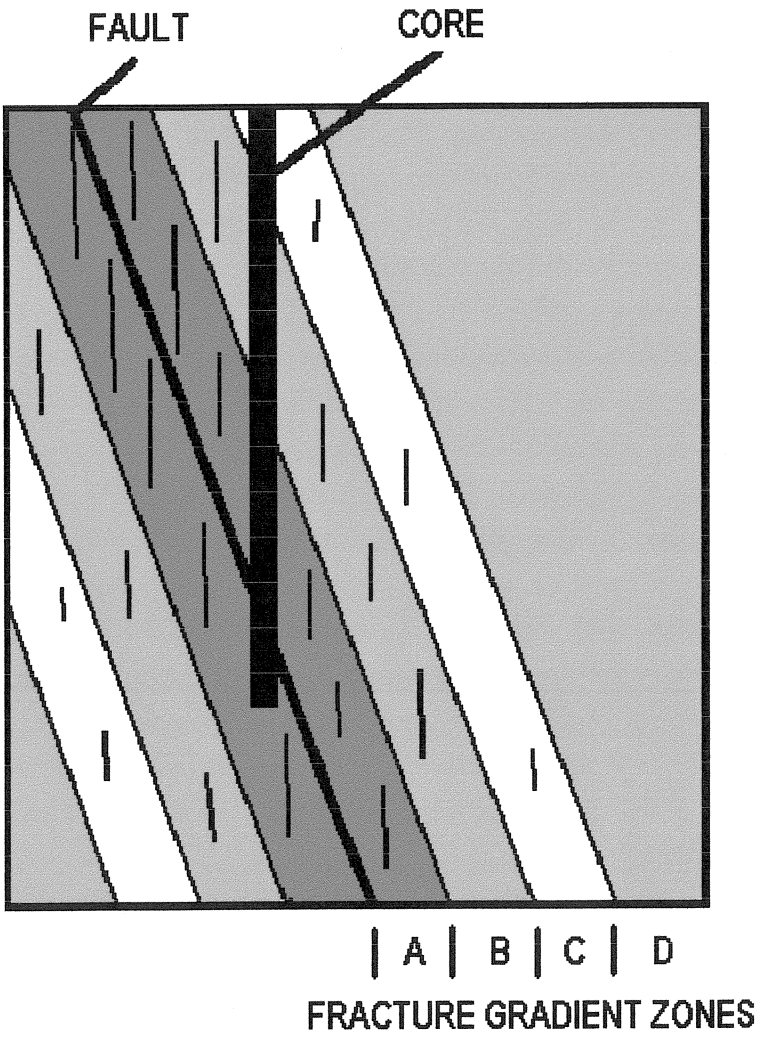

Figure 78. A diagrammatic representation of the fracture gradient zones that parallel the plane of the fault. There is a decreasing amount of fractures within the bedrock with distance from the fault. Zone A is the most fractured zone; zone D is unfractured bedrock.

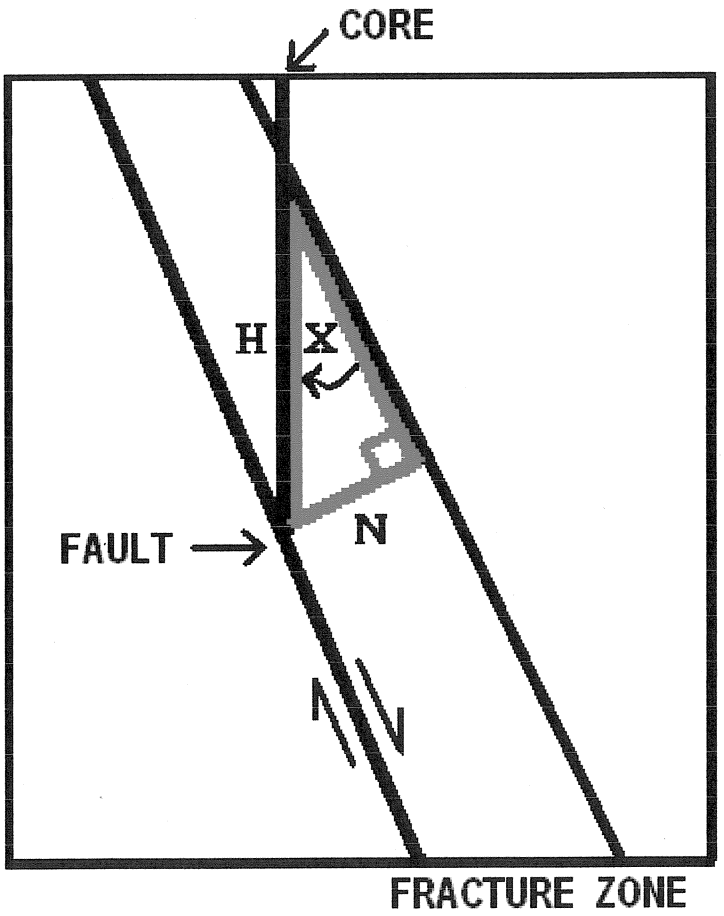

Figure 79. The geometric relationship between the core interval length (H), the angle between the fault plane and the core (X) and the width of the fracture gradient zones, normal to the plane of the fault (N). This particular fracture zone is in the hanging wall block.

known, but the displacements of the faults in the study area are known to increase to the east as the orogenic front is approached (Bradley and Kidd, 1991). The Imperial Paper Co. core is located approximately 55 km northeast of core 74-NY-11. This eastward location may have resulted in a fault displacement that is greater than the fault intersected by core 74-NY-11. In support of this, several faults in the graben system where the Imperial Paper Co. core was taken have displacements of 850 and 1500 meters (Isachsen and McKendree, 1977).

The widths of the fracture zones in the footwall blocks penetrated by cores 74-NY-10 and 74-NY-6 were both very similar in size (Table 30). The widths of the fracture zones in the hanging wall blocks penetrated by core 74-NY-11 and the Imperial Paper Co. core were three to four times greater than the widths of the fracture zones in the footwall blocks. The width of the fracture zone in the hanging wall block penetrated by the Imperial Paper Co. core is 40 % to 60 % greater than the width of the fracture zone in the hanging wall block penetrated by core 74-NY-11.

INTERPRETATION

The similarity in the widths of the fracture zones in the footwall blocks was expected, since the change in average fracture spacing with depth was virtually identical for cores 74-NY-10 and 74-NY-6 (Table 29 and Figure 44). This is not surprising, since the lithology and stress history is the same for the bedrock where both of these two cores were taken. This similarity suggests that the fracture zones within many of the footwall blocks in the Beekmantown carbonates may also be similar in width.

The fracture zones in the hanging wall blocks penetrated by cores 74-NY-11 and the Imperial Paper Co. core are wider than the fracture zones in the footwall blocks penetrated by cores 74-NY-10 and 74-NY-6 (Table 30). This is consistent with the findings of Nelson (2004) who has indicated that there is a greater amount of fracturing in the hanging wall block than the footwall block. This is due to the fact that the hanging wall block slides over the irregular fault surface, which produces an increased amount of fracturing in that block.

The wider fracture zone in the hanging wall block penetrated by the Imperial Paper Co. core, compared to the fracture zone in the hanging wall block penetrated by core 74-NY-11, may be a function of fault displacement. The faults to the east are known to have higher displacements, which would have resulted in an increased amount of fracturing in the hanging wall block as it slid over the footwall block.

Table 30. A comparison between the widths of the fracture zones in footwall blocks and hanging wall blocks. This width is the distance it takes for the fracture spacing to increase from 0.001 to 3 meters on one side of the fault plane. The value of 0.001 meters is meant to represent the spacing at the fault plane.

Core	Block type	Displacement in meters	Length of core in meters	Width of process zone in meters
74-NY-10	FW [(1)]	350 – 400	87 – 97	7.6 – 8.5
74-NY-6	FW	37	100 – 110	8.7 – 9.6
74-NY-11	HW	60	50	25.0
Imperial P.	HW	N/A	70 – 80	35.0 – 40.0

(1) FW – footwall, HW – hanging wall

The fractures zones within the footwall blocks were similar in width despite great differences in fault displacement. The faults adjacent to cores 74-NY-6 and 74-NY-10 are nearly vertical. The fact that these two faults are very steeply dipping may be the reason why there is little difference in the width of the fracture zones despite great differences in fault displacement. The steepness of the faults may have resulted in very little slip related fracturing during fault movement.

FRACTURES WITHIN PROCESS ZONES

The fracture patterns along cores 75-NY-2, 75-NY-14 and 74-NY-9 were attributed to the fact that these cores were taken from fault process zones, where the rock was in a state of stress that was very close to faulting, or in the case of core 75-NY-14, the initial stages of faulting (Figures. 17, 24 and 56, respectively).

The widths of the fault process zones intersected by cores 75-NY-2, 75-NY-14 and 74-NY-9 were calculated using Pythagorean's theorem, in a manner similar to what was done above. The width measured was the distance it took the fracture spacing to decrease from 3 meters to the lowest fracture spacing value calculated for each of the cores. The lowest fracture spacing value was 0.52 for core 75-NY-2, 0.58 for core 74-NY-9 and 0.20 for core 75-NY-2. An angle of 60° was used for the dip of the faults that would have eventually passed through the process zones, since this is a common dip angle for faults in the Mohawk River Valley (Bradley and Kidd, 1991). The length of core used for the hypotenuse of the right triangle was taken from the graphs plotting average fracture spacing versus depth for these three cores (Figures. 21, 28 and 60 for cores 75-NY-2, 75-NY-14 and 74-NY-9, respectively).

The widths of the process zones for cores 75-NY-2, 75-NY-14 and 74-NY-9 ranged in size from 8.5 to 15 meters (Table 31). These widths are comparable to the widths of the fracture zones in the footwall blocks intersected by cores 74-NY-10 and 74-NY-6, but significantly smaller than the widths of the fracture zones in the hanging wall blocks intersected by core 74-NY-11 and the Imperial Paper Co. core (Tables 30 and 31).

INTERPRETATION

The similarity in the widths of the process zones with the fractures zones in the footwall blocks, intersected by cores 74-NY-10 and 74-NY-6, suggests that the process zones penetrated by cores 75-NY-2, 75-NY-14 and 74-NY-9 were very close to faulting. Supporting this is the fact that core 75-NY-14 had some rubble in the interval that had the most fractures. It is believed that this fault had

Table 31. A comparison between the widths of three fault process zones. The width is the distance it takes for the fracture spacing to decrease from 3 meters to the lowest fracture spacing value found on the core.

Core	Block type	Length of core in meters	Width of process zone bedrock in meters
75-NY-2	PZ (1)	22	11.0
74-NY-9	PZ	17	8.5
75-NY-14	PZ	30	15.0

(1) PZ – process zone

experienced a very small amount of displacement, so it is the most highly developed process zone. As such, it should be have the widest process zone, which it does.

The wider fracture zone in the hanging wall blocks, intersected by core 74-NY-11 and the Imperial Paper Co. core, is consistent with the fact that an increased amount of fractures is generated in hanging wall blocks during fault movement (Tables 29 and 30).

REGIONAL CHANGES IN FRACTURE DENSITY

EXTENSION FRACTURE DENSITY

The changes in fracture density over a larger regional area were analyzed by plotting the average number of extension fractures per 12 meter interval of core, for the entire length of core, against the distance to the nearest fault. Averaging the number of fractures enabled cores of different lengths to be used in the analysis.

Cores 74-NY-7, 74-NY-13, the Comstock core and the upper section of the Imperial Paper Co. core were used for this analysis, since each of these cores were taken several kilometers from the nearest surface exposure of a fault. A second order polynomial indicates that the minimum average number of extension fractures, per 12- meter interval of core, can be found at a distance of approximately 7 to 8 kilometers from the nearest fault (Figure 80).

INTERPRETATION

If the distance where the minimum number of extension fractures per 12-meter interval of core is taken to be the point midway between two adjacent faults, then the average distance between faults in the study area is between 14 and 16 km. This distance is in agreement with Bradley and Kidd (1991), who indicated that the average distance between the major faults in the Mohawk River Valley is between 10 and 20 km. This is a very strong indication that the source of the fractures within the Beekmantown Group carbonates is the stress field that produced the faults, which is known to have been produced by the Taconic Orogeny.

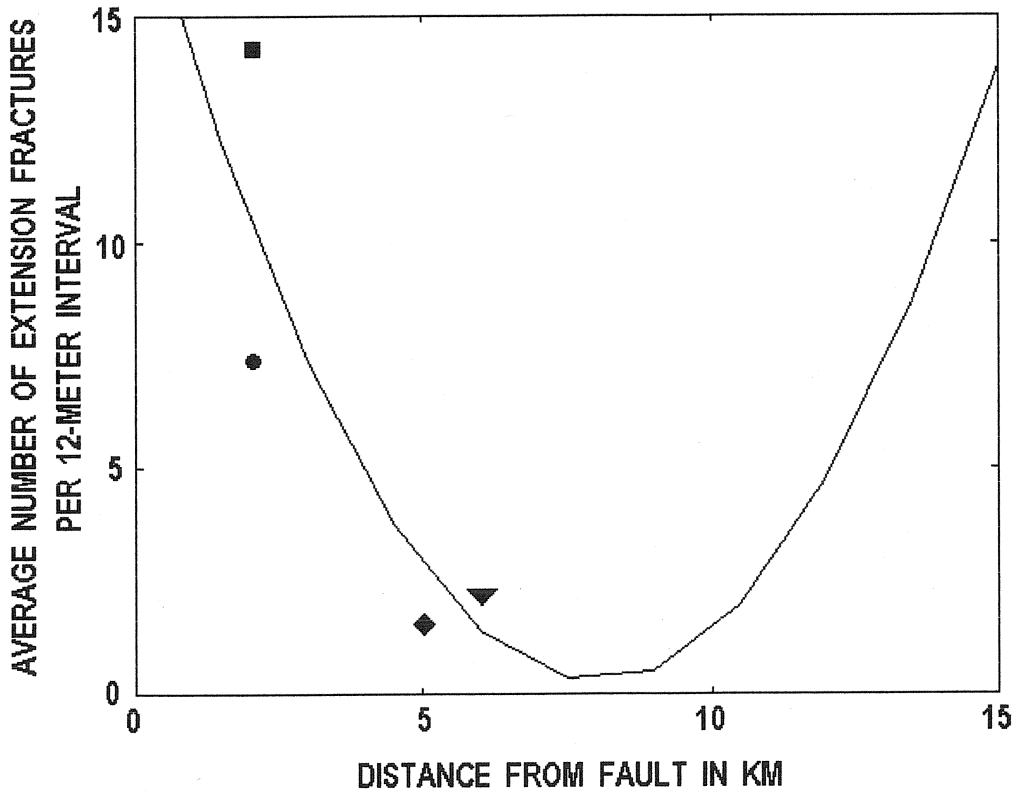

Figure 80. The decrease in the average number of extension fractures, per 12 meter interval of core, with increasing distance from the nearest fault. Square - Core 74-NY-7; circle - Comstock core; inverted triangle - core 74-NY-13; diamond - Imperial Paper Co. core. The line is a second order polynomial.

EXTENSION FRACTURE SPACING

The average fracture spacing between the extension fractures for cores 74-NY-7, 74-NY-13, the Comstock core and the upper section of the Imperial Paper Co. core, were plotted against the distance to the nearest fault to determine if fracture spacing increased with increasing distance from the faults (Figure 81). The average fracture spacing values for each of these cores was calculated as a single value for the entire length of each core. This was done to measure the relationship between the fracture spacing within a larger mass of bedrock and the distance from the faults on a regional scale. The maximum fracture spacing is between 3 and 4 meters at a distance of between 8.5 and 10 kilometers from the nearest fault.

INTERPRETATION

If the distance where the maximum fracture spacing is taken to be the point midway between two adjacent faults, then the average distance between faults in the study area is between 17 and 20 km. This distance is in agreement with Bradley and Kidd (1991), who indicated that the average distance between the major faults in the Mohawk River Valley is between 10 and 20 km. These results indicate that the source of the fractures within the Beekmantown Group carbonates is the stress field that produced the faults, which is known to have been produced by the Taconic Orogeny.

The graph in Figure 81 seems to contradict the average fracture spacing curves in previously sections of this report, which showed that the average fracture spacing increased to three meters within several tens of meters from the fault zones. This apparent discrepancy is due to the size of the bedrock sampled. When measuring the change in average fracture spacing close to individual faults, 12-meter core intervals were used. This size interval was very sensitive to localized changes in fracture spacing. Figure 81, on the other hand, used the entire core length to determine the average fracture spacing. These cores ranged between 60 and 104 meters in length. Using the whole core to make average fracture spacing calculations smoothed over localized changes in fracture spacing and presented a clearer picture of the fracture intensity in a larger volumes of bedrock taken various distances from the faults in the study area.

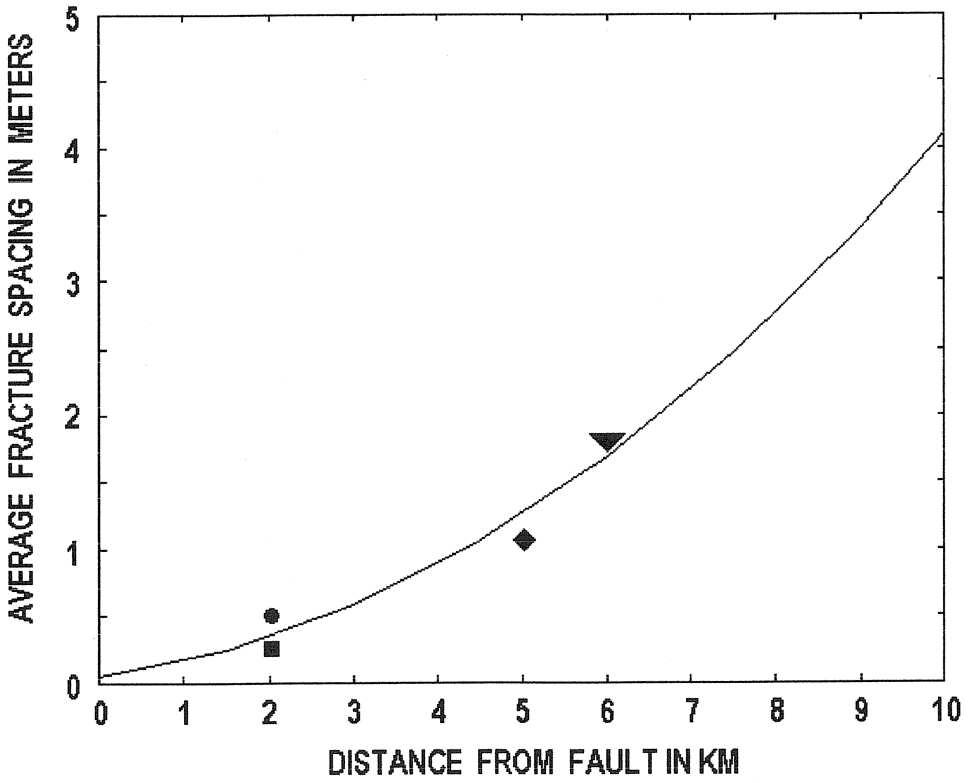

Figure 81. The increase in spacing between the extension fractures with increasing distance from the nearest fault. Square - Core 74-NY-7; circle - Comstock core; inverted triangle - core 74-NY-13; diamond - Imperial Paper Co. core. The line is a second order polynomial.

DIFFERENCES BETWEEN SHEAR AND EXTENSION FRACTURE DISTRIBUTION PATTERNS

Both on a regional scale, and on a local scale, the number of extension fractures increased and the spacing between these fractures decreased as faults were approached. Shear fractures, on the other hand, were not found in any meaningful numbers in areas that were distant from faults. Instead, shear fractures were found clustered very close to the faults.

In order to quantify the apparent differences in these distribution patterns, a comparison was made between the number of extension fractures and the number of shear fractures that were found in a single 12-meter interval of core. Using a single 12-meter interval of core allowed for the comparison of cores of different lengths.

A comparison was made from cores that intersected faults and from cores that were taken further distances from faults. For the cores that intersected faults, this 12-meter interval was the interval closest to the fault. For cores that were taken further distances from faults, the maximum number of both types of fractures tended to be in the same 12-meter interval.

For all the cores that intersected faults, the ratio of the number of extension fractures to the number of shear fractures, in this single 12-meter interval, averaged 1:1 (Table 32). For all the cores that were taken several kilometers from faults, the ratio of the number of extension fractures to the number of shear fractures in this single 12-meter interval, was 3.8:1.

INTERPRETATION

These comparisons quantified the observation that the extension fractures formed over a much greater geographic area than the shear fractures. This indicates that the development of shear fractures is more closely associated with faulting than the development of extension fractures. These results also suggest that the formation of shear fractures occurred after the formation of the extension fractures. This conclusion is based on the fact that there were intervals where extension fractures are found, but no shear fractures.

Table 32. A comparison between the fracture types from cores that intersected fault zones versus cores that were taken greater distances from fault zones. For the cores that intersected faults, the sample numbers were taken from the intervals closest to the faults. For the cores that were taken further distances from faults, the sample numbers were taken from the 12-meter intervals that had the highest number of fractures.

Core	Maximum number of extension fractures	Maximum number of shear fractures	Extension/ shear ratio	Distance to closest fault (km)
74-NY-11	4	5	0.8:1	Intersected fault
74-NY-10	6	5	1.2:1	Intersected fault
75-NY-2	7	7	1.0:1	Intersected incipient fault
75-NY-14	13	12	1.1:1	Intersected incipient fault
Willsboro	14	15	0.9:1	Intersected fault
Beekmantown	11	11	1.0:1	Intersected fault
Average	9.17	9.16	1:1	
SD	4.07	4.12		
74-NY-6	7	0	7.0:0	0.5
74-NY-7	9	3	3.0:1	2.0
Comstock	9	0	9.0:0	2.0
74-NY-9	6	2	3.0:1	3-6
74-NY-13	7	5	1.4:1	6.0
Average	7.60	2.00	3.8:1	
SD	1.34	2.12		

FRACTURE SPACING COMPARISONS BETWEEN SURFACE FRACTURES AND SUBSURFACE FRACTURES

Fracture spacing and strike and dip measurements were taken from a series of outcrops in the study area, so that surface fractures could be compared to subsurface fractures calculated from cores (Figure 82). All of the fractures measured came from Sauk Sequence carbonates. All of the fractures had vertical dips. Single sets of fractures, striking between 60° and 90°, were measured at Lester Park, at the intersection of McQuade and Cranes Hollow Road (east of Amsterdam), in Fort Hunter Quarry and along River Road (south of St. Johnsville). Orthogonal sets of fractures striking 100° to 110° and 10° to 30° were measured in St. Johnsville and in the Crystal Grove Campsite, north of St. Johnsville (Table 33). The present day maximum compressive stress in northeastern North America has a northeast – southwest orientated (Muller et al., 2003).

INTERPRETATION

The single fracture set that strikes between 60° and 90° is very similar in description to the neotectonic joints described by Hancock and Engelder (1989) (Figure 4) and will be given this classified. Neotectonic joints are very shallow features, usually forming in the upper 500 meters of crust due to uplift and erosion. These are the most recently formed joints in the area and, as such, propagate parallel to, or approximately parallel to the direction of the present maximum compressive stress.

Because the fracture spacing between these neotectonic joints ranged between 0.44 and 0.69 meters, it would be expected that a significant, but decreasing number of neotectonic fractures would have been found on the cores in the study area. Core 74-NY-11, for example, was drilled from a depth of 129 to 249 meters, yet the upper 40 meters of this core had no vertically dipping fractures at all (Figure 10). The number of vertically dipping fractures actually increased with depth, to a maximum of 4 per 12-meter interval, at a depth of 196 meters. Core 75-NY-2 had a similar pattern. There was a notable lack of vertical fractures at shallow depths, 340 to 460 meters, followed by an increase in the number of vertical fractures with increasing depth (Figure 18).

The fracture patterns found in these two core samples are the opposite of what would have been expected if they were neotectonic joints. As a result, they cannot be classified as such. The apparent lack of neotectonic joints at the depths from which the cores were taken indicates that neotectonic joints are extremely shallow features in the study area. This means that the fractures that are found in the cores are not neotectonic joints.

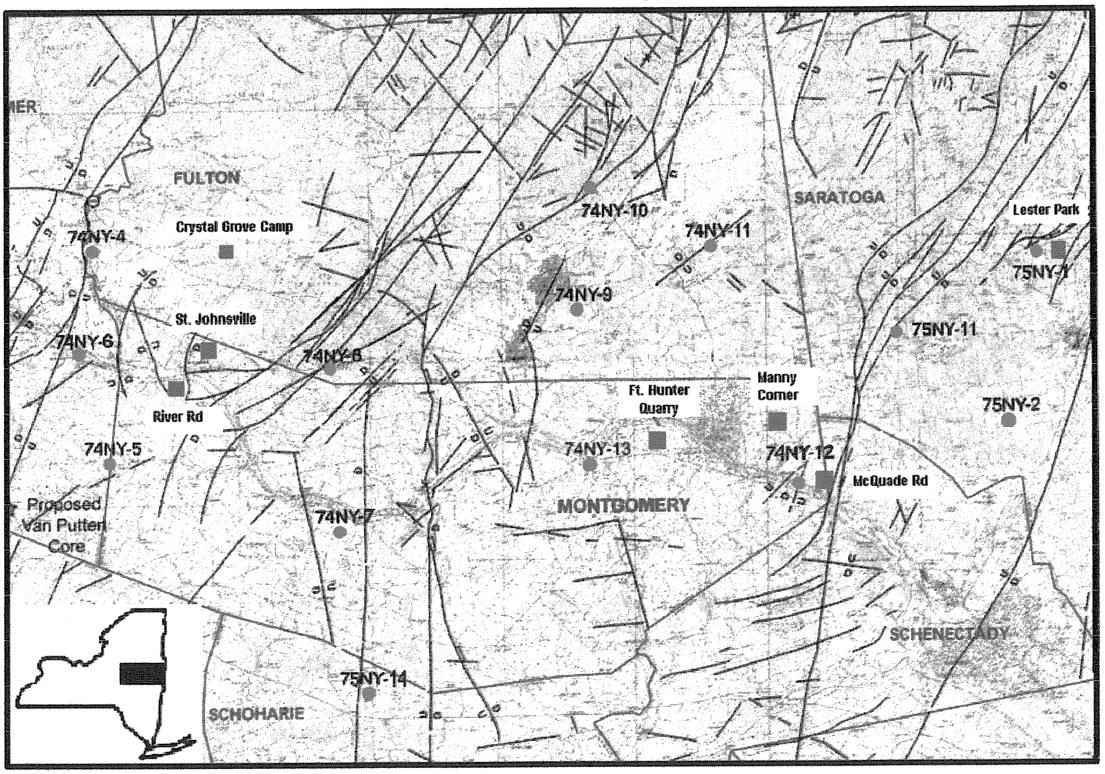

Figure 82. Map of the study area showing the locations of the outcrops where fractures measurements were taken (blue squares). The core locations are also shown on this map (red dots).

Table 33. Surface fracture measurements from outcrops in the Mohawk River Valley. All formations are from the Sauk Sequence.

Location	Formation	Strike	Number of Fractures	Avg. Spacing in meters	SD
Lester Park	Hoyt LS	60°	22	0.69	0.5
Manny Corner	Amsterdam LS	70°	5	0.71	0.40
		160°	8	0.66	0.13
McQuade Rd & Cranes H. Rd.	Cranesville DS	90°	18	0.59	0.41
Fort Hunter Quarry	Fort Johnson, Tribes Hill	60°	25	0.51	0.19
River Road, St. Johnsville	Palatine Bridge	60°	4	0.44	0.19
St. Johnsville	Little Falls	30°	6	0.97	0.23
		110°	6	0.67	0.17
Crystal Grove Campsite	Galway	100°	9	0.37	0.18
		10°	1		

It is not clear if the fractures striking 100° to 110° are also neotectonic joints. Their orientation implies they are not, since the present day maximum horizontal compressive stress field has a northeast – southwest orientation (Muller, et al., 2003). The 10° to 30° striking joints that are orthogonal to the 100° to 110° striking fractures are cross joint fractures that formed after the 100° to 110° striking fractures. Taken together, these two sets of fractures, the 100° to 110° striking joints and the younger set of cross joint fractures, are most probably regional fractures.

The 100° to 110° and the 10° to 30° striking fractures were only measured in the Little Falls and Galway formations. These formations are older than the overlying formations where the other surface fracture measurements where taken. As a result, the Little Falls and Galway formations were subjected to a greater amount of stress, due to deeper burial, and a greater amount of stress release, due to a higher amount of uplift, than the overlying formations. It is very probable that the 100° to 110° dipping fractures were formed due to deep burial whereas the 10° to 30° were formed due to uplift. This interpretation is consistent with the interpretation of others as to the origin of regional fractures (Lorenz, et al., 1991). The deeper depth of burial would explain why these two sets of fractures are unique to these two formations.

DISCUSSION

FRACTURE CONTROLS

Within carbonate rocks, fracture intensity is controlled by a variety of factors, such as bedding thickness, grain size, porosity, lithology and depth of burial (Nelson, 2001). Decreasing bedding thickness, grain size and porosity all increase fracture intensity in carbonate rocks. Carbonate rocks with higher percentages of quartz, feldspar and dolomite have higher fracture intensities than rocks with lower percentages of these minerals and higher percentages of calcite, gypsum and halite. Fracture intensity also increases with depth of burial (in the presence of elevated pore pressure) and with an increase in the amount of overburden that is removed by erosion (Engelder, 1985 and Lorenz, et al., 1991). Fracture intensity is also controlled by structural position (Nelson, 2001). Specifically, and of particular interest to this study, is the fact that flexure related fracturing will be highest where the curvature is at its maximum. It should be noted that within the zone of maximum curvature, lithology (specifically dolomite vs. calcite) plays a much lower role in controlling fracture intensity than outside the zone of maximum curvature (Nelson, 2001).

When determining the cause of the fracturing, it is important to determine if each of the above mentioned characteristics acted as a major control over the formation of the fractures within the Beekmantown Group carbonates. Each of these controls, specific to the study area, will be examined below.

The bedding of the Beekmantown group carbonates in the core samples ranged from massively bedded to thinly bedded. Phillips and Freidman (2001) indicated that within the carbonate units of the Mohawk River Valley, subtidal deposits tended to be massively bedded whereas inter and supratidal deposits tended to be thinly bedded. The transition from subtidal to supratidal facies within the Sauk Sequence carbonates represent 1 to 5 meter thick (and sometimes thicker) parasequences that were formed during fifth-order (50 – 100 ky duration) epeiric platform cycles (Friedman, 1994). If the fracture distribution patterns found on the cores were controlled by bedding thickness, they would have been correlated to the parasequence boundaries. In other words, the number of fractures found along the cores would have increased from subtidal to supratidal areas, as the bedding became thinner. This pattern was not detected on the cores. Instead, individual fractures were often found to pass through sections of rock where there was a noticeable transition from massive bedding to thin bedding. Individual fractures were also found to pass right through parasequence boundaries (Figure 83). This indicated that bedding thickness was not a significant mechanism controlling fracture distribution patterns in the study area.

Needham (2005) indicated that fractures tend to be either strata bound or non-strata bound. Strata bound fractures terminate at boundaries, such as bedding planes, and typically are regularly spaced. Non-strata bound fractures are not constrained by layering and, as a result, are vertically persistent. Non-strata bound fractures are often found in clusters and are found associated with faults. The majority of fractures found on the cores taken from the study area were non-strata bound fractures, which also indicates that bedding was not a mechanism controlling fracture distribution patterns (Figure 83).

It was very difficult to correlate fracture distribution patterns with grain size in the study area due to the extensive diagenesis that has occurred to the carbonate rocks of the Sauk Sequence. Phillips and Friedman (2001) indicated that at least four separate stages of dolomitization occurred in the study area. These stages occurred during or shortly after the deposition of the carbonate material, during deep burial and during uplift of the area. These stages resulted in multiple episodes of textural and geochemical changes to the existing rock as well as the precipitation of additional dolomite crystals within vugs and void spaces. Diagenetic changes to the rock would certainly have occurred after fracturing, since the fractures would have acted as conduits for diagenetic fluids. As a result, the grain sizes and fabric of the rock that existed before and during fracturing would have been altered, making it difficult to impossible to determine original grain size and fabric. As a result fracture distribution patterns were not correlated with grain size.

The extensive diagenesis that changed the grain size and fabric of the rocks also would have significantly changed the original porosity of the rock. A reduction in porosity would have been the result of both compaction, due to deep burial, and the precipitation of dolomite within void spaces. In addition, additional porosity may also have been created due to the dissolution of carbonate material by either hydrothermal fluids or meteoric water. As a result, porosity at the time of fracturing cannot be determined, so fracture distribution patterns cannot be correlated with original porosity. Despite knowing that it impossible to determine the original porosity at the time of fracturing, the fracture distribution pattern along one core, the Beekmantown core, was compared to the porosity along the core (Figure 84). The number of fractures along this core appears to increase with increasing porosity. This conclusion would indicate that fracture intensity increases with increasing porosity, but this is contrary to the well known fact that fracturing actually decreases with increasing porosity (Nelson, 2001). This is due to the fact that rock strength and brittleness decrease with increasing porosity, which decreases fracture intensity.

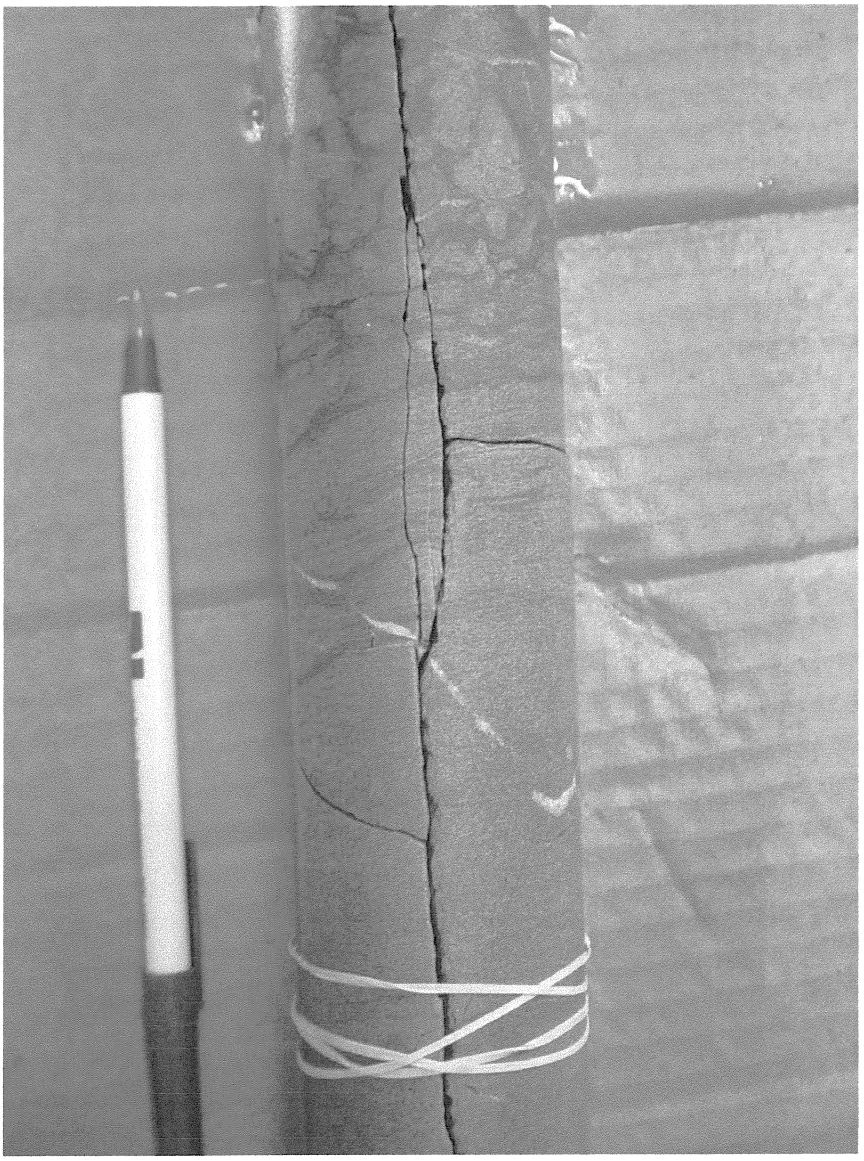

Figure 83. Beekmantown core. An extension fracture passing through a parasequence boundary. This parasequence is an upward coarsening storm parasequence, identified by the presence of a round-pebble conglomerate at the top of the parasequence. Beds become thinner at the top of the parasequence, indicating a change from a subtidal zone to an intertidal or supratidal zone. This fracture is classified as a non-strata bound fracture, since it was not constrained by either the bedding planes or the parasequence boundary (Needham, 2005).

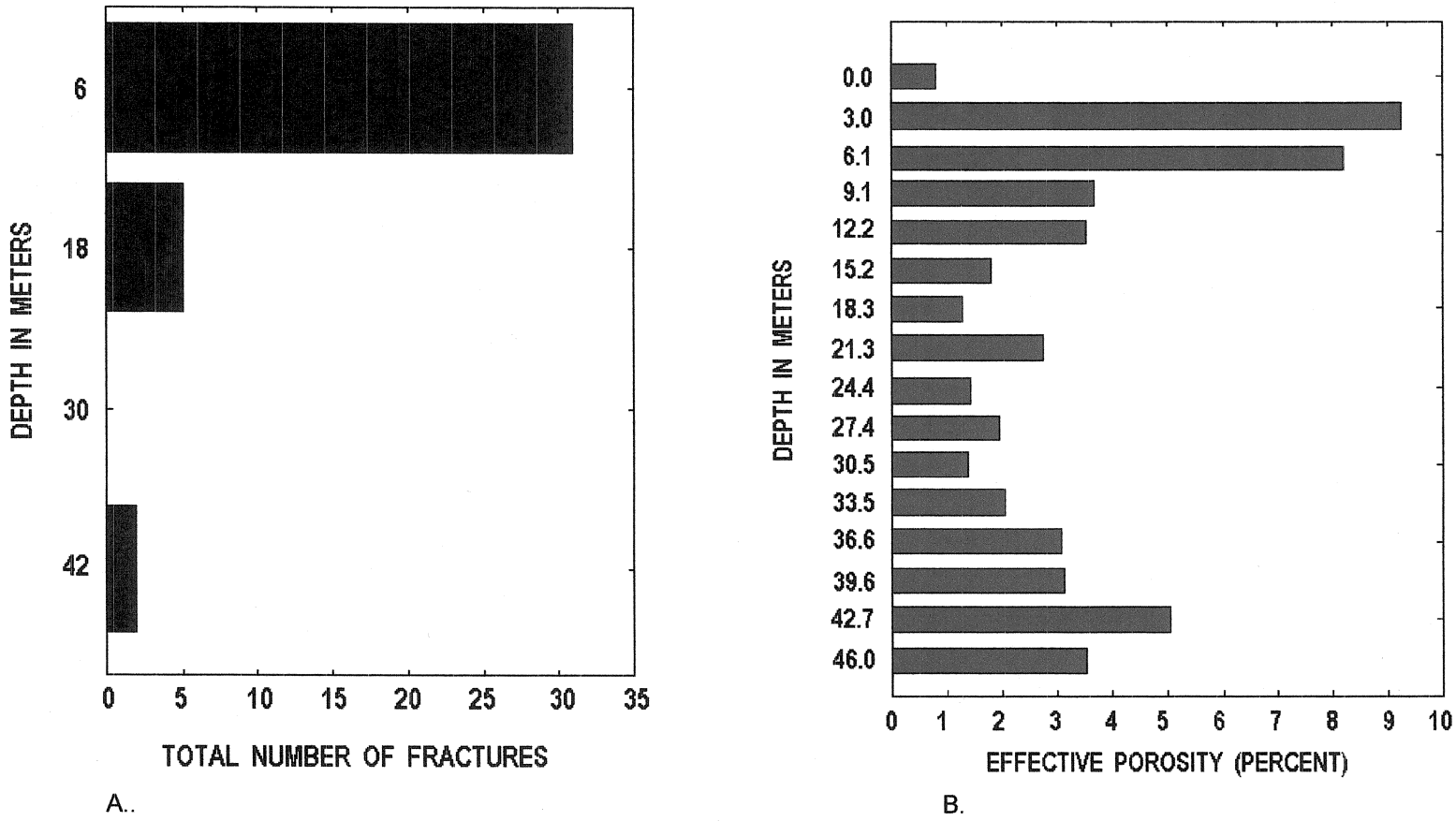

Figure 84. The Beekmantown core. A comparison between the change in the total number of fractures, per 24 meter interval, with depth (A) and the change in matrix porosity with depth (B). The porosity decreases as the number of fractures decrease. The top of the core is level with the Knox unconformity surface.

Instead, the fracture pattern seen in Figure 84 indicates that porosity along the Beekmantown core has increased where there are an increased number of fractures. This is due to the fact that the fractures acted as conduits for meteoric water flow in the vadose or upper phreatic zone, while the area was subaerially exposed. The undersaturated meteoric water dissolved the carbonate material, increasing its porosity. This is consistent with the theory that the original porosity at the time of fracturing cannot be determined.

The majority of the cores came from the Little Falls formation. Some of the cores that passed through the Little Falls formation extended into the Galway formation. The Little Falls formation is a quartzose to low quartz, medium to course crystalline dolostone (Zenger, 1981). The Galway is a medium to coarse crystalline dolostone (Mazzullo, 1977). The quartz content of the Galway formation decreases toward the top of the formation. The core sample from Beekmantown, N.Y. was taken from the Providence Island formation, which is a fine to medium crystalline, low quartz dolostone. Authigenic potassium feldspar is ubiquitous in the dolostones of the Sauk Sequence (Buyce and Friedman, 1975). The Authigenic feldspar occurs as overgrowths over detrital feldspar grains as a result of digenesis of volcanic tuff in a hypersaline environment. Changes in lithology along the cores can largely be ruled out as a mechanism controlling fracture distribution patterns, due to the fact that the rock is primarily composed of brittle minerals (quartz, feldspar and dolomite).

Differences in lithology may be a control affecting the distribution of the fractures in core 75-NY-2. Core 75-NY-2 was the only core to pass through limestone units of significant thickness, the Hoyt, Ritchie and Slade Creek limestones. There were no fractures along the sections of core that passed through these limestone formations. All, but one of the fractures on this core were found in the dolomitic Galway formation, which is located at the bottom of the core. For this reason it could certainly be argued that lithology controlled fracture intensity along this core, since calcite is less brittle than dolomite, feldspar and quartz (Nelson, 2001).

A shallow depth of burial, during the time that fracturing occurred, may have minimized the control that lithology had on the fracturing of the rock extracted by core 75-NY-2. This study has indicated that a significant amount of fracturing in the area occurred during the time of the Knox unconformity. During this time, both the Gailor and Galway formations were only shallowly buried (up to a maximum of several hundred meters). Stearns and Friedman (1972) indicated that the differences in brittleness between limestone and dolostone are minimal in the near surface. Minimal differences between the brittleness of limestone and dolostone at this shallow depth of burial may have limited the control that lithology had on fracturing in the area where the core was taken.

Core 75-NY-2 was taken the farthest distance from the surface exposures of any of the faults in the study area. This indicates that the area where the core was taken was an area where the stress levels were lower.

Ultimately, this lower stress structural position, not differences in lithology, was most probably the factor resulting in the low number of fractures found on this core.

If depth of burial was the mechanism controlling fracture intensity, then there would have been a relatively consistent increase in the number of fractures with depth. In addition, there should also have been some uniformity between the various cores as to the number of fractures found on the cores at a particular depth of burial. Conversely, if uplift due to the removal of overburden was the mechanism controlling fracture intensity, then there would have been a relatively consistent decrease in the number of fractures with depth. Along all the cores that were examined there were both increases and decreases in the number of fractures with depth (Table 34). In addition, there was no consistency between depth of burial and the number of fractures found on the cores. Extension fractures (mode I fractures) were used for this comparison, since they are the type of fractures that form due to deep burial and subsequent uplift (Engelder, 1985).

Within the study area, fracture intensity was only controlled by structural position, specifically, the distance, both locally and regionally, that the core was taken from a fault. Locally, the relationship between structural position and fracture intensity was seen in the cores that intersected or came close to intersecting faults.

This includes cores 74-NY-11, 75-NY-14, 74-NY-10, the Imperial Paper co. core and the Beekmantown core (Figures. 8, 24, 30, 62 and 71, respectively). Along each of these cores, the number of fractures increased dramatically as a fault was approached. These findings are consistent with the findings of other workers, both within and outside of the study area, who found an increase in the number of fractures as fault zones were approached (Thamm, 1939; Shepard, et al., 1981 and Geraghty and Isachsen, 1981).

Most recently, Bahat (2004) identified syntectonic vertical joints that subparalleled the strike of a normal fault in chalks in the Beer Sheva syncline, Israel, (Figure 85). These joints show a significant decrease in spacing as the fault is approached and were formed in the same stress field as the fault. Clearly these fractures are associated with the fault, indicating that structural position was the mechanism controlling fracture intensity.

Regionally, the relationship between structural position and fracture intensity was indicated by the decrease in the average number of extension fractures, per 12-meter interval of core, with distance from the faults (Figure 80). This relationship indicated that the average distance between faults in the study area is between 14 and 16 km. This distance is consistent with the measured average distance between the major faults in the study area (Bradley and Kidd, 1991) and confirms that a regional relationship exists between fractures and faults in the study area.

Table 34. The depth where the greatest number of extension fractures, per interval of core, was found and the trend whether there is an increase or decrease in the number of fractures with depth.

Core	Number of extension fractures	Depth (m)	Trend with depth
74-NY-11	4	196	increase
75-NY-2	5	485	increase
75-NY-14	13	718	decrease
74-NY-10	11	254	decrease
74-NY-6	7	86	decrease
74-NY-7	19	196	no trend
74-NY-13	6	245	no trend
74-NY-9	6	276	decrease
Imperial Paper	11	299	increase
Comstock	9	23	no trend
Beekmantown	11	6	decrease

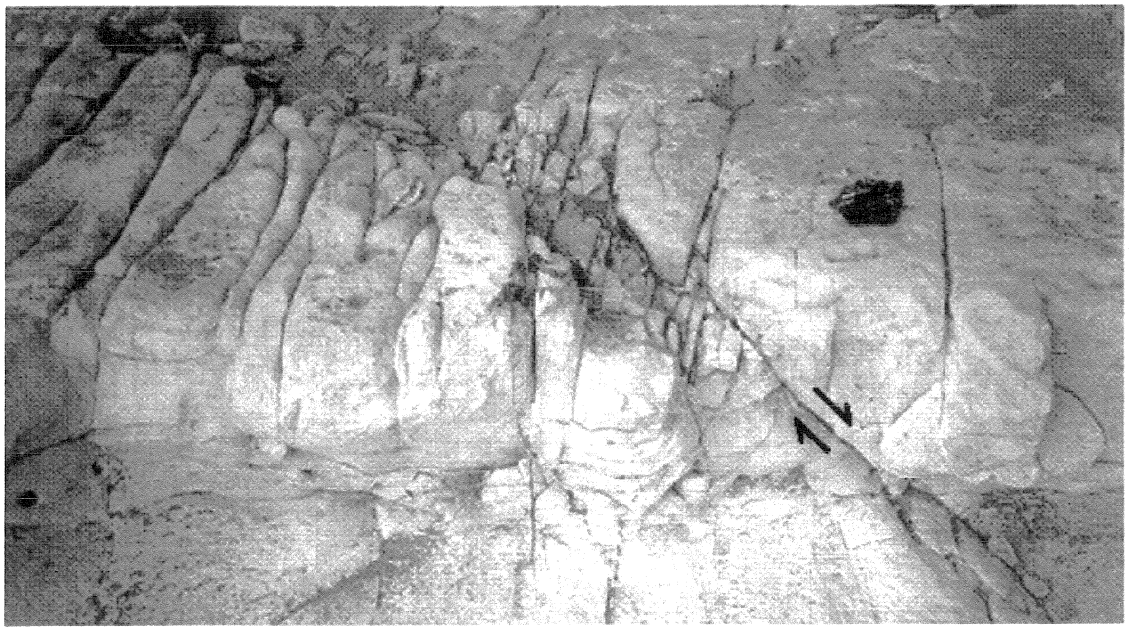

Figure 85. Vertical fracture set found in association with a normal fault in chalk in the Beer Sheva Syncline, Israel. The strike of the fractures is subparallel to the strike of the fault. The fracture spacing decreases as the fault is approached. Backpack on hanging wall block for scale.

Source: Bahat, 2004.

FRACTURE AND FAULT DEVELOPMENT WITHIN EASTERN NEW YORK STATE

The fracture distribution patterns found in core samples taken from the Mohawk and Champlain Valleys indicate that the normal faults that bisect the area developed from an initial fracture network. This development followed an orderly sequence of events. The initial stage of fracture development resulted in the formation of vertical extension fractures in the carbonate bedrock (Figure 86). The extension fractures formed parallel to the greatest and intermediate principal stress axes and perpendicular to the least principal stress axis. This stage most likely occurred as the peripheral bulge first began uplifting the area as it moved cratonward, in advance of the Taconic island arc (Jacobi, 1981). The Sauk Sequence was exposed during this time (post Sauk unconformity), which indicates that the carbonate formations were only subjected to shallow burial. A shallow depth of burial produces low confining pressures, which in turn causes the bedrock to behave as a brittle material during deformation (Price, 1966). The formation of extension fractures is consistent with these conditions. The greatest principal stress axis was vertical at this time, the intermediate principal stress axis was parallel to the strike of the peripheral bulge and the least principal stress axis was perpendicular to it. As a result, the strike of the fractures was parallel to the strike of the peripheral bulge. The bedrock recovered by core 74-NY-13 represents this stage of fracture development (Figure 53 and 55).

The second stage of fracture development resulted in the concentration of extension fractures into linear fracture swarms, or fault process zones (Figure 87). These process zones had 60° to 80° dips and formed as conjugate sets. The presence of both eastward and westward dipping normal faults in the Mohawk River Valley confirms the fact that the process zones formed as conjugate sets. The fracture spacing between the extension fractures in the process zones was close, but not close enough to permit faulting to occur.

During this stage of fracture development, shear and hybrid extension fractures formed between the extension fractures within the fault process zones. Fracturing at this stage probably was not extensive enough to allow faulting to occur. This stage most likely occurred during the continued uplift of the area due to the cratonward migration of the peripheral bulge. The bedrock recovered by core 74-NY-9 represents this stage of fracture development (Figures. 57 and 60).

The presence of hybrid extension (oblique extension) fractures strongly supports the view that the fractures formed during the passage of the peripheral bulge, since they form due to extension across the fracture surface, under a tensile normal stress component (Dennis, 1972). The outer most arc of the bulge would have experienced a significant amount of extension and tensile stress during this time.

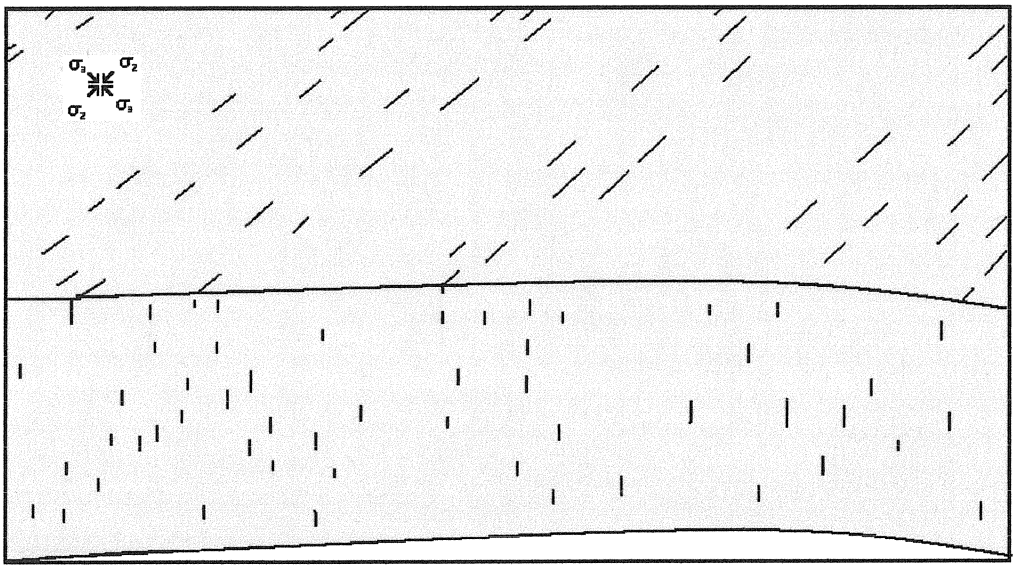

Figure 86. The first stage of fracture development. This stage started as the peripheral bulge, that preceded the Taconic Orogeny, started to uplift the area. At this stage, extension fractures are beginning to develop parallel to the greatest and intermediate principal axes and perpendicular to the least principal stress. Present day east is to the right. Diagram not to scale.

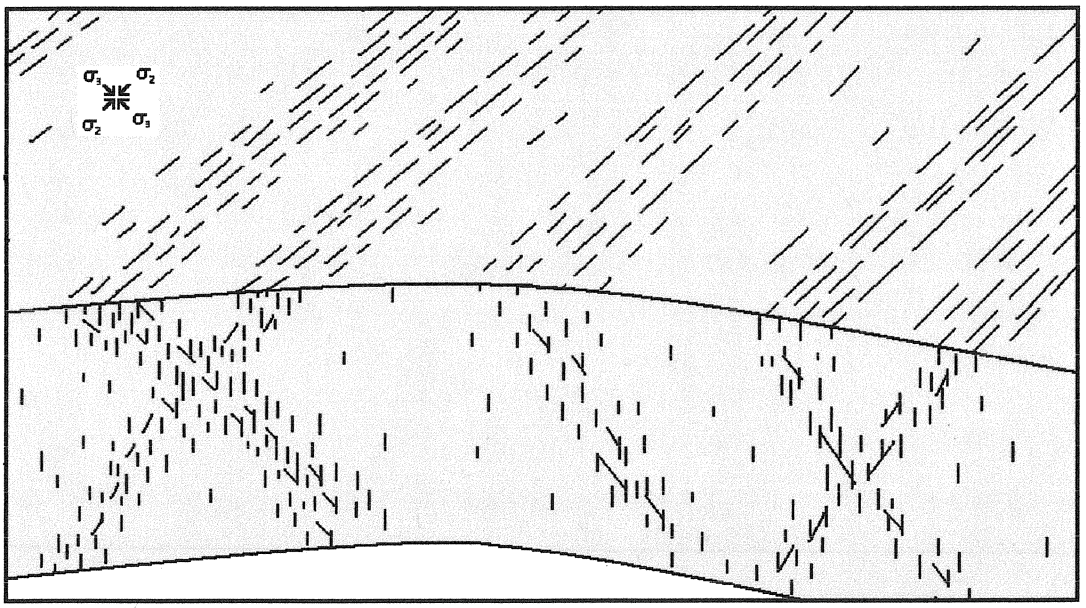

Figure 87. The second stage of fracture development. This stage was the result of an increased amount of uplift due to the passage of the peripheral bulge. At this stage, the extension fractures had become concentrated into a series of conjugate, linear arrays. These concentrated arrays of fractures are fault process zones. During this stage of fracture development, shear fractures and hybrid extension fractures formed between the extension fractures within the fault process zones, but not enough of them formed to permit faulting to occur. Present day east is to the right. Diagram not to scale.

The third stage of fracture development resulted in a decrease in the spacing between the extension fractures and an increase in the number of shear fractures and hybrid extension fractures within the fault process zones (Figure 88). At this time, fault planes developed within some of the fault process zones. Offset along these fault planes also occurred at this time. It is important to note that fault planes need not have formed in all the process zones. The strike of the faults was parallel to the strike of the extension fractures and to the strike of the peripheral bulge. The bedrock recovered by cores 75-NY-2 and 75-NY-14 represents this stage of fracture development (Figures. 17, 21 and 24, 28, respectively).

This stage probably occurred when the peripheral bulge uplift of the area was at its maximum and the area was exposed to subaerial weathering. The best evidence to support this is the presence of extensive paleokarst within the Sauk Sequence carbonates. The fracture networks within the fault process zones formed conduits for meteoric water flow, which resulted in the dissolution of the carbonate bedrock to form karst features. Evaporite minerals were also exposed to the flow of meteoric water at this time and were dissolved and removed, leaving both voids and dissolution collapse breccias behind. Knight, James and Lane (1991) recorded karst to a depth of at least 120 meters below the Sauk Sequence unconformity surface in Newfoundland. Dix, Robinson and McGregor (1998) recorded karst features in Ontario. Friedman (1996), Rubin and Friedman (1977) and Conway and Friedman (1984) all reported evidence of karst in the Sauk Sequence carbonates in New York State. As part of this study, a 45 meter core was drilled in the town of Beekmantown, N.Y. There was a paleokarst surface on the Providence Island formation, at the edge of a normal fault, where the core was drilled (Figure 75). Infilled karst features were present throughout the core, to a depth of 36 meters. Potentially, karst dissolution may even have extended to greater depths, but since the core was only drilled to a depth of 45 meters this cannot now be determined.

The final stage of fracture development is characterized by large scale offset along the fault planes. During this stage, slip related fractures primarily build up within the hanging wall blocks as the blocks slid over the irregular fault surface. This stage took place as the continental crust entered the Taconic foredeep (Bradley and Kidd, 1991). The bedrock recovered by cores 74-NY-11 and 74-NY-10 represents this stage of fracture development (Figures. 8, 14 and 30, 33, respectively).

STRIKE SLIP ANALOG

A very similar sequence of events was used to describe the fracture and fault history of the Sella Group dolomites of northern Italy (Antonellini and Mollema, 2000). In the Sella Group dolomites, joints (extension fractures) first formed parallel to the greatest principal stress (Figure 89). With increasing deformation, the joints localized into conjugate, en echelon arrays with cross joints forming between them.

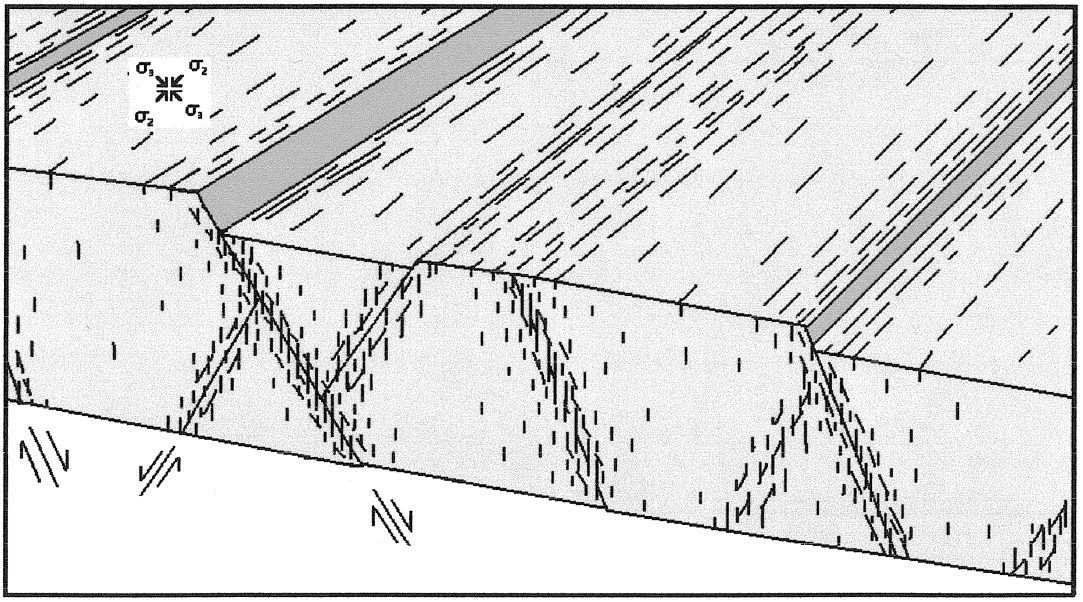

Figure 88. Third stage of fracture development. At this stage, the peripheral bulge had increased the level of deformation to the point where fault planes had developed and small scale faulting had occurred. At this stage there may have been some fault process zones that did not experience faulting. Present day east is to the right. Diagram not to scale.

Antonellini and Mollema (2000) referred to these arrays as joint zones and felt that they represented incipient faults. These joint zones are equivalent to the fault process zones that are found in the Sauk Sequence dolomites in the Mohawk and Champlain Valleys. At the onset of faulting, the bridges between the joints in the joint zones broke up, forming breccias. Shearing was localized within the breccia and increased as large offset faulting progressed.

The depositional and diagenetic history of the upper complex of the Sella Group dolomites is very similar to the Sauk Sequence carbonates and has produced very similar lithologies (Antonellini and Mollema, 2000; Conway and Friedman, 1984; Guo, Sanders and Friedman, 1990; Mazzullo et al., 1978; Philips and Friedman, 2001). Both groups were deformed at a shallow depth of burial, where the dolostone behaved as a brittle material. In both areas, extension fractures formed parallel to the greatest and intermediate principal stresses and perpendicular to the least principal stress and bisected the conjugate angle between the fault planes. In the Sella Group dolomites, the greatest principal stress was horizontal and compressional, resulting in a strike slip tectonic environment. In the Sauk Sequence dolomites, the greatest principal stress was vertical and the area was subjected to extension as a result of the passage of the peripheral bulge. This resulted in normal faulting.

The differences between the tectonic environments initially makes a comparison between the two different areas implausible, but this difference may be negated if the two environments are looked at strictly from the standpoint of the principal stress axes. When strike slip faults and normal faults form as conjugate pairs, the dihedral angle separating the conjugate shear planes is commonly 60° (Figure 90) (Price, 1966). Extension fractures bisect this angle and are parallel to the greatest and intermediate principal stresses and perpendicular to the least principal stress. The geometric relationship between the principal stresses and the faults and fractures in a strike slip environment is the same as in a normal fault environment, but rotated 90°. In the Sella Group dolomites, the strikes of the extension fractures and faults differ by 15° to 35°. In the Sauk Sequence dolostones, the dips of the extension fractures, 90°, and the dips of the majority of the faults, 60°, differ by 30°. The similarity between the orientations of the extension fractures, the faults and the principal stress axes allows for the comparison of the development of the two different fault types.

POROSITY AND PERMEABILITY WITHIN FRACTURE ZONES

The Knox unconformity surface has many productive natural gas reservoirs throughout the United States (Friedman, 1999). Many of these reservoirs are found in Beekmantown correlative rocks, such as the Knox, Arbuckle and Ellenberger formations.

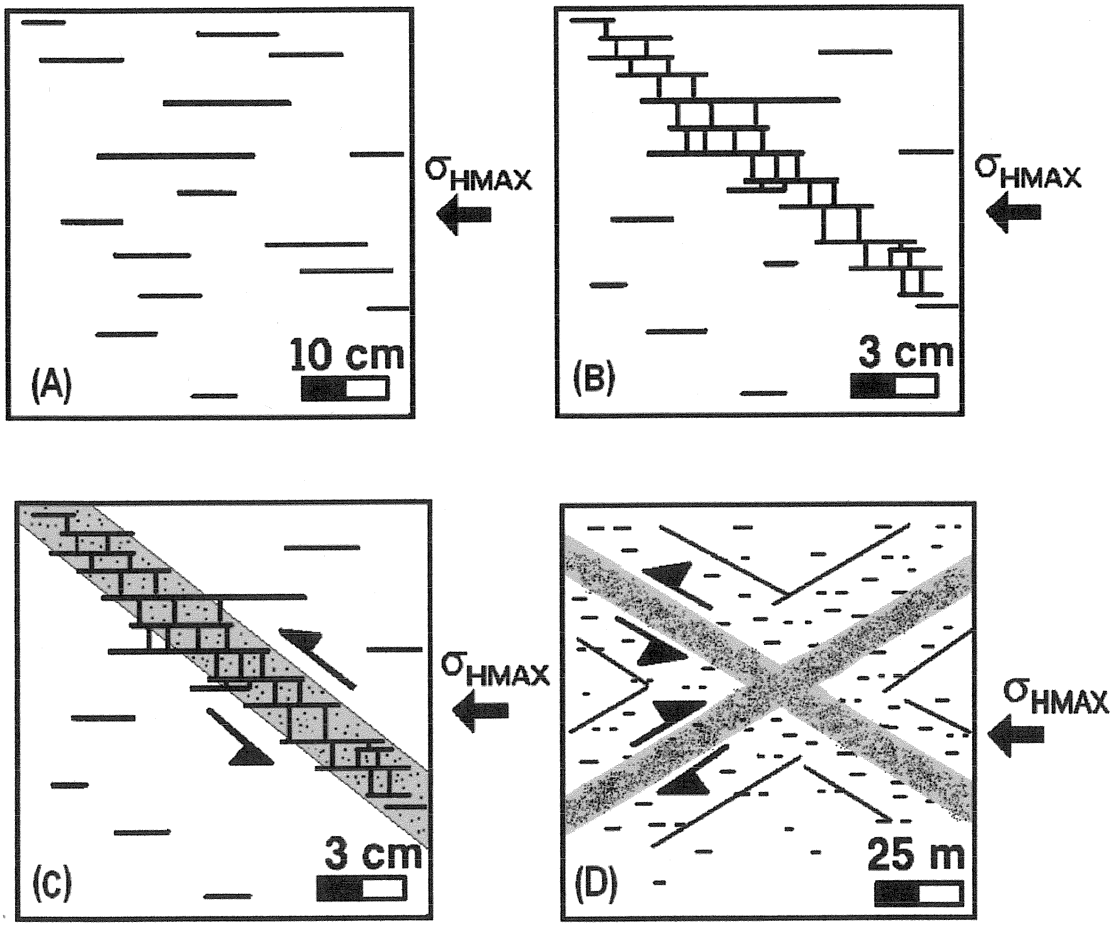

Figure 89. Diagrammatic representation of joint and fault development within the Sella Group dolomites of Northern Italy. (A) The development of joints parallel to the greatest principal stress. (B) The localization of the joints into en echelon arrays (joint zones). (C) The breakup of joint zones as small scale fault movement begins and the formation of breccia zones. (D) The formation of large scale conjugate strike slip faults parallel to and within the joint zones.

Source. Antonellini and Mollema, 2000.

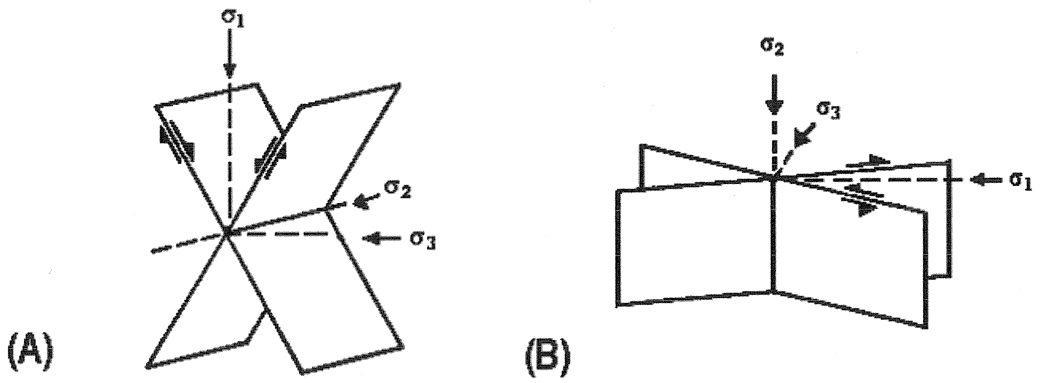

Figure 90. The principal stress axes corresponding to (A) normal faults and (B) strike slip faults, where σ_1 is the greatest principal stress, σ_2 is the intermediate principal stress and σ_3 is the least principal stress. The plane surfaces are conjugate shear planes. Extension fractures bisect the shear planes and are parallel to σ_1 and σ_2 and perpendicular to σ_3.

Source: Price (1966).

Weathering and solution enhancement, due to subaerial exposure, has significantly increased the porosity and permeability of the upper Arbuckle formation in Kansas (Franseen, 2000). Most of the natural gas and oil reservoirs in Kansas are within the top 15 meters of the formation. This has resulted in the practice of drilling into the top 3 meters of the formation, just beneath the Knox unconformity surface.

Subaerial exposure has also enhanced the porosity of petroleum and natural gas reservoirs within the Beekmantown in Ohio (Smosna, et al., 2005). From 1980 to 2002, the Bakersville field in eastern Ohio has produced 18.3 Bcf of gas and 357,000 barrels of oil from paleohighs that were subjected to vadose and upper phreatic meteoric diagenesis (Figure 91). Of special interest to this report is the fact that the paleohighs were produced by the reactivation of normal faults within the basement rock. The upthrown fault blocks are the paleohighs. Within these paleohighs, good porosity is confined to the upper 17 meters of the Beekmantown, just beneath the unconformity surface. Porosity values of 10 to 15% are found just beneath the unconformity surface. Porosity values diminish with depth.

As part of this study, a core was taken from the upthrown fault block of a normal fault in Beekmantown, New York (Figure 70). The bedrock outcrop surface at this site, the Providence Island formation, is the Knox unconformity surface. This outcrop was a paleohigh that had experienced substantial karst erosion. The upper portion of the core was extremely fractured due to the fact that the core was taken right next to the fault scarp (Figures 71 and 72). Fold related fractures were also found at the top of the core. These fractures were produced by the stress field that produced gentle anticlinal folding in the area. The fractures acted as conduits for meteoric water flow, which greatly enhanced the size of some of the fractures (Figure 75). Meteoric water flow also increased the matrix porosity of the bedrock (Figure 84). There is a positive correlation between the number of fractures within the bedrock and the matrix porosity of the bedrock (the greater the number of fractures the greater the porosity). The porosity profile from the upper 25 meters of the Beekmantown core (Providence Island formation) is nearly identical to the porosity profile for the top 25 meters of the Beekmantown Dolomite from the Bakersville field in eastern Ohio (Figures 91 and 84). This comparison strongly suggests that the Beekmantown formation in New York State, just beneath the Knox unconformity surface, contains high quality reservoir rock in areas where paleohighs can be identified. Clearly, the upthrown fault blocks of the normal faults that bisect eastern New York State should be the first areas of exploration for paleohigh reservoirs.

Jacobi (1981) and Knight James and Lane (1991) indicated that the post Sauk erosional unconformity (Knox unconformity in the Appalachian region and the St. George unconformity in Newfoundland) formed due to the cratonward migration of a peripheral bulge in advance of the Taconic Orogeny. Jacobi (1981) suggested that the peripheral bulge may have uplifted the area several hundred meters above sea level. Karst features, seen along the full length of the 45-meter Beekmantown core, support this. Knight, James and Lane (1991) reported that karst features are seen at depths of as much as 120 meters in western

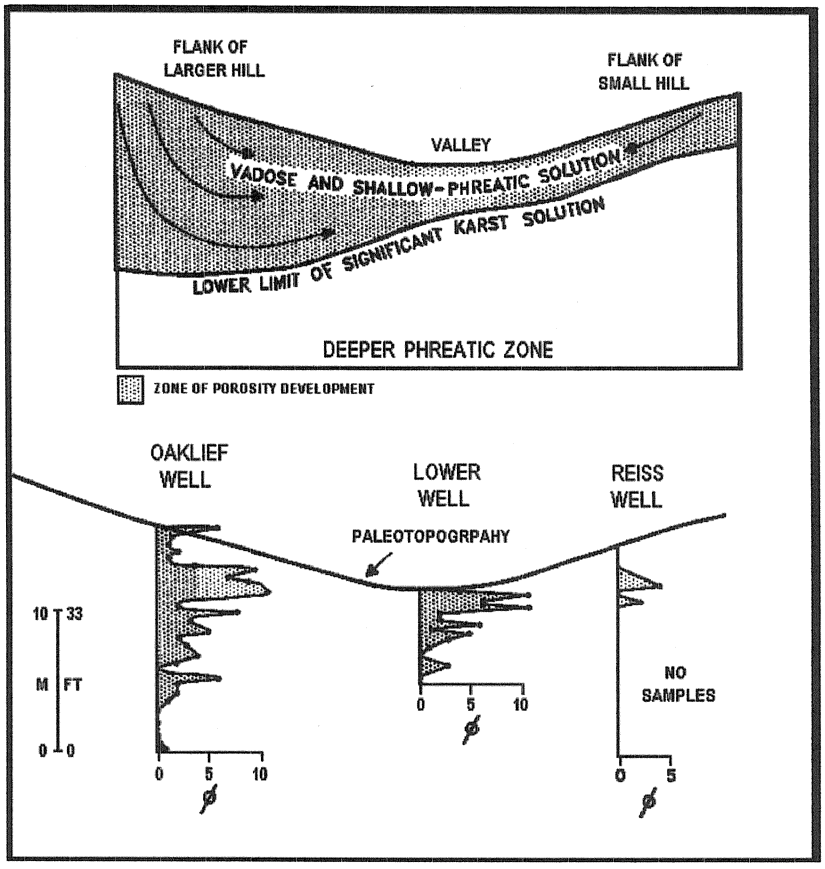

A.

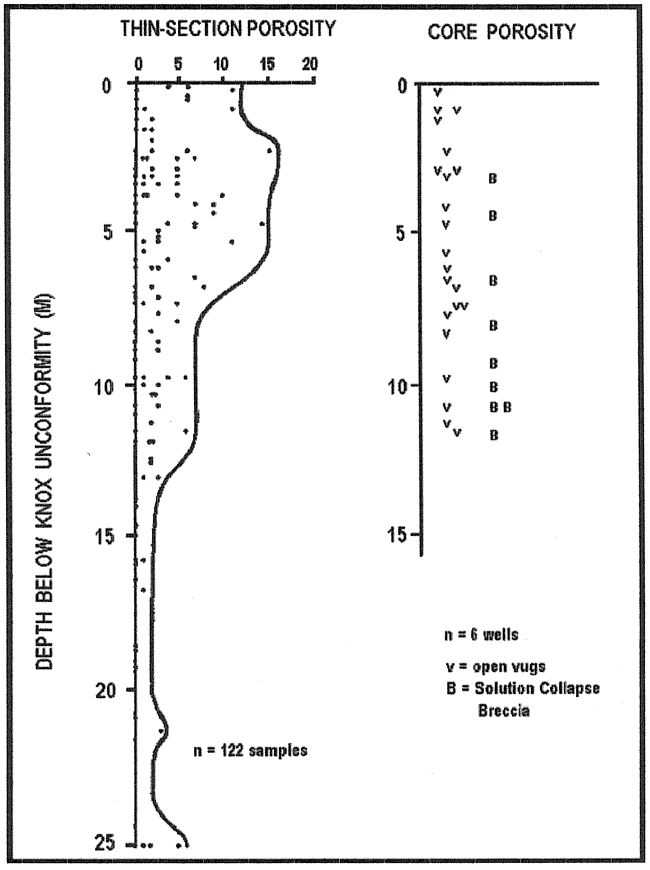

B.

Figure 91. Paleohighs from the Bakersville natural gas field were subjected to both upper phreatic and vadose diagenesis (A), which dramatically increased the porosity within the top 17 meters of the Beekmantown Dolomite in eastern Ohio (B).

Source. Smosna, et al., 2005.

Newfoundland. This also supports the idea that a substantial amount of uplift had occurred during the peripheral bulge uplift. This indicates that a substantial amount of secondary porosity, due to meteoric diagenesis, should be found at depths of up to several hundred meters along fault and fracture networks within the Beekmantown of New York, since these networks acted as conduits for meteoric water flow.

Total reservoir porosity along fault and fracture zones is a combination of fracture porosity and matrix porosity. Fracture porosity is a function of both aperture size and fracture spacing. Fracture porosity increases as fracture spacing decreases and aperture size increases. Fracture porosity for the extension fractures was calculated using Narr's (1996) average fracture spacing method for several of the cores in the study area. The extension fractures were ideally suited for this technique, since Narr's (1996) method requires that fractures are long, relative to the diameter of the core and are perpendicular to bedding. Each set of fractures must be analyzed individually. For the cores that intersected faults, the assumption was made that the extension fractures composed a single set, whose strike was parallel or subparallel to the strike of the fault. This assumption is supported by rock fracture theory, since fractures that are associated with faults, are the result of the same stress field that produced the fault (Nelson, 2001 and Nelson, 2004). As indicated above, this has already been shown to be true in the study area (Geraghty and Isachsen, 1980). The fracture and matrix porosity of several hypothetical fractured reservoirs surrounding faults in the study area were calculated and will be discussed in detail below.

FRACTURED RESERVOIR PENETRATED BY CORE 74-NY-10

Core 74-NY-10 was taken from the footwall block of the East Stone Arabia fault (Figure 7). The apertures of the fractures found on this core ranged in size from 0.005 to 0.20 cm. Using an average aperture value of 0.056 cm and 24-meter interval lengths, the fracture porosity decreased from a high of 0.33% to a low of 0.03% with increasing depth and increasing distance from the fault (Table 35). In order to estimate the fracture porosity closer to the fault, a third order polynomial curve was extrapolated from the center of the shallowest interval (241 to 265 meters) to the estimated depth of the fault, 220 meters (Figure 92). From this curve, the extension fracture porosity is estimated to be 0.8% near the plane of the fault. Along the length of this core, there is an obvious decrease in fracture porosity with an increase in fracture spacing. It needs to be emphasized that this is only the fracture porosity that is associated with the extension fractures. There is additional fracture porosity associated with the hybrid extension fractures that were found along the length of this core and with any fractures that are found within the fault damage zone. The fracture porosity for these fractures was not calculated, since they did not fit the characteristics for using Narr's (1996) method.

Table 35. Core 74-NY-10. Fracture porosity, calculated after Narr (1996), for the vertical extension fracture set. Interval length - 24 meters.

Interval depth (m)	Fracture porosity (%)
241 – 265	0.33
265 – 289	0.10
289 – 317	0.03

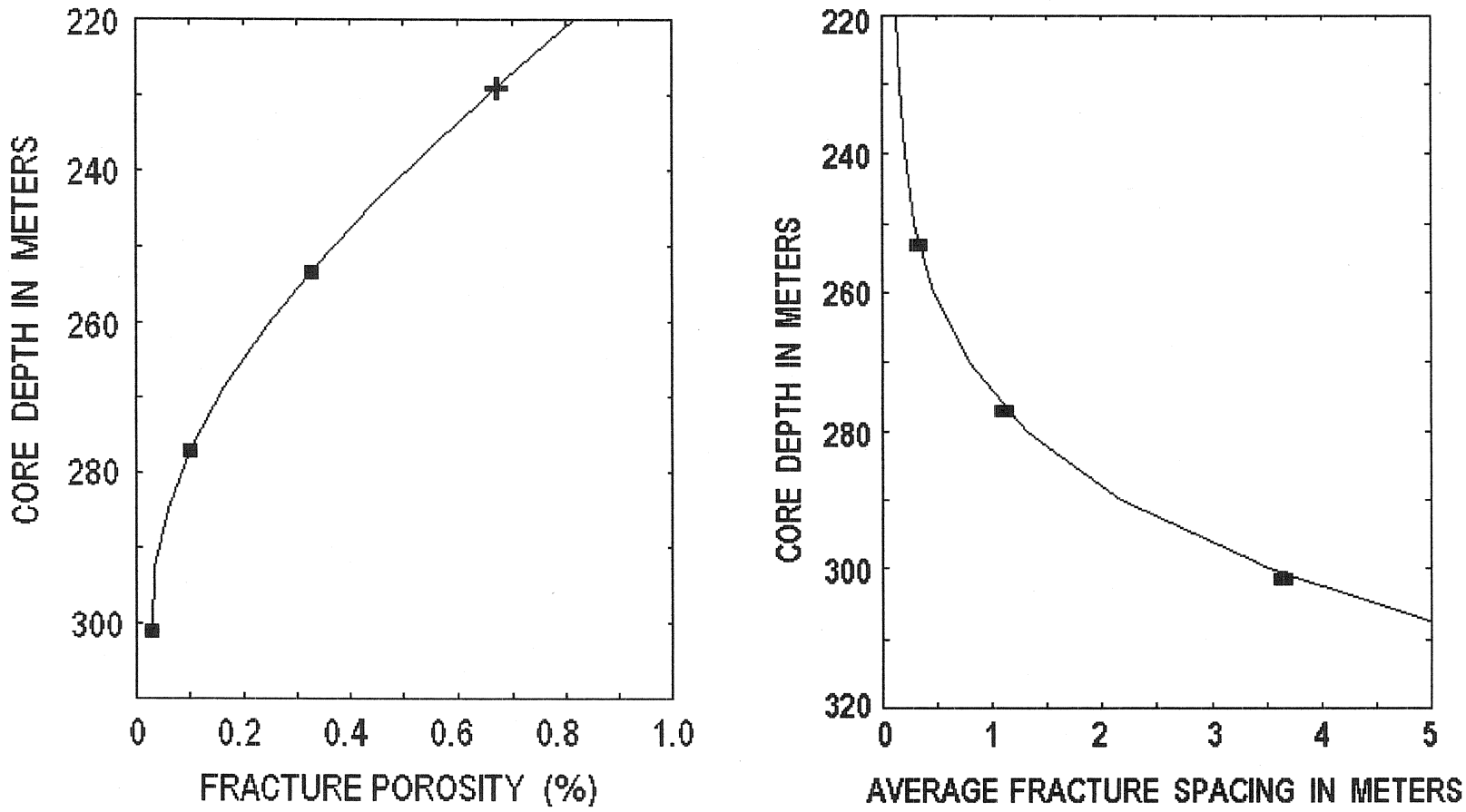

Figure 92. Core 74-NY-10. The change in fracture porosity (A) and fracture spacing (B) with depth and increasing distance from the East Stone Arabia fault. The bars are the centers of each of the 24-meter intervals; the cross is the polynomial intercept at the center of the missing interval between 218 and 242 meters.

There is a distinct fracture gradient surrounding these faults that is roughly perpendicular to the fault plane (Figures 78). The width of each of the fracture gradient zones, normal to the plane of the fault, can be calculated using Pythagorean's theorem, if the interval length is used as the hypotenuse of the right triangle (Figure 79). The East Stone Arabia fault is a high angle normal fault (Isachsen and McKendree, 1977). If the dip angle is estimated to be 85°, the angle between the fracture plane and the core is 5°. If the core interval length, 24 meters, is taken as the hypotenuse of a right triangle, the width of each of the intervals, normal to the fault, is 2.1 meters (sin 5° = N/H). Since core 74-NY-10 had a total of three 24-meter fractured intervals, the known width of the band of fractured bedrock in the footwall block of this fault is 6.3 meters. If the fault is, in fact, at an elevation of 220 meters, then there is an additional 21 meters of missing core between the actual fault and the start of the first interval, at a depth of 241 meters. This is equivalent to an additional 1.8 meters of fractured bedrock, normal to the fault. Therefore, the total width of the band of fractured bedrock in the foot wall block of this fault is 8.1 meters. It is important to note that the band of fractured bedrock on the hanging wall block may be wider, since the hanging wall block often is more fractured than the footwall block (Nelson, 2004).

FRACTURE AND MATRIX PORE VOLUME

From the data above, the total pore volume due to the vertical extension fractures can be calculated for a hypothetical section of fractured reservoir surrounding this fault. This volume does not include the fracture porosity of the hybrid extension fractures or the porosity associated with the fractures within the fault damage zone, so should be viewed as the minimum fracture porosity volume that can be expected.

Fractured reservoirs associated with faults are known to be linear structures (Nelson, 2004). If a fractured reservoir surrounding this fault has a length of 10 km, a height parallel to the plane of the fault of 100 meters and a width equal to the width of the zone of fractured rock in the footwall block, 8.1 meters, then the total volume of fracture porosity is 21,720 m^3 from 8,100,000 m^3 of fractured reservoir (Table 36). Again, this is a minimum value, since this does not include the fracture porosity from the shear fractures or from the damage zone along the fault plane.

This volume of pore space is what would be expected if the fractures are the only source of porosity, a type I fractured reservoir (Nelson, 2004). If the reservoir is a type II, or type III reservoir, the rock matrix adds additional porosity. If the hypothetical reservoir just examined has a porosity of 4%, then there is an additional 324,000 m^3 of pore volume in this reservoir, for a total of 345,720 m^3 of pore space (Table 36). If the hypothetical reservoir just examined has a porosity of 10%, then there is an additional 810,000 m^3 of pore volume in this reservoir, for a total of 831,720 m^3 of pore space.

Table 36. Core 74-NY-10. The extension fracture and matrix porosity volumes of a reservoir from the footwall block of the East Stone Arabia fault.

Fracture zone	Volume reservoir	Percent porosity (%)	Pore volume
Zone A	1,800,000 m^3	0.67(1)	12,060 m^3
Zone B	2,100,000 m^3	0.33	6,930 m^3
Zone C	2,100,000 m^3	0.10	2,100 m^3
Zone D	2,100,000 m^3	0.03	630 m^3
Total	8,100,000 m^3		21,720 m^3
Matrix	8,100,000 m^3	4.0	324,000 m^3
Matrix + fracture	8,100,000 m^3		345,720 m^3
Matrix	8,100,000 m^3	10.0	810,000 m^3
Matrix + fracture	8,100,000 m^3		831,720 m^3

(1) Estimated value based on extrapolation

FRACTURED RESERVOIR PENETRATED BY CORE 74-NY-11

Core 74-NY-11 was taken from the hanging wall block of one of the faults that forms the graben that holds that Sacandaga reservoir (Figure 7). As with most of the other cores examined, the apertures of the fractures found on this core ranged in size from 0.005 to 0.20 cm. Using an average aperture value of 0.056 cm and 12-meter interval lengths, the fracture porosity decreased from a high of 0.13% to a low of 0.02% with decreasing depth and increasing distance from the fault (Table 37). It should be noted that the 12-meter interval from a depth of 202 to 214 meters was severely fractured and does contain any extension fracture porosity. The reason that the fracture porosity for this interval was 0 % is due to the fact that there were no extension fractures within this interval (Figures 8, 10 and 11). This interval is close to the fault plane and is within the damage zone that surrounds the fault plane. The damage zone surrounding the fault plane is severely fractured and has a complex fracture geometry. Due to this complex geometry, the fracture porosity from the fractures within the damage zone cannot be calculated using the method developed by Narr (1996).

In order to estimate the fracture porosity closer to the fault, a third order polynomial curve was extrapolated from a depth of 160 meters to the estimated depth of the fault, 220 meters (Figure 93). The extension fracture porosity is estimated to be 0.8% near the plane of the fault. This increase in fracture porosity is consistent with the decrease in fracture spacing as the fault is approached.

FRACTURE AND MATRIX PORE VOLUME

It is clear that there is a distinct fracture gradient surrounding these faults that is roughly perpendicular to the fault plane (Figure 78). The width of each of the fracture gradient zones, normal to the plane of the fault, can be calculated using Pythagorean's theorem, if the interval length is used as the hypotenuse of the right triangle (Figure 79). In this case, the 12-meter core interval length is the hypotenuse of the right triangle. Using an estimated fault dip of 60°, the angle between the plane of the fracture gradient zones and the vertical core is 30° (90° – 60° = 30°). The width of each of the 12-meter intervals, normal to the plane of the fault is 6 meters ($\sin 30^\circ = n/12$; $n = 6$). Four full 12-meter intervals (centered at 172, 184, 196 and 208 meters) and half of one 12-meter interval (centered at 220 meters) is equal to a 27-meter band of fractured rock on the hanging wall side of the fault plane.

From this data, the pore volume due to the vertical extension fractures was calculated for a hypothetical fractured reservoir within the hanging wall block of this fault. This volume should be viewed as the minimum fracture pore volume that can be expected, since the fracture porosity from the fractures within the fault rubble zone was not calculated.

Table 37. Core 74-NY-11. Fracture porosity, calculated after Narr (1996), for the vertical extension fracture set. Interval length, 12-meters.

Interval depth (m)	Fracture porosity (%)
130 – 142	0.00
142 – 154	0.00
154 – 166	0.00
166 – 178	0.02
178 – 190	0.04
190 – 202	0.13
202 – 214	0.00[(1)]

(1) Values of 0 % are due to an absence of vertical fracture in the interval.

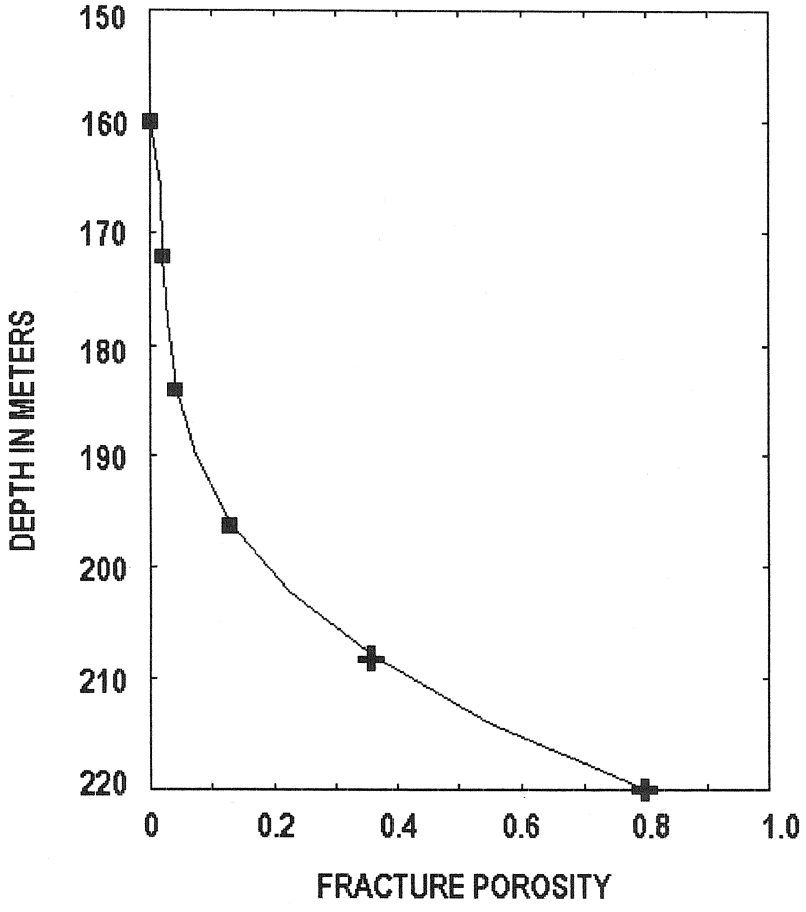

A..

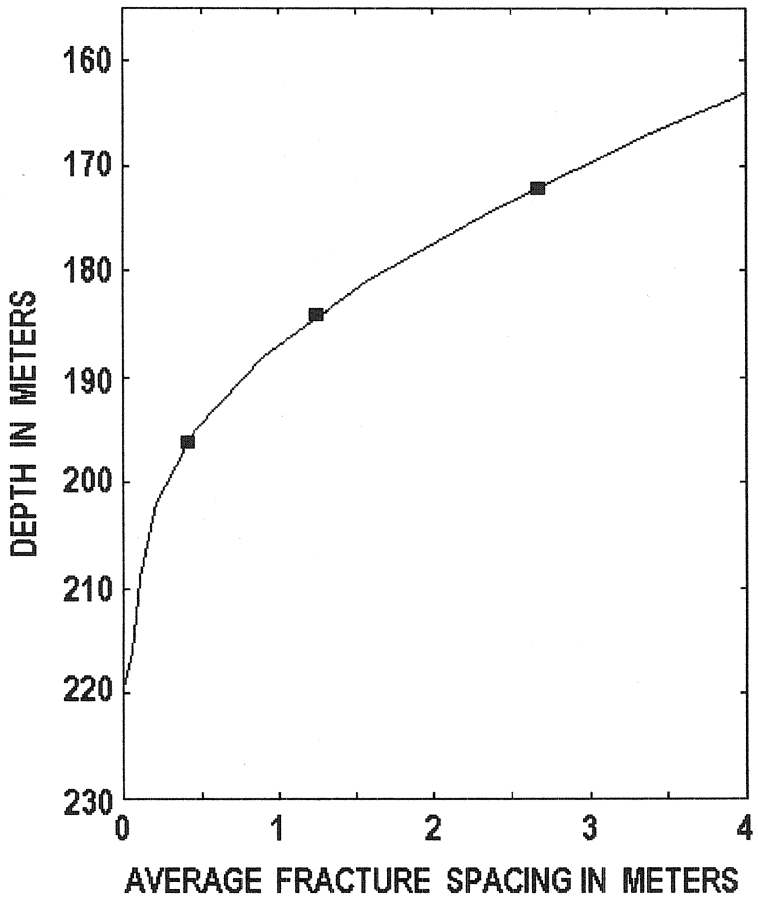

B.

Figure 93. Core 74-NY-11. The change in fracture porosity (A) and fracture spacing (B) with increasing depth and decreasing distance from the fault. The bars are the centers of each of the 12-meter intervals; the crosses are the extrapolated values for the interval between 202 and 214 meters and for the value at the estimated location of the fault plane, at 220 meters.

Fractured reservoirs associated with faults are known to be linear structures (Nelson, 2004). If a fractured reservoir surrounding this fault has a length of 10 km, a height parallel to the plane of the fault of 100 meters and a width equal to the width of the zone of fractured rock in the footwall block, 27 meters, then the total volume of fracture porosity is 57,630 m^3 from 27,000,000 m^3 of fractured reservoir (Table 38). Again, this is a minimum value, since this does not include the fracture porosity from the shear fractures or from the fractures within the damage zone close to the fault plane. This is also a minimum value, since the fracture reservoir within the footwall block is not included in these calculations.

This volume of pore space is what would be expected if the fractures are the only source of porosity, a type I fractured reservoir (Nelson, 2004). If the reservoir is a type II, or type III reservoir, the rock matrix adds additional porosity. If the hypothetical reservoir just examined has a porosity of 4%, then there is an additional 1,080,000 m^3 of pore volume in this reservoir, for a total of 1,137,630 m^3 of pore space (Table 38). If the hypothetical reservoir just examined has a porosity of 10%, then there is an additional 2,700,000 m^3 of pore volume in this reservoir, for a total of 2,757,630 m^3 of pore space.

FRACTURED RESERVOIR PERMEABILITY

Within each of the above cases, it is clear that the matrix porosity is substantially larger than the fracture porosity. The fractures are much more important in increasing the permeability within the reservoir than increasing reservoir volume.

With respect to permeability, the dominance of parallel or subparallel vertical extension fractures will create a highly anisotropic reservoir. Because the extension fractures are subparallel or parallel to each other and parallel or subparallel to the strike of the fault, the permeability parallel to the plane of the fault can be several orders of magnitude greater than the permeability perpendicular to the strike of the fault (Nelson, 2001and Nelson, 2004). The presence of shear and hybrid extension fractures within the fractured reservoir is extremely beneficial, since they interconnect the parallel and subparallel vertical extension fractures, increasing permeability perpendicular to the strike of the fault. More importantly, the shear fractures interconnect the parallel vertical extension fractures, so that the reservoir is not compartmentalized.

Stylolites were found along many of the cores. Stylolites will impede flow in the direction perpendicular to the stylolite (Nelson, 2001) (Figure 94). Unloading fractures are often found associated with stylolites and form parallel to the stylolite seam. The presence of these unloading fractures can greatly increase the permeability of the rock parallel to the plane of the stylolite. Nelson (2001) warns that many of these fractures form as a result of the coring operation and may not be

Table 38. Core 74-NY-11. The extension fracture and matrix porosity volumes of a hypothetical reservoir from the hanging wall block penetrated by core 74-NY-11.

Fracture zone	Volume reservoir	Percent porosity	Total porosity volume
Fault zone	3,000,000 m^3	0.80(1)	24,000 m^3
Zone A	6,000,000 m^3	0.36(1)	21,600 m^3
Zone B	6,000,000 m^3	0.13	7,830 m^3
Zone C	6,000,000 m^3	0.05	3,000 m^3
Zone D	6,000,000 m^3	0.02	1,200 m^3
Total	27,000,000 m^3		57,630 m^3
Matrix	27,000,000 m^3	4.0	1,080,000 m^3
Matrix + fracture	27,000,000 m^3		1,137,630 m^3
Matrix	27,000,000 m^3	10.0	2,700,000 m^3
Matrix + fracture	27,000,000 m^3		2,757,630 m^3

(1) Intercept values taken from the polynomial curve in figure 88.

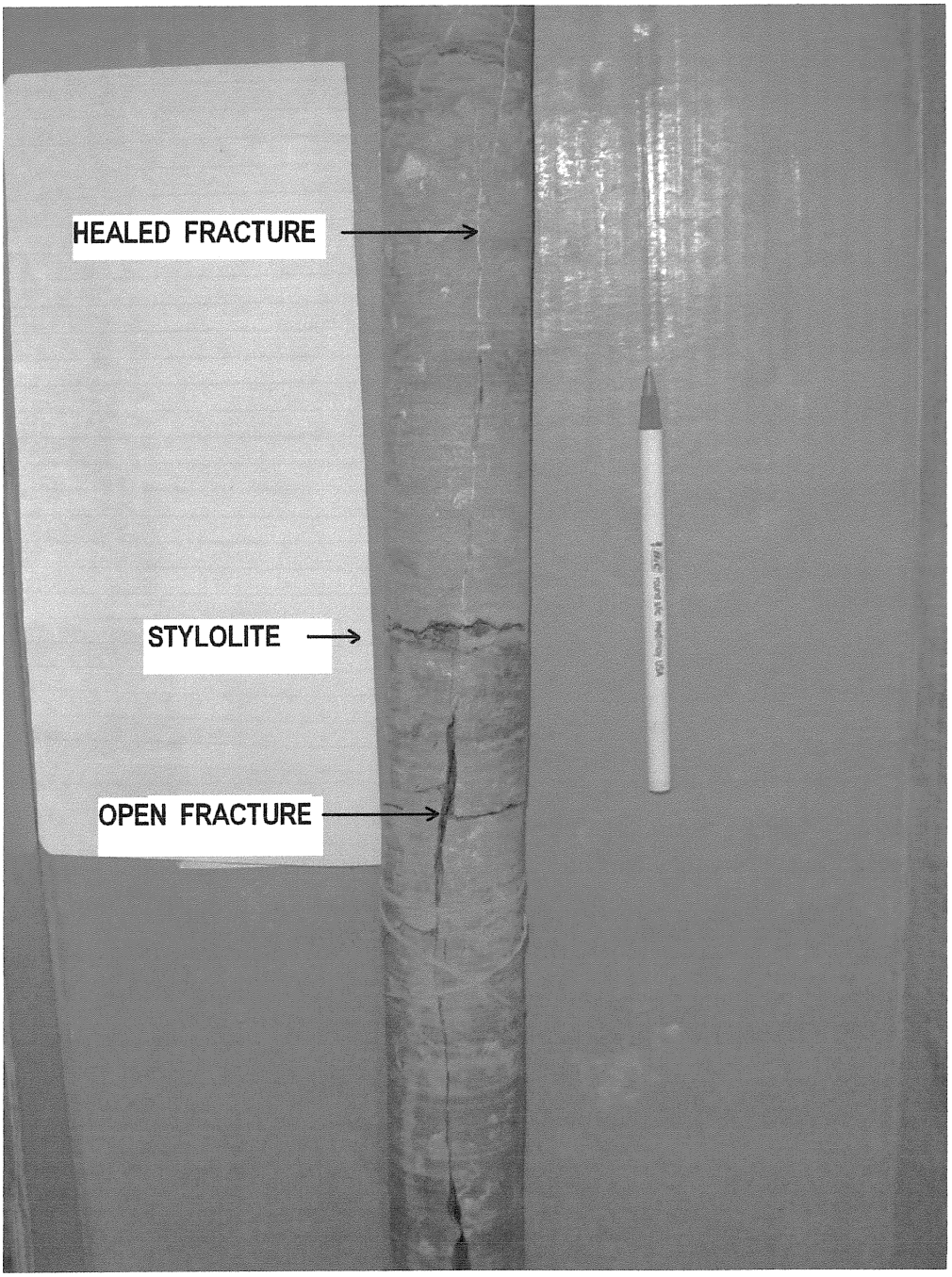

Figure 94 Core 74-NY-9. A stylolite at a depth of 311 meters. The top of the core is pointed toward the top of the picture. Above the stylolites the fracture is filled with carbonate cement. Below the stylolites, the fracture is open. This demonstrates the ability of a stylolite to limit flow perpendicular to the plane of the stylolite, in this case, mineral rich water was not able to flow below the stylolite. As a result, the fracture below the stylolite remained open.

found at depth. Therefore, increased permeability parallel to and close to the plane of stylolites at depth cannot be guaranteed. Where present, stylolites may act to compartmentalize reservoirs.

Mineral filled fractures form permeability barriers in fractured reservoirs (Nelson, 2001). Partially filled fractures can actually increase fracture porosity since the mineral growth prevents the closure of the fracture due to an increase in overburden pressure during burial. Although completely mineral filled fractures were found along the length of the core, the majority of the fractures examined for this study were open fractures. Partially filled fractures were also found along the cores.

Where present, gouge and slickensides can act as permeability barriers in fractured reservoirs (Nelson, 2001). Gouge is finely abraded material that forms between the walls of a fracture. It forms as a result of grinding and cataclasis during movement along a fracture or fault plane. When cemented, gouge can form a very low permeability barrier to fluid flow. Slickensides form from frictional sliding along a fault or fracture plane. The formation of both gouge and slickensides result from movement parallel to a fracture or fault plane. The vertical fractures found on the cores are extension or mode I fractures, which are defined by movement perpendicular to the fracture plane. This type of movement would not form either gouge or slickensides. As a result, these morphologic features were not found along the extension fractures. These morphologic features were also absent from the shear fractures, despite the fact that the displacement along shear fractures is the type of movement that would produce these morphologic features. Gouge is most often found in porous sandstones, so the absence of gouge within the shear fractures that formed in the dolomite rock may certainly be due to lithology. Carbonate rocks typically have slickensides, but none were found on the fractures that were found on the cores. Interestingly, well formed slickensides were found on fracture faces in the Precambrian metamorphic rocks that were found stratigraphically beneath the Sauk Sequence carbonate rocks. The absence of slickensides on the carbonate rocks may be the result of meteoric diagenesis, since the fractures acted as conduits for meteoric water. As discussed above, there is widespread evidence of karst dissolution throughout the study area. The lack of slickensides may be yet another example of karst. The reason that the metamorphic rocks still had the slickensides on the fracture faces is due to the fact that the minerals that make up the metamorphic rocks are much less susceptible to dissolution by meteoric water flow than the carbonate minerals.

OPTIMAL DRILLING ORIENTATION

The dominant fracture set surrounding the faults in the study area are the vertically dipping extension fractures that are parallel to, or subparallel to the strikes of the faults. As a result, a vertical bore hole would intersect the fewest number of these fractures in a fractured reservoir surrounding any of the faults in the study area. The optimal drilling orientation with regard to the vertically dipping extension

fractures is clearly a horizontal well drilled normal to the strike of the fault and these fractures. This bore hole should pass through the fault zone and not stop until unfractured bedrock is encountered. This would ensure that the maximum number of vertically dipping extension fractures was intercepted. The anisotropic nature of the permeability of a fractured reservoir surrounding a fault would not require close well spacing along the strike of the fault in order to extract the maximum amount of natural gas from the reservoir. The horizontal bore hole should ideally be drilled just below the Know unconformity surface. This would place the bore hole in the section of the Beekmantown that has the highest porosity.

ERROR ANALYSIS

In any study it is important to examine possible sources of error that would compromise the accuracy of the study. Sources of error for this study may have been introduced during data collection, data analysis and the interpretation of the data. Each will be analyzed separately.

DATA COLLECTION

The majority of the data collected for this study came from cores that had been drilled for various academic studies during the past 30 years and are now stored in the New York State Museum core repository. Before coming to the core repository, the cores had been handled by different workers, transported numerous times and stored in a variety of facilities that were not designed for core storage. Damage to these cores, in the form of additional fracturing, may have occurred during the coring operation or during subsequent handling, transportation, analysis or storage. During the data collection stage of study, it is very important to be able to differentiate between natural fractures and non-natural fractures.

Probably the greatest cause of non-natural fracturing is drilling. Unfortunately, it is often difficult to differentiate between drilling induced fractures and natural fractures. Friedman (1969) designated fractures as unequivocal natural fractures (identified by the presence of gouge, secondary mineral growth or shear offset), very probable natural fractures (identified by the presence of slickensides) and probable natural fractures (identified by clean, fresh planar surfaces that are accompanied by parallel incipient fractures that are parallel to unequivocal natural fractures).

Nelson (2001) indicated that the sometimes common practice of removing jammed cores from the core barrel with a sledge hammer often causes numerous fractures. In addition, unloading fractures, perpendicular to the core, often form in shale or along shale partings. These fractures often lead to the

formation of multiple "poker chip" fractures along the core. The twist of the core barrel during coring also can lead to spiral shaped fractures. One particularly troublesome form of drilling induced fracturing is referred to as centerline fracturing. These are extension fractures that propagate through the center of the core in front of the coring bit. These fractures form due to the weight of the drill string.

The guidelines of Friedman (1969) and Nelson (2001) were used when differentiating natural from drilling induced and core mishandling fractures. Fractures that were suspected of being drilling induced or the byproduct of mishandling were not recorded or used in the analyses. When examining the cores, euhedral and subhedral crystal growth on the fracture surface, bedding offset on either side of the fracture, and incipient fractures, parallel to the fractures in question, were often the best means of identifying natural fractures. Striations and plumose markings were all but absent from the fracture surfaces. Interestingly, striations were often present along fractures in the Precambrian metamorphic rock from those cores that penetrated the Precambrian. The reason that the striations and plumose markings were absent from the Sauk Sequence carbonate rocks is most likely due to meteoric diagenesis, which occurred during the time that the peripheral bulge uplifted and subaerially exposed the area. Meteoric water dissolved both striations and plumose markings from fracture faces as it flowed through the carbonate rocks. The meteoric water did not have the same effect on the Precambrian metamorphic rocks, due to the lower solubility of the minerals in them. It is strongly believed that, by using these guidelines, both artificial and natural fractures were correctly identified during this study. As a result, misidentification of fractures should not have been a significant source of error in this study.

A second potential problem associated with data collection was the accurate measurement of fracture strike and dip. Dip measurements were taken from the core with the assumption that the core was parallel to the vertical axis. If the core deviated from the vertical axis, the dip measurements would be in error. Where bedding was present, it was very nearly normal to the vertical axis of the cores. Bradley and Kidd (1991) indicated that the dip of the beds in the Mohawk Valley was only 1° to 2°. This indicates that there was very little deviation of the cores from the vertical, so any error in dip angle should be minimal.

Strike measurements could not be measured, since the cores were not orientated at the time of drilling. Strikes could not be measured based on the dip of the bedding, since the bedding of the formations in the study area are nearly horizontal. A significant amount of the carbonate rock that was cored showed massive bedding, which further eliminated the possibility of using regional bedding dip as a method of measuring strike.

The strike of the fractures was assumed to be parallel, or subparallel to the strike of the faults that were adjacent to the areas where the cores were taken. This assumption was based on the fact that the strikes of fractures are parallel to, or subparallel to the strike of the faults that they are associated with (Thamm 1939; Friedman, 1969; Stearns and Friedman, 1972; Nelson, 2001; Nelson, 2004, Bahat, 2004). This parallel relationship is the result of the fact that both the fractures and the faults form in the same stress field. This has already been shown to be true in the study area. Geraghty and Isachsen (1981) reported that the strike of the fractures adjacent to the McGregor-Saratoga-Ballston fault system had a good correspondence with the strike of the fault trend in 14 out of 16 fault segments that were studied. Although rock fracture theory and field observation indicate that there is a very high degree of certainty that the strikes of the fractures found along the cores parallel the strikes of adjacent faults, a certain degree of uncertainty still remains, since direct measurement of the fracture strikes could not be taken.

DATA ANALYSIS

As indicated above, there is a certain degree of uncertainly in differentiating between natural and drilling induced fractures when examining cores. Chi-square goodness of fit testing was used to determine if the distribution of fractures was dependent or independent of position along the length of the core. For all, but two, cases (the 90° dipping fractures for core 74-NY-11 and the 70° dipping fractures for core 74-NY-10), the results of the chi-square goodness of fit testing indicated that the fracture distributions were either in strong disagreement or strong agreement with the null hypothesis (there is no relationship between the positions of the fractures along the length of the core with respect to an adjacent fault). Because chi-square testing was so conclusive, either one way or the other, a small recording error in the actual number of natural fractures found along the lengths of the cores would not have changed the results of the chi-square analysis. Therefore, small errors in fracture identification would not have changed the conclusions of the study.

Fracture spacing was determined using the average fracture spacing method developed by Narr (1996). This method treats the core as a three dimensional sample of the bedrock from which it was taken. It requires that fractures occur in arrays of parallel fractures that form sets, are perpendicular to bedding and are long, relative to the core diameter. If, as indicated above, there were errors in data collection then there would also be errors in the calculation of fracture spacing. Specifically, if drilling induced fractures were mistakenly included in the fracture spacing calculations, then the resultant fracture spacing values would be too close together. Conversely, if natural fractures were misidentified as drilling induced fractures and kept out of the fracture spacing calculations, then the resultant fracture spacing values would be too far apart. Since considerable care was used to identify natural and non-

natural fractures, it is not believed that errors of this type will adversely affect the average fracture spacing calculations.

The comparison of the fracture spacing curves for cores 75-NY-2, 75-NY-14 and 74-NY-11 strongly suggests that Narr's (1996) average fracture spacing method did an excellent job in calculating the differences in fractures spacing between a fault process zone (core 75-NY-2), an incipient fault (core 75-NY-14) and a fault with just several tens of meters of offset (core 74-NY-11) (Figure 29). Clearly, as a fault process zone develops into an active fault zone, the spacing between the fractures will get closer and the zone of fractured rock surrounding the fault will become greater. The comparison between the fracture spacing curves for these three cores showed a consistent decrease in fracture spacing and an enlargement in the fracture zone surrounding the fault with each successive stage of fault development. This is a very strong indication that Narr's method was correctly modeling the fracture behavior of the rock.

The comparison between the fracture spacing curves for cores 74-NY-10 and 74-NY-6 also is a very strong indication that Narr's (1996) average fracture spacing method is correctly calculating changes in fracture spacing with distance from a fault (Figure 44). Both cores passed through the same formation, the Little Falls formation, both cores passed very close to nearly vertical normal faults and both cores share the same stress history. As a result, the fracture spacing around the two faults is very similar which resulted in fracture spacing curves that are nearly identical. This is certainly a good indication that there was a minimal amount of error when using this method in this study.

DATA INTERPRETATION

In order to eliminate errors in the interpretation of the data, it is important to be able to differentiate between the various types of joints that can be found in an area. The various types of joints, such as regional, neotectonic and tectonic fractures all have distinguishing characteristics that can be used to differentiate them from each other.

By definition, regional fractures are extension fractures that form over an extremely large area (Stearns and Friedman, 1972; Lorenz, et al., 1991 and Nelson, 2001). They form perpendicular to major bedding surfaces, have a very consistent orientation, show no offset and cut across local structures Within the study area, the presence of 45° to 60° dipping shear fractures, the reduction in fracture spacing as tectonic structures (faults) are approached, the presence of offset in many of the fractures and the relative absence of fractures in cores taken great distances from faults clearly indicates that the fractures found on the cores are not part of a regional fracture network.

By definition, neotectonic joints are very shallow features (less than 500 m) that form due to uplift and erosion (Hancock and Engelder, 1989). They are the most recently formed joints in the area and, as such, propagate parallel to, or approximately parallel to the direction of the present maximum compressive stress. They typically form as vertical fractures, or less commonly as steeply dipping conjugate fractures. Because they form due to uplift and erosion, they would be expected to die out with depth, indicated by a consistent increase in the spacing between the fractures with depth. The fracture patterns found on the cores that were taken from the study area indicate that fracture spacing both increased and decreased with depth. This strongly suggests that the fractures that were found on the cores are not neotectonic fractures. In addition, 45° to 60° dipping shear fractures were identified on the cores. The shear fractures are not related to the processes that formed neotectonic joints, so clearly cannot be identified as such. There is little evidence to suggest that the fractures that were found on the cores are neotectonic joints.

By definition, tectonic joints are associated with tectonic features, such as folds and faults and are produced by the same forces and stress field that produced the faults and folds (Nelson, 2001 and Nelson, 2004). Tectonic fractures are typically made up of conjugate sets of shear fractures and extension fractures that bisect the acute angles between the shear fractures. Specific to fault related tectonic fractures, the formation of both shear and extension fractures predates faulting and are found concentrated in fault process zones, or fracture swarms. The fault passes through the process zone, which produces a fracture pattern that is characterized by a reduction in the number of fractures and an increase in the spacing between the fractures with distance from the fault. The types of fractures and the fracture patterns that were found in the cores from the study area are consistent with all aspects of fault related tectonic fractures and are given this designation.

A COMPARISON BETWEEN THE FAULT PROCESS ZONES IN THE MOHAWK AND CHAMPLAIN VALLEYS AND THE FRACTURE INTENSIFICATION DOMAINS IN THE FINGER LAKES REGION OF NEW YORK STATE

A Fracture Intensification Domain is defined by a concentration of fractures that is much higher than the concentration of fractures found in the surrounding rocks (Lugert, 2005) (Figure 95). The spacing of the fractures within the Fracture Intensification Domain is too close to be the result of widespread regional stresses that produce regional fractures within the same area. For this reason, the formation of Fracture Intensification Domains is strongly believed to be the result of a stress build up that is associated with the reactivation of subsurface faults below the area where the Fracture Intensification Domains are found. Lugert (2005) found a close association between Fracture Intensification Domains and subsurface faults (observed in proprietary seismic data), the orientation of regional

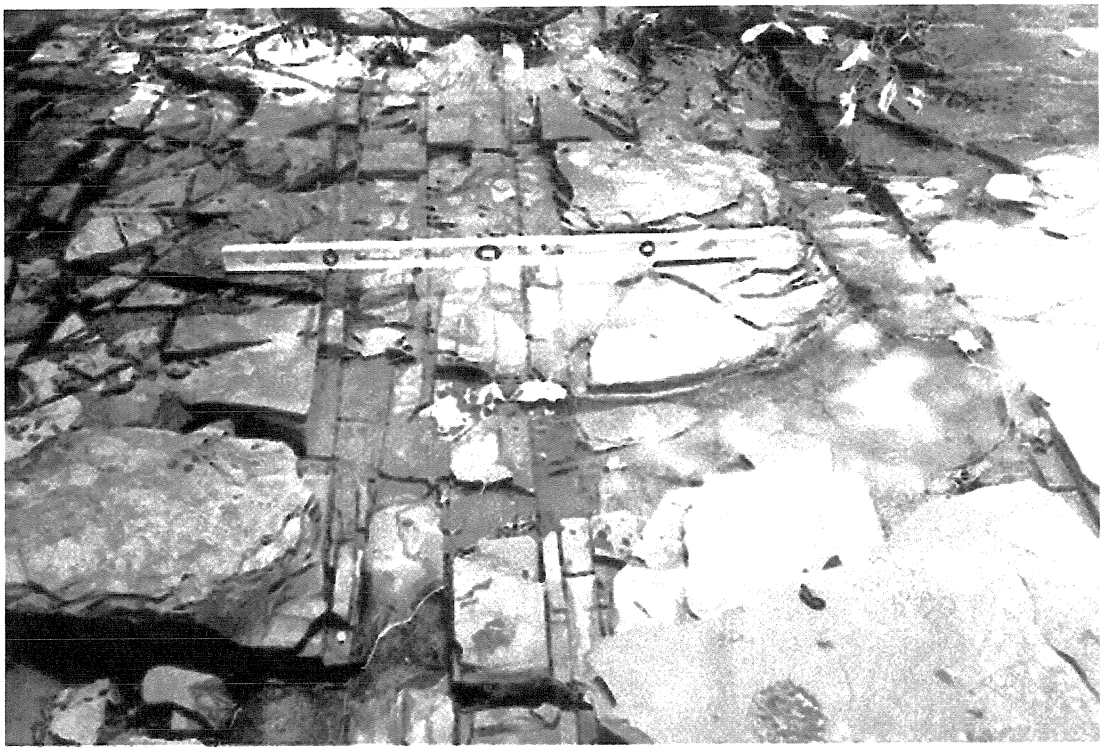

Figure 95. North-northwest striking Fracture Intensification Domain on the southeastern shore of Seneca Lake, New York. The Fracture Intensification Domain is identified by fracture spacing between parallel to subparallel extension fractures that is much closer than the fracture spacing of the regional fractures within the same area. Four foot level for scale.

Source. Lugert (2005)

aeromagnetic data and the orientation of surface lineaments in the Finger Lakes region of New York State. Interestingly Lugert (2005) indicated that lithology did not appear to be a significant control affecting fracture spacing. The close spacing of the fractures within the Fracture Intensification Domains was similar in limestone, sandstone, siltstone and shale formations.

Lugert (2005) defined the Fracture Intensification Domains in her study area as any site where the fracture frequency within the Domain exceeded a value equal to the mean of that set plus one standard deviation from the mean. The mean is the fracture frequency of background areas (areas outside the Fracture Intensification Domain).

Lugert (2005) determined that a NNW trending ($324^{\circ} - 349^{\circ}$) fracture set was the most common in her study area (Figure 95). The average fracture frequency for this NNW striking regional fracture set is 1.08 f/m (0.926 meter spacing) and the threshold for the NNW striking Fracture Intensification Domain is 2.77 f/m (0.36 meter spacing). Within the Fracture Intensification Domain, fracture frequency values as high as 12 f/m (0.083 meter fracture spacing) were recorded.

Lugert (2005) determined that a NNE trending ($54^{\circ} - 89^{\circ}$) fracture set was the second most common fracture set in her study area. The average fracture frequency for this NNE striking regional fracture set is 1.32 f/m (0.758 meter fracture spacing) and the threshold for the NNE Fracture Intensification Domain is 3.30 f/m (0.303 m spacing). Within the Fracture Intensification Domain, fracture frequency values as high as 6 f/m (0.167 meter fracture spacing) were recorded.

From this study, it was determined that core 74-NY-11 penetrated a hanging wall block of a normal fault with approximately 60 meter offset, core 75-NY-14 penetrated an incipient fault, or a fault with only meter scale displacement and core 75-NY-2 penetrated a fault process zone that had not achieved offset. When comparing the extension fracture spacing between these cores, two patterns were clearly seen (Figures 22 and 29). First, the fracture spacing curve for core 74-NY-11was larger than the fracture spacing curve for core 75-NY-14, which was larger than the fracture spacing curve for core 75-NY-2. This indicated that the width of a typical process zone within the study area increased in size as the process zone developed into a fault (Tables 30 and 31). Second, the minimum extension fracture spacing was approximately 0.3 meters for the fault process zone (core 75-NY-2), 0.2 meters for the incipient fault (core 75-NY-14) and millimeter to centimeter scale for the fault zone (core 74-NY-11). These estimates for subsurface fracture spacing, using Narr's (1996) method, indicate that fracture spacing between 0.3 meters and 0.2 meters is the minimum fracture spacing threshold that needs to be achieved before faulting can occur.

Lugert (2005) identified a fracture spacing of approximately 0.3 meters as the fracture spacing threshold for the Fracture Intensification Domains in her study area whereas this study concluded that a fracture spacing of 0.3 meters was the minimum fracture spacing threshold that needed to be obtained before faulting could occur. If the comparisons hold true, then several of the Fracture Intensification Domains identified by Lugert (2005) were close to achieving offset, since the spacing within the Domains was as close as 0.08 to 0.16 meters. This spacing, measured at the surface, may indicate that actual offset of the fault has occurred at a fairly shallow depth.

Lugert (2005) concluded that Fracture Intensification Domains are associated with and were produced by the same stresses that reactivated subsurface faults within her study area. This conclusion indicates that the Fracture Intensification Domains are equivalent to the fault process zones found in the Sauk Sequence formations within the Mohawk River and Champlain valleys. Specifically, both Fracture Intensification Domains and fault process zones are formed by the stresses that are associated with faulting, both are composed of a set of parallel to subparallel extension fractures, both are identified by a significant decrease in the spacing between the extension fractures and both will experience offset if the stress build up is significant enough. The comparison between the Fracture Intensification Domains and the fault process zones becomes even stronger when the actual fracture spacing values within these two areas are compared.

CONCLUSIONS

A subsurface fracture analysis of the Beekmantown Group (Sauk Sequence) in eastern New York State was conducted using fracture distribution and fracture spacing patterns found in cores. The purpose of this study was to determine the origin and development of the fractures within the subsurface Beekmantown Group carbonate rocks.

It has been determined that the fractures found within the Beekmantown Group carbonates formed during the passage of a peripheral bulge, as it migrated cratonward in advance of the Taconic orogeny. This conclusion was based on multiple lines of evidence.

First, the fracture distribution and fracture spacing patterns were shown to be spatially related to the faults that bisect the study area. This was done both locally and regionally. Locally, the spatial relationship was confirmed using individual cores to shown that the number of fractures increases as faults are approached. Chi-square goodness of fit testing was used to confirm that these fracture distribution patterns were significant. Using these same cores, the spacing between individual fractures was also shown to decrease as faults were approached. Regionally, the spatial relationship was confirmed by plotting the average number of fractures per 12-meter interval of core against the distance to the nearest fault affecting the area where the fault was taken. This indicated that there was a measurable decrease in the number of fractures within the bedrock as the distance from a fault increased. This decrease could be measured for kilometers and was consistent with the distance separating major faults in the study area. The types of fractures and the fracture patterns that were found on the cores are consistent with the characteristics of fault related tectonic fractures.

Second, the possibility that the fractures could have been produced by other causes or were fractures that belonged to a category of fractures other than tectonic fractures was conclusively determined not to be the case. The fractures are not part of a regional fracture system and do not fit the definition of fractures that are part of such a regional fracture system. The fractures are not neotectonic joints and do not fit the definition of fractures that are part of a neotectonic system. The fractures are not part of a fracture system that was caused due to deep burial, or uplift due to erosion and do not fit the definition of fractures that formed in this manner. Eliminating the possibility that these fractures are regional fractures or neotectonic fractures strengthens the conclusion that they are tectonic fractures.

Third, fracture development was shown to follow an orderly sequence of events that started with the formation of widely spaced extension fractures, then progressed to the formation of conjugate fault process zones and ended with the formation of normal faults. Previous studies have proven that the normal faults that bisect the Mohawk and Champlain Valleys formed during the Taconic Orogeny due

to flexural extension of the crust (Bradley and Kidd, 1991). Since the faults developed from the fault process zones, it is clear that the fractures predated faulting and formed during the early stages of the Taconic orogeny, as a result of the peripheral bulge uplift.

Fourth, previous studies have indicated that there is widespread karst dissolution within the carbonate beds of the Sauk Sequence (Dix, Robinson and McGregor, 1998; Friedman, 1996; Kolkas and Friedman, 1999; Rubin and Friedman, 1977 and Conway and Friedman, 1984). Fractures within these carbonate beds would have acted as conduits for meteoric water flow during subaerial exposure. Subaerial exposure occurred during the time that the area was uplifted, due to the passage of peripheral bulge. Evidence of meteoric diagenesis includes the presence of vuggy fractures, the absence of surface ornamentation (striations and slickensides) on the fracture face and an increase in matrix porosity where there is an increased number of fractures. These diagenetic changes are consistent with the flow of undersaturated meteoric water through the fractures.

Presenting multiple lines of evidence linking the fractures found within the study area to the Taconic Orogeny, while at the same time eliminated all other causes of fracturing, has resulted in the very definite conclusion that the fractures within the subsurface Beekmantown carbonates of eastern New York State resulted from the tectonic events leading up to, and culminating with the Taconic Orogeny.

Vadose and upper phreatic diagenesis of the Beekmantown formation, just below the Knox unconformity, has resulted in a significant increase in secondary porosity in the upthrown fault block of a normal fault in the town of Beekmantown, New York. It is very probable that the upthrown fault blocks of other normal faults within the study area have had similar increases in porosity due to meteoric diagenesis. These upthrown fault blocks should make excellent natural gas reservoirs, especially where fault movement has placed the overlying Utica Black Shale along side the fractured dolomite.

REFERENCES

Antonellini, M. and P. N. Mollema, A Natural Analog for a fractured and Faulted Reservoir in Dolomite: Triassic Sella Group, Northern Italy, AAPG Bulletin, vol. 84, no. 3, p. 314-344.

Bahat, D., 2004, Eight distinct fault-joint geometric/genetic relationships in the Beer Sheva syncline, Israel. In: Cosgrove, J. W. and T. Engelder (eds.) 2004. The initiation, propagation and arrest of joints and other fractures. Geological Society, London, Special Publications, 231 pgs. 257-267.

Bradley, D. C. and W. S. F. Kidd, 1991, Flexural extension of the upper continental crust in collisional foredeeps: GSA Bulletin, v. 103, p. 1416 – 1438.

Buyce, M. R. and G. M. Friedman, 1975, Significance of Authigenic K-feldspar in Cambrian-Ordovician carbonate rocks of the Proto-Atlantic shelf in North American: Jour. Of Sed. Petrology, v. 45 p. 808 – 821.

Condie, K. C., 1997, Plate Tectonics and Structural Evolution, Butterworth-Heinemann, Oxford, 828 pgs.

Conway, S. W. and G. M. Friedman, 1984, Depositional environments and diagenesis of the Lower Ordovician Gailor Formation, Schenectady County, New York: Northeastern Geology, vol. 6, no. 3, p. 135 – 150.

Curl, M. W., 1983, Peritidal Carbonate Lithofacies, Diagenetic Sabkha Overprinting, and Paleoenvironment Correlation of the subsurface Tribes Hill Formation (Lower Ordovician), Mohawk Valley, New York, Master of Science Thesis, Rensselaer Polytechnic Institute, Troy, N. Y.

Curl, M. W., T. W. Zagorski, and G. M. Friedman, 1984, Depositional environments and diagenesis (Ordovician), Mohawk Valley, New York: The Compass, v. 61, no. 4, p. 216-243.

Davis, J. C. 1986, Statistics and data analysis in geology. John Wiley and sons, New York, 442 pgs.

Dennis, J. G., 1972, Structural Geology. John Wiley and sons, New York, 532 pgs.

Dix, G. R., G. W. Robinson and D. C. McGregor, 1998, Paleokarst in the Lower Ordovician Beekmantown Group, Ottawa Embayment: Structural control inboard of the Appalachian orogen: GSA Bulletin, vol. 110, no. 8, p. 1046 – 1059.

Dolfi, R. U. and G. M. Friedman, 1983, Regional Lithofacies of Lower Ordovician (Canadian age) Strata of New York and New England: Northeastern Geology, vol. 4, no. 2, p. 40-53.

Dykstra, J. C. F. and M. W. Longman, 1995, Gas Reservoir Potential of the Lower Ordovician Beekmantown Group, Quebec Lowlands, Canada: AAPG Bulletin, v.79, no. 4 (April 1995), p. 513-530.

Engelder, T., 1985, Loading paths to joint propagation during a tectonic cycle: an example from the Appalachian Plateau, U.S.A.: Journal of structural geology, v. 7 nos. 3/4 p. 459 – 476.

Franseen, E. K., 2000, A review of Arbuckle Group strata in Kansas from a sedimentologic perspective: insights for future research from past and recent studies. The Compass of Sigma Gamma Epsilon, vol. 75 No. 2 and 3. pgs. 68 – 89.

Friedman, M., 1969. Structural analysis of fractures in cores from Saticoy Field, Ventura County, California. AAPG Bulletin, vol. 53, no. 2 pgs. 367-389.

Friedman, G. M., 1980, Dolomite is an evaporite mineral: Evidence from the rock record and from sea-marginal ponds of the Red Sea. SEPM special publication no.28, Concepts and Models of Dolomitization, p. 69-80.

Friedman, G. M., 1994, Stacking patterns of cyclic parasequences in Cambro-Ordovician carbonates of eastern New York State. Northeastern Geology, v. 16, no.2, p. 145-157.

Friedman, G. M., 1996, Gas Reservoir Potential of the Lower Ordovician Beekmantown Group, Quebec Lowlands, Canada: Discussion: AAPG Bulletin, v.80, no. 10 (October 1996), P.1674-1677.

Friedman, G. M., M. M. Kolkas and B.Y. Ching, 1999, Petrophysical evaluation of the Beekmantown Group in the Hubbard #1 Borehole, Steuben County New York: Northeastern Geology and Environmental Science, v. 21, no. 4, p. 261-274.

Friedman, G. M. and J. E. Sanders, 1967, Origin and occurrence of dolostone. In Chilingar, G. V., H. J. Cissell and R. W. Fairbridge, (eds.), Carbonate rocks, p. 267-348. New York: Elsevier.

Friedman, G. M., J. E. Sanders and D. C. Kopaska-Merkel, 1992, Principals of Sedimentary Deposits, Macmillan Publishing Co., New York, 717 pgs.

Friedman, M., 1969, Structural Analysis of Fractures in Cores from Saticoy Field, Ventura County, California, A. A. P. G. bulletin Vol. 53, no. 2 (February, 1969) p. 367 – 389.

Geraghty, E. P., and Isachsen, Y. W., 1981, Investigation of the McGregor-Saratoga-Ballston Lake Fault System, East-Central New York. U.S. Nuclear Regulatory Commission, Report NUREG/CR-1866, 44p.

Guo, Baiying, J. E. Sanders and G. M. Friedman, 1990, Columbia Gas Company No.1 Finnegan Boring, Washington County, New York: Microlithofacies and Petroleum Prospects in Lower Paleozoic Platform Strata Beneath Taconic Allochthon: Northeastern Geology, v. 12, no. 4, p. 238–265.

Hancock, P. L. et al., 1984, Regional Joint Sets in the Arabian Platform as Indicators of Intraplate Processes: Tectonics, v. 3, no. 1, p. 27-43.

Hancock, P. L. and T. Engelder, 1989, Neotectonic joints: Geological Society of America Bulletin, v. 101 p. 1197-1208.

Isachsen, Y. W. and W. McKendree, 1977, Preliminary Brittle Structure Map of New York. New York State Museum and Science Services, Map and Chart Series No.31.

Jacobi, R. D., 1981, Peripheral Bulge - a causal mechanism for the Lower/Middle Ordovician unconformity along the western margin of the Northern Appalachians: Earth and Planetary Science Letters, v. 56, p. 245-251.

Keith, B. D. and G. M. Friedman, 1977, A Slope-Fan-Basin-Plain Model, Taconic Sequence, New York and Vermont: Journal of Sedimentary Petrology, Vol. 47, no. 3, p. 1220-1241.

Knight, I., N. P. James and T. E. Lane, 1991, The Ordovician St. George Unconformity, northern Appalachians: The relationship of plate convergence at the St. Lawrence Promontory to the Sauk/Tippecanoe sequence boundary: GSA bulletin, vol. 103, p. 1200-1225.

Kolkas M. M. and G. M. Friedman, 1999, Regional Stratigraphy, Facies distributions, and Depositional Environments of the Beekmantown Group (Sauk Sequence) of Central and Western New York: Northeastern Geology and Environmental Sciences, v. 21, no. 4, p. 247–260.

Lim, Chul, Kidd, W.S.F. and Howe, S.S., 2005, Late shortening and extensional structures and veins in the western margin or the Taconic Orogen (New York and Vermont): Journal of Geology, v. 113, p419-438.

Lorenz, J. C., L. W. Teufel and N.R. Warpinski, 1991, Regional Fractures I: A Mechanism for the Formation of Regional Fractures at Depth in Flat-Lying Reservoirs: A.A.P.G. Bulletin, vol. 75, no.11, p. 1714 – 1737.

Lugert (2005), Fractures and their relation to other geological data sets along the southeastern shore of Seneca Lake, New York: Implications for fault systems in the Appalachian Plateau. Unpublished Master's thesis, SUNY Buffalo, New York, 141 pgs.

Mazzullo, S. J., P. Agostino, J. N. Seitz and D. Fisher, 1978, Stratigraphic and depositional environments of the upper Cambrian-Lower Ordovician sequence, Saratoga Springs, New York: Journal of Sedimentary Petrology, vol. 48, no. 1, p. 99-116.

Muller, B., V. Wehrle, S. Hettel, B. Sperner and K. Fuchs, 2003. A new method for smoothing orientated data and its application to stress data. In Ameen, M. (ed.) Fracture and in-situ stress characterization of hydrocarbon reservoirs. Geological Society, London, Special Publications, 209, 107-126

Narr, W., 1996, Estimating Average Fracture Spacing in Subsurface Rock: A.A.P.G. Bulletin, v.80, no.10 (October 1996), p.1565-1586.

Needham, T., 2005, Fault and fracture characterization and modeling in carbonate reservoirs. Petroleum Exploration Society of Great Britain carbonate conference, November 15th and 16th, 2005.

Nelson, R.A., 2001, Geologic Analysis of Naturally Fractured Reservoirs, Butterworth-Heinemann, Woburn, Ma., 332 pgs.

Nelson, R. A., 2004, Exploration and Evaluation of Fractured Reservoirs, AAPG Eastern Section Meeting short coarse, Oct. 6, 2004, Columbus, Ohio.

New York State Museum, The University of the State of New York/ The State Education Department/ Albany, New York

Phillips, S. S. and G. M. Friedman, 2001, Carbonate Diagenesis and Dolomitization of Cambro-Ordovician (Sauk Sequence) Platform Strata in Central New York: Depositional Environments, Parasequences and Facies: Northeastern Geology and Environmental Science, v. 23, no. 2, p. 127-169.

Price, N. J., 1966, Fault and Joint Development in Brittle and Semi-brittle Rock, Pergamon Press, Oxford, 176 pgs.

Rickard, L. V., 1973, Stratigraphy and Structure of the Subsurface Cambrian and Ordovician Carbonates of New York. New York State Museum and Science Services, Map and Chart Series No. 18, 26 pgs.

Rubin, D. M. and G. M. Friedman, 1977, Intermittent Emergent Shelf Carbonates: An example from the Cambro-Ordovician of Eastern New York State, Sedimentary Geology, vol. 19, pgs. 81-106.

Shepherd, J., J. F. Huntington and J. W. Creasey, 1981, Surface and underground geological prediction of bad roof conditions in collieries of the Western coalfield, New South Wales, Australia, Trans. Instn. Min. Metall. (Sec.B: Appl. Earth sci.) Vol. 90 (February, 1981), p. B1 – B14.

Smosna, R., K. R. Bruner and R. A. Riley, Paleokarst and reservoir porosity in the Ordovician Beekmantown dolomite of the central Appalachian Basin. Carbonates and Evaporites, vol. 20, no. 1, pgs. 50 – 63.

Stearns D. W. and M. Friedman, 1972, Reservoirs in Fractured Rock, A.A.P.G. Memoir no.16 p. 82-100.

Thamm, N., 1939, Certain methods of mapping faults in the Pretoria and Dolomite Series on West Witwatersrand areas, Ltd., Transactions of the Geological Society of South Africa, Vol. XLII, 1939.

Zagorski, T.W., 1981, Depositional Environments and Diagenesis of the Subsurface Tribes Hill Formation (Lower Ordovician) of the Mohawk Valley Region, New York. Master of Science Degree thesis, Rensselaer Polytechnic Institute, Troy, New York

Zenger, D. H., 1980, Stratigraphy and Petrology of the Little Falls Dolostone (Upper Cambrian), East-Central New York. New York State Museum and Science Services, Map and Chart Series No. 34, 138 pgs.